

Synthesis and Characterization of Carboxylic Acid Functionalized Silicon Nanoparticles

An abstract

Submitted on the Eighth day of January, Two Thousand Sixteen

To the Department of Chemistry

In Partial fulfillment of the Requirements

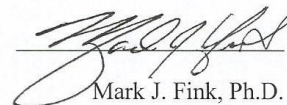
Of the Graduate School of Tulane for the

Degree of Doctor of Philosophy

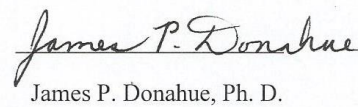
By



Ted V. Shaner



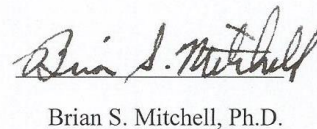
Mark J. Fink, Ph.D.



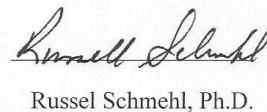
James P. Donahue, Ph. D.



Janarthanan Jayawickramarajah, Ph. D.



Brian S. Mitchell, Ph.D.



Russel Schmehl, Ph.D.

Abstract

Silicon nanoparticles are of great interest in a great number of fields. Silicon nanoparticles show great promise particularly in the field of bioimaging. Carboxylic acid functionalized silicon nanoparticles have the ability to covalently bond to biomolecules through the conjugation of the carboxylic acid to an amine functionalized biomolecule. This thesis explores the synthesis of silicon nanoparticles functionalized by both carboxylic acids and alkenes and their carboxylic acid functionality. Also discussed is the characterization of the silicon nanoparticles by the use of x-ray spectroscopy. Finally, the nature of the Si-H bond that is observed on the surface of the silicon nanoparticles will be investigated using photoassisted exciton mediated hydrosilation reactions.

The silicon nanoparticles are synthesized from both carboxylic acids and alkenes. However, the lack of solubility of diacids is a significant barrier to carboxylic acid functionalization by a mixture of monoacids and diacids. A synthesis route to overcome this obstacle is to synthesize silicon nanoparticles with terminal vinyl group. This terminal vinyl group is distal to the surface of the silicon nanoparticle. The conversion of the vinyl group to a carboxylic acid is accomplished by oxidative cleavage using ozonolysis.

The carboxylic acid functionalized silicon nanoparticles were then successfully conjugated to amine functionalized DNA strand through an n-hydroxy succinimide ester activation step, which promotes the formation of the amide bond. Conjugation was characterized by TEM and polyacrylamide gel electrophoresis (PAGE). The PAGE results show that the silicon nanoparticle conjugates move slower through the polyacrylamide gel, resulting in a significant separation from the nonconjugated DNA.

The silicon nanoparticles were then characterized by the use of x-ray absorption near edge spectroscopy (Xanes) and x-ray photoelectron spectroscopy (XPS) to investigate the bonding and chemical environment of the silicon surface of the nanoparticles. Modeling of the silicon nanoparticles and theoretical XANES spectra were also accomplished through the use of the FEFF9 software package. Results validate the infrared spectra results of more oxygen bound to the surfaces of larger silicon nanoparticles and less oxygen bound to smaller silicon nanoparticles.

The photoluminescence was shown to greatly increase in yield after photoassisted exciton mediated hydrosilation. This has led to an increase of the luminescence yield of over an order of magnitude.

Synthesis and Characterization of Carboxylic Acid Functionalized Silicon Nanoparticles

A Dissertation

Submitted on the Eighth day of January, Two Thousand Sixteen

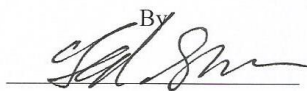
To the Department of Chemistry

In Partial fulfillment of the Requirements

Of the Graduate School of Tulane for the

Degree of Doctor of Philosophy

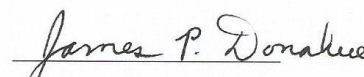
By



Ted V. Shaner



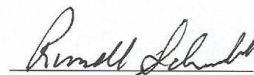
Mark J. Fink, Ph.D.


James P. Donahue, Ph. D.

Janarthanan Jayawickramarajah, Ph. D.



Brian S. Mitchell, Ph.D.



Russel Schmehl, Ph.D.

Acknowledgements

I would like to thank Dr. Mark Fink for all of his assistance, patience, and guidance during my graduate career. His allowing of my to study what I found interesting and to pursue lines of investigation on my own was a truly rewarding experience.

I would also like to thank the members of my committee, Dr. James Donahue, Dr. Brian Mitchell, Dr. Janarthanan Jayawickramarajah, and Dr. Russ Schmehl not only for their assistance in preparing and evaluating my thesis, but also for the help throughout my career at Tulane. I would also like to thank all of the faculty, staff , and fellow graduate students who have helped me along my exploration and journey that was my time at Tulane. It is the people of the Chemistry department who truly make this a great department both academically and socially. I would also like to thank all of the people who I have met during my stay in New Orleans who have helped to expose me to such culture, great food, and friendship that makes this the great city that it is.

I would also like to extend heartfelt thanks and gratitude to my parents without whom this would not have been possible. Their continued love and support is without end.

Table of Contents:

	Page
Chapter 1: General Introduction	
Background	1
Quantum confinement	1
Quantum Dots	3
Silicon Quantum Dots	5
Methods of silicon nanoparticle synthesis	12
Bottom up methods	12
Top down methods	23
Functionalization of silicon nanoparticles	27
Applications of silicon nanoparticles	30
Motivation for thesis	37
Chapter 2: Synthesis of passivated silicon nanoparticles using Reactive High Energy Ball Milling (RHBM) with carboxylic acids.	
Introduction	47
Experimental	55

Results and discussion	61
RHEBM of silicon with monocarboxylic acids	61
RHEBM with monocarboxylic acids and dicarboxylic acids	77
RHEBM of silicon and monocarboxylic acid in an inert solvent	85
Conclusion	90
Chapter 3: Biologically relevant transformations of the vinyl terminated silicon nanoparticle.	
Introduction	95
Synthesis of vinyl terminated silicon nanoparticles	101
Results and discussion	104
Oxidation of terminal vinyl groups	114
Conjugation of amine to carboxylic acid terminated silicon nanoparticles	124
Conjugation with DNA	129
Conclusion	135
Chapter 4. X-ray investigation and characterization of silicon nanoparticles.	
Introduction	139

Experimental	146
Results and discussion	150
Modeling	169
XPS	177
Conclusion	183

Chapter 5. Attempts to elucidate reactivity of the Si-H bond on alkenyl passivated silicon nanoparticles.

Introduction	190
Experimental	190
Results and discussion	194
Reaction of D ₂ O with silicon nanoparticles	197
Reaction of silicon dangling bonds using D ₂ O and sonication	200
Hydrosilation of passivated silicon nanoparticles	204
Hydrosilation of 1-octene passivated silicon nanoparticles with halogenated solvents.	209
Future work	218
Conclusion	219

Chapter 6: Summary and Prospectus 221

Biography 228

List of Figures

	Page
Chapter 1:	
Figure 1.1 Schematic of the energy levels of molecular dyes, quantum dots, and bulk semiconductors	2
Figure 1.2 Luminescence of CdSe QD's of increasing size from left to right	3
Figure 1.3 Indirect band gap of silicon. 1) Direct Γ - Γ transition. 2) Least energetic transition (needs phonon assistance)	6
Figure 1.4. Observed absorbance spectra of silicon nanoparticles	8
Figure 1.5 Calculated absorbance spectra of silicon nanoparticles	8
Figure 1.6. Photographs showing photoluminescence from styrene grafted silicon nanoparticles after different periods of time under 254 nm UV illumination.	10
Figure 1.7. UV-Vis absorbance (left axis) and uncorrected emission spectra observed at various excitation wavelengths (right axis) of alkenyl passivated silicon nanoparticles produced by milling in 1-octyne for 24 hours	11
Figure 1.8. Korgel's supercritical reactor	20

Figure 1.9. CO ₂ laser apparatus for the synthesis of silicon nanoparticles by laser pyrolysis	22
Figure 1.10. Silicon nanoparticles that have been etched to for a oxide layer and the resulting change in color of luminescence that corresponds to change in the size of the silicon nanoparticle.	24
Figure 1.11. Hydrosilylation on hydrogen terminated bulk silicon (111) surface	29
Figure 1.12. Exciton mediated photohydrosilylation on silicon nanoparticle surface	30
Figure 1.13. PET images of mice injected with silicon nanoparticles	32
Figure 1.14. CHO cells stained using Poly acrylic acid passivated silicon nanoparticles	33
Figure 1.15. BV2 cells stained with a) DRAQ5, b) silicon nanoparticles, c) confocal image of both DRAQ5 and silicon nanoparticles	34
Figure 1.16. Mice injected with silica nanoparticles (LPSiNP) and dextran coated silica nanoparticles (D-LPSiNP).	35

Chapter 2:

Figure 2.1 8000D Mixer/Mill	56
-----------------------------	----

Figure 2.2 ^1H NMR of 1-octanoic acid passivated silicon nanoparticles in CDCl_3	62
Figure 2.3 Infrared spectrum of 1-octanoic acid passivated silicon nanoparticles	63
Figure 2.4 IR spectra of octanoic acid from Heintz et al	64
Figure 2.5 Photoluminescence of octanoic acid passivated silicon nanoparticles	65
Figure 2.6 EDS spectrum of Figure 2.7 TEM image	66
Figure 2.7 TEM image of octanoic acid passivated silicon nanoparticles	67
Figure 2.8 High resolution image of octanoic acid passivated silicon nanoparticles with lattice fringes.	69
Figure 2.9 Photoluminescence of 1-hexanoic acid passivated silicon nanoparticles	70
Figure 2.10 Infrared spectrum of hexanoic acid passivated silicon nanoparticles	71
Figure 2.11 ^1H NMR of hexanoic acid passivated silicon nanoparticles	72
Figure 2.12 Absorbance and photoluminescence spectrum of 1-pentanoic acid passivated silicon nanoparticles in ethyl acetate	74

Figure 2.13 ^1H NMR spectrum of 1-pentanoic acid passivated silicon nanoparticles in CDCl_3	75
Figure 2.14 Infrared spectrum of 1-pentanoic acid passivated silicon nanoparticles	76
Figure 2.15 Initially formed silicon nanoparticle passivated by 1,6-hexanedioic acid/hexanoic acid.	77
Figure 2.16 Photoluminescence of hexanoic acid/ 1,6-heanedioic acid nanoparticle attempt	78
Figure 2.17 Photoluminescence of 1-pentanoic acid/ 1,7-heptanedioic acid (5%) passivated silicon nanoparticles	80
Figure 2.18 Infrared spectrum of 1-pentanoic acid/ 1,7-heptanedioic acid (5%) passivated silicon nanoparticles	81
Figure 2.19 ^1H NMR spectrum of 1-pentanoic acid/ 1,7-heptanedioic acid (5%) passivated silicon nanoparticles	82
Figure 2.20 Low resolution TEM of 1-pentanoic acid/ 1,7-heptanedioic acid (5%) passivated silicon nanoparticles	83
Figure 2.21. EDS of 1-pentanoic acid/ 1,7-heptanedioic acid (5%) passivated silicon nanoparticles	84

Figure 2.22 Photoluminescence of benzoic acid passivated silicon nanoparticles	86
Figure 2.23 Infrared spectrum of benzoic acid passivated silicon nanoparticles	87
Figure 2.24 ^1H NMR spectrum of benzoic acid passivated silicon nanoparticles	88
Chapter 3	
Figure 3.1 TEM and EDS of 50% 1,7-octadiene/1-pentene silicon nanoparticles with histogram	105
Figure 3.2 EDS of 50% 1,7-octadiene/1-pentene silicon nanoparticles	106
Figure 3.3 NMR spectra of 50% 1,7-octadiene/1-pentene silicon nanoparticles	106
Figure 3.4 infrared Spectra of 50% 1,7-octadiene/1-pentene silicon nanoparticles	107
Figure 3.5 Photoluminescence of 1,7-octadiene/1-pentene silicon nanoparticles	108
Figure 3.6 Absorption spectrum of 1,7-octadiene/1-pentene silicon nanoparticles	109

Figure 3.7 Photoluminescence of 1,6-hexadiene(20%)/1-pentene passivated silicon nanoparticles	110
Figure 3.8 Infrared spectrum of 1,6-hexadiene (20%)/1-pentene passivated silicon nanoparticles	112
Figure 3.9 ¹ H NMR spectrum of 1,6-hexadiene (20%)/1-pentene passivated silicon nanoparticles	113
Figure 3.10 ¹ H NMR of 1,7-octadiene/1-pentene (50%) Silicon nanoparticles after KMnO ₄ oxidation	114
Figure 3.11 IR of 1,7-octadiene/1-pentene (50%) silicon nanoparticles after reaction with KMnO ₄ .	115
Figure 3.12 ¹ H NMR of 1,7-octadiene/1-pentene (50%) silicon nanoparticles after increased reaction time (>72 hours stirring with KMnO ₄)	116
Figure 3.13 Characteristic blue color of dichloromethane containing dissolved ozone	117
Figure 3.14 Photoluminescence of carboxylic acid terminated silicon nanoparticles	118
Figure 3.15 Water solubility of carboxylic acid terminated	120

nanoparticles at pH 2 on the left and at pH 8 on the right

Figure 3.16 Infrared spectra of carboxylic acid terminated silicon nanoparticles	121
Figure 3.17 ^1H NMR of carboxylic acid terminated silicon nanoparticles in CDCl_3	122
Figure 3.18 Infrared spectra of Amine terminated silicon nanoparticles	125
Figure 3.19 ^1H NMR of amine terminated silicon nanoparticles in CD_2Cl_2	126
Figure 3.20 Photoluminescence of amine terminated silicon nanoparticles	127
Figure 3.21 Polyacrylamide gel of 1,7-octadiene/1-pentene (50%) silicon nanoparticles conjugated with DNA	129
Figure 3.22 Polyacrylamide gel of 1,7-octadiene/1-pentene (25%) silicon nanoparticles conjugated with DNA which was hybridized with a fluorescent marker	130
Figure 3.23 TEM of 1,7-octadiene/1-pentene (25%) silicon nanoparticles conjugated to DNA	131
Figure 3.24 EDS of TEM of 1,7-octadiene/1-pentene (25%) silicon nanoparticles conjugated to DNA	132
Figure 3.25 TEM and EDS of 1,7-octadiene/1-pentene (50%) silicon nanoparticles conjugated with DNA	131

Figure 3.26 Histogram of TEM particles of 1,7-octadiene/1-pentene (50%) passivated silicon nanoparticles conjugated with DNA.	133
 Chapter 4	
Figure 4.1. Energy levels of synchrotrons	139
Figure 4.2 Transmission experiment setup of sample in ionization chamber	141
Figure 4.3 Total electron yield method	142
Figure 4.4 Silicon K-edge XANES of methylfluorosilane	144
Figure 4.5 Silicon K-edge XANES of silicon minerals	145
Figure 4.6. Schematic drawing of double crystal monochromator	147
Figure 4.7. XANES spectra of silicon dioxide standard	150
Figure 4.8. Silicon powder standard	151
Figure 4.9 XANES results of 1-octyne passivated silicon nanoparticle fractions	152
Figure 4.9B. Close up view of all normalized peaks of 1-octyne passivated silicon nanoparticles	153
Figure 4.10 XANES results of 1-octene passivated silicon nanoparticles	154
Figure 4.10B. Close up view of all normalized peaks of 1-octene passivated silicon nanoparticles	155

Figure 4.11 Infrared spectra of 1-octene nanoparticles	156
Figure 4.12 XANES spectra of octaphenyl –T8- silsequioxane	159
Figure 4.13 XANES spectrum of octakis(dimethylsiloxy)-T8-silsequioxane	160
Figure 4.14 XANES spectra of octakis(tetramethylammonium)-T8 -silsequioxane hydrate	161
Figure 4.15 XANES spectra of octavinyl –T8-silsequioxane	162
Figure 4.16 XANES spectra of octaphenylcyclotetrasiloxane	163
Figure 4.17 XANES spectra of hexaphenylcyclotrisiloxane	164
Figure 4.18 XANES K-edge spectra of silicon nanoparticles prepared as described in Chapter 1 from silicon rich silicon oxides	166
Figure 4.19 TEY-XANES spectra for silicon rich silicon nitride films	167
Figure 4.20 Model of 29 at silicon nanoparticle with propyl chains passivating surface	170
Figure 4.21 FEFF calculations of chain length on 29 atom silicon nanoparticle	171
Figure 4.22 FEFF calculations of propyl passivated silicon nanoparticle size	173
Figure 4.23 Microfluidic chip reaction that allows for the <i>in situ</i> monitoring of the growth of gold nanoparticles using L ₃ edge XANES	174

Figure 4.24 XANES spectra of Au L ₃ -edge of gold nanoparticles monitored using XANES	175
Figure 4.25 XANES spectra of time resolved formation of colloidal copper nanoparticles	176
Figure 4.26 Silicon XPS of 1-octyne passivated silicon nanoparticles	178
Figure 4.27 Silicon XPS of 1-octene passivated silicon nanoparticles	179
Figure 4.28 Carbon XPS of 1-octyne passivated silicon nanoparticles	180
Figure 4.29 Carbon XPS of 1-octene passivated silicon nanoparticles	181
Figure 4.30. XPS control experiments	182
Chapter 5	
Figure 5.1. Stainless steel milling vial with adapted gas sidearm	192
Figure 5.1B. Dimensions for the adaptation of stainless steel milling vial	193
Figure 5.2. ¹ H NMR of 1-octene passivated silicon nanoparticles, in CD ₂ Cl ₂	195
Figure 5.3. FTIR spectra of 1-octene passivated silicon nanoparticles	196
Figure 5.4. Photoluminescence of the 1-octene passivated silicon nanoparticles	197
Figure 5.5. Photoluminescence of 1-octene passivated silicon nanoparticles after 24 hours exposure to D ₂ O	198

Figure 5.6. 1-Octene passivated silicon nanoparticles denoted as control and 1-octene passivated silicon nanoparticles that had been exposed to D ₂ O for 24 hours, denoted as D ₂ O.	199
Figure 5.7. 1-Octene passivated silicon nanoparticles after 12 hours sonication with D ₂ O	201
Figure 5.8. IR spectra of 1-octene passivated silicon nanoparticles after sonication for 12 hours with D ₂ O	202
Figure 5.9. The IR spectra of hydrogen, deuterium, and tritium bound to silicon	203
Figure 5.10. 1-Octene passivated silicon nanoparticles, purged with ethylene under 254 nm light for 30 minutes	206
Figure 5.11. 1-Octene passivated silicon nanoparticles, purged with ethylene under 254 nm light for 1 hour	207
Figure 5.12. IR of 1-octene passivated silicon nanoparticles, purged with ethylene under 254 nm light for 12 hours	208
Figure 5.13. Reduction potentials of halogen solvents compared to porous silicon	210
Figure 5.14. 1-Octene passivated silicon nanoparticles purged with ethylene in CCl ₄ for 12 hours under 254 nm light	211

Figure 5.15. IR of 1-octene passivated silicon nanoparticles purged with ethylene for 12 hours under 254 nm light with chloroform	212
Figure 5.16. 1-Octene passivated silicon nanoparticles purged with ethylene in CCl ₄ for 12 hours under 254 nm light, fraction 1	213
Figure 5.17. 1-Octene passivated silicon nanoparticles purged with ethylene in CCl ₄ for 12 hours under 254 nm light, fraction 2	214
Figure 5.18. 1-Octene passivated silicon nanoparticles purged with ethylene in CCl ₄ for 12 hours under 254 nm light, fraction 3	215
Figure 5.19. IR of 1-octene passivated silicon nanoparticles purged with ethylene in CCl ₄ under 254 nm light for 12 hours	217

List of Schemes

	Page
Scheme 1.1. Synthesis of silicon nanoparticles by <i>Heath</i>	13
Scheme 1.2. Synthesis of silicon nanoparticles by the oxidation of magnesium silicide	13
Scheme 1.3. Oxidation of Zintl salt synthesis of silicon nanoparticles	14
Scheme 1.4 Synthesis of silicon nanoparticles by reduction of SiCl_4 using the Zintl Salt NaSi	15
Scheme 1.5. Reduction of Silicon tetrachloride by sodium naphthlaide to synthesis silicon nanoparticles	15
Scheme 1. 6. Synthesis of Mn doped silicon nanoparticles	16
Scheme 1.7. Synthesis of silicon nanoparticles using potassium and the transfer agent, crown ether, to reduce silicon tetrachloride	17
Scheme 1.8. Synthesis of silicon nanoparticles by sonochemical approach	18
Scheme 1.9. Surface passivation of chloride terminated silicon nanoparticle by the alkyl lithium reagent butyllithium	27
Scheme 2.1 Synthesis of alkyne passivated silicon nanoparticles	48

Scheme 2.2. Radical addition of alkyne and alkene reactive organic liquids to fresh (111) silicon surface	49
Scheme 2.3 The 2+2 mode of cycloaddition to a silicon (100) fresh silicon surface with liquid alkyne and alkenes	50
Scheme 2.4 Passivation by carboxylic acid of silicon nanoparticle	52
Scheme 2.5 Synthesis of silicon nanoparticle conjugated to DNA by hydrosilation method	53
Scheme 2.6 Synthesis of silicon nanoparticle passivated with free carboxylic acid	54
Scheme 3.1 Reaction scheme for the production of carboxylic acid functionalized silicon nanoparticles from silicon wafers and 1,7-octadiene/1-pentene	97
Scheme 3.2 General mechanism of ozonolysis reaction	98
Scheme 3.3 Activation of carboxylic acid	123
Scheme 5.1. Exciton mediated hydrosilation mechanism on silicon nanoparticle	209

Chapter 1: Introduction.

Section 1.1: Background

Nanotechnology is a developing field with much interest due to its use in biomedical diagnostics, electronics, and in energy storage and generation.¹ The term Nanotechnology was coined by Professor Norio Taniguchi while studying the use of ultrafine machining. It wasn't until 1981 that the tunneling microscope was invented which was the first time that atoms themselves could be visualized. This advance really catalyzed the growth of nanotechnology. With the ability to verify the size and conformation of structures composed of just several atoms, the field began to slowly grow and has become one of the leading interests in research today. A nanostructure is generally defined as objects having a characteristic dimension between 1 and 100 nanometers, shown increased control of light spectrum, and increased chemical reactivity than their larger-scale counterparts.² The field of nanotechnology includes such topics as: micro-machining, synthesis of nanotubes, nanoparticles, and nanowires.

Section 1.2: Quantum confinement

Semiconductors are materials with electronic properties between those of conductors (metals) and insulators. A bulk solid semiconductor can be described as having a filled valence band and an empty conduction band. At $T = 0$ K there is no probability of an electron

being promoted from the valence band to the conduction band, which would make it act like an insulator at that temperature. Insulators are defined by the fact that the conduction band is either completely filled or is completely empty and that the bandgap is much higher than the available Boltzmann energy. However, when $T > 0^\circ\text{K}$, there is an increasing probability that an electron can be promoted to the conduction band. This probability, which is increased by the temperature is what defines the material as a semiconductor.³ A conductor (metal) already has one partially filled conduction band and thus can easily accept an electron. When the size of the material is shrunk till it approaches the Bohr radius, these band structures take on discrete energy levels which are more reminiscent of discrete molecular orbitals. This is illustrated in Figure 1.1.

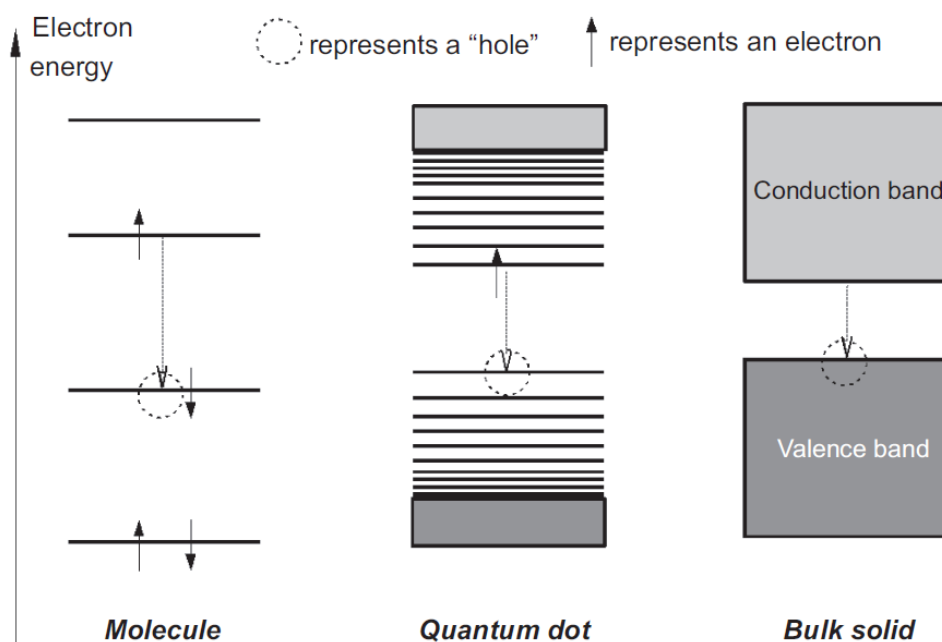


Figure 1.1 Schematic of the energy levels of molecular dyes, quantum dots, and bulk semiconductors.³

Silicon particles smaller than the Bohr radius (5 nm in silicon) gives rise to size dependent bandgaps in a phenomenon known as quantum confinement. As the size of the particle decreases there is an increase in the size of the band gap.^{1, 4-5} This leads to the ability to tune the luminescence by the bandgap of the nanoparticle.⁶ The resulting luminescence is equal to the energy of the band gap, giving rise to photons of different color (energy).

Section 1.3: Quantum Dots

Semiconductor nanoparticles are commonly referred to as quantum dots, as quantum confinement dominates their luminescence properties.⁷ Two of the most studied systems are that of semiconductor group II-VI materials such as CdSe and CdS. These systems produce QD's with very well defined luminescence that corresponds to the quantum confinement theory based on their size.⁸ The visible colors from the luminescence of CdSe QD's of different sizes can be seen in Figure 1.2.



Figure 1.2 Luminescence of CdSe QD's of increasing size from left to right.⁸

QD's have shown the potential for use in the biomedical field, photodetectors, and photovoltaics. Their use in the biomedical field shows great promise over the molecular dyes that were previously used. QD's absorb over a large spectrum which is a great advantage over molecular dyes. Molecular dyes normally have very narrow excitation ranges and broad emission spectra. Molecular dyes normally have to be excited in close proximity to the emission range. This leads to background scattering which decreases their usefulness as a biolabel.

However, since QD's can be excited over such a broad range, the emission can easily be differentiated from the excitation. Also, since QD's can emit in such narrow well defined emissions, several QD's of different sizes can be used to label several different targets without obscuring each other.⁹ This is usually done using a single excitation source as the QD's absorb over such a large range.

Another advantage of QD's over molecular dyes is the stability of the QD's to photobleaching. Molecular dyes have short lifetimes before their use is degraded by the excitation wavelength causing chemical changes to the dye. QD's are stable to the excitation light source and will display continuous strong fluorescent emission.⁹ Also, the QD's have higher quantum yields which means less concentration of QD's are needed as compared to molecular dyes.⁹

Since one application for QD's is its use in bioimaging of living tissues, QD's must be water soluble. This has been done by encapsulating the QD's with a shell of block copolymers or phospholipid micelles which have shown excellent results in increasing the water solubility properties of the QD's. Also, the QD's must be able to be conjugated to

different biomolecules to be able to target the tissues of interest. This has also been done through the use of the encapsulating ligands.⁹

While the CdSe and other such group II-VI QD's show great promise in their use based on the tailorability of the luminescence, stability to photobleaching, water solubility, and their ability to be conjugated to biomolecules, they are not suitable for use in biomedical devices due to their cytotoxicity.^{1, 3, 10} Leaching of cadmium leads to heavy metal poisoning which has led to a need for "cadmium-free quantum dot" research to find a replacement.¹ One such candidate that is showing great promise is silicon.

Section 1.4: Silicon Quantum Dots

Silicon is of great interest because of how well the chemistry is developed. It is used extensively throughout the electronics industry and is the second most abundant element in the earth's crust. The extensive study of silicon chemistry on flat surfaces under ultrahigh vacuum conditions has given extensive insight into how chemical reactions on the silicon nanoparticles surfaces occur.¹¹ Silicon nanoparticles are luminescent, non-cytotoxic, water soluble through surface ligands, and able to be conjugated to biomolecules. Having met these requirements, silicon presents itself as a positive candidate for further research into its use as a bio-labeling platform.

Origin of Luminescence

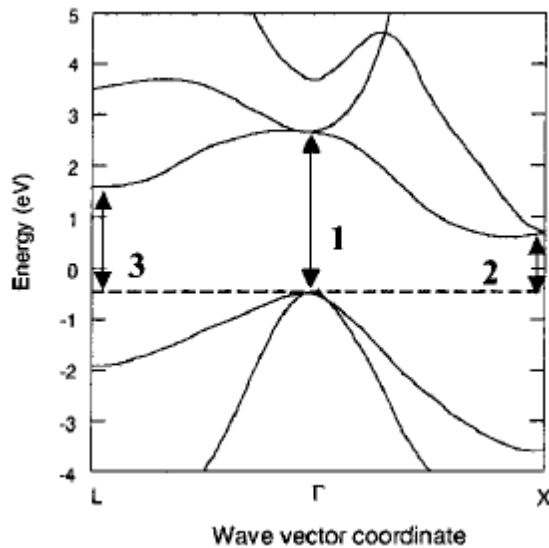


Figure 1.3 Indirect band gap of silicon. 1) Direct Γ - Γ transition. 2) Γ -X transition, least energetic transition (needs phonon assistance). 3) Γ -L transition (needs phonon assistance).¹²

Silicon as an indirect band gap semiconductor requires the use of a phonon to assist in a transition of an electron between the valence band and the conduction band. This required phonon emission or absorption decreases the probability of the electron transition. This addition barrier causes silicon to have a lower efficiency of light absorption and also a lower efficiency of photoluminescence. As seen in Figure 1.3, the maximum of the valence band does not line up with the minimum of the conduction band, which requires the assistance of a phonon to match the energy of the electron transition.

However, when the size of the silicon is reduced to a nanocrystal, the periodic boundaries disappear.¹³ This means that the Bloch states and the K vector (crystal momentum) disappear and the nature of the band gap becomes more direct-like.¹³ Shrinking the size 3-dimensionally increases the probability of luminescence, as the probability of the exciton encountering a grain boundary or surface defect, which could result in a non-radiative electron-hole recombination.¹⁴⁻¹⁵ That is to say, that an electron bound in a very small space will have a higher probability of recombining and luminescing, than finding a defect or grain boundary. Silicon nanocrystals prepared from high purity reagents prepared at high temperatures or using gas-phase methods do exhibit quantum confinement size dependent luminescence.¹ However, not all silicon nanocrystals described in the literature follow this.

Nanocrystals prepared in the gas phase were studied by *Meier* et al. and found to be mostly spherical. Meier found that the absorbance and emission spectra showed indirect bandgap characteristic that was in agreement with calculations done based on a size dependent oscillator strength (Figure 1.4 and 1.5).⁴ Meier used Fermi's golden rule and the common definition of the oscillator strength to link the radiative recombination time to the oscillator strength, thus allowing for extraction of size data from the spectral data.

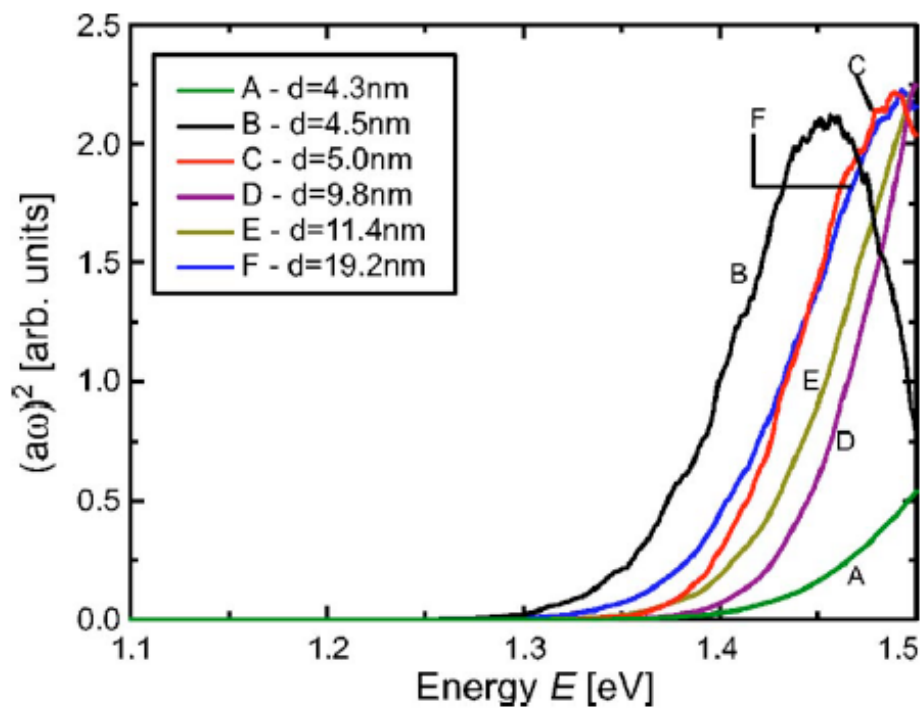


Figure 1. 4. Observed absorbance spectra of silicon nanoparticles.⁴

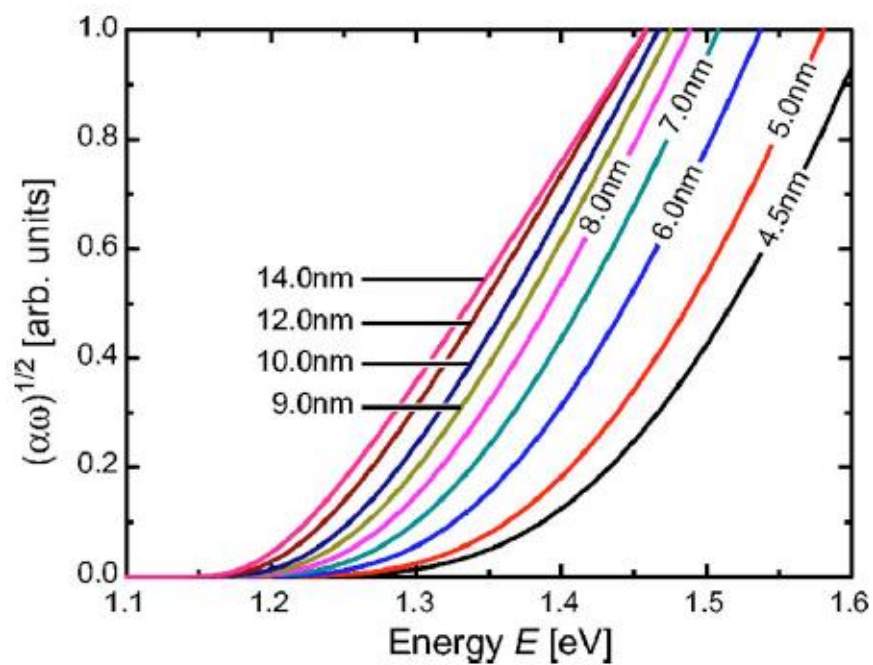


Figure 1.5 Calculated absorbance spectra of silicon nanoparticles.⁴

These results show indirect band gap character is observed with the experimental results as well as with the calculated results. A direct band gap character would have manifested itself as a linear fit of oscillator strength with decreasing nanoparticles size, which is not observed.⁴

While the luminescence is generally controlled by the quantum confinement effect, it is also influenced by surface defect states and by oxygen being present on the surface of the nanoparticle. There is still much discussion about the origin of the luminescence in many of the silicon nanoparticles that do not follow the effective mass approximation (EMA) of quantum confinement. Studies have shown that blue luminescence can arise from surface radiation recombination created by trapping on surface dimer sites or constrained relaxation on the surface in 1 nm silicon nanoparticles.¹⁶

Surface oxidation also plays a role in the luminescence energy of the nanoparticles. *Hua et al.* showed that by oxidizing the surface of silicon nanoparticles, yellow emitting silicon nanoparticles would become blue emitting nanoparticles as shown in Figure 1.6.¹⁷

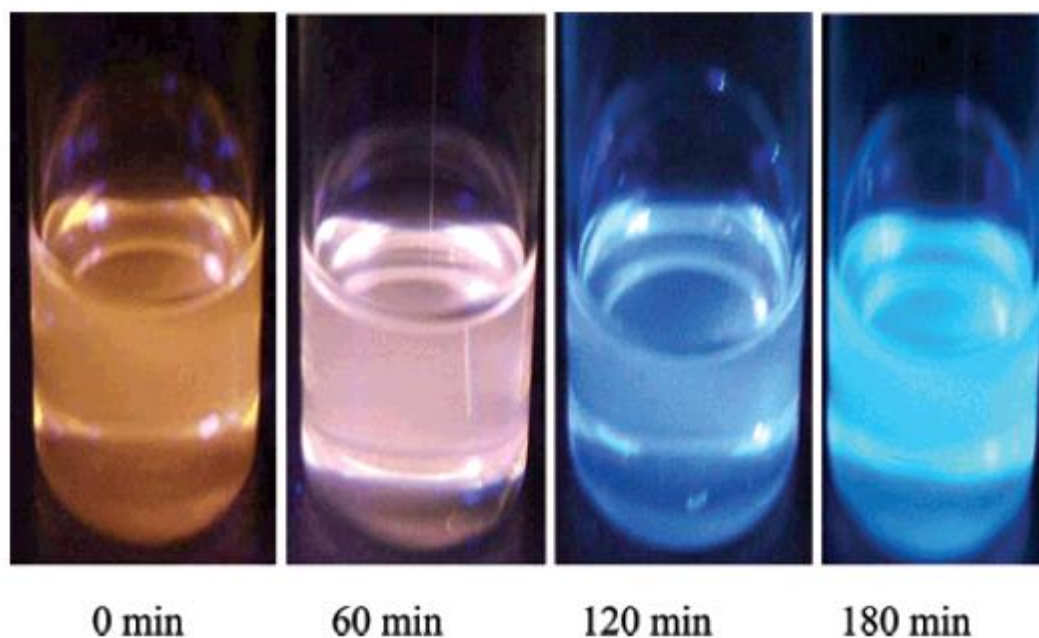


Figure 1. 6. Photographs showing photoluminescence from styrene grafted silicon nanoparticles after different periods of time under 254 nm UV illumination. For the photographs, the particles were illuminated with a 355 nm handheld UV lamp.

Some nanoparticle syntheses only report blue emitting silicon nanocrystals. *Heintz et al.* reported silicon nanoparticles with a variety of surface coverages including Si-O and Si-C passivation of the surface, yet only observed blue luminescence (Figure 1.7).⁵

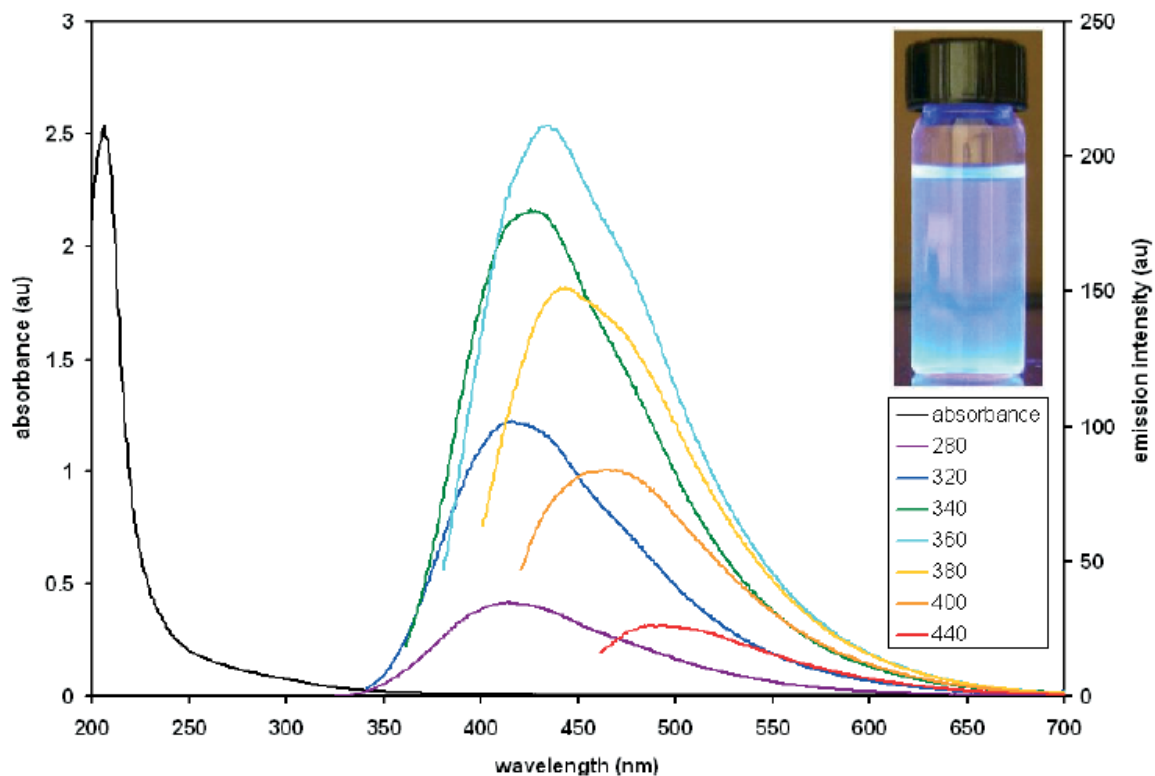


Figure 1.7. UV-Vis absorbance (left axis) and uncorrected emission spectra observed at various excitation wavelengths (right axis) of alkenyl passivated silicon nanoparticles produced by milling in 1-octyne for 24 hours (inset: photograph of the PL of the nanoparticles).⁵

The origin of luminescence in silicon nanoparticles is still a field of interest and controversy. Depending on the method of synthesis, different photoluminescence may be obtained. Due to this, a more complete understanding of the origins of luminescence in silicon nanoparticles is still needed.

Section 1.5: Methods of Silicon nanoparticle synthesis

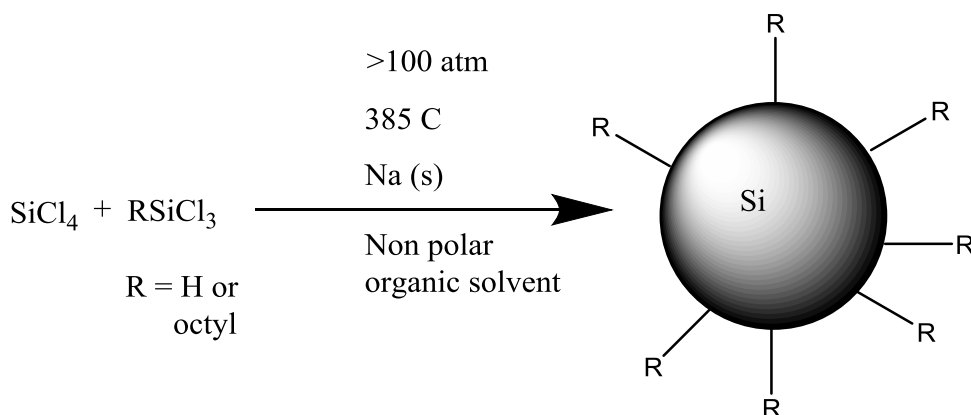
Numerous methods have been implemented for the synthesis of silicon nanoparticles. These methods of synthesis can generally be broken down to either: top down or bottom up methods. Top down methods are characterized as methods in which bulk silicon is the starting point and it is reduced to the nanometer size regime. Bottom up methods are when molecular precursors are reacted to form larger nanometer sized particles.

Section 1.5.1: Bottom up methods

Bottom up methods start with molecular silicon precursors which are reacted to form nanoparticles, resulting in silicon nanoparticles that are capped with hydrogen or halides. Silicon nanoparticles generally require protection from oxygen to prevent the particle from being oxidized and therefore quenching the luminescence. Usually a further chemical step is needed to protect the surface, such as a hydrosilation reaction for hydrogen terminated surfaces, or nucleophile displacement with polar organometallics for halide surfaces. The surfaces are therefore stabilized by strong Si-C bonds.

Reduction of Silanes

The first method of producing silicon nanoparticles was reported by *Heath*.¹⁸ A liquid-solution phase reaction was used to synthesize nanoparticles in the submicron range. A schematic of the reaction is shown below in Scheme 1.1.

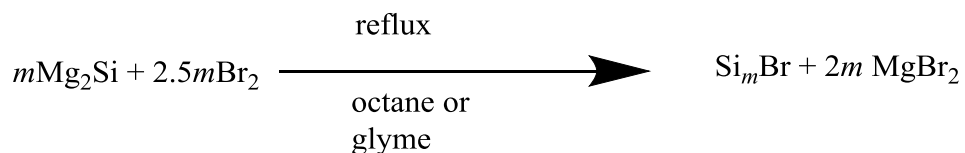


Scheme 1.1. Synthesis of silicon nanoparticles by *Heath*.

This synthesis was performed in a bomb reactor due to the high temperatures and pressures that were required. The results of the reaction were silicon nanoparticles of 5-3000 nm for R = H. For reactions using R = octyl the result was nanoparticles of size 5.5 ± 2.5 nm. In both cases, hexagonal shaped silicon crystals were obtained.

Oxidation and reduction methods to form silicon nanoparticles

Kauzlaurich et al. have developed several methods of preparing silicon nanoparticles from metal silicides involving metathesis reactions using Zintl salts. One approach is the oxidation of magnesium silicide with bromine, as shown in Scheme 1.2.¹⁹



Scheme 1.2. Synthesis of silicon nanoparticles by the oxidation of magnesium silicide.

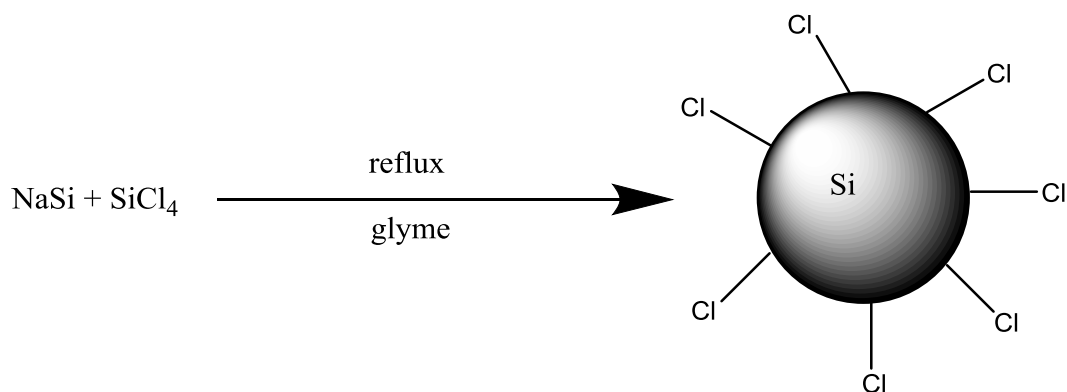
The size of the silicon nanoparticles synthesized by this method is controlled by the stoichiometry. The yield of the reaction was 10.9% in octane and 41.8% when performed in glyme. As the product is a bromine capped particle, further reactions with alkyl lithium reagents were needed to passivate the surface.

Another method used by the Kauzlarich group is the oxidation of Zintl salts as shown in Scheme 1.3. This reaction is carried out in dimethoxyethane (DME) at 80° C or in dioctyl ether (DOE) at 260°C. This method also requires a further reaction step with an alkyl lithium reagent for the passivation of the surface of the nanoparticle. This method results in sizes of 4.91 ± 1.23 nm for DME reaction and sizes of 3.85 ± 1.03 nm for the reaction carried out in DOE.



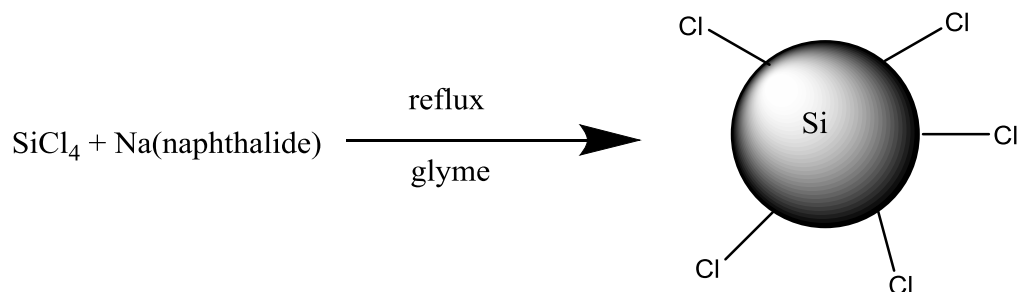
Scheme 1.3. Oxidation of Zintl salt synthesis of silicon nanoparticles.²⁰

Another reaction employed by the Kauzlarich group is the reduction of silicon tetrachloride with the Zintl salt, sodium silicide as shown in Scheme 1.4. This method produces small silicon nanocrystals along with larger amorphous silicon nanoparticles.²¹ As with the previous method, the nanoparticle must undergo a further reaction with an alkyl lithium reagent to passivate the surface and protect it from oxidation.



Scheme 1.4 Synthesis of silicon nanoparticles by reduction of SiCl_4 using the Zintl Salt NaSi .

The reduction of silicon tetrachloride can also be accomplished with sodium naphthalide, as shown in Scheme 1.5.



Scheme 1.5. Reduction of Silicon tetrachloride by sodium naphthalide to synthesis silicon nanoparticles.²²

As with the other reactions, this also requires a further reaction step with an alkyl lithium reagent or silanization reagent to passivate the surface to protect from oxidation. The average size of this reaction yields particles of 4.51 ± 1.10 nm when reacted for 12 hours.

The Zintl salt metathesis route offers a way to produce monodisperse samples with good control over the surface termination. However, a further step is needed to passivate the

nanoparticles to protect them from oxidation. One other positive aspect of this method is the ability to dope the silicon nanoparticles, shown in Scheme 1.6.



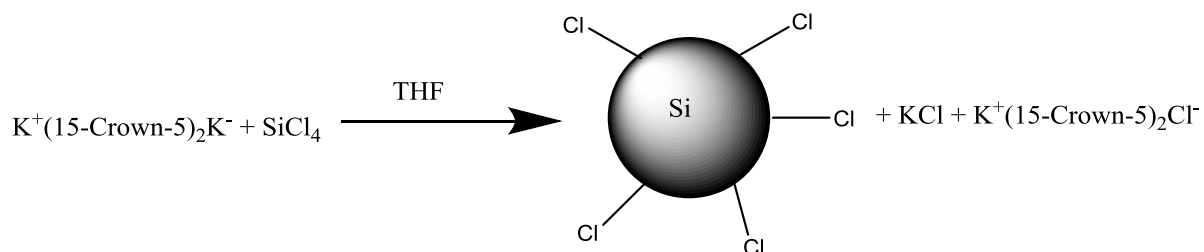
Scheme 1. 6. Synthesis of Mn doped silicon nanoparticles.²³

The addition of the manganese dopant allows the silicon nanoparticles to be used as an MRI imaging agent. Elemental analysis showed that the nanoparticles were within experimental error the same composition as the starting reagents, meaning that control of the level of doping had been achieved. Comparison of photoluminescence spectra of the un-doped silicon nanoparticles prepared in the same manner v. the doped silicon nanoparticles showed an obvious red shift from an emission maxima of 430 nm to 520 nm.

Silicon nanoparticles were also developed in the same manner using iron as the dopant. Similar results were seen, though higher levels of doping were observed to quench the photoluminescence of the nanoparticles. Through the use of dopants, bimodal imaging particles are easily synthesized which are of great interest due to their increased functionality. (These increased functionalities will be discussed in the applications section.)

Reduction of SiCl₄ using crown ether

Sletnes et al. have developed a method for the synthesis of silicon nanoparticles using potassium complexes with a crown ether as the reducing agent. This is shown in scheme 1.7.



Scheme 1.7. Synthesis of silicon nanoparticles using potassium and the transfer agent, crown ether, to reduce silicon tetrachloride.

Size distribution of 3-7 nm was found by this method. The controlling factor in the size of the silicon nanoparticles was the concentration of SiCl₄ that was present in the reaction. The particles showed a blue-green luminescence that was attributed to surface defect states rather than from the EMA.²⁴

Synthesis of silicon nanoparticles by sonochemical approach.

A novel method of producing silicon nanoparticles was discovered by *Dhas* et al. This method involves the use of sonication to create silicon nanoparticles. It has been found that within the collapsing bubble formed by sonication, temperatures can reach 5000°K with

pressures of 1800 atm.²⁵ The reduction of silicon to form silicon nanoparticles is shown in scheme 1.8.



Scheme 1.8. Synthesis of silicon nanoparticles by sonochemical approach.

The yield reported for this process is $70 \pm 5\%$ after a reaction time of 3 hours. The reported size of the nanoparticles was of the range from 2 nm to 5 nm. This process has the advantages of this method are reduced reaction time, reduced temperatures (-70°C), and high yield.

Synthesis of silicon nanoparticles in inverse micelles

Wilcoxon et al. have reported a method of synthesizing silicon nanoparticles using inverse micelles.²⁶⁻²⁷ A micelle, composed of nonionic aliphatic polyethers, of 10 nm diameter is formed in a hydrophobic solvent such as octane. The interior of the micelle is hydrophilic in nature and as such salts can be solvated by the hydrophilic portion of the micelle. This allows for the anhydrous salts SiX_4 ($X = \text{Cl}, \text{Br}, \text{or I}$) to dissolve without any water present, or else the product would be silica. The reduction of the silicon tetrahalide is performed by reaction with LiAlH_4 in dry THF. The cluster size of the nanoparticles is controlled by the controlling the micelle size and the reaction stoichiometry.²⁶ The nanoparticle products are hydrogen terminated and need addition reactions to hydrosilate. However, due to the experimental set up, purification is not trivial.

Tilley et al. also report synthesis of silicon nanoparticles using reverse micelle methods.²⁸ The surfactant used is tetraoctyl ammonium bromide (TOAB) in anhydrous toluene or pentaethylene glycol monododecyl ether (C12E5) in anhydrous hexane. Again the exclusion of water is absolutely necessary for the formation of silicon nanoparticles and not silica. Silicon tetrachloride is reduced by hydride reducing agents such as LiAlH_4 in dry THF. After the reaction is completed, the surface of the silicon nanoparticles are hydrogen terminated. The particles are then hydrosilated catalytically using H_2PtCl_6 and reacting with 1-heptene or allylamine.²⁸ This method yields particles with uniform sizes that have been reported between $1\text{-}4\text{ nm} \pm 0.2\text{nm}$. The nanoparticles exhibit a blue luminescence for all sizes synthesized, as has been seen with other methods of silicon nanoparticle synthesis.

Supercritical fluid synthesis of silicon nanoparticles.

Korgel et al. have shown that they are able to produce monodisperse populations of silicon nanoparticles using supercritical fluids.¹² Korgel applies the same wet chemistry approaches (thermal degradation of precursors) that have been so successful with group II-VI semiconductors. However, the temperatures needed to be reached are above the boiling points of the capping ligands used for silicon nanoparticles. To solve this problem, Korgel has designed a pressure reactor system which allows him to heat and pressurize the solvents above their critical point (Figure 1.8). This allows the silicon precursors to reach the temperature needed for their degradation, while also keeping the particles solvated.^{12, 29}

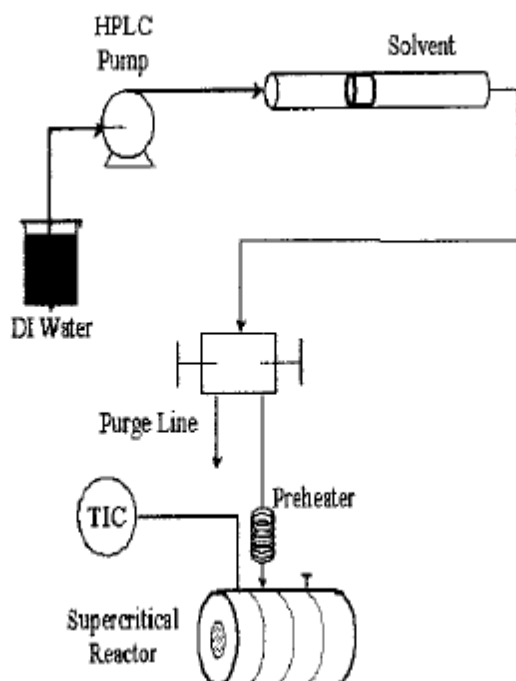


Figure 1.8. Korgel's supercritical reactor. An HPLC pump is used to reach the high pressures needed.¹²

Diphenylsilane is degraded in the reactor in the presence of octanol and hexane. The reaction is done at a temperature of 500°C and a pressure of 345 bar. This is well above the critical points of octanol and hexane: octanol: T_c : 385 °C, P_c : 34.5 bar; hexane: T_c : 235 °C, P_c : 30 bar.¹² The pressure is achieved by using a HPLC pump to pump the solvent into the Inconel high pressure cell. The cell is then wrapped in heat tape and is heated to 500°C to create the supercritical fluid reactor.

This method is advantageous as this process caps the nanoparticles as the nanoparticles are synthesized, requiring no further reaction steps. This results in the size distribution of the nanoparticles being very monodisperse. However, the yield of the reaction varies 0.5% to 5% for the incorporation of silane precursor into silicon nanoparticle.

Analysis of the photoluminescence of these particles shows there is some size dependent shift in the luminescence. However, there is an indirect bandgap transition even for the particles which are 1.4 nm in diameter. Also, observed was IR evidence for the capping (passivation) of the silicon surface with octanol, showing that the silicon is covalently bonded to the oxygen of the octanol. As stated before, the luminescence of the silicon nanoparticles is complex and not yet entirely understood.

Laser pyrolysis synthesis of silicon nanoparticles.

Swihart et al. have reported a laser pyrolysis method of producing silicon nanoparticles at high rates such as 200 mg/h.³⁰ The CO₂ laser apparatus needed to produce this nanoparticles is shown in Figure 1.9.

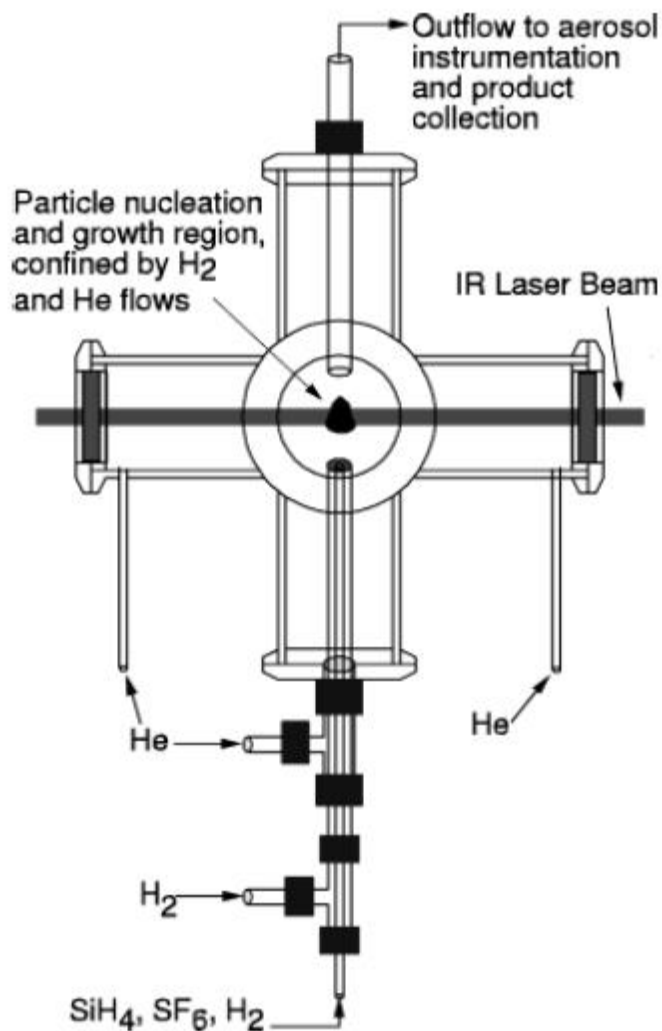


Figure 1.9. CO₂ laser apparatus for the synthesis of silicon nanoparticles by laser pyrolysis.

The laser pyrolysis method uses silane to decompose to silicon nanoparticles. The silane absorbs the laser and absorbs heat for the decomposition of the silane to silicon. The SF₆ and hydrogen is used to increase the heat at the nucleation site, promoting the decomposition of the silane. Helium is used as the carrier gas. The silicon nanoparticles are then collected on a grid from the gas stream. The nanoparticles are not luminescent at this point.

Laser pyrolysis produces gram sized quantities of silicon nanoparticles which are loosely agglomerated.³⁰⁻³¹ This method also shows good control of ability to control particle

size and particle size distribution. These particles are etched with HF acid to further diminish their size and to increase their luminescence. The particles when first synthesized, show little luminescence due to the size being larger than 5 nm. However, after etching the particles in HF/HNO₃, bright luminescence is observed.^{30, 32} This etching can also be done by allowing the nanoparticles to be exposed to air and form an oxide layer, the layer can then be removed by HF etching, allowing control of the size of the nanoparticles.^{17, 33}

Section 1.5.2: Top down methods of synthesizing silicon nanoparticles.

Canham et al. first reported luminescence silicon made from etching of silicon wafers in 1990.³⁴ This discovery has led to decades of research into porous silicon.

Electrochemical etching synthesis of silicon nanoparticles.

Nayfeh et al. have developed a process of preparing small (1 nm) silicon nanoparticles using a catalyzed electrochemical process.^{16, 35} They use a combination of HF acid and H₂O₂ to etch the wafers. The hydrogen peroxide forms an oxide layer with the silicon which the HF acid can easily remove.³⁶⁻³⁷

Sailor et al. has prepared colloidal solutions of silicon nanoparticles by electrochemical etching of silicon wafers with HF acid and ethanol.³⁸⁻³⁹ While the wafers are being etched sonication is used to aid in the decomposition of the silicon, allowing silicon nanoparticles to be released into solution.⁴⁰ The resultant nanoparticles, upon analysis with TEM were shown to be irregularly shaped and had a wide size distribution from many

micrometers to the nanometer range. The colloidal suspension showed red luminescence which was attributed to EMA (quantum confinement).⁴⁰

Kang *et al.* synthesized silicon nanoparticles and then etched them to create a series of nanoparticles whose photoluminescence spanned the visible spectrum.⁴¹

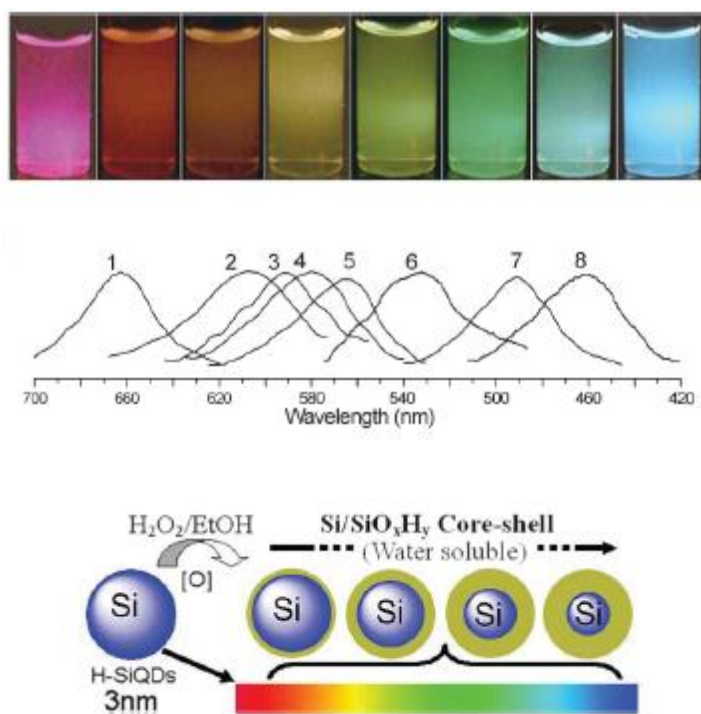


Figure 1.10. Silicon nanoparticles that have been etched to form an oxide layer and the resulting change in color of luminescence that corresponds to change in the size of the silicon nanoparticle.

Etching of silicon rich silicon oxides

Silicon nanoparticles can be synthesized by etching of silicon rich suboxide powder that contains silicon nanocrystals that are larger than 10 nm in diameter. The HF and HNO₃ acid rapidly attacks and dissolves silicon dioxide.⁴²⁻⁴³ This releases the silicon nanoparticles and also decreases their size as they are also etched. Decreasing their size below 5 nm leads to hydrogen terminated silicon nanoparticles that are luminescent.

Veinot *et al.* have synthesized silicon nanoparticles from annealing hydrogen silsesquioxane. The silicon nanocrystals that form during the thermal annealing process are contained in a matrix of SiO₂. The matrices are ground and etched using HF and ethanol/water.⁴⁴⁻⁴⁶ These nanoparticles can then be further etched to produce smaller nanoparticles, allowing a range of sizes to be obtained. The resultant nanoparticles are hydrogen terminated and need a further reaction step to passivate the surface. This has been done by both thermal hydrosilation and photohydrosilation.⁴⁷ This method, while being a top down method, shows luminescence which agrees with the EMA model.

Laser ablation

Laser ablation methods occur by focusing a laser on a silicon wafer and irradiating the surface. Laser ablation methods depend on the frequency of the laser. A femtosecond laser will produce silicon nanoparticles by means of heating the precursor material till it thermally expands, and then cools causing a contraction and fragmentation of the material.⁴⁸ A nanosecond frequency laser however, forms nanoparticles by a vapor condensation mechanism.⁴⁸ The size of the silicon nanoparticles produced vary based on experimental conditions. However, crystalline nanoparticles have been reported.⁴⁸⁻⁴⁹ These particles are not passivated and require further reactions to passivate the surface to stabilize the particles to oxidation.

Mechanochemical synthesis of silicon nanoparticles

High energy ball milling is a technique that has been used to form nanocomposite material.⁵⁰ Early experiments of ball milling of silicon powder showed results of crystalline silicon being converted to amorphous silicon due to the extreme temperatures reached during the ball milling.⁵¹⁻⁵² Silicon has also been ball milled with graphite in an attempt to synthesize carbon-silicon composite nanoparticles for the use of lithium ion batteries.⁵³

Heintz *et al.* reported colloidal silicon nanoparticles can be produced by high energy ball milling.⁵ This procedure is discussed more in depth in chapter 2. This method uses silicon wafers which are degraded by mechanical means of a ball mill while in the presence of a reactive organic liquid. This method has the advantage of being a one-step synthesis of the nanoparticles with passivation and this method has been shown to work with a great

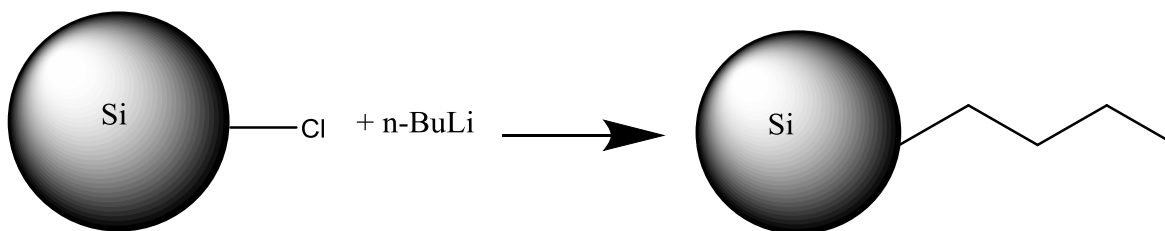
many organic ligands: alkynes, alkenes, aldehydes, carboxylic acids, and alcohols.^{5-6, 54-58}

These particles have also been shown to successfully act as a platform for the attachment of DNA.⁵⁹

Section 1.6: Functionalization of silicon nanoparticles

Most of the methods of synthesis of silicon nanoparticles results in a surface that is hydrogen or halide terminated. These surfaces if not further protected by passivation will be oxidized which leads to changes in the photoluminescence of the nanoparticles.⁶⁰⁻⁶² There are a few methods such as alkyl lithium reagents or hydrosilylation that have been employed depending on the surface termination.

Nanoparticles that are halide terminated have been passivated using alkyl lithium reagents such as n-butyl lithium.²¹



Scheme 1.9. Surface passivation of chloride terminated silicon nanoparticle by the alkyl lithium reagent butyllithium.

Another route for the passivation of halide terminated silicon nanoparticles is to react the particle with primary alcohols, resulting in alkoxy linkages. These linkages do introduce oxygen to the particle surface, but the covalent bond and alkyl chain length protect the silicon surface from further oxidation.^{12, 19}

As most chemical etching processes result in hydrogen terminated particles, hydrosilylation is a more common method of surface passivation and functionalization.⁶³ Hydrosilylation can occur in three separate methods. There is thermal hydrosilylation, photohydrosilylation, and catalytic hydrosilylation.⁶⁴

Thermal hydrosilylation has the advantage of shorter reaction times and less purification needed than catalytic hydrosilylation.⁶³ Catalytic hydrosilylation is very useful for inverse micelle synthesis of silicon nanoparticles, allowing for the nanoparticles to be passivated before being exposed to oxidation by air.²⁸ Other methods of hydrosilylation would require purification of the nanoparticles first, which would expose the nanoparticles to oxygen, leading to the need for an etching step to remove the oxide layer.

Photohydrosilylation is of particular interest due to its ease of use. It has also been extensively studied on flat silicon surfaces for use in the electronics industry.¹¹ The mechanism of hydrosilylation on a flat hydrogen terminated surface is shown in Figure 1.11.

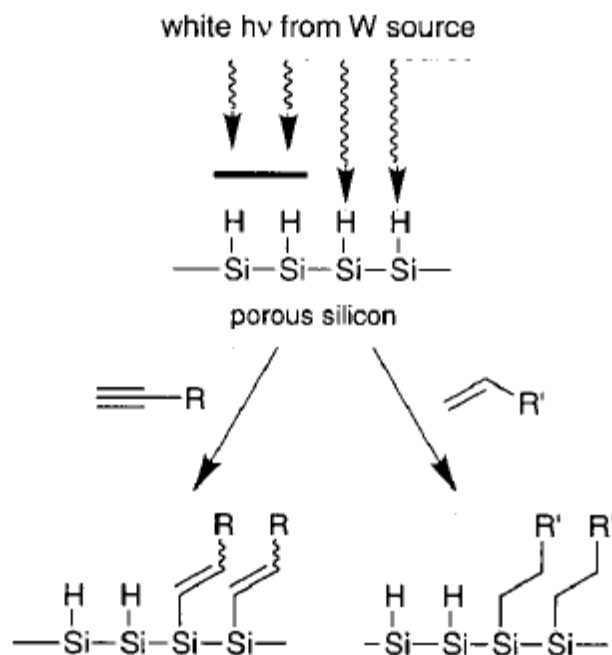


Figure 1.11. Hydrosilylation on hydrogen terminated bulk silicon (111) surface.⁶⁵

One possible mechanism for the hydrosilylation mechanism is the photo-assisted exciton mediated mechanism shown in Figure 1.12.

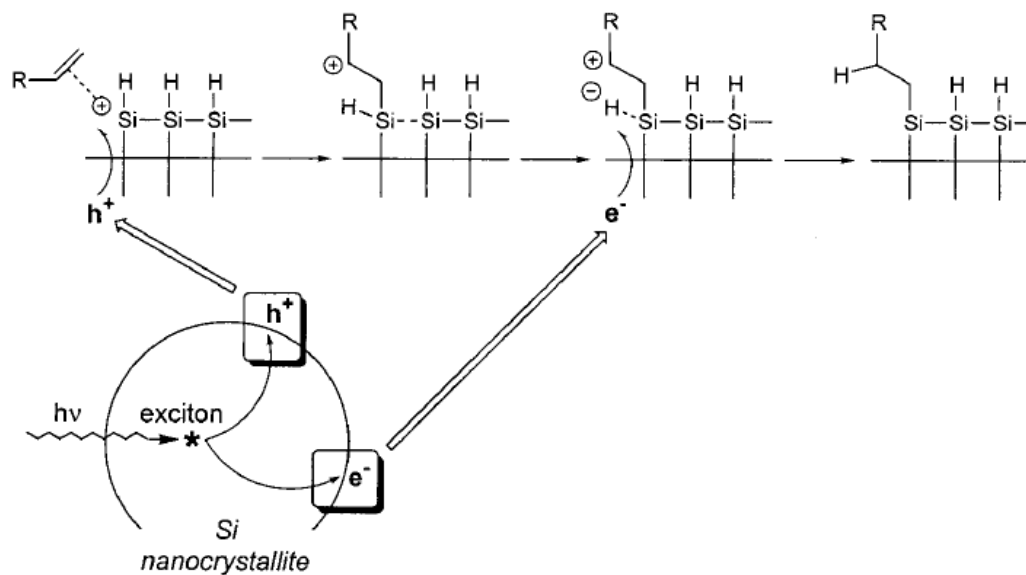


Figure 1.12. Exciton mediated photohydrosilylation on silicon nanoparticle surface.¹¹

Through this mechanism, white light is able to catalyze the hydrosilylation. Normal conditions call for a radical initiator or shorter wavelength light (254 nm) to drive the hydrosilylation.⁶⁶

Section 1.7: Applications of silicon nanoparticles

Silicon nanoparticles are of interest in an array of applications from electronic devices,⁶⁷⁻⁶⁸ photovoltaics,⁶⁹⁻⁷⁰ biomedical applications,⁷¹⁻⁷² and energy storage.⁷³⁻⁷⁵

Biomedical applications are especially important for silicon nanoparticles since previously used nanoparticles based on group II-VI semiconductors such as CdSe QD's have been shown to be toxic and as such are not suitable for *in vivo* experimentation.⁷⁶⁻⁷⁸ Silicon nanoparticles however show very little toxicity.¹⁰ Most toxicity shown in experiments with silicon nanoparticles can be attributed to surface chemistry, positive charges located on the surface tend to increase the toxicity of the particles.¹⁰ The size of the nanoparticles is also important since only nanoparticles < 5.5 nm can be successfully cleared by the kidneys.¹⁰ This however is not an obstacle for silicon nanoparticles as the particles of interest are those that are smaller than the Bohr exciton radius of about 5 nm, allowing them to be luminescent.

In order for silicon nanoparticles to be useful as biological agents there are some requirements that they first have to meet. First, they must be nontoxic. Second, they must be luminescent. Thirdly, they must be water soluble as this is the medium in which they will be dispersed for *in vivo* applications. Fourth, they must be able to be functionalized so that they can be tailored for specific purposes, such as targeting certain tissue or receptors.

Many experiments have been performed showing the use of silicon nanoparticles as bio-labeling platforms that are far superior to molecular dyes.

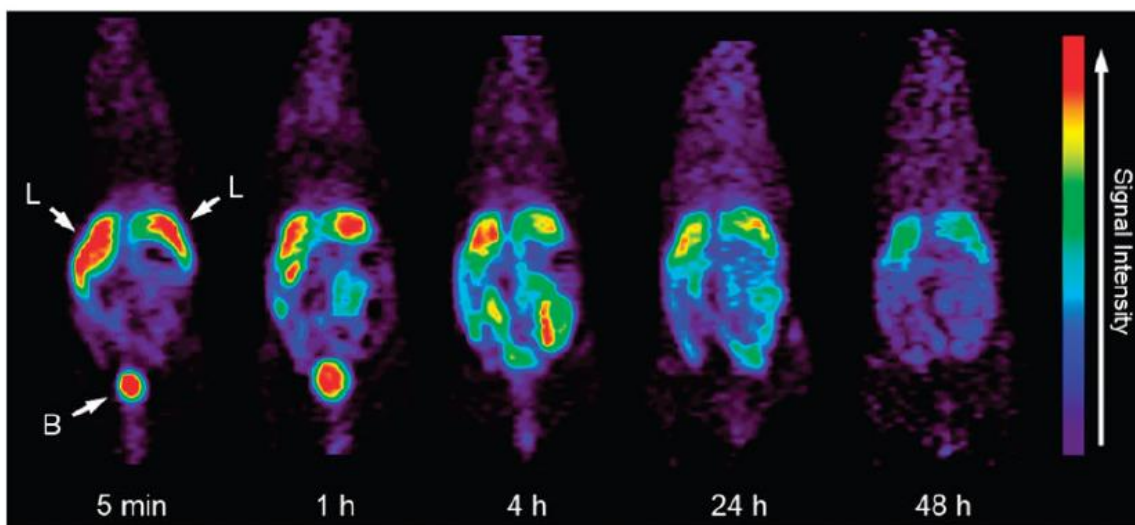


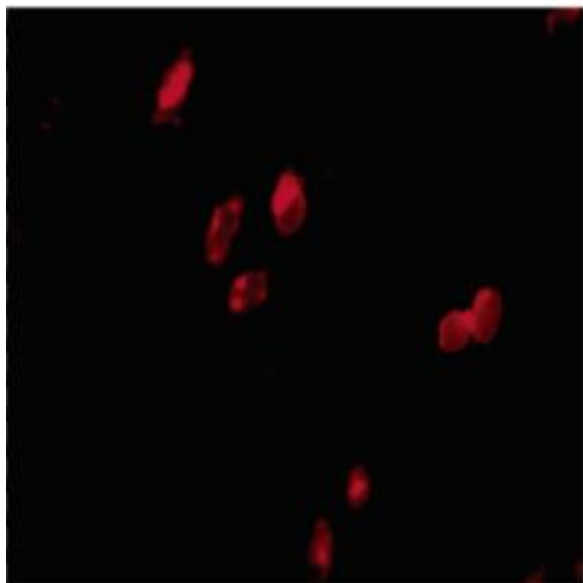
Figure 1.13. PET images of mice injected with silicon nanoparticles showing that they target the liver and are cleared by the kidneys as they are also observed in the bladder. Liver is denoted as L and the bladder is denoted as B in the figure.⁷⁹

In Figure 1.13 we see mice that have been injected with silicon nanoparticles that were coated with dextran and then complexed to a macrocyclic ligand with the radioisotope- $^{64}\text{Cu}^{2+}$. The average hydrodynamic diameter of the particles were 15.1 ± 7.6 nm. As can be seen from the figure, most of the nanoparticles are rapidly filtered from the blood stream very quickly. They are quickly filtered through the kidney and eliminated through the bladder. After just 1 hour, most of the nanoparticles had already been removed and after 48 hours, only low concentration were only detected in the liver.

Another study used poly acrylic acid to increase the water solubility of the silicon nanoparticles. In this study, 3-5 nm silicon nanoparticles were passivated by poly acrylic acid. Using a hydrosilation reaction, the acrylic acid was covalently linked to the silicon

surface. This passivating ligand increased both the water solubility and also the luminescence of the nanoparticles.⁸⁰ Chinese hamster ovary cell tissue was then stained using the silicon nanoparticles.

A)



B)

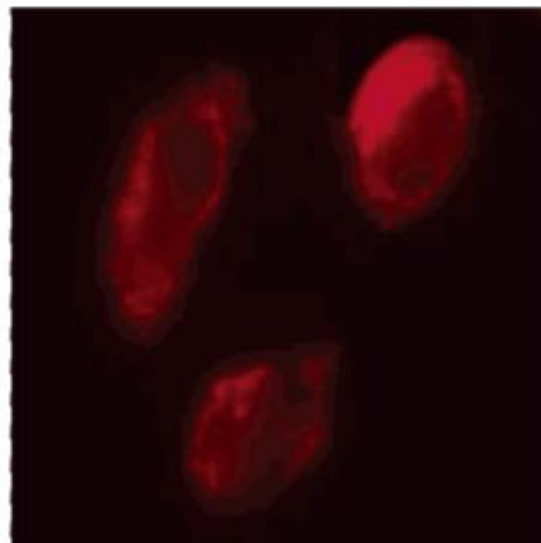


Figure 1.14. CHO cells stained using Poly acrylic acid passivated silicon nanoparticles. (B is a higher magnification of A)⁸⁰

These results show that silicon nanoparticles can be synthesized that are water soluble, stable, and luminescent quantum yields necessary for use as a biolabel. Also, these results show once again that the use of QD's is superior to molecular dyes as there is no issue with photo bleaching as seen with some molecular dyes.

Another example of the use of amine terminated silicon nanoparticles as bioimaging labels is seen in the imaging of BV2 cells undergoing mitosis. In this study the cells were suspended in a phosphate buffer and mixed with the nanoparticles in a 1:1 ratio. The cells were then separated by centrifugation.

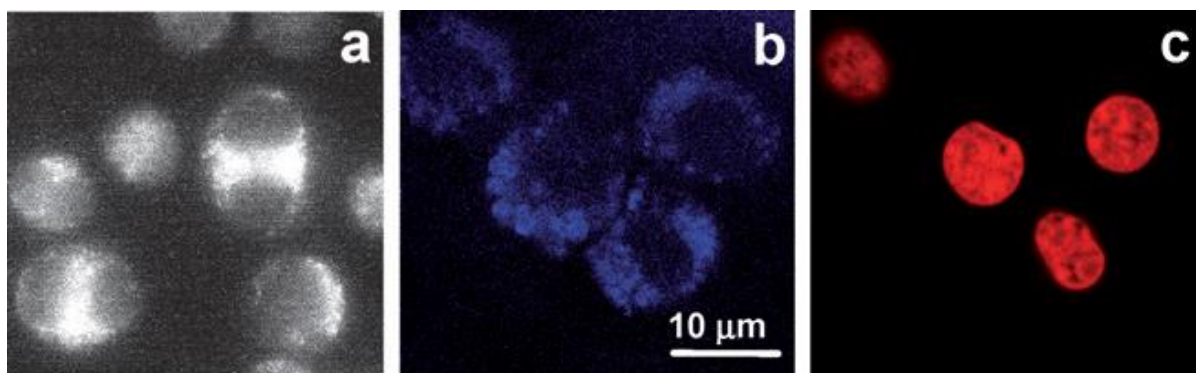


Figure 1.15. Epifluorescence image of BV2 cells stained with a) DRAQ5, b) silicon nanoparticles, c) confocal image of both DRAQ5 and silicon nanoparticles.⁸¹

The most interesting thing about this study is that it showed that multiple generations of cells could be followed without having to apply additional stain to the samples. Due to the stability of the nanoparticles to photobleaching, the nanoparticles were useful as labels in several generations of daughter cells that formed during mitosis.⁸¹

Another issue with nanoparticles for biological application is the outcome of nanoparticles that do not get cleared from the organism by way of renal filtering. Sailor *et al.* have reported biodegradable silicon nanoparticles that will break down in the organism if they are not cleared.

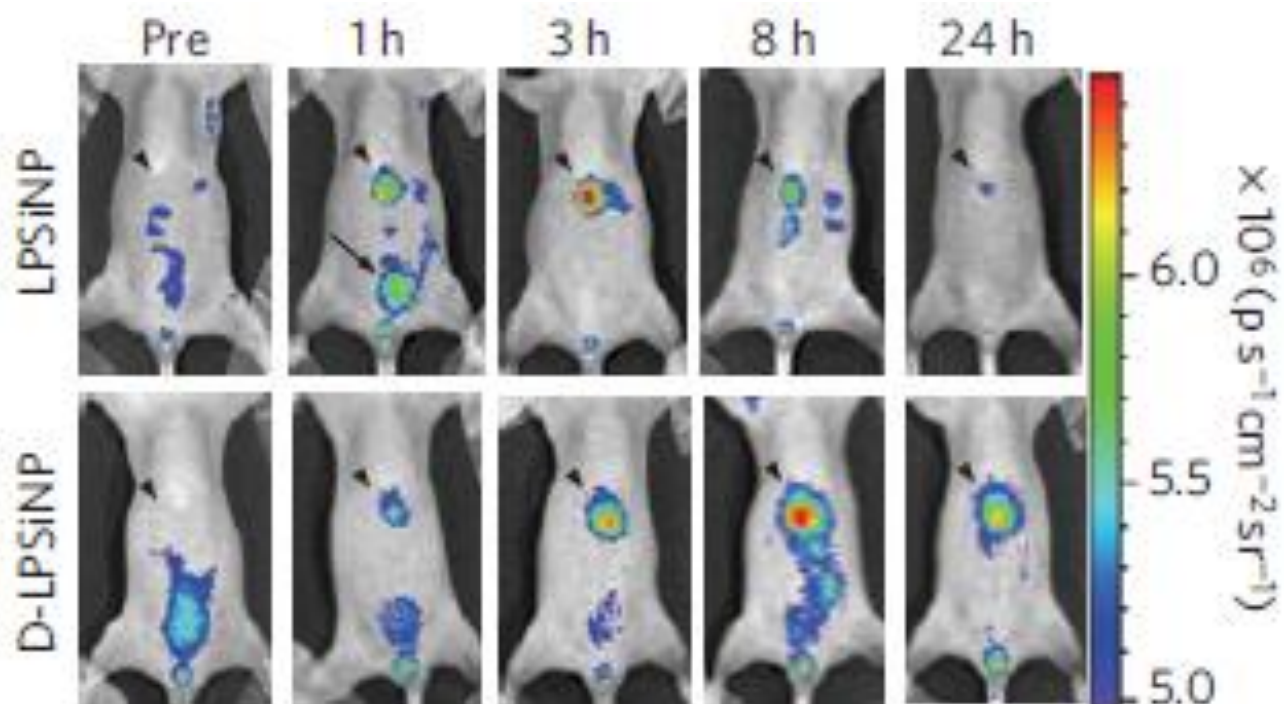


Figure 1.16. *In vivo* fluorescence imaging (370 and 488 nm excitation) of mice injected with silicon nanoparticles (LPSiNP) and dextran coated silicon nanoparticles (D-LPSiNP). Arrows point to liver and bladder.⁸²

As can be seen in Figure 1.16 the silicon nanoparticles are broken down over the 24 hours that the mice were monitored. The dextran coated silicon nanoparticles break down at a much slower rate. As silicon nanoparticles are oxidized in an organism, their oxidized silicon core will safely biodegrade to silica and be excreted. The only issue is the surface coverage of the silicon nanoparticles as noted before.

Silicon nanoparticles can also be functionalized with targeting molecules that are covalently bound to the silicon nanoparticles. This allows the particles to be tuned to reach

specific targets in a host.⁸³⁻⁸⁴ Unspecific silicon nanoparticles are mainly bound by their size as to what locations they travel to in the host. This is normally the liver and then excretion by the renal glands as seen in figures 1.13 and 1.16

One of the ways in which to accomplish this targeting functionalization is to attach DNA to the silicon nanoparticle.⁸⁵⁻⁸⁷ This is easily done by activation of a terminal carboxylic acid on a silicon nanoparticle.⁸⁸⁻⁸⁹ This activation is accomplished by attaching a molecule such as n-hydroxysuccinimide which acts as a better leaving group, promoting the formation of an amide bond with an amine functionalized biomolecule.⁹⁰

Future uses of Silicon nanoparticles in energy

One of the newest fields of interest for silicon nanoparticles and silicon wires, is the field of lithium ion batteries. Current technology uses graphite for anode material. However, the volume change cycles of being swelled with lithium ions when charged, and the subsequent shrinking when the battery is depleted leads to mechanic stress on the anode material.⁹¹ Silicon nanoparticles have been proposed as an anodic material due to their ability to swell easily without large mechanical stress due to their small volume. However, they still do experience mechanical stress and do break down, which reduces the effectiveness of the battery, through loss of conductive contact from mechanical stress failure.⁹² It has been hypothesized that supporting silicon nanoparticles using a cheap, conductive, and strong material like graphene in conjunction with silicon nanoparticles might lead to increased cycling of lithium ion batteries.⁹² These same ideas are also the focus of silicon nanowires,

which are of similar research focus as silicon nanowires, as they many similar properties due to being in the nano size regime.^{29, 93}

Motivation for thesis

The use of silicon nanoparticles for use in bioimaging applications has been shown throughout the literature to be a very promising field. To contribute to this field, the use of carboxylic acid functionalized nanoparticles which are able to easily be conjugated to biomolecules is a major focus of this thesis. This thesis also is focused on increasing the luminescence of the nanoparticles as well and seeking new ways using the instrumentation available to us to better characterize the silicon nanoparticles that we synthesize.

To synthesize carboxylic acid functionalized silicon nanoparticles we first attempt a passivation of silicon nanoparticles using carboxylic acids. This is then followed by the use of α - ω dicarboxylic acids. However, as shown in Chapter 2, the solubility of the diacids due (due to hydrogen bonding forming oligomers) are not easily dissolved in the mono carboxylic acids. Because of this barrier, a new route to carboxylic acid functionalized silicon nanoparticles was sought. The use of alkene passivated silicon nanoparticles with terminal vinyl groups distal to the silicon surface were synthesized. The oxidation of the terminal vinyl groups provided us with the carboxylic acid functionalized silicon nanoparticles.

The carboxylic acid functionalized silicon nanoparticles were then conjugated to DNA sequences in a proof of concept experiment, to show that these silicon nanoparticles can be covalently conjugated to biomolecules. This was done through the activation of the

carboxylic acid using n-hydroxysuccinimide to form ester activated silicon functionalized nanoparticles. The n-hydroxysuccinimide acts as a better leaving group than the proton which promotes the rate of the reaction. This was characterized using TEM and gel electrophoresis.

Another focus of this thesis is to better characterize the silicon nanoparticles that we synthesized. As this is a top down method, the size and of the chemistry on the surface is not as controllable as silicon nanoparticles formed by the bottom up methods mentioned previously. To characterize the silicon nanoparticles we used x-ray absorption near edge spectroscopy (XANES). To analyze our results modeled the silicon nanoparticles and used the FEFF9 software package to obtain theoretical XANES spectra. Also, x-ray photoelectron spectroscopy (XPS) was used to investigate the bonds in the silicon nanoparticles.

One of the main focuses throughout every stage of these projects is to observe the influence of these reactions on the luminescence of the silicon nanoparticles. Since one of the envisioned applications for these nanoparticles is bioimaging, the luminescence is of great importance. To increase the luminescence, the complete passivation of the silicon surface of the nanoparticles was attempted through a post processing step of hydrosilation. This step is mean to passivate any Si-H that is on the surface as well as to react with any dangling bonds that are remaining from the fractured silicon nanoparticle surface due to the milling process.

The results of these reactions and investigations are reported hereafter. The carboxylic acid functionalized silicon nanoparticles have been synthesized and conjugated to DNA. The nanoparticles have been further characterized by XANES and XPS. Also, the results of further hydrosilation to increase the photoluminescence of the nanoparticles is show.

References

1. Dasog, M.; Yang, Z.; Regli, S.; Atkins, T. M.; Faramus, A.; Singh, M. P.; Muthuswamy, E.; Kauzlarich, S. M.; Tilley, R. D.; Veinot, J. G. C., Chemical Insight into the Origin of Red and Blue Photoluminescence Arising from Freestanding Silicon Nanocrystals. *ACS Nano* **2013**, *7* (3), 2676-2685.
2. Manhat, B. A.; Brown, A. L.; Black, L. A.; Ross, J. B. A.; Fichter, K.; Vu, T.; Richman, E.; Goforth, A. M., One-Step Melt Synthesis of Water-Soluble, Photoluminescent, Surface-Oxidized Silicon Nanoparticles for Cellular Imaging Applications. *Chemistry of Materials* **2011**, *23* (9), 2407-2418.
3. O'Farrell, N.; Houlton, A.; Horrocks, B. R., Silicon nanoparticles: applications in cell biology and medicine. *International Journal of Nanomedicine* **2006**, *1* (4), 451-472.
4. Meier, C.; Gondorf, A.; Lüttjohann, S.; Lorke, A.; Wiggers, H., Silicon nanoparticles: Absorption, emission, and the nature of the electronic bandgap. *Journal of Applied Physics* **2007**, *101* (10), 103112.
5. Heintz, A. S.; Fink, M. J.; Mitchell, B. S., Mechanochemical Synthesis of Blue Luminescent Alkyl/Alkenyl-Passivated Silicon Nanoparticles. *Advanced Materials* **2007**, *19* (22), 3984-3988.
6. Heintz, A. S.; Fink, M. J.; Mitchell, B. S., Silicon nanoparticles with chemically tailored surfaces. *Applied Organometallic Chemistry* **2010**, *24* (3), 236-240.
7. Reed, M. A.; Randall, J. N.; Aggarwal, R. J.; Matyi, R. J.; Moore, T. M.; Wetsel, A. E., Observation of discrete electronic states in a zero-dimensional semiconductor nanostructure. *Physical Review Letters* **1988**, *60* (6), 535-537.
8. Chan, W. C. W.; Maxwell, D. J.; Gao, X.; Bailey, R. E.; Han, M.; Nie, S., Luminescent quantum dots for multiplexed biological detection and imaging. *Current Opinion in Biotechnology* **2002**, *13* (1), 40-46.
9. Barroso, M. M., Quantum Dots in Cell Biology. *Journal of Histochemistry and Cytochemistry* **2011**, *59* (3), 237-251.
10. Bhattacharjee, S.; Rietjens, I. M. C. M.; Singh, M. P.; Atkins, T. M.; Purkait, T. K.; Xu, Z.; Regli, S.; Shukaliak, A.; Clark, R. J.; Mitchell, B. S.; Alink, G. M.; Marcelis, A. T. M.; Fink, M. J.; Veinot, J. G. C.; Kauzlarich, S. M.; Zuilhof, H., Cytotoxicity of surface-functionalized silicon and germanium nanoparticles: the dominant role of surface charges. *Nanoscale* **2013**, *5* (11), 4870-4883.
11. Buriak, J. M., Organometallic Chemistry on Silicon and Germanium Surfaces. *Chemical Reviews* **2002**, *102* (5), 1271-1308.
12. Holmes, J. D.; Ziegler, K. J.; Doty, R. C.; Pell, L. E.; Johnston, K. P.; Korgel, B. A., Highly Luminescent Silicon Nanocrystals with Discrete Optical Transitions. *Journal of the American Chemical Society* **2001**, *123* (16), 3743-3748.

13. Kocevski, V.; Eriksson, O.; Ruzs, J., Transition between direct and indirect band gap in silicon nanocrystals. *Physical Review B* **2013**, *87* (24), 245401.
14. Llansola Portolés, M. J.; Rodriguez Nieto, F.; Soria, D. B.; Amalvy, J. I.; Peruzzo, P. J.; Mártire, D. O.; Kotler, M.; Holub, O.; Gonzalez, M. C., Photophysical Properties of Blue-Emitting Silicon Nanoparticles. *The Journal of Physical Chemistry C* **2009**, *113* (31), 13694-13702.
15. Llansola Portolés, M. J.; Pis Diez, R.; Dell'Arciprete, M. L.; Caregnato, P.; Romero, J. J.; Mártire, D. O.; Azzaroni, O.; Ceolín, M.; Gonzalez, M. C., Understanding the Parameters Affecting the Photoluminescence of Silicon Nanoparticles. *The Journal of Physical Chemistry C* **2012**, *116* (20), 11315-11325.
16. Rao, S.; Mantey, K.; Therrien, J.; Smith, A.; Nayfeh, M., Molecular behavior in the vibronic and excitonic properties of hydrogenated silicon nanoparticles. *Physical Review B* **2007**, *76* (15), 155316.
17. Hua, F.; Erogbogbo, F.; Swihart, M. T.; Ruckenstein, E., Organically Capped Silicon Nanoparticles with Blue Photoluminescence Prepared by Hydrosilylation Followed by Oxidation. *Langmuir* **2006**, *22* (9), 4363-4370.
18. Heath, J. R., A Liquid-Solution-Phase Synthesis of Crystalline Silicon. *Science* **1992**, *258* (5085), 1131-1133.
19. Pettigrew, K. A.; Liu, Q.; Power, P. P.; Kauzlarich, S. M., Solution Synthesis of Alkyl- and Alkyl/Alkoxy-Capped Silicon Nanoparticles via Oxidation of Mg₂Si. *Chemistry of Materials* **2003**, *15* (21), 4005-4011.
20. Neiner, D.; Chiu, H. W.; Kauzlarich, S. M., Low-Temperature Solution Route to Macroscopic Amounts of Hydrogen Terminated Silicon Nanoparticles. *Journal of the American Chemical Society* **2006**, *128* (34), 11016-11017.
21. Mayeri, D.; Phillips, B. L.; Augustine, M. P.; Kauzlarich, S. M., NMR Study of the Synthesis of Alkyl-Terminated Silicon Nanoparticles from the Reaction of SiCl₄ with the Zintl Salt, NaSi. *Chemistry of Materials* **2001**, *13* (3), 765-770.
22. Zou, J.; Baldwin, R. K.; Pettigrew, K. A.; Kauzlarich, S. M., Solution Synthesis of Ultrastable Luminescent Siloxane-Coated Silicon Nanoparticles. *Nano Letters* **2004**, *4* (7), 1181-1186.
23. Zhang, X.; Brynda, M.; Britt, R. D.; Carroll, E. C.; Larsen, D. S.; Louie, A. Y.; Kauzlarich, S. M., Synthesis and Characterization of Manganese-Doped Silicon Nanoparticles: Bifunctional Paramagnetic-Optical Nanomaterial. *Journal of the American Chemical Society* **2007**, *129* (35), 10668-10669.
24. Sletnes, M.; Maria, J.; Grande, T.; Lindgren, M.; Einarsrud, M. A., Octoxy capped Si nanoparticles synthesized by homogeneous reduction of SiCl₄ with crown ether alkalide. *Dalton Transactions* **2014**, *43* (5), 2127-2133.
25. Arul Dhas, N.; Raj, C. P.; Gedanken, A., Preparation of Luminescent Silicon Nanoparticles: A Novel Sonochemical Approach. *Chemistry of Materials* **1998**, *10* (11), 3278-3281.

26. Wilcoxon, J. P.; Samara, G. A., Tailorable, visible light emission from silicon nanocrystals. *Applied Physics Letters* **1999**, *74* (21), 3164.
27. Wilcoxon, J. P.; Samara, G. A.; Provencio, P. N., Optical and electronic properties of Si nanoclusters synthesized in inverse micelles. *Physical Review B* **1999**, *60* (4), 2704-2714.
28. Tilley, R. D.; Yamamoto, K., The Microemulsion Synthesis of Hydrophobic and Hydrophilic Silicon Nanocrystals. *Advanced Materials* **2006**, *18* (15), 2053-2056.
29. Chan, C. K.; Patel, R. N.; O'Connell, M. J.; Korgel, B. A.; Cui, Y., Solution-Grown Silicon Nanowires for Lithium-Ion Battery Anodes. *ACS Nano* **2010**, *4* (3), 1443-1450.
30. Li, X.; He, Y.; Talukdar, S. S.; Swihart, M. T., Process for Preparing Macroscopic Quantities of Brightly Photoluminescent Silicon Nanoparticles with Emission Spanning the Visible Spectrum. *Langmuir* **2003**, *19* (20), 8490-8496.
31. Li, Z. F.; Swihart, M. T.; Ruckenstein, E., Luminescent Silicon Nanoparticles Capped by Conductive Polyaniline through the Self-Assembly Method. *Langmuir* **2004**, *20* (5), 1963-1971.
32. Hua, F.; Swihart, M. T.; Ruckenstein, E., Efficient Surface Grafting of Luminescent Silicon Quantum Dots by Photoinitiated Hydrosilylation. *Langmuir* **2005**, *21* (13), 6054-6062.
33. Li, X.; He, Y.; Swihart, M. T., Surface Functionalization of Silicon Nanoparticles Produced by Laser-Driven Pyrolysis of Silane followed by HF-HNO₃ Etching. *Langmuir* **2004**, *20* (11), 4720-4727.
34. Canham, L. T., Silicon quantum wire array fabrication by electrochemical and chemical dissolution of wafers. *Applied Physics Letters* **1990**, *57* (10), 1046.
35. Nayfeh, M. H.; Barry, N.; Therrien, J.; Akcakir, O.; Gratton, E.; Belomoin, G., Stimulated blue emission in reconstituted films of ultrasmall silicon nanoparticles. *Applied Physics Letters* **2001**, *78* (8), 1131-1133.
36. Belomoin, G.; Rogozhina, E.; Therrien, J.; Braun, P. V.; Abuhassan, L.; Nayfeh, M. H.; Wagner, L.; Mitas, L., Effects of surface termination on the band gap of ultrabright nanoparticles: Experiments and computational models. *Physical Review B* **2002**, *65* (19), 193406.
37. Rao, S.; Sutin, J.; Clegg, R.; Gratton, E.; Nayfeh, M. H.; Habbal, S.; Tsolakidis, A.; Martin, R. M., Excited states of tetrahedral single-core nanoparticles. *Physical Review B* **2004**, *69* (20), 205319.
38. Lee, E. J.; Bitner, T. W.; Ha, J. S.; Shane, M. J.; Sailor, M. J., Light-Induced Reactions of Porous and Single-Crystal Si Surfaces with Carboxylic Acids. *Journal of the American Chemical Society* **1996**, *118* (23), 5375-5382.
39. Lee, E. J.; Ha, J. S.; Sailor, M. J., Photoderivatization of the Surface of Luminescent Porous Silicon with Formic Acid. *Journal of the American Chemical Society* **1995**, *117* (31), 8295-8296.
40. HEINRICH, J. L.; CURTIS, C. L.; CREDO, G. M.; SAILOR, M. J.; KAVANAGH, K. L., Luminescent Colloidal Silicon Suspensions from Porous Silicon. *Science* **1992**, *255* (5040), 66-68.

41. Kang, Z.; Liu, Y.; Tsang, C. H. A.; Ma, D. D. D.; Fan, X.; Wong, N.-B.; Lee, S.-T., Water-Soluble Silicon Quantum Dots with Wavelength-Tunable Photoluminescence. *Advanced Materials* **2009**, *21* (6), 661-664.
42. Sato, S.; Swihart, M. T., Propionic-Acid-Terminated Silicon Nanoparticles: Synthesis and Optical Characterization. *Chemistry of Materials* **2006**, *18* (17), 4083-4088.
43. Bley, R. A.; Kauzlarich, S. M.; Davis, J. E.; Lee, H. W. H., Characterization of Silicon Nanoparticles Prepared from Porous Silicon. *Chemistry of Materials* **1996**, *8* (8), 1881-1888.
44. Hessel, C. M.; Henderson, E. J.; Veinot, J. G. C., Hydrogen Silsesquioxane: A Molecular Precursor for Nanocrystalline Si-SiO₂ Composites and Freestanding Hydride-Surface-Terminated Silicon Nanoparticles. *Chemistry of Materials* **2006**, *18* (26), 6139-6146.
45. Dasog, M.; De los Reyes, G. B.; Titova, L. V.; Hegmann, F. A.; Veinot, J. G. C., Size vs Surface: Tuning the Photoluminescence of Freestanding Silicon Nanocrystals Across the Visible Spectrum via Surface Groups. *ACS Nano* **2014**, *8* (9), 9636-9648.
46. Veinot, J. G. C., Synthesis, surface functionalization, and properties of freestanding silicon nanocrystals. *Chemical Communications* **2006**, (40), 4160-4168.
47. Yang, Z.; De los Reyes, G. B.; Titova, L. V.; Sychugov, I.; Dasog, M.; Linnros, J.; Hegmann, F. A.; Veinot, J. G. C., Evolution of the Ultrafast Photoluminescence of Colloidal Silicon Nanocrystals with Changing Surface Chemistry. *ACS Photonics* **2015**, *2* (5), 595-605.
48. Amoruso, S.; Bruzzese, R.; Spinelli, N.; Velotta, R.; Vitiello, M.; Wang, X.; Ausanio, G.; Iannotti, V.; Lanotte, L., Generation of silicon nanoparticles via femtosecond laser ablation in vacuum. *Applied Physics Letters* **2004**, *84* (22), 4502-4504.
49. Seto, T.; Orii, T.; Hirasawa, M.; Aya, N., Fabrication of silicon nanostructured films by deposition of size-selected nanoparticles generated by pulsed laser ablation. *Thin Solid Films* **2003**, *437* (1-2), 230-234.
50. Ying, D. Y.; Zhang, D. L., Processing of Cu-Al₂O₃ metal matrix nanocomposite materials by using high energy ball milling. *Materials Science and Engineering: A* **2000**, *286* (1), 152-156.
51. Gaffet, E.; Harmelin, M., Crystal-amorphous phase transition induced by ball-milling in silicon. *Journal of the Less Common Metals* **1990**, *157* (2), 201-222.
52. Shen, T.; Koch, C.; McCormick, T.; Nemanich, R.; Huang, J.; Huang, J., The structure and property characteristics of amorphous/nanocrystalline silicon produced by ball milling. *Journal of materials research* **1995**, *10* (01), 139-148.
53. Wang, C.; Wu, G.; Zhang, X.; Qi, Z.; Li, W., Lithium insertion in carbon-silicon composite materials produced by mechanical milling. *Journal of the Electrochemical Society* **1998**, *145* (8), 2751-2758.

54. Hallmann, S.; Fink, M. J.; Mitchell, B. S., Wetting properties of silicon films from alkyl-passivated particles produced by mechanochemical synthesis. *Journal of Colloid and Interface Science* **2010**, *348* (2), 634-641.
55. Hallmann, S.; Fink, M. J.; Mitchell, B. S., Mechanochemical synthesis of functionalized silicon nanoparticles with terminal chlorine groups. *Journal of Materials Research* **2011**, *26* (08), 1052-1060.
56. Hallmann, S.; Fink, M. J.; Mitchell, B. S., Williamson ether synthesis: an efficient one-step route for surface modifications of silicon nanoparticles. *Journal of Experimental Nanoscience* **2013**, *10* (8), 588-598.
57. Kuang, L.; Mitchell, B. S.; Fink, M. J., Silicon nanoparticles synthesised through reactive high-energy ball milling: enhancement of optical properties from the removal of iron impurities. *Journal of Experimental Nanoscience* **2014**, 1-9.
58. Verdoni, L. P.; Fink, M. J.; Mitchell, B. S., A fractionation process of mechanochemically synthesized blue-green luminescent alkyl-passivated silicon nanoparticles. *Chemical Engineering Journal* **2011**, *172* (1), 591-600.
59. Su, X.; Kuang, L.; Battle, C.; Shaner, T.; Mitchell, B. S.; Fink, M. J.; Jayawickramarajah, J., Mild Two-Step Method to Construct DNA-Conjugated Silicon Nanoparticles: Scaffolds for the Detection of MicroRNA-21. *Bioconjugate Chemistry* **2014**, *25* (10), 1739-1743.
60. Eckhoff, D. A.; Sutin, J. D. B.; Clegg, R. M.; Gratton, E.; Rogozhina, E. V.; Braun, P. V., Optical Characterization of Ultrasmall Si Nanoparticles Prepared through Electrochemical Dispersion of Bulk Si. *The Journal of Physical Chemistry B* **2005**, *109* (42), 19786-19797.
61. Fojtik, A.; Henglein, A., Surface Chemistry of Luminescent Colloidal Silicon Nanoparticles. *The Journal of Physical Chemistry B* **2006**, *110* (5), 1994-1998.
62. Yoonjung, B.; Doh, C. L.; Elena, V. R.; David, C. J.; Brian, A. K.; Allen, J. B., Electrochemistry and electrogenerated chemiluminescence of films of silicon nanoparticles in aqueous solution. *Nanotechnology* **2006**, *17* (15), 3791.
63. Rogozhina, E. V.; Eckhoff, D. A.; Gratton, E.; Braun, P. V., Carboxyl functionalization of ultrasmall luminescent silicon nanoparticles through thermal hydrosilylation. *Journal of Materials Chemistry* **2006**, *16* (15), 1421-1430.
64. Ahire, J. H.; Wang, Q.; Coxon, P. R.; Malhotra, G.; Brydson, R.; Chen, R.; Chao, Y., Highly Luminescent and Nontoxic Amine-Capped Nanoparticles from Porous Silicon: Synthesis and Their Use in Biomedical Imaging. *ACS Applied Materials & Interfaces* **2012**, *4* (6), 3285-3292.
65. Stewart, M. P.; Buriak, J. M., Exciton-Mediated Hydrosilylation on Photoluminescent Nanocrystalline Silicon. *Journal of the American Chemical Society* **2001**, *123* (32), 7821-7830.
66. Kolasinski, K. W., The Mechanism of Photohydrosilylation on Silicon and Porous Silicon Surfaces. *Journal of the American Chemical Society* **2013**, *135* (30), 11408-11412.

67. Patolsky, F.; Zheng, G.; Lieber, C. M., Fabrication of silicon nanowire devices for ultrasensitive, label-free, real-time detection of biological and chemical species. *Nat. Protocols* **2006**, *1* (4), 1711-1724.
68. Ameya, B.; Curtis, A.; Christopher, R. P.; Carter, C. B.; Stephen, A. C.; Uwe, K., Plasma synthesis of single-crystal silicon nanoparticles for novel electronic device applications. *Plasma Physics and Controlled Fusion* **2004**, *46* (12B), B97.
69. Kelzenberg, M. D.; Turner-Evans, D. B.; Kayes, B. M.; Filler, M. A.; Putnam, M. C.; Lewis, N. S.; Atwater, H. A., Photovoltaic Measurements in Single-Nanowire Silicon Solar Cells. *Nano Letters* **2008**, *8* (2), 710-714.
70. Matheu, P.; Lim, S. H.; Derkacs, D.; McPheeters, C.; Yu, E. T., Metal and dielectric nanoparticle scattering for improved optical absorption in photovoltaic devices. *Applied Physics Letters* **2008**, *93* (11), 113108.
71. Xu, H.; Yan, F.; Monson, E. E.; Kopelman, R., Room-temperature preparation and characterization of poly (ethylene glycol)-coated silica nanoparticles for biomedical applications. *Journal of Biomedical Materials Research Part A* **2003**, *66A* (4), 870-879.
72. Vivero-Escoto, J. L.; Huxford-Phillips, R. C.; Lin, W., Silica-based nanoprobe for biomedical imaging and theranostic applications(). *Chemical Society reviews* **2012**, *41* (7), 2673-2685.
73. Shin, D.; Banerjee, D., Enhancement of specific heat capacity of high-temperature silica-nanofluids synthesized in alkali chloride salt eutectics for solar thermal-energy storage applications. *International Journal of Heat and Mass Transfer* **2011**, *54* (5-6), 1064-1070.
74. Li, Y.; Guo, B.; Ji, L.; Lin, Z.; Xu, G.; Liang, Y.; Zhang, S.; Toprakci, O.; Hu, Y.; Alcoutlabi, M.; Zhang, X., Structure control and performance improvement of carbon nanofibers containing a dispersion of silicon nanoparticles for energy storage. *Carbon* **2013**, *51*, 185-194.
75. Yoo, J.-K.; Kim, J.; Jung, Y. S.; Kang, K., Scalable Fabrication of Silicon Nanotubes and their Application to Energy Storage. *Advanced Materials* **2012**, *24* (40), 5452-5456.
76. Wang, L.; Nagesha, D. K.; Selvarasah, S.; Dokmeci, M. R.; Carrier, R. L., Toxicity of CdSe Nanoparticles in Caco-2 Cell Cultures. *Journal of Nanobiotechnology* **2008**, *6*, 11-11.
77. Kirchner, C.; Liedl, T.; Kudera, S.; Pellegrino, T.; Muñoz Javier, A.; Gaub, H. E.; Stölzle, S.; Fertig, N.; Parak, W. J., Cytotoxicity of Colloidal CdSe and CdSe/ZnS Nanoparticles. *Nano Letters* **2005**, *5* (2), 331-338.
78. Ron, H., A Toxicologic Review of Quantum Dots: Toxicity Depends on Physicochemical and Environmental Factors. *Environmental Health Perspectives* **2006**, *114* (2), 165-172.
79. Tu, C.; Ma, X.; House, A.; Kauzlarich, S. M.; Louie, A. Y., PET Imaging and Biodistribution of Silicon Quantum Dots in Mice. *ACS Medicinal Chemistry Letters* **2011**, *2* (4), 285-288.

80. Li, Z. F.; Ruckenstein, E., Water-Soluble Poly(acrylic acid) Grafted Luminescent Silicon Nanoparticles and Their Use as Fluorescent Biological Staining Labels. *Nano Letters* **2004**, *4* (8), 1463-1467.
81. Rosso-Vasic, M.; Spruijt, E.; Popovic, Z.; Overgaag, K.; van Lagen, B.; Grandidier, B.; Vanmaekelbergh, D.; Dominguez-Gutierrez, D.; De Cola, L.; Zuilhof, H., Amine-terminated silicon nanoparticles: synthesis, optical properties and their use in bioimaging. *Journal of Materials Chemistry* **2009**, *19* (33), 5926-5933.
82. Park, J.-H.; Gu, L.; von Maltzahn, G.; Ruoslahti, E.; Bhatia, S. N.; Sailor, M. J., Biodegradable luminescent porous silicon nanoparticles for in vivo applications. *Nat Mater* **2009**, *8* (4), 331-336.
83. Erogbogbo, F.; Yong, K.-T.; Roy, I.; Hu, R.; Law, W.-C.; Zhao, W.; Ding, H.; Wu, F.; Kumar, R.; Swihart, M. T.; Prasad, P. N., In Vivo Targeted Cancer Imaging, Sentinel Lymph Node Mapping and Multi-Channel Imaging with Biocompatible Silicon Nanocrystals. *ACS Nano* **2011**, *5* (1), 413-423.
84. Erogbogbo, F.; Yong, K.-T.; Roy, I.; Xu, G.; Prasad, P. N.; Swihart, M. T., Biocompatible Luminescent Silicon Quantum Dots for Imaging of Cancer Cells. *ACS Nano* **2008**, *2* (5), 873-878.
85. Wang, L.; Reipa, V.; Blasic, J., Silicon Nanoparticles as a Luminescent Label to DNA. *Bioconjugate Chemistry* **2004**, *15* (2), 409-412.
86. Voicu, R.; Boukherroub, R.; Bartzoka, V.; Ward, T.; Wojtyk, J. T. C.; Wayner, D. D. M., Formation, Characterization, and Chemistry of Undecanoic Acid-Terminated Silicon Surfaces: Patterning and Immobilization of DNA. *Langmuir* **2004**, *20* (26), 11713-11720.
87. Tabasi, O.; Falamaki, C.; Khalaj, Z., Functionalized mesoporous silicon for targeted-drug-delivery. *Colloids and Surfaces B: Biointerfaces* **2012**, *98* (0), 18-25.
88. Sam, S.; Touahir, L.; Salvador Andresa, J.; Allongue, P.; Chazalviel, J. N.; Gouget-Laemmel, A. C.; Henry de Villeneuve, C.; Moraillon, A.; Ozanam, F.; Gabouze, N.; Djebbar, S., Semiquantitative Study of the EDC/NHS Activation of Acid Terminal Groups at Modified Porous Silicon Surfaces. *Langmuir* **2010**, *26* (2), 809-814.
89. Yang, M.; Teeuwen, R. L. M.; Giesbers, M.; Baggerman, J.; Arafat, A.; de Wolf, F. A.; van Hest, J. C. M.; Zuilhof, H., One-Step Photochemical Attachment of NHS-Terminated Monolayers onto Silicon Surfaces and Subsequent Functionalization. *Langmuir* **2008**, *24* (15), 7931-7938.
90. Choi, J.; Wang, N. S.; Reipa, V., Conjugation of the Photoluminescent Silicon Nanoparticles to Streptavidin. *Bioconjugate Chemistry* **2008**, *19* (3), 680-685.
91. Poizot, P.; Laruelle, S.; Grugeon, S.; Dupont, L.; Tarascon, J. M., Nano-sized transition-metal oxides as negative-electrode materials for lithium-ion batteries. *Nature* **2000**, *407* (6803), 496-499.
92. Lee, J. K.; Smith, K. B.; Hayner, C. M.; Kung, H. H., Silicon nanoparticles-graphene paper composites for Li ion battery anodes. *Chemical Communications* **2010**, *46* (12), 2025-2027.

93. Lee, B.-S.; Son, S.-B.; Park, K.-M.; Seo, J.-H.; Lee, S.-H.; Choi, I.-S.; Oh, K.-H.; Yu, W.-R., Fabrication of Si core/C shell nanofibers and their electrochemical performances as a lithium-ion battery anode. *Journal of Power Sources* **2012**, *206*, 267-273.

Chapter 2.

Synthesis of passivated silicon nanoparticles with carboxylic acids using Reactive High Energy Ball Milling (RHEBM).

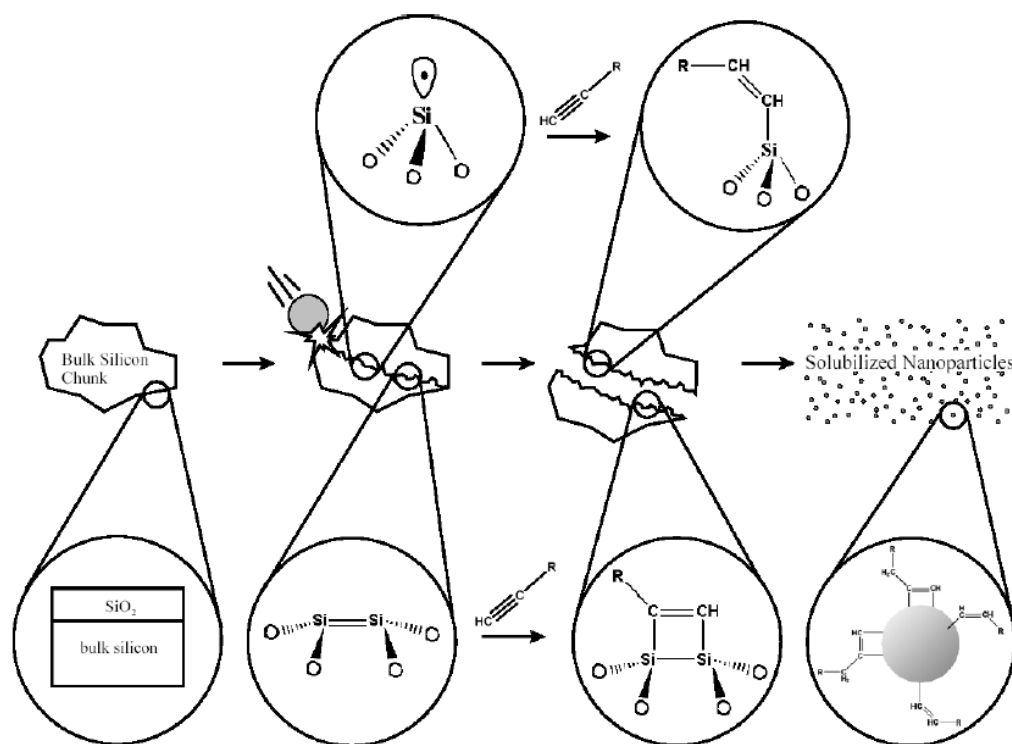
Section 2.1: Introduction:

Silicon nanoparticles have been synthesized from numerous methods, including reduction of chlorosilanes in inverse micelles,¹ chemical etching of silicon,²⁻⁴ oxidation of Zintl salts,⁵⁻⁷ thermolysis of silanes in supercritical fluids,⁸ and reductive thermal annealing of silsequioxanes.⁹ However, many of these methods require high temperatures, further modification of the surfaces, or the use of highly reactive chemicals. A promising method of producing silicon nanoparticles in a one-step method with the required surface passivation is reactive high energy ball milling (RHEBM).¹⁰

RHEBM allows for a wide array of passivating ligands to be attached to the silicon nanoparticles during the synthesis step. Alkynes,¹⁰⁻¹¹ alkenes,¹²⁻¹³, alcohols, carboxylic acids, and aldehydes have all shown to act as passivating reactive organic liquids during the synthesis of silicon nanoparticles by RHEBM. This allows for several different surface passivations to easily be utilized, simply by changing the reactive organic liquid that the silicon is milled in.

RHEBM milling has the advantage of not needing high pressure or potentially dangerous reagents such as HF acid, and it has been shown to have a wide range of use

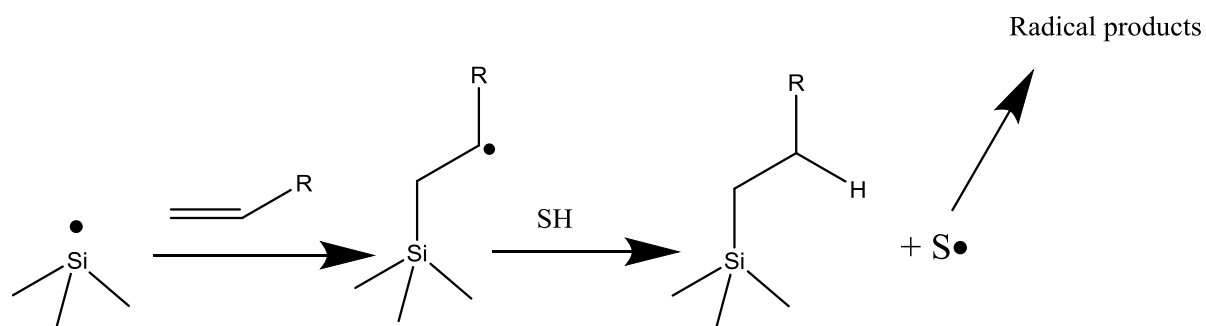
with different passivating reactive organic liquids. The synthesis of silicon nanoparticles by RHEBM is performed by filling a milling vial with silicon, a degassed reactive organic liquid, and a set of milling balls. The process is generally done in a dry box with an inert atmosphere of N_2 . The vial is closed gas tight and then milled in a Spex SamplePrep 8000D mill for 12 hours. The suspension is then removed and separated from any insoluble sediments by means of centrifugation. The solution is then purified by means of gel permeation chromatography in order to remove molecular impurities. This simple method results in the introduction of a covalent bond between the reactive organic liquid and the silicon surface of the nanoparticle. This process is presented schematically below using an alkyne to illustrate the process.



Scheme 2.1 Synthesis of alkyne passivated silicon nanoparticles.¹⁰

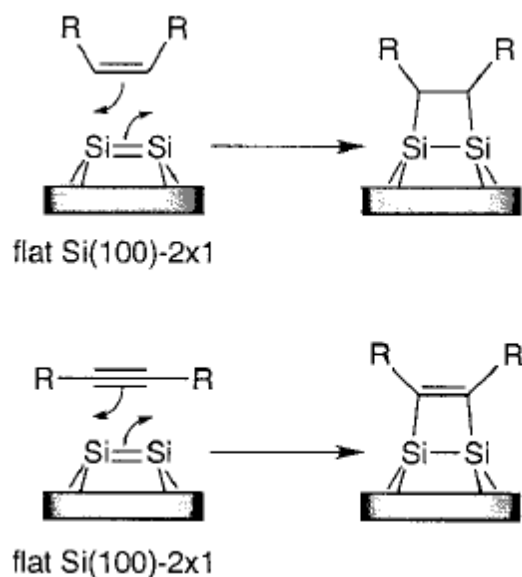
As can be seen in scheme 2.1 the bulk silicon wafers are broken when struck by the milling ball. This exposes a clean surface that has not been oxidized by atmospheric oxygen prior to entering the milling vial. This new surface reacts with the reactive organic liquid generally through the formation of a strong Si-C bond and the surface therefore becomes passivated. This process continues for the duration of the milling time, resulting in solubilized silicon nanoparticles that have been passivated by the reactive organic liquid, in this case an alkyne. The process is general and can accommodate a wide variety of functional groups.

Alkynes and alkenes can bond to the surface in two distinct modes. The first mode is an end on radical addition to silicon radical sites, as on a (111) surface to give an initial carbon centered radical as shown in (scheme 2.2).¹⁴ The carbon centered radical can then abstract a hydrogen from the solvent to give the resultant surface ligand.



Scheme 2.2. Radical addition of alkyne and alkene reactive organic liquids to fresh (111) silicon surface.¹⁴

The second mode is a 2+2 cycloaddition with silicon dimers as found on the (100) silicon surface (scheme 2.3).¹⁴⁻¹⁵



Scheme 2.3 The 2+2 mode of cycloaddition to a silicon (100) fresh silicon surface with liquid alkyne and alkenes.¹⁴

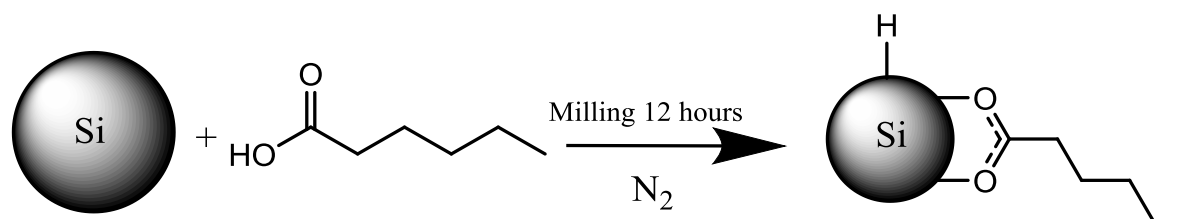
These bonding modes occur because of the differences in the surface morphology of the (111) vs. (100) surfaces. The 7x7 (111) surface is characterized by single dangling bonds as well as silicon dimers that can be readily reacted via a radical mechanism to form products as seen in scheme 2.2. The silicon 2x1 (100) surface is characterized by a series of dimers between neighboring silicon atoms. The neighboring atoms are not coplanar, with one end being slightly elevated and the other end being slightly depressed.^{14, 16} The difference in the heights of the ends of the dimers is associated with a zwitterionic character of the dimer.^{14, 17}

The chemistry that is known from the flat surfaces in high vacuum conditions is well reported and can be extrapolated to the nanoparticle surfaces. The nanoparticle surface is not ideal and may likely be an intermediate between (111) and (100) surfaces and therefore likely to contain both silicon radical sites as well as silicon-silicon dimers. This chemistry results from the reconstruction of the cleaved silicon surfaces. The RHEBM process also allows for different reactive organic liquids to be milled at the same time. This is of great interest as the use of α - ω reactive organic liquids provides a passivating surface that can undergo further chemistry. Mixtures of these α - ω diynes and α - ω dienes can be used along with monoynes and monoenes to produce silicon nanoparticles in a one-step synthesis which can undergo further chemistry on the terminal functionalities.

Using RHEBM, the surface coverage of mixture of difunctionalized and nonfunctionalized reactive organic liquids can be controlled by the mole fraction of the mixture. As long as the functionalities of the reactive organic liquid are the same, *Kuang* has shown that the percent surface coverage of the silicon nanoparticle corresponds to the starting molar percentage of the milling liquid within experimental error.¹⁵

The focus of this project is to produce silicon nanoparticles that are passivated by carboxylic acids and have a free terminal carboxylic acid functionality. These silicon nanoparticles would be of great interest for their ability to conjugate biomolecules with an accessible amine to form an amide. This route of linkage of biomolecules has shown great promise with many reports in the literature.¹⁸⁻²⁷ Biomolecules have been successfully tethered to flat surfaces through this route as well as the conjugation of biomolecules to nanoparticles using the conjugation of an carboxylic acid functionality

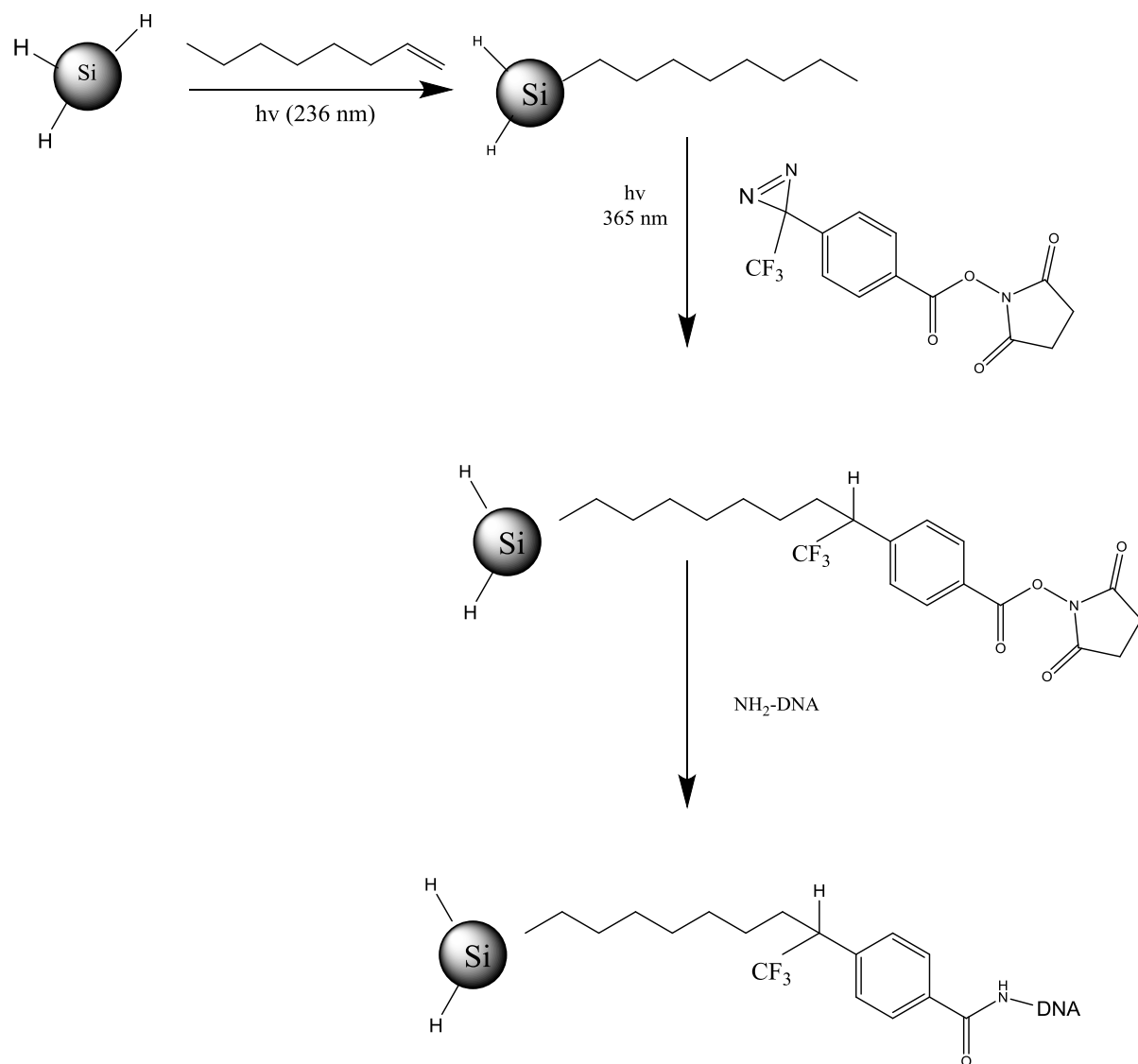
and an amine functionality. The scheme for bonding of carboxylic acid to the silicon surface is shown in scheme 2.4. First the hydroxyl group bonds to the silicon surface, resulting in both an Si-O bond and an Si-H bond. The Si-H bond is most likely further oxidized to Si-OH upon exposure to atmospheric oxygen and water. The carbonyl will also interact with the silicon surface, resulting in a bidentate bonding mode for the bound carboxylic acid as reported by Heintz *et al.*²⁸



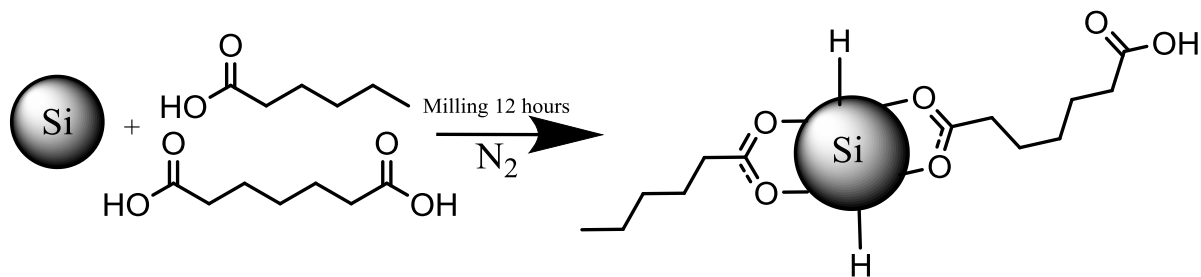
Scheme 2.4 Passivation by carboxylic acid of silicon nanoparticle.

Examples of silicon nanoparticles with terminal carboxylic acid groups have been reported in the literature. This has been accomplished using hydrosilation²¹⁻²² and expensive and complex cross linkers.^{20, 23} Swihart *et al* have produced carboxylic acid terminated silicon nanoparticles through the hydrosilation of acrylic acid.² Wang *et al* have grafted linker ligands to the surface of silicon nanoparticles as shown in Figure 2.5. The hydrogen passivated silicon nanoparticle is chemically stabilized through the hydrosilation of the nanoparticles surface with 1-octene. The 1-octene is further linked with 4'-[3-(trifluoromethyl-3*H*-diazirin-3-yl)]-benzoic acid and *N*-hydroxysuccinimide ester via a C-H insertion reaction.²⁰ The resultant chain now possesses an activated carboxylic acid group as an NHS ester. The NHS ester is a good leaving group and was

subsequently displaced by a DNA residue. This is the same method of conjugation to biomolecules as will be used in this project.



Scheme 2.5 Synthesis of silicon nanoparticle conjugated to DNA by hydrosilation method.



Scheme 2.6 Synthesis of silicon nanoparticle passivated with free carboxylic acid.

RHEBM provides potentially a more direct route to carboxylic acid functionalized nanoparticles. A mixture of monocarboxylic acid (*eg.* 1-pentanoic acid) and dicarboxylic acid (*eg.* 1,7-heptanedioic acid) as reactive organic milling liquids should provide a surface which has carboxylic acid functionality. This one step synthesis should produce silicon nanoparticles that can be later conjugated with an amine group of a biomolecule of interest (*eg.* DNA) in a direct fashion.

Section 2.2: Experimental:

Materials

The following chemicals were obtained from Sigma Aldrich and used without further purification: 1-octanoic acid (98 %), 1-hexanoic acid (98 %), 1,6-hexanedioic acid (99 %), 1-pentanoic acid (99 %), 1,7-heptanedioic acid (98 %), benzoic acid (99.5 %), 1-hexadiene (97 %). 1-pentene (>95%) was obtained from Gelest and used without further purification. The dialysis membrane was purchased from Spectra/Por[®] and was a regenerated cellulose membrane with a molecular weight cut off (MWCO) of 1,000 Da. This was chosen for its stability with most organic solvents including toluene and dichloromethane. The solvents toluene, dichloromethane, and ethanol were obtained from Fisher Scientific. Dichloromethane was dried over calcium hydride and then distilled. The other solvents were not further purified.

General procedure for RHEBM

The silicon wafers were stored in a nitrogen filled dry box. The milling vial and 2 stainless steel balls were taken into the dry box along with the degassed reactive organic liquid. The vial was filled with 1.25 g of silicon wafer and 25 mL of reactive organic liquid. The two milling balls, each weighing approximately 2.1 cm in diameter and 8.1 g, were then added to the vial and it was sealed using Teflon tape and screwed tight. The vial was milled for 12 hours in a cold room at 4°C at 1060 cycles per minute in a Spex SamplePrep 8000D mill (Figure 2.1).²⁹ When the milling had been completed, the milling mixture was centrifuged in air in a plastic centrifuge tube for 30 minutes at 511 G using a

Thermo IEC[®] Centra CL2 centrifuge. The supernatant was then separated from the insoluble sediments and then purified.

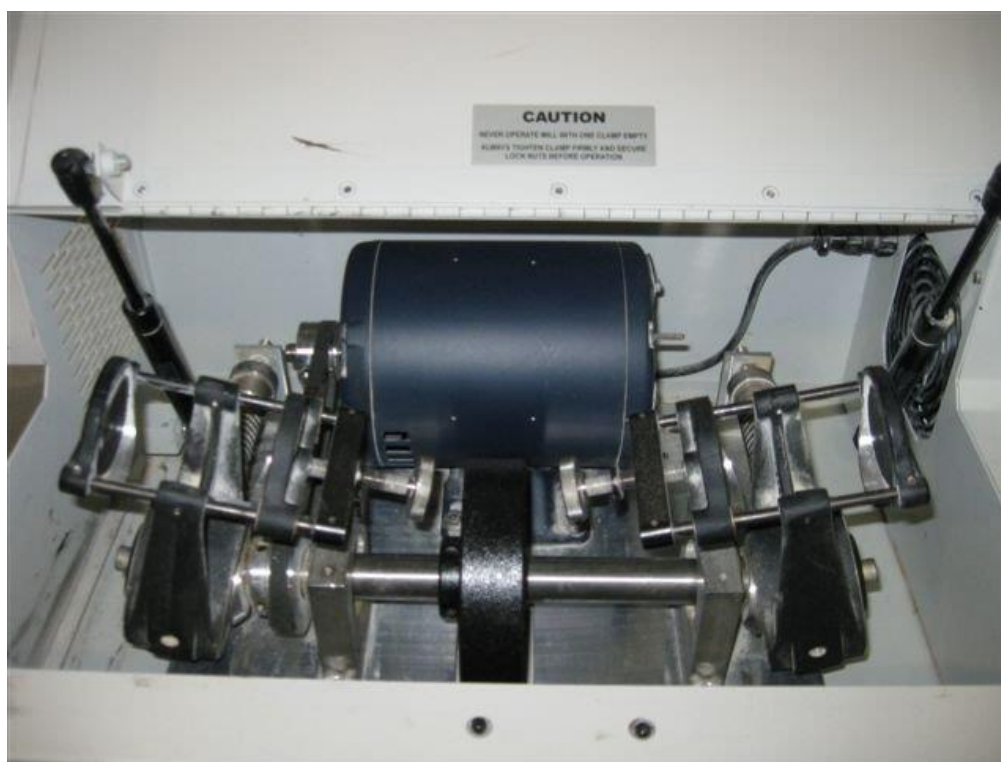


Figure 2.1 8000D Mixer/Mill

Synthesis of 1-octanoic acid passivated silicon nanoparticles

1-Octanoic acid (25 mL), 1.25 grams of silicon chips, and 2 milling balls were added to a stainless steel milling vial in a nitrogen filled dry box. After milling the product solution was purified by Soxhlet extraction using dichloromethane for 36 hours. A brown solid was recovered giving an average yield of 45 mg. The product was then characterized by ¹H NMR, photoluminescence, UV-Vis, and TEM.

Synthesis of 1-hexanoic acid passivated silicon nanoparticles

1-Hexanoic acid (25 mL), 1.25 g silicon chips were added to a stainless steel milling vial in a nitrogen filled dry box. After milling and centrifugation the remaining starting material (1-hexanoic acid) was removed by dialysis in ethanol/ toluene (10%). The product was a brownish solid. The average yield was 30 mg.

Synthesis of 1-hexanoic acid/1,6-hexanedioic acid passivated silicon nanoparticles

1- Hexanoic acid (25 mL), 1,6-hexandioic acid 4g ($C_6H_{10}O_4$) (which was not soluble in the hexanoic acid), and 1.25 grams of silicon chips were added to a stainless steel milling vial in a nitrogen filled dry box.. The product solution was purified by dialysis for 72 hours in a mixture of toluene/ethanol (10%) to remove starting material. The resulting yield was 9 mg of a gray solid.

Synthesis of 1-pentanoic acid passivated silicon nanoparticles.

1-Pentanoic acid (25 mL) was combined with 1.25 g silicon chips in a stainless steel milling vial in a nitrogen filled dry box. After milling and centrifugation, the remaining starting material (1-pentanoic acid) was removed by dialysis in ethanol/ toluene (10%). The product was a brownish solid. The average yield was 25 mg.

Synthesis of 1-pentanoic acid / 1,7-heptanedioic acid (5%) passivated silicon nanoparticles.

1-Pentanoic acid (25 mL), 1.25 grams of silicon wafer, and 3.6 g of 1,7-heptanedioic acid were added to a stainless steel vial in a nitrogen filled dry box. After milling and centrifugation, the supernatant was collected and purified by dialysis for 48 hours in dichloromethane using a regenerated cellulose membrane. The yield was 35 milligrams of a brown solid.

Synthesis of benzoic acid passivated silicon nanoparticles.

Toluene (30 mL), 2 g silicon wafer, and 2 g benzoic acid were added to a stainless steel vial in a nitrogen filled dry box. The vial was capped in the dry box and was then milled for 12 hours at 4°C in a cold room. The contents of the vial were then centrifuged in a plastic centrifuge tube to separate the nanoparticle supernatant from the insoluble sediments. The product was then separated from the starting material using Soxhlet extraction with toluene and a regenerated cellulose membrane for 36 hours. The yield was 20 mg of brown solid.

Characterization

Elemental Analysis was done using a FEI TECNAI G² Transmission Electron Microscope (TEM). The TEM was fitted with a Bruker AXS XFlash energy dispersive X-ray detector for elemental analysis. Spectral analysis of the particles were

characterized using a combination of TEM, NMR, IR, UV-Vis, and photoluminescence.

^1H analysis of the silicon nanoparticles was done using an Advance Bruker UltraShield 300 MHz Spectrometer. All spectra were taken at room temperature. All IR spectra were taken using a Thermo Nicolet NEXUS 870 FTIR E.S.P spectrometer. Sample preparation was a thin film was prepared on a KBr plate by the evaporation of a drop of a solution of the nanoparticles in dichloromethane on the KBr plate. A Varian Cary 50 Bio UV-Visible Spectrophotometer was used for all UV-Vis measurements. The instrument was always operated in medium voltage mode and was run with a medium rate of scan of 300 nm/minute. The photoluminescence spectra were obtained by a Varian Cary Eclipse Fluorescence Spectrometer operated in the medium voltage mode of 600 volts. The slits were 5 nm and a scan rate of 120 nm/minute was used. All spectra were taken using dichloromethane as the solvent unless otherwise noted.

Photoluminescence comparison

The photoluminescence spectra were all taken using the same instrument and under the same conditions as described in the previous chapter. Quantum yield measurements were not taken however. For purposes of comparison of the luminescence yields, all luminescence spectra were normalized by the UV-vis absorbance. The wavelength of the excitation was compared to the UV-vis and the optical density at that wavelength was noted. The luminescence spectra were then normalized by dividing the emission amplitudes by the optical density from the absorbance spectra.

This is not an absolute quantum yield and cannot be used to compare to other yields of silicon nanoparticles in the literature and from different groups. It does however, provide us with an ability to compare the luminescence of silicon nanoparticles synthesized with different passivating ligands to compare the luminescence yields. The operating conditions of the instrument are kept constant and the solvent used are also kept constant, leaving the passivated silicon nanoparticles as the only part of the experiment that changes.

Size separation and purification

All products were purified by Gel Permeation Chromatography (GPC) prior to characterization. This was done using BioBeads X-1 as the immobile phase and dichloromethane that had been dried and distilled as the mobile phase. These characterization and purification steps have been done for all silicon nanoparticles whose synthesis is described in this thesis.

Section 2.3: Results and Discussion

Section 2.3.1 RHEBM of silicon with monocarboxylic acids

Various aliphatic carboxylic acids were used to passivate silicon nanoparticles. Different chain lengths were chosen so that the effect of solubility and of the percent yield could be assessed. One hypothesis was that longer chain length should result in a greater percentage yield as it would better suspend the nanoparticles due to increased solvation and also that it would better protect the surface from oxidation due to oxygen.

1-Octanoic acid passivated silicon nanoparticles.

1-octanoic acid passivated silicon nanoparticles were first synthesized by Andrew Heintz.²⁸ They were synthesized in the course of this project for the purpose of comparison to his work. The 1-octanoic acid passivated silicon nanoparticles were characterized by ¹H NMR, photoluminescence, UV-Vis, TEM, and infrared spectroscopy. 1-Octanoic acid passivated silicon nanoparticles were investigated thoroughly as they were the first system that showed good results of formation of passivated silicon nanoparticles with a carboxylic acid.

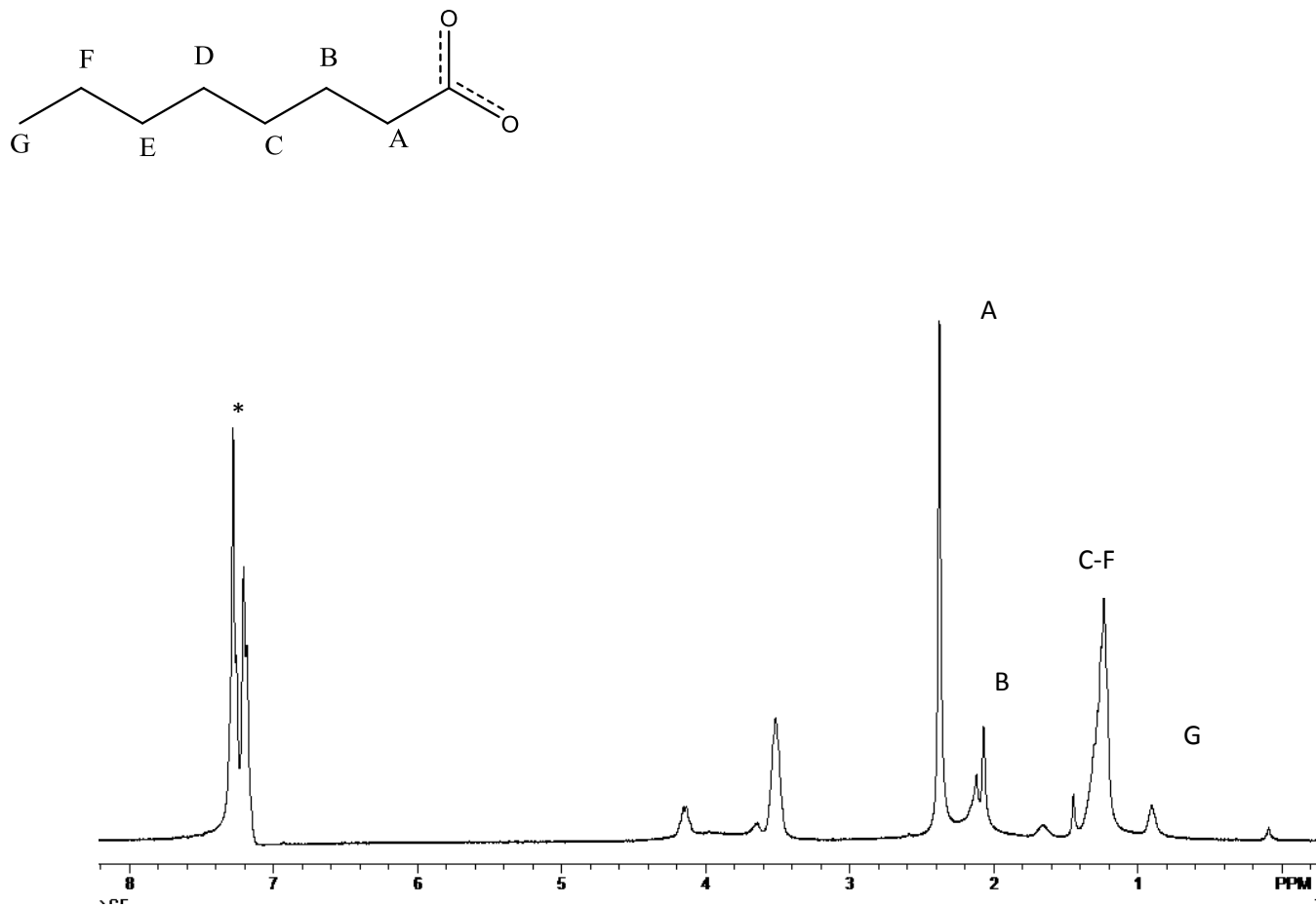


Figure 2.2 ¹H NMR of 1-octanoic acid passivated silicon nanoparticles in $CDCl_3$.

(* = $CDCl_3$)

The purification of the octanoic acid passivated silicon nanoparticles was challenging due to the boiling point of octanoic acid being $237^\circ C$. The starting material could not be removed except by using Soxhlet dialysis extraction in which the dialysis membrane was placed inside a Soxhlet extractor³⁰ and exposed to multiple changes of

dichloromethane over a 36 hour period. As can be seen from the ^1H NMR, there still remains some impurities between 3.5 ppm and 4.2 ppm. However, failure to observe any peaks between 10-12 ppm shows that no free 1-octanoic acid is present and that the spectrum is presumably that of the remaining nanoparticles.

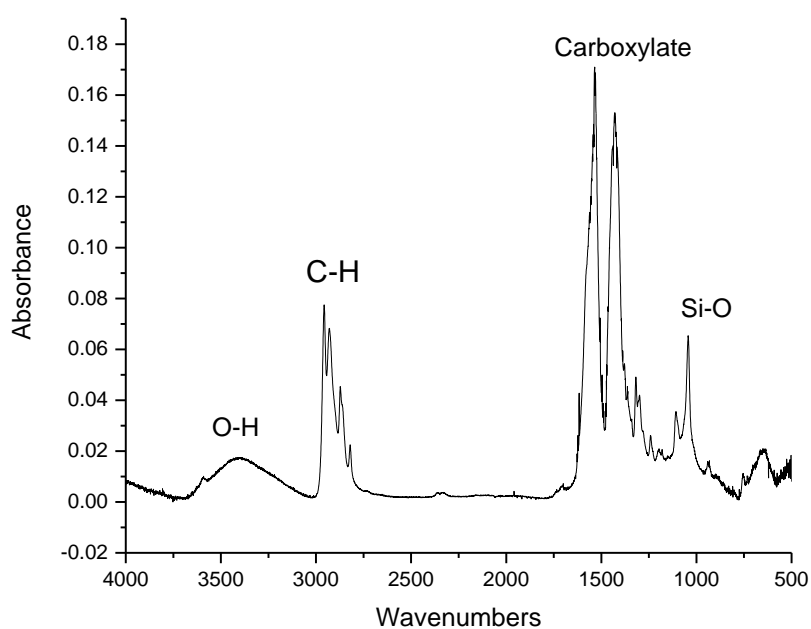


Figure 2.3 Infrared spectrum of 1-octanoic acid passivated silicon nanoparticles.

The infrared spectrum of the 1-octanoic acid passivated silicon nanoparticles shows two stretches at 1536 and 1431 wavenumbers which correspond to a bidentate carboxylate group.³¹ The absence of any stretch around 1715 wavenumbers indicates the absence of any remaining carboxylic acid starting material. There is also the expected

alkane stretches around 2900 wavenumbers. A stretch for O-H is observed centered around 3300 wavenumbers, this is most likely due to Si-OH which formed from Si-H on the nanoparticle surface being oxidized.²⁸ Also observed is a strong peak around 1100 wave numbers that is due to Si-O vibrations. These finding are very similar to those found by Heintz et al. Shown in Figure 2.4 is the infrared spectrum they observed.

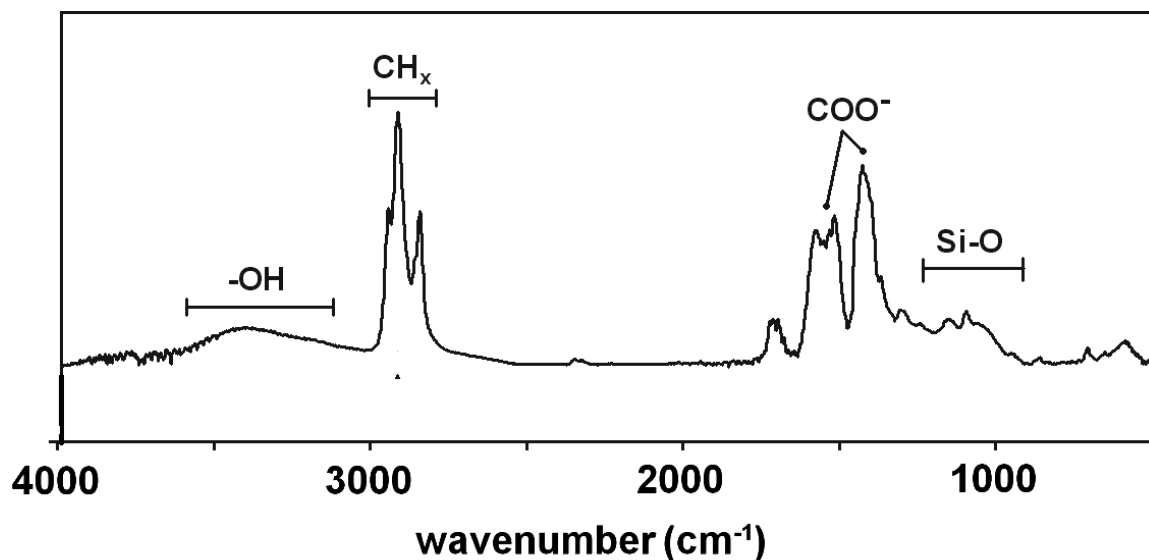


Figure 2.4 IR spectra of octanoic acid adapted from Heintz et al.²⁸

The primary difference between the two spectra is the appearance of a carbonyl peak around 1715 cm⁻¹ in Heintz's spectra which is probably due to unremoved starting material. The Si-O peak is broader and weaker compared to the current method. These differences are probably due to the method of purification. Where Heintz relied on a vacuum oven to remove the unreacted starting material, the purification using Soxhlet dialysis which is a more efficient method, for the removal of the high boiling point 1-octanoic acid.

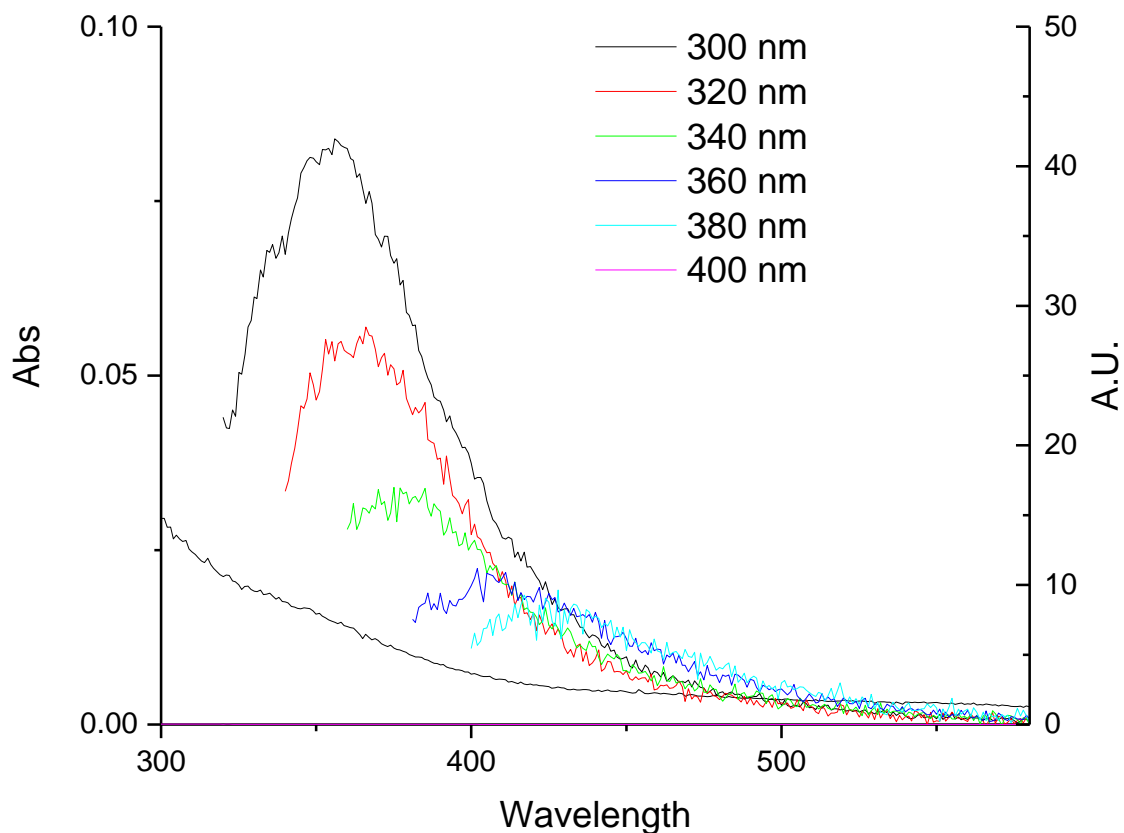


Figure 2.5 Photoluminescence of octanoic acid passivated silicon nanoparticles (in DCM). Normalized by the UV-vis absorbance.

The photoluminescence spectrum was taken in dichloromethane and shows the expected absorbance/emission shift that is typically observed with silicon nanoparticles. An absorbance of 300 nm results in an emission at 356 nm. The other shifts average about 40 nm. A red shift is observed as the increasing wavelength of light excites populations of larger nanoparticles.¹⁰ When viewed using a bench top UV-lamp, a blue

luminescence is observed for the octanoic acid passivated silicon nanoparticles. After fractionation by GPC, there is no discernible change in the color of the different fractions.

The absorbance spectrum of the nanoparticles was also taken in dichloromethane. There is a long absorbance tail that is characteristic of indirect bandgap nanoparticles.^{7, 10,}

12, 15

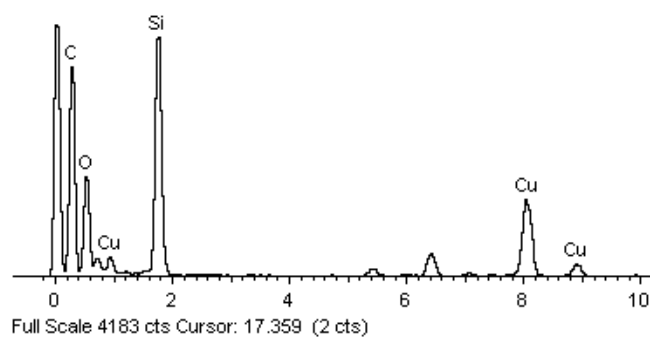


Figure 2.6 EDS spectrum of Figure 2. TEM image of octanoic acid passivated silicon nanoparticles.

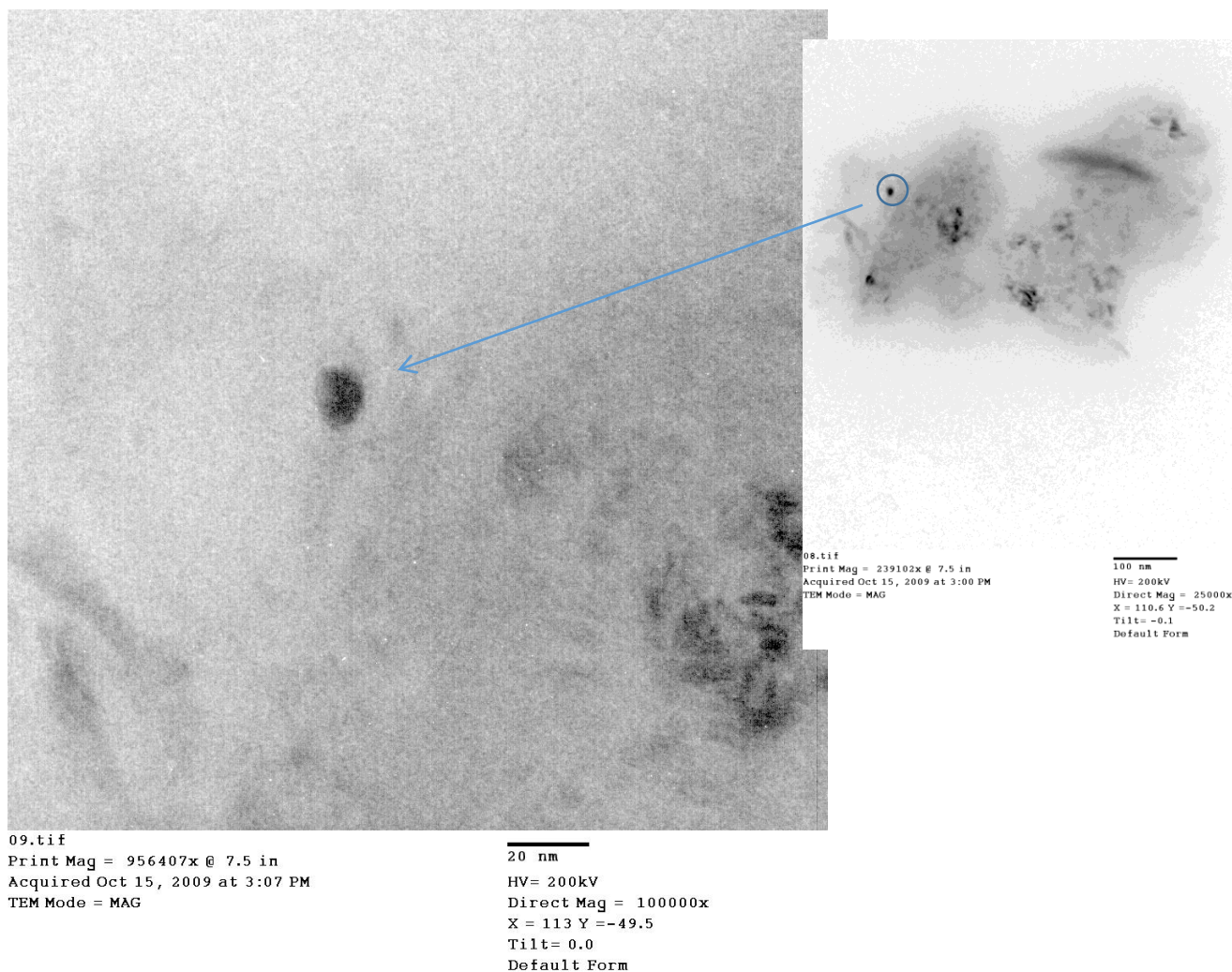


Figure 2.7 TEM image of octanoic acid passivated silicon nanoparticles.

The TEM image was taken using toluene as the solvent and was dispersed on a formvar coated copper grid. The images show that the particles tend to aggregate as seen in Figure 2.7. The corresponding EDS spectrum shows that there is a strong silicon signal at 1.9 KeV. There is also a strong carbon signal, though that is also partially due to the

formvar coating on the grid. The silicon signal though is very good evidence for silicon nanoparticles.

An HRTEM of the same sample, shown in Figure 2.8, reveals lattice fringes reflecting the crystallinity of the silicon nanoparticles. This result shows that the RHEBM process does not destroy the crystallinity of the starting crystalline chips. The lattice fringes are spaced at an average distance of approximately 3.2 Å which corresponds to the silicon $d_{(111)}$ spacing of 3.135 Å.³² Lattice fringes were measured using ImageJ software. Ten consecutive lattice fringes were counted and then measured using a calibrated straight line. This line is shown as a red bar in Figure 2.8.

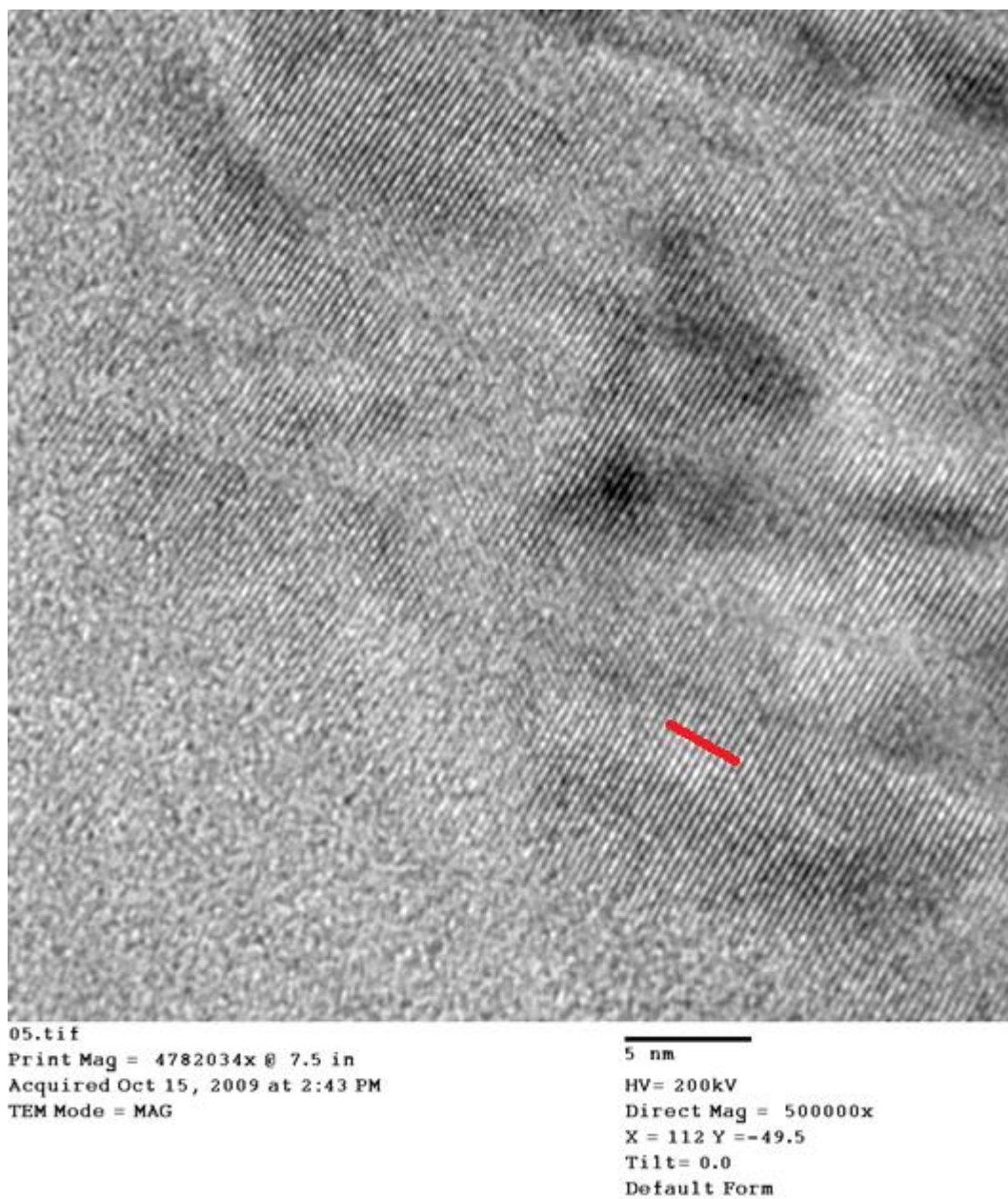


Figure 2.8 High resolution image of octanoic acid passivated silicon nanoparticles with lattice fringes.

1-Hexanoic acid passivated silicon nanoparticles.

1-Hexanoic acid passivated silicon nanoparticles were synthesized by milling 25 mL of 1-hexanoic acid with 1.25 grams of silicon chips for 12 hours. After milling, the product was purified by Soxhlet extraction.

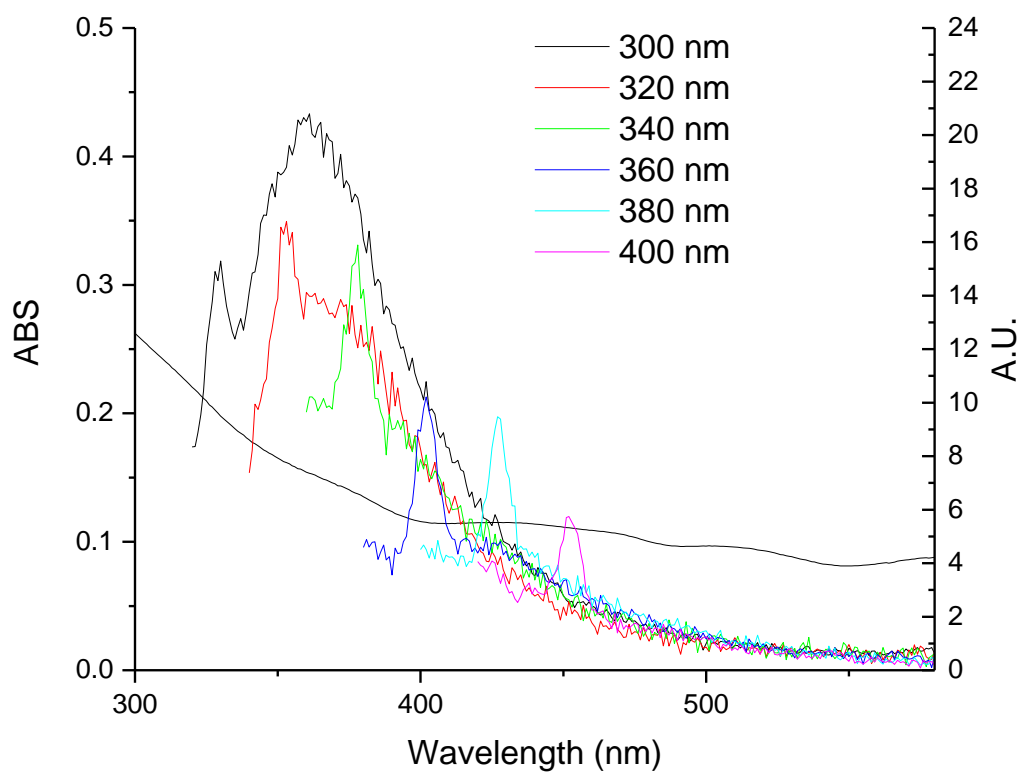


Figure 2.9 Photoluminescence of 1-hexanoic acid passivated silicon nanoparticles.

Normalized by UV-vis absorbance.

The photoluminescence of the hexanoic acid passivated silicon nanoparticles is very weak. There is still a typical absorbance/emission shift to the red with increasing excitation wavelength. The changing of the filter during the recording of the spectrum has introduced artifacts into the spectrum which are amplified by the low luminescence intensity of the particles.

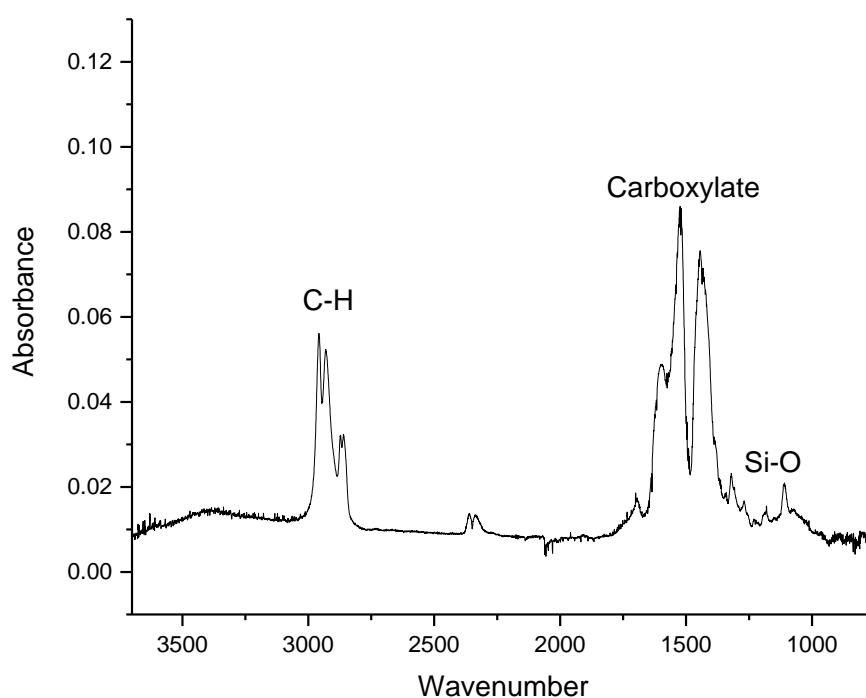


Figure 2.10 Infrared spectrum of hexanoic acid passivated silicon nanoparticles.

The sample was prepared for IR by depositing a solution of nanoparticles in dichloromethane on a KBr plate and allowing the dichloromethane to evaporate, leaving

behind a thin film. The infrared spectrum shows that the carboxylate bonds in a bidentate fashion with the silicon nanoparticle. This is evident from the symmetric and antisymmetric stretching vibrations seen at 1526 and 1442 wavenumbers. The absence of any stretch at 1715 wavenumbers shows that no free carboxylic acid is present in the sample. There is a small feature centered around 3300 wavenumbers which is likely due to the Si-OH that was formed on the surface of the nanoparticle, from the oxidation of Si-H. There is also a small feature at about 2300 wavenumbers that might be attributed to Si-H. It could possibly be an overtone, or combination band, perhaps of the Si-O which is present at around 1100 wavenumbers.

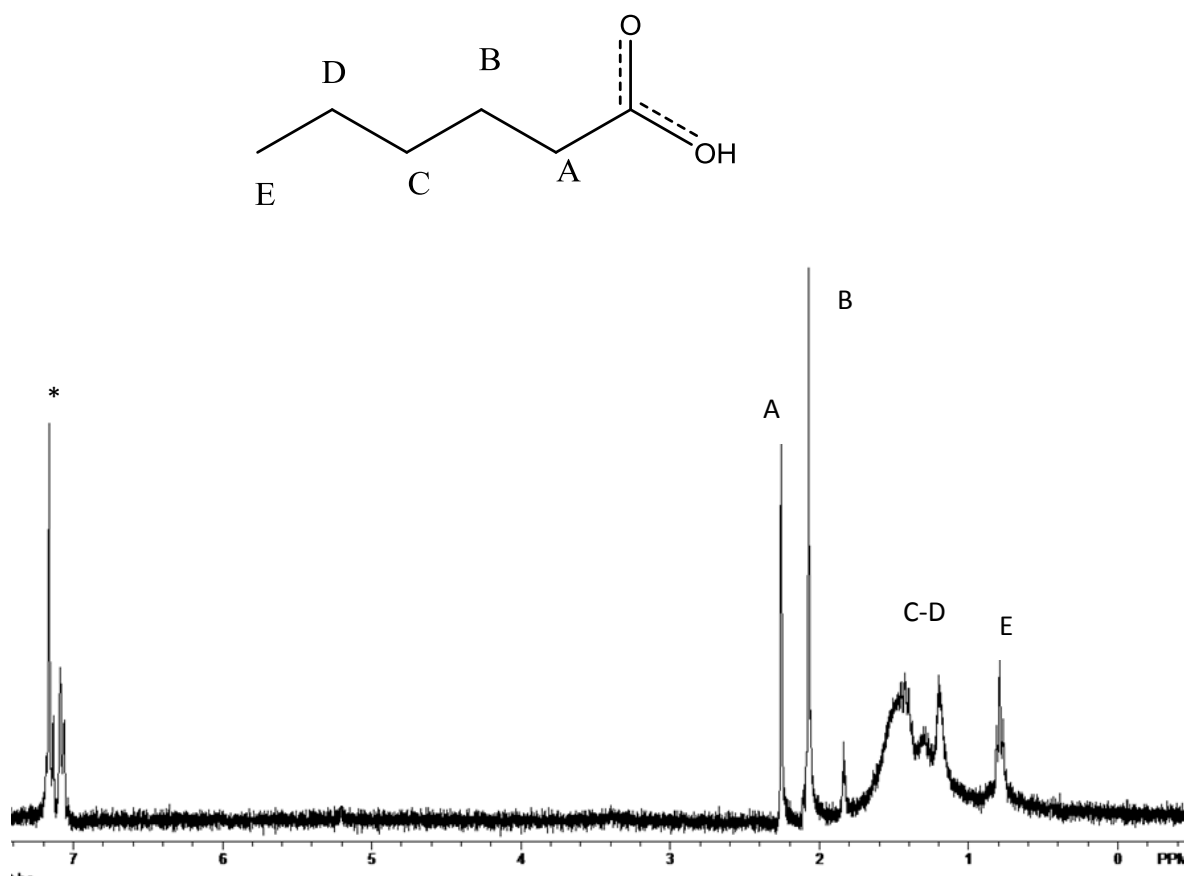


Figure 2.11 ^1H NMR of hexanoic acid passivated silicon nanoparticles. (* = CDCl_3)

The ^1H NMR shows the hexanoic acid functionalized nanoparticles in a reasonably pure state. Purification is a concern with all of the carboxylic acid systems as the boiling points do not allow for easy removal of the starting material. The peaks denoted as A and B are expected to be the protons closest to the carboxylate group. Also shown is the aliphatic region shown between 1 ppm and 1.8 ppm. The methyl group, denoted as E is shown at 0.8 ppm. These peak differ from that of pure 1-hexanoic acid, with a slight shift up field, which also lends evidence of the formation of a covalent bonding to the silicon nanoparticle.

The hexanoic acid passivated silicon nanoparticles showed decent luminescence, a clean infrared spectrum, and a ^1H NMR spectrum that was largely free of impurities. The boiling point of hexanoic acid being 205°C is the largest problem with the synthesis. Such a high boiling point does not allow efficient removal of starting material by evaporation. Soxhlet dialysis had to be used which is time consuming as it requires 36 hours. However, the data shows that silicon nanoparticles can be successfully synthesized by this process.

1-Pentanoic acid passivated silicon nanoparticles.

1-Pentanoic passivated silicon nanoparticles were synthesized by milling 25 mL of 1-pentanoic acid with 1.25 grams of silicon chips for 12 hours. 1-Pentanoic acid has a boiling point of 186°C , so the same issues of purification were still present. Namely the inability to evaporate the starting material and the need to use Soxhlet extraction using a regenerated cellulose membrane. This was done for 36 hours which is a considerable

longer time for purification than the removal of the starting material by rotary evaporation which is done within 30 minutes.

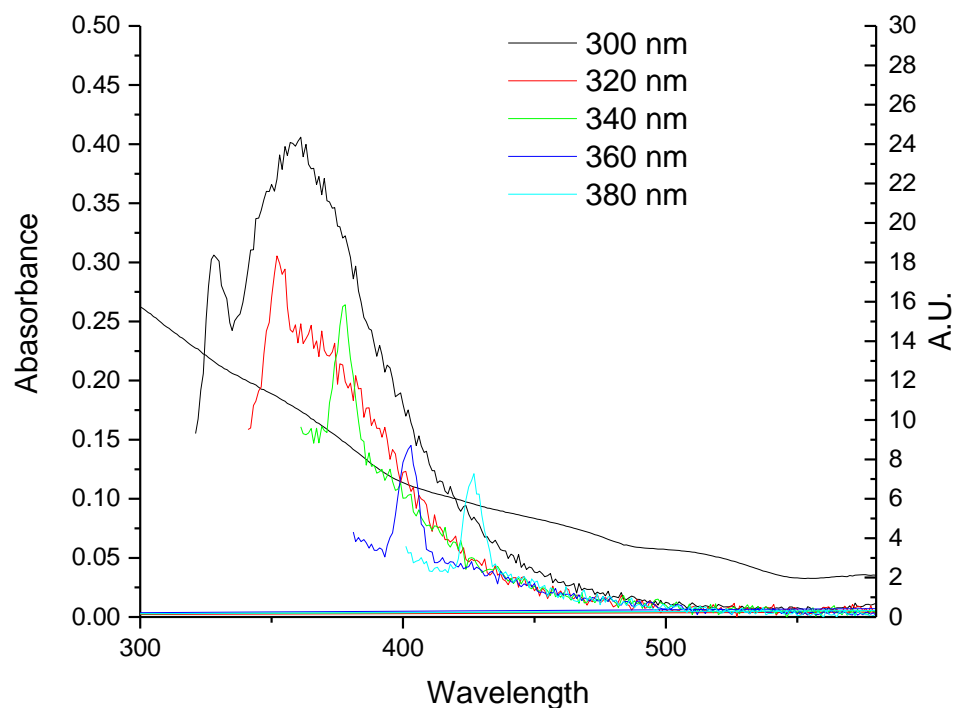


Figure 2.12 Absorbance and photoluminescence spectrum of 1-pentanoic acid passivated silicon nanoparticles in ethyl acetate. Normalized by the UV-vis absorbance.

The photoluminescence spectrum is similar to the systems already discussed in this chapter. The luminescence of the 1-pentanoic acid passivated silicon nanoparticles is not strong, with a maximum intensity of 20 arbitrary units based on the normalized spectra

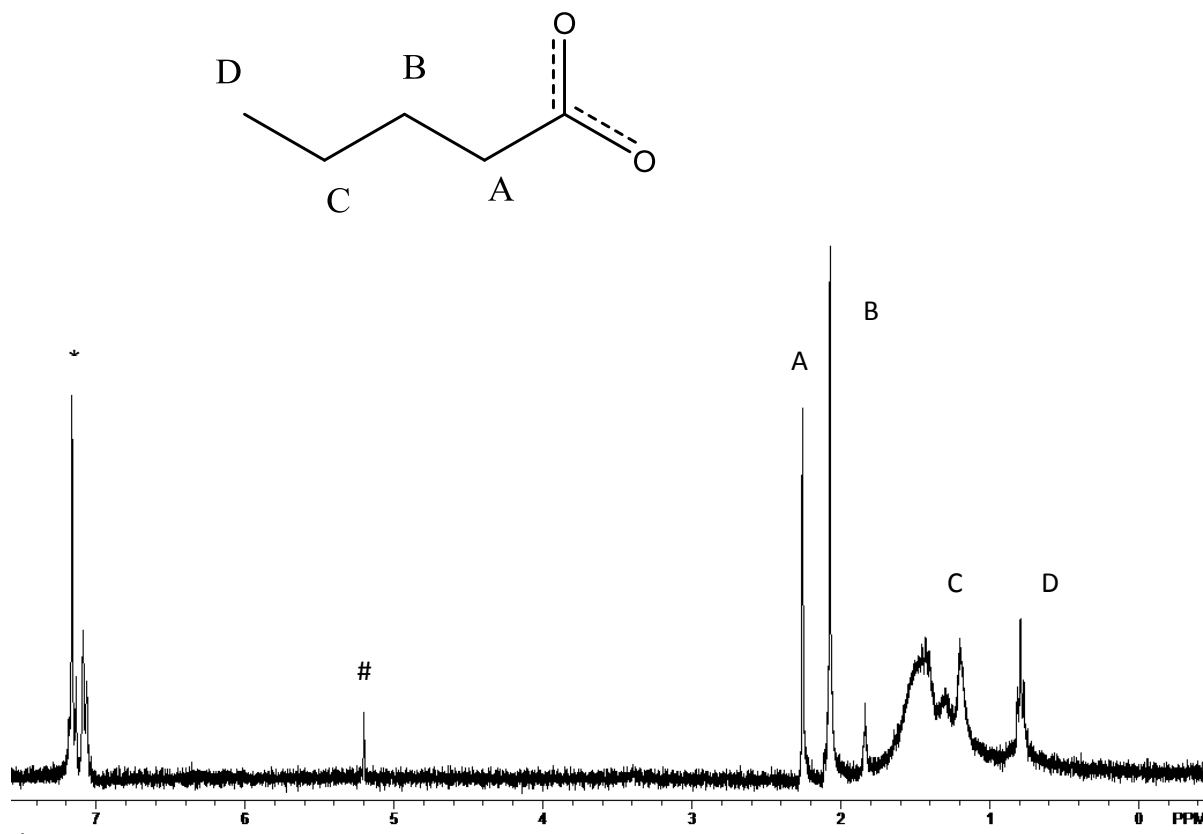


Figure 2.13 ^1H NMR spectrum of 1-pentanoic acid passivated silicon nanoparticles in CDCl_3 . * = CDCl_3 and # = CH_2Cl_2

The ^1H NMR spectrum shows the peaks denoted by A at 2.2 ppm and B at 2.0 ppm. The methyl group denoted D is seen at 0.8 ppm with the aliphatic region with C from 1.0 ppm to 1.6 ppm. The spectrum shows that the nanoparticles are largely free

from impurities except for a small peak at 5.2 ppm which is attributed to dichloromethane.

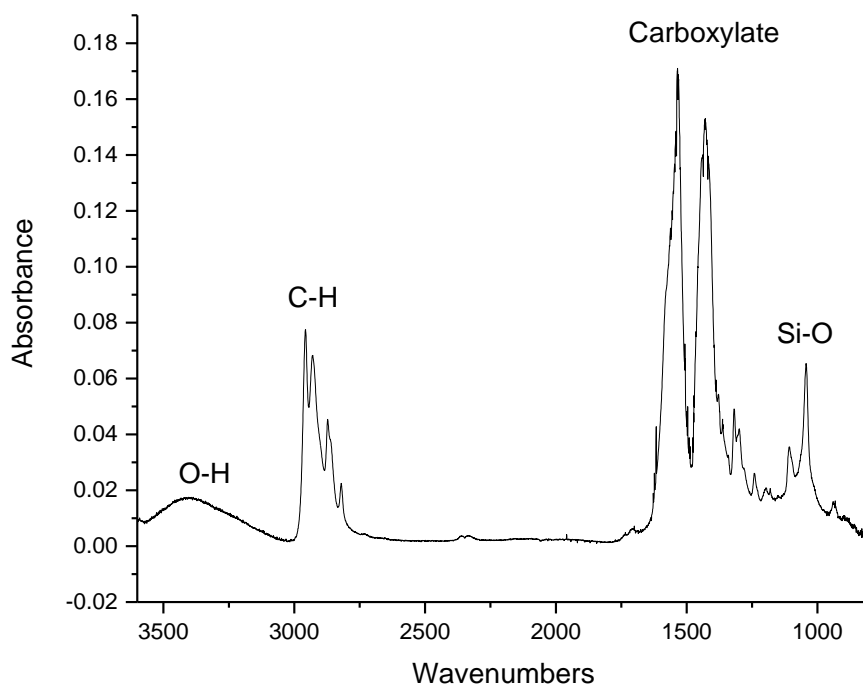


Figure 2.14 Infrared spectrum of 1-pentanoic acid passivated silicon nanoparticles.

The infrared spectrum show the carboxylate peaks at 1532 and 1428 wavenumbers.³¹ A broad peak centered around 3300 wavenumbers is most likely adventitious water from sample preparation as seen before in previous sections. Also, as seen before in previous sections there is a broad peak around 1100 wavenumbers for Si-O. There is no carbonyl peak observed at 1715 wavenumbers showing that there is no free carboxylic acid starting material remaining in the product.

Section 2.3.2: RHEBM of silicon with monocarboxylic acids and dicarboxylic acids

Once it was confirmed that carboxylic acids passivated silicon nanoparticles by the synthesis of silicon nanoparticles with monoacids, the addition of a functional group distal from the surface of the silicon nanoparticle was attempted by the use of α,ω -diacids. These acids are mixed with monoacids to prevent the diacids from forming hair pins and both ends reacting with the silicon surface, by diluting the percentage of diacid chains.

1-Hexanoic acid/ 1,6-hexanedioic acid passivated silicon nanoparticles.

1,6-Hexanedioic acid, a six carbon chain di-carboxylic acid was chosen as a coreactant in order to introduce a carboxylic group, distal from the surface, as illustrated in Figure 2.14.

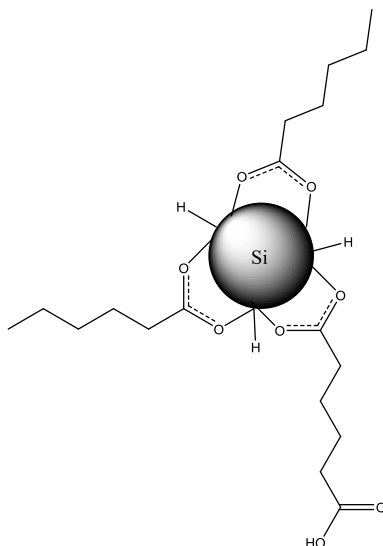


Figure 2.15 Initially formed silicon nanoparticle passivated by 1,6-hexanedioic acid/hexanoic acid.

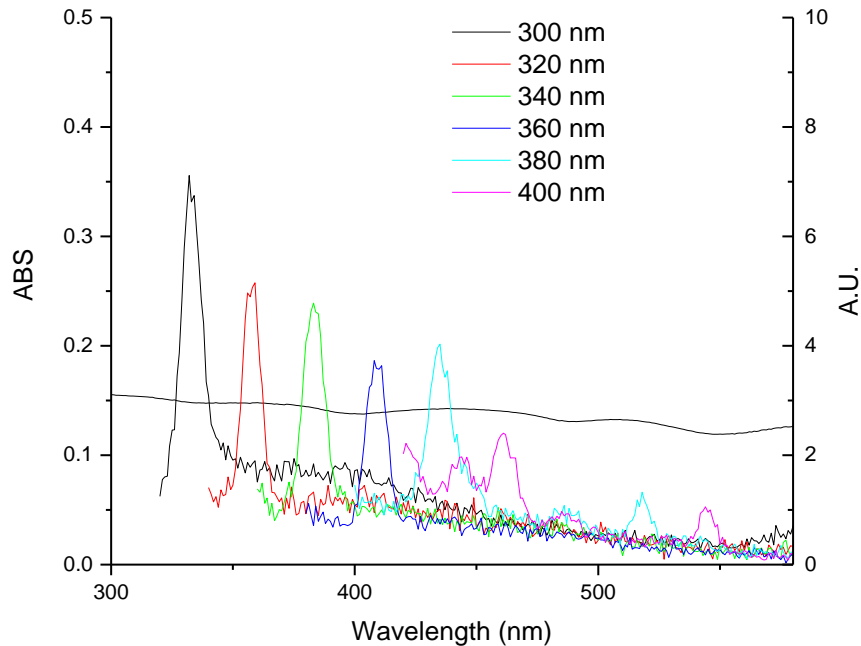


Figure 2.16 Photoluminescence of hexanoic acid/ 1,6-hexanedioic acid nanoparticle attempt.

The unsuccessful synthesis of silicon nanoparticles can clearly be seen in the photoluminescence spectrum. Very little luminescence was observed and major features could be characterized as noise and artifacts from the filters being changed during the recording of the spectrum. This failure however, shows that the solubility is very important to the process. Not only were the anticipated silicon nanoparticles not produced, but also no hexanoic acid passivated nanoparticles were evident. As shown in the preceding section, hexanoic acid passivated silicon nanoparticles are produced by RHEBM in the presence of hexanoic acid.

The unsuccessful synthesis of the 1,6-hexanedioic acid/hexanoic acid functionalized silicon nanoparticles is probably due to the insolubility of the solid 1,6-

heanedioic acid in the hexanoic acid, which results in a two phase system in the milling vial. The 1,6-hexanedioic acid which was not soluble in the hexanoic acid likely provided a soft barrier between the milling ball, silicon wafer, and the wall of the steel vial. While the wafers were reduced in size after the milling was completed, the yield was a very low 9 mg.

1-Pentanoic acid/ 1,7-heptanedioic acid (5%) passivated silicon nanoparticles.

The α,ω - dicarboxylic acid, 1,7-heptanedioic acid, was chosen as a coreactant due to its significantly longer chain length relative to 1-pentanoic acid (7 carbons versus 5) which should eventually facilitate the amide bond conjugation reaction. In addition, 1,7-heptanedioic acid shows slight solubility in 1-pentanoic acid. As seen in the system with hexanoic acid and 1,6-hexanedioic acid, this is a very important aspect, as insoluble material prohibited the formation of any silicon nanoparticles. The 1,7-heptanedioic acid was only slightly soluble though, which is the limiting factor in the percentage of terminal carboxylic acids that can be added to the silicon nanoparticle. Only 5% molar solution of 1,7-heptanedioic acid dissolved in 1-pentanoic acid was possible before the solubility limit was reached.

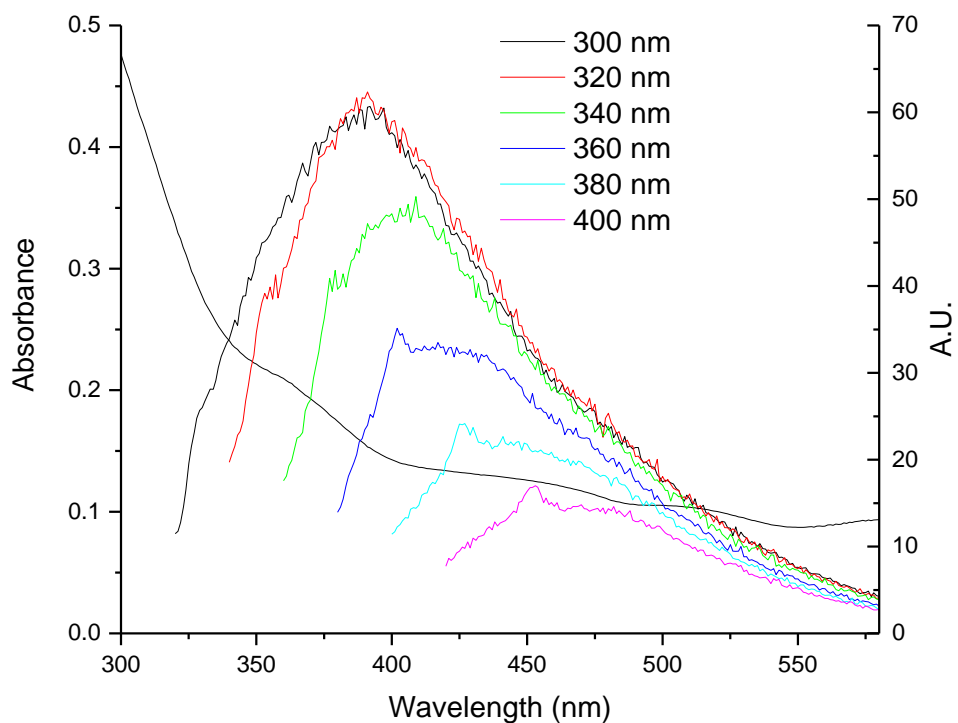


Figure 2.17 Photoluminescence of 1-pentanoic acid/ 1,7-heptanedioic acid (5%) passivated silicon nanoparticles. Normalized by the UV-vis absorbance.

The photoluminescence spectrum shows the greatest intensity of all the carboxylic acid functionalized silicon nanoparticles. As can be seen in figure 2.16, the emission maxima reaches over 60 arbitrary units.

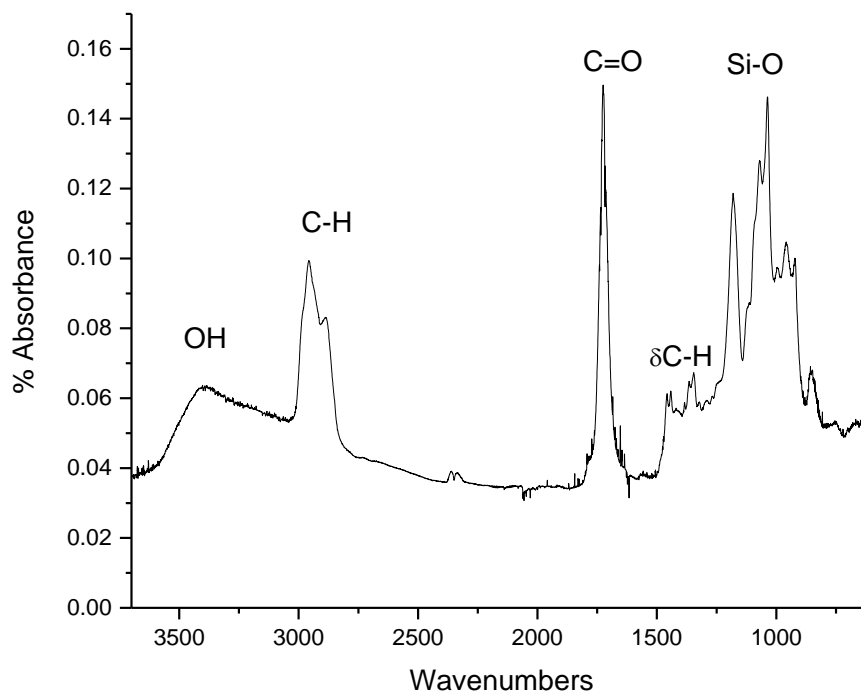


Figure 2.18 Infrared spectrum of 1-pentanoic acid/ 1,7-heptanedioic acid (5%) passivated silicon nanoparticles.

The infrared spectrum of the 1-pentanoic acid/1,7-heptanedioic acid (5%) silicon nanoparticles shows the wide absorption of a carboxylic acid. From 3500-2000 wavenumbers is a very broad peak which is indicative of a carboxylic acid with hydrogen bonding.³¹ A peak at 1725 wavenumbers is the carbonyl stretch of the carboxylic acid and suggests a monodentate bonding mode. Also, a very broad and prominent peak is observed centered around 1100 wavenumbers attributable to the Si-O stretching vibration.

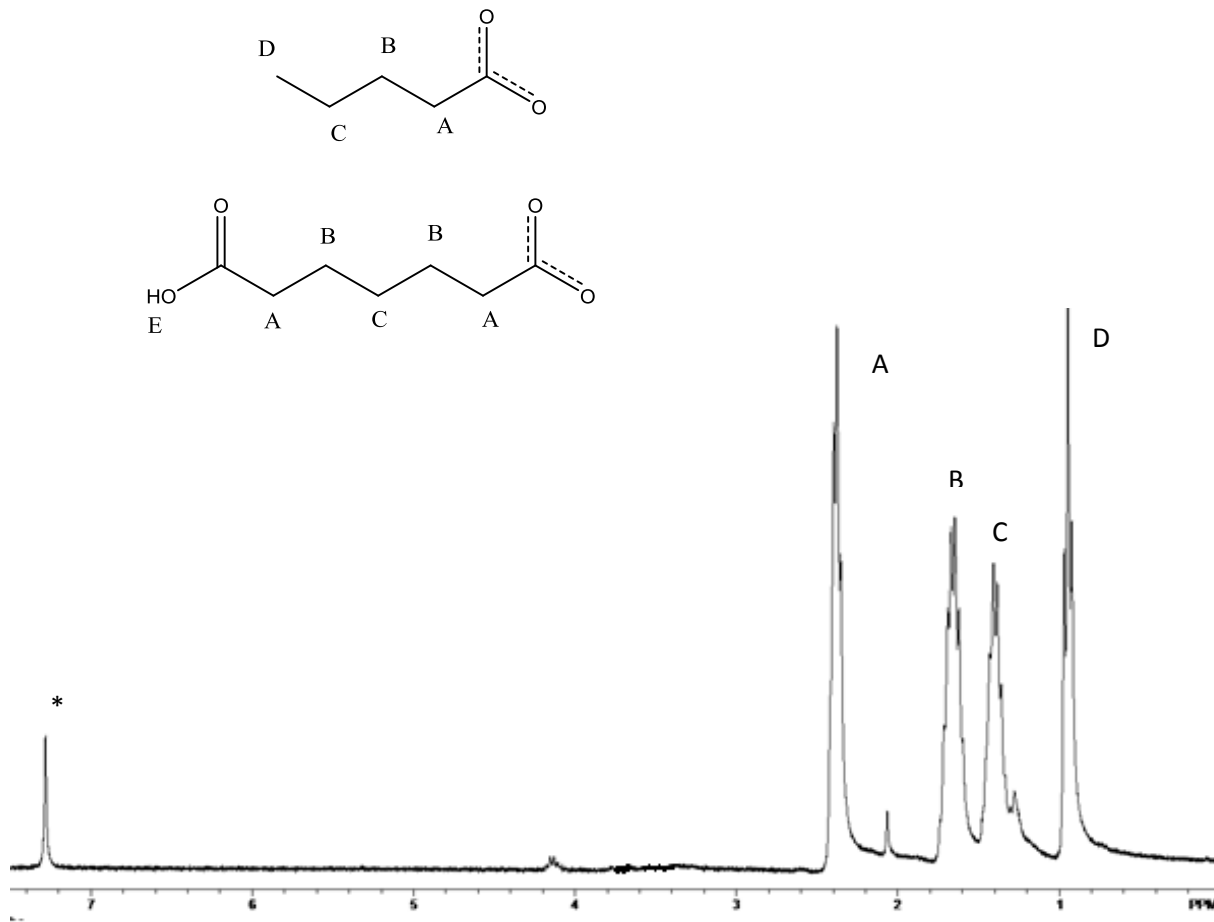
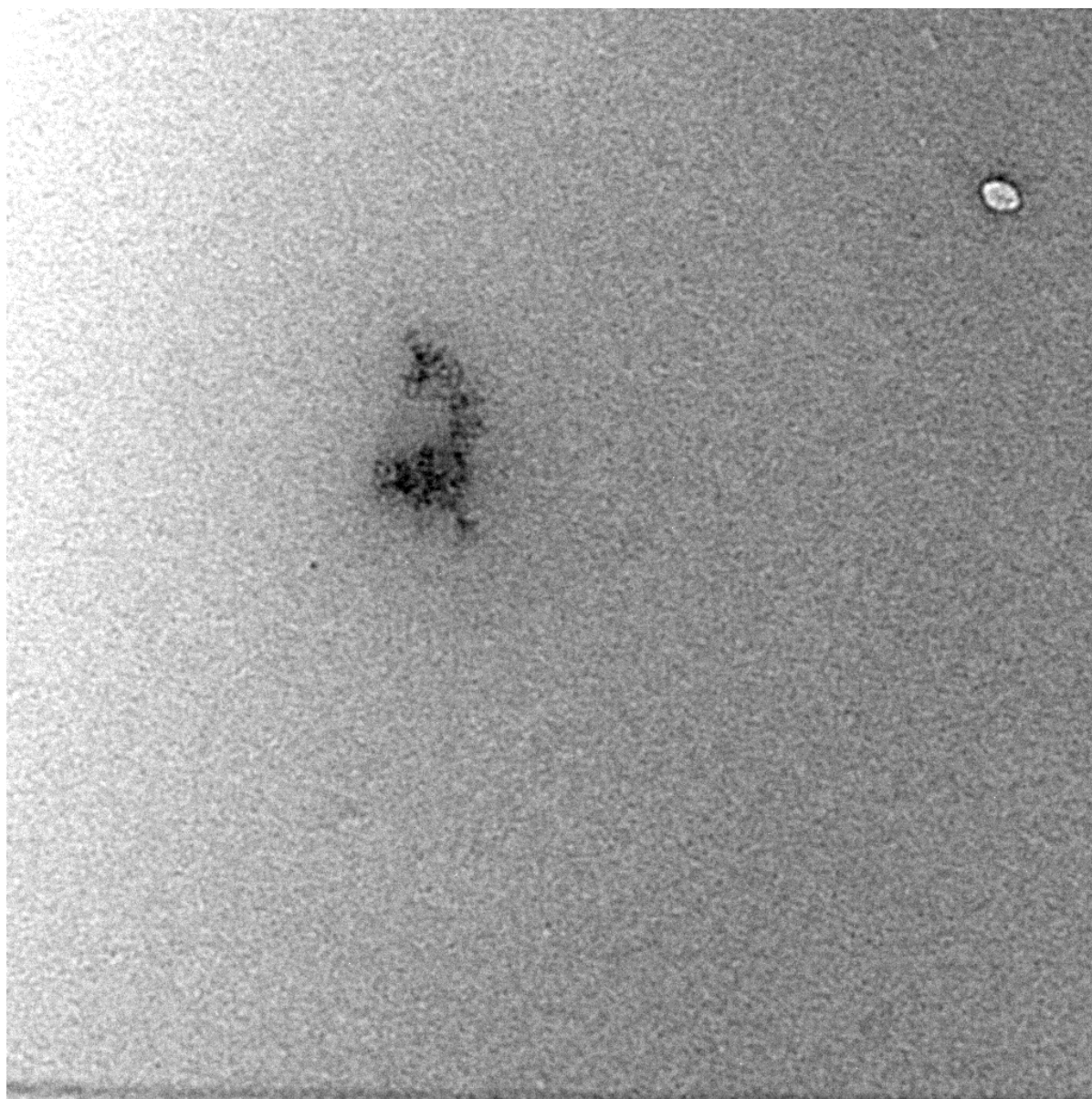


Figure 2.19 ^1H NMR spectrum of 1-pentanoic acid/ 1,7-heptanedioic acid (5%) passivated silicon nanoparticles. (* = CDCl_3)

The ^1H NMR spectrum shows the expected peaks A,B,C, and D. Their assignments are noted on the inset of figure 2.19. A peak for E, the carboxylic acid proton, is not observed. However, the IR spectrum shows that there is a carboxylic acid functional group present with a high degree of hydrogen bonding.



img11.tif

Print Mag = 143461x @ 7.5 in

Acquired Mar 1, 2012 at 4:12 PM

TEM Mode = MAG

100 nm

HV=200.0kV

Direct Mag = 15000x

X = 620 Y = -41

Tilt=

Default Form

Figure 2.20 Low resolution TEM of 1-pentanoic acid/ 1,7-heptanedioic acid (5%) passivated silicon nanoparticles.

The TEM showed that the 1-pentanoic acid/ 1,7-heptanedioic acid (5%) passivated silicon nanoparticles were agglomerated. This is perhaps due to hydrogen bonding between the carboxylic acids which promotes agglomeration. Also, the EDS shows low concentration of silicon as seen in Figure 2.21 at 1.8 KeV.

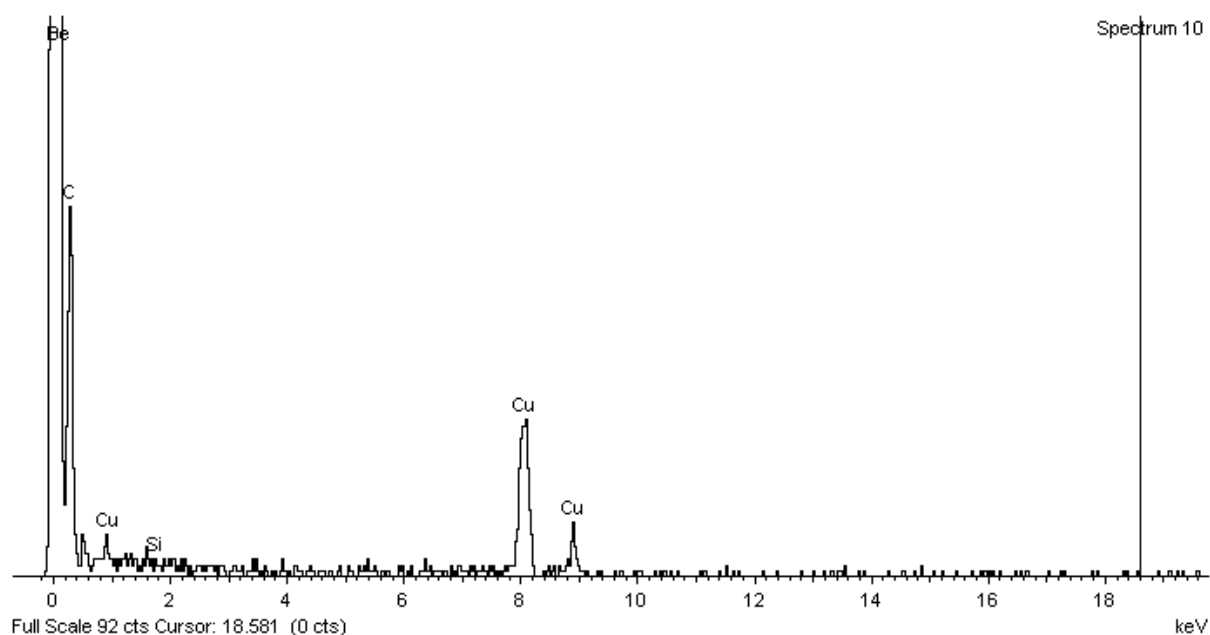


Figure 2.21. EDS of 1-pentanoic acid/ 1,7-heptanedioic acid (5%) passivated silicon nanoparticles.

The existence of the terminal carboxylic acid, was tested by a conjugation reaction with a strand of DNA in collaboration with Dr. David Harris previously of the Dr. Jayawickramarajah group. However, the reaction failed. This could be because of two problems. First, the carboxylic acid has formed an ester. Secondly, the amount of terminal carboxylic acid was too low. The solubility of the 1,7-heptanedioic acid limits the amount of possible free carboxylic acid to just 5% by molar concentration. This may

have been too small a concentration and so a method for a larger concentration of terminal carboxylic acid became the new goal.

Section 2.3.3: RHEBM of complexes in an inert solvent

The solubility of the di-carboxylic acids is the limiting factor in the synthesis of silicon nanoparticles that have a terminal carboxylic acid functional group. This can be seen in the preceding section of the 1-pentanoic acid/ 1,7-heptanedioic acid(5%) passivated silicon nanoparticles. One method of trying to solve this problem is the use of a solvent that will dissolve the carboxylic acids but will not react with the silicon wafers to form nanoparticles or side products. One solvent that was found to meet these requirements was toluene. A control experiment was run using benzoic acid dissolved in toluene.

Benzoic acid passivated silicon nanoparticles.

The synthesis of benzoic acid passivate silicon nanoparticles was attempted by the milling of 30 mL of Toluene, 2 grams of silicon wafer, and 2 grams of benzoic acid for 12 hours in a nitrogen atmosphere. The larger insoluble sediment was separated by centrifugation and purified by Soxhlet extraction. The average yield was about 20 mg.

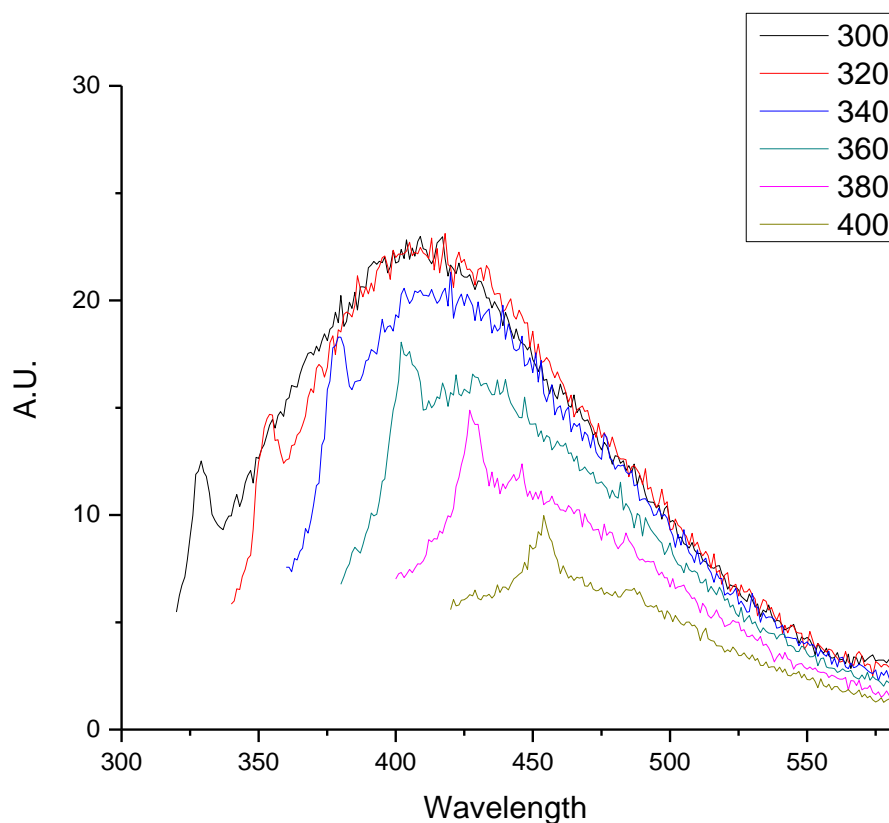


Figure 2.22 Photoluminescence of benzoic acid passivated silicon nanoparticles. Normalized by UV-vis absorbance.

The photoluminescence spectrum for the benzoic acid passivated silicon nanoparticles shows decent luminescence. The absorption/emission shift is once again observed as with all of the silicon nanoparticle systems that have been studied. The first absorbance of 300 nm, shows an emission maxima at 408 nm. The second absorbance wavelength of 320 nm, shows an emission maxima at 416 nm. The third absorbance of 340 nm shows the emission maxima at 418 nm. These emission maximums do not shift to the same degree as shown with other silicon nanoparticles that were passivated with other

carboxylic acids. This may be due to the fact that we do not see a difference in populations of different sizes. This milling process did not produce as many silicon nanoparticles (yield of only 20 mg) and those particles may not be as polydisperse, resulting in a photoluminescence spectra that does not show the shift exhibited by other passivated silicon nanoparticles.

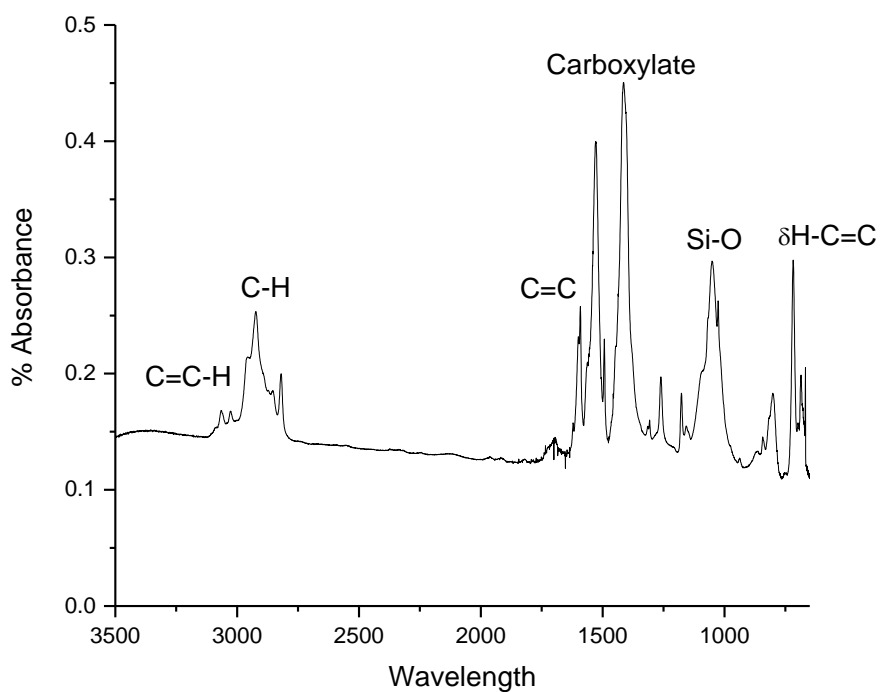


Figure 2.23 Infrared spectrum of benzoic acid passivated silicon nanoparticles.

The infrared spectrum shows the characteristic peaks of a carboxylate at 1530 and 1417 wavenumbers. Also observed is the alkene hydrogen stretch at 3067 wavenumbers, the aromatic alkene vibration at 1591 wavenumbers, and the alkene bending vibrations at 717 wavenumbers. These peaks show that the benzoic acid is bound to the silicon

nanoparticle and that there is no free benzoic acid present as there is no carbonyl peak observed at 1715 wavenumbers. Also, observed is the Si-O vibration around 1100 wavenumbers. The presence of these expected peaks, and the absence of the peaks associated with the starting material proves that the benzoic acid has been successfully attached to the silicon nanoparticle through the carboxylic acid.

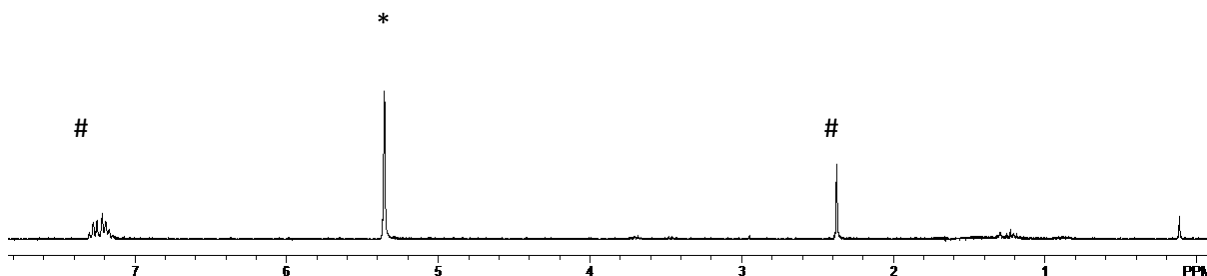


Figure 2.24 ^1H NMR spectrum of benzoic acid passivated silicon nanoparticles. (* = CDCl_2) (# = residual protons of toluene)

The ^1H NMR of the benzoic acid passivated silicon nanoparticles shows toluene. Toluene was used in the milling process and was also used during the purification process. The reason for such unexpected results is likely due to the small amount of product formed and the sparing solubility of the product in the NMR solvent, chloroform. This leads to the results shown by the NMR to be inconclusive.

The spectral data shows that benzoic acid passivated silicon nanoparticles may have been synthesized. However, it needed the help of an addition solvent that is

unreactive with silicon. While this does show that there is a possibility of using an unreactive solvent to synthesize carboxylic acid passivated silicon nanoparticles, the volume of solvent needed becomes an issue. The milling vial should only be filled about 50% (30 mL max) with liquid. Increased volume will likely have an impact of the production of silicon nanoparticles as the increased volume may impact the velocity and momentum of the milling balls. As seen with the hexanoic acid/ 1,6-hexanoic acid system, the production of nanoparticles is affected by the conditions in the milling vial. The addition of an insoluble mass in the vial resulted in no nanoparticles. The degree to which the increased volume would affect the production of silicon nanoparticles was not examined as part of this project.

Section 2.4: Conclusion

Silicon nanoparticles were synthesized from monocarboxylic acids, a mixture of monocarboxylic acids and dicarboxylic acids. They were characterized using photoluminescence, UV-Vis absorption spectroscopy, ^1H NMR, and TEM. The different systems were chosen in an effort to reach the goal of silicon nanoparticles with a terminal carboxylic acid.

The carboxylic acids presented several problems. They had high boiling points which meant that the purification was limited to dialysis. Moving to Soxhlet dialysis presented a large gain in both the time reduction needed to purify the products and also a savings in the volumes of organic solvents needed to purify the products. The use of dicarboxylic acids for a straight forward reaction with the carboxylic acids to produce terminal carboxylic acids, was severely hampered by the solubility problems that the dicarboxylic acids presented. As seen with the hexanoic acid/1,6-hexanedioic acid system, the insoluble 1,6-hexanedioic acid not only prevented the formation of a terminal carboxylic acid nanoparticle, but it also prevented the hexanoic acid passivated particle from being formed. Earlier experiments had been able to produce the hexanoic acid passivated nanoparticle, but the insoluble 1,6-hexanedioic acid acted in some way to prevent this from happening. It is most likely that the insoluble 1,6-hexanedioic acid acted as a cushion between the milling ball and the wafer, or it increased the viscosity of the milling solution, inducing drag on the milling ball and decreasing its momentum.

Nanoparticles synthesized with the aid of an unreactive solvent to dissolve the carboxylic acid was successfully completed. This was done with the solid carboxylic acid benzoic acid as a control experiment. Toluene was shown to be a possible solvent as it is

unreactive and does not lead to side products. However, using increasingly complicated milling solutions led to increasing the volume of liquid required for each milling. The milling vial is recommended to only be filled with 25 mL.³³ For this reason, this line of investigation was discontinued and a new approach was sought.

Another drawback to the carboxylic acid systems is the low intensity of photoluminescence as compared to the alkene systems. The major goal of the entire project is to produce silicon nanoparticles which will have applications that are relevant to biology. In order for this goal to be obtained, it is necessary that the nanoparticles display sufficient quantum yield of luminescence that they are biologically relevant for labeling processes.

The original hypothesis that the chain length would have an impact on the yield was upheld by the results. Silicon nanoparticles passivated with 1-octanoic yield an average yield of 45 mg, 1-hexanoic acid yield an average of 30 mg, and 1-pentanoic acid yielded an average yield of 25 mg. All experimental variables were held constant except for the chain length carboxylic acid used. Also, the use of a dicarboxylic acid greatly decreased the yields as it prohibited the formation of a product in most cases.

References

1. Baldwin, R. K.; Pettigrew, K. A.; Ratai, E.; Augustine, M. P.; Kauzlarich, S. M., Solution reduction synthesis of surface stabilized silicon nanoparticles. *Chemical Communications* **2002**, (17), 1822-1823.
2. Sato, S.; Swihart, M. T., Propionic-Acid-Terminated Silicon Nanoparticles: Synthesis and Optical Characterization. *Chemistry of Materials* **2006**, *18* (17), 4083-4088.
3. Rogozhina, E. V.; Eckhoff, D. A.; Gratton, E.; Braun, P. V., Carboxyl functionalization of ultrasmall luminescent silicon nanoparticles through thermal hydrosilylation. *Journal of Materials Chemistry* **2006**, *16* (15), 1421-1430.
4. Eckhoff, D. A.; Sutin, J. D. B.; Clegg, R. M.; Gratton, E.; Rogozhina, E. V.; Braun, P. V., Optical Characterization of Ultrasmall Si Nanoparticles Prepared through Electrochemical Dispersion of Bulk Si. *The Journal of Physical Chemistry B* **2005**, *109* (42), 19786-19797.
5. Mayeri, D.; Phillips, B. L.; Augustine, M. P.; Kauzlarich, S. M., NMR Study of the Synthesis of Alkyl-Terminated Silicon Nanoparticles from the Reaction of SiCl₄ with the Zintl Salt, NaSi. *Chemistry of Materials* **2001**, *13* (3), 765-770.
6. Zou, J.; Baldwin, R. K.; Pettigrew, K. A.; Kauzlarich, S. M., Solution Synthesis of Ultrastable Luminescent Siloxane-Coated Silicon Nanoparticles. *Nano Letters* **2004**, *4* (7), 1181-1186.
7. Manhat, B. A.; Brown, A. L.; Black, L. A.; Ross, J. B. A.; Fichter, K.; Vu, T.; Richman, E.; Goforth, A. M., One-Step Melt Synthesis of Water-Soluble, Photoluminescent, Surface-Oxidized Silicon Nanoparticles for Cellular Imaging Applications. *Chemistry of Materials* **2011**, *23* (9), 2407-2418.
8. Holmes, J. D.; Ziegler, K. J.; Doty, R. C.; Pell, L. E.; Johnston, K. P.; Korgel, B. A., Highly Luminescent Silicon Nanocrystals with Discrete Optical Transitions. *Journal of the American Chemical Society* **2001**, *123* (16), 3743-3748.
9. Hessel, C. M.; Henderson, E. J.; Veinot, J. G. C., Hydrogen Silsesquioxane: A Molecular Precursor for Nanocrystalline Si-SiO₂ Composites and Freestanding Hydride-Surface-Terminated Silicon Nanoparticles. *Chemistry of Materials* **2006**, *18* (26), 6139-6146.
10. Heintz, A. S.; Fink, M. J.; Mitchell, B. S., Mechanochemical Synthesis of Blue Luminescent Alkyl/Alkenyl-Passivated Silicon Nanoparticles. *Advanced Materials* **2007**, *19* (22), 3984-3988.
11. Verdoni, L. P.; Fink, M. J.; Mitchell, B. S., A fractionation process of mechanochemically synthesized blue-green luminescent alkyl-passivated silicon nanoparticles. *Chemical Engineering Journal* **2011**, *172* (1), 591-600.
12. Hallmann, S.; Fink, M. J.; Mitchell, B. S., Mechanochemical synthesis of functionalized silicon nanoparticles with terminal chlorine groups. *Journal of Materials Research* **2011**, *26* (08), 1052-1060.

13. Kuang, L.; Mitchell, B. S.; Fink, M. J., Silicon nanoparticles synthesised through reactive high-energy ball milling: enhancement of optical properties from the removal of iron impurities. *Journal of Experimental Nanoscience* **2014**, 1-9.
14. Buriak, J. M., Organometallic Chemistry on Silicon and Germanium Surfaces. *Chemical Reviews* **2002**, 102 (5), 1271-1308.
15. Kuang, L. Mechanochemical Synthesis, Characterization, and functionalization of Vinyl-Terminated Silicon Nanoparticles. Tulane, 2014.
16. Sieval, A. B.; Demirel, A. L.; Nissink, J. W. M.; Linford, M. R.; van der Maas, J. H.; de Jeu, W. H.; Zuilhof, H.; Sudhölter, E. J. R., Highly Stable Si-C Linked Functionalized Monolayers on the Silicon (100) Surface. *Langmuir* **1998**, 14 (7), 1759-1768.
17. Chadi, D. J., Atomic and Electronic Structures of Reconstructed Si(100) Surfaces. *Physical Review Letters* **1979**, 43 (1), 43-47.
18. Voicu, R.; Boukherroub, R.; Bartzoka, V.; Ward, T.; Wojtyk, J. T. C.; Wayner, D. D. M., Formation, Characterization, and Chemistry of Undecanoic Acid-Terminated Silicon Surfaces: Patterning and Immobilization of DNA. *Langmuir* **2004**, 20 (26), 11713-11720.
19. Yang, M.; Teeuwen, R. L. M.; Giesbers, M.; Baggerman, J.; Arafat, A.; de Wolf, F. A.; van Hest, J. C. M.; Zuilhof, H., One-Step Photochemical Attachment of NHS-Terminated Monolayers onto Silicon Surfaces and Subsequent Functionalization. *Langmuir* **2008**, 24 (15), 7931-7938.
20. Wang, L.; Reipa, V.; Blasic, J., Silicon Nanoparticles as a Luminescent Label to DNA. *Bioconjugate Chemistry* **2004**, 15 (2), 409-412.
21. Sam, S.; Touahir, L.; Salvador Andresa, J.; Allongue, P.; Chazalviel, J. N.; Gouget-Laemmel, A. C.; Henry de Villeneuve, C.; Moraillon, A.; Ozanam, F.; Gabouze, N.; Djebbar, S., Semiquantitative Study of the EDC/NHS Activation of Acid Terminal Groups at Modified Porous Silicon Surfaces. *Langmuir* **2010**, 26 (2), 809-814.
22. Rosso-Vasic, M.; Spruijt, E.; Popovic, Z.; Overgaag, K.; van Lagen, B.; Grandidier, B.; Vanmaekelbergh, D.; Dominguez-Gutierrez, D.; De Cola, L.; Zuilhof, H., Amine-terminated silicon nanoparticles: synthesis, optical properties and their use in bioimaging. *Journal of Materials Chemistry* **2009**, 19 (33), 5926-5933.
23. Choi, J.; Wang, N. S.; Reipa, V., Conjugation of the Photoluminescent Silicon Nanoparticles to Streptavidin. *Bioconjugate Chemistry* **2008**, 19 (3), 680-685.
24. Guo, D.-J.; Xiao, S.-J.; Xia, B.; Wei, S.; Pei, J.; Pan, Y.; You, X.-Z.; Gu, Z.-Z.; Lu, Z., Reaction of Porous Silicon with Both End-Functionalized Organic Compounds Bearing α -Bromo and ω -Carboxy Groups for Immobilization of Biomolecules. *The Journal of Physical Chemistry B* **2005**, 109 (43), 20620-20628.
25. Park, J.-H.; Gu, L.; von Maltzahn, G.; Ruoslahti, E.; Bhatia, S. N.; Sailor, M. J., Biodegradable luminescent porous silicon nanoparticles for in vivo applications. *Nat Mater* **2009**, 8 (4), 331-336.

26. Erogbogbo, F.; Yong, K.-T.; Roy, I.; Xu, G.; Prasad, P. N.; Swihart, M. T., Biocompatible Luminescent Silicon Quantum Dots for Imaging of Cancer Cells. *ACS Nano* **2008**, 2 (5), 873-878.
27. Li, Z. F.; Ruckenstein, E., Water-Soluble Poly(acrylic acid) Grafted Luminescent Silicon Nanoparticles and Their Use as Fluorescent Biological Staining Labels. *Nano Letters* **2004**, 4 (8), 1463-1467.
28. Heintz, A. S.; Fink, M. J.; Mitchell, B. S., Silicon nanoparticles with chemically tailored surfaces. *Applied Organometallic Chemistry* **2010**, 24 (3), 236-240.
29. 8000D Mixer/Mill. http://www.spexsampleprep.com/equipment-and-accessories/equipment_product/6.
30. Jensen, W. B., The Origin of the Soxhlet Extractor. *Journal of Chemical Education* **2007**, 84 (12), 1913.
31. Robert M. Silverstein, F. X. W., David J. Kiemle, *Spectrometric Identification of Organic Compounds*. 7 ed.; John Wiley & Sons: Hoboken, 2005.
32. Chih-Hang Tung, G. T. T. S., Chih-Yuan Lu, *ULSI Semiconductor Technology Atlas*. John Wiley & Sons: Hoboken New Jersey, 2003.
33. 8007 - Stainless Steel Grinding Vial Set. http://www.spexsampleprep.com/equipment-and-accessories/accessory_product/8007 (accessed 6/22/2015).

Chapter 3: Biologically relevant transformations of the vinyl terminated silicon nanoparticle.

Section 3.1: Introduction

In chapter 2, the attempted synthesis of carboxylic acid terminated silicon nanoparticles by reactive high energy ball milling (RHEBM)¹ was described. However, the low solubility of the diacids in the co-reactant monoacids limited the production of carboxylic acid terminated silicon nanoparticles. Even the nanoparticles that were produced were hampered by a low percentage of terminal acid functional groups due to the low solubility of the di-carboxylic acids. Another route envisioned for obtaining terminal carboxylic acid functionalized silicon nanoparticles is from the oxidation of terminal vinyl functionalized silicon nanoparticles.

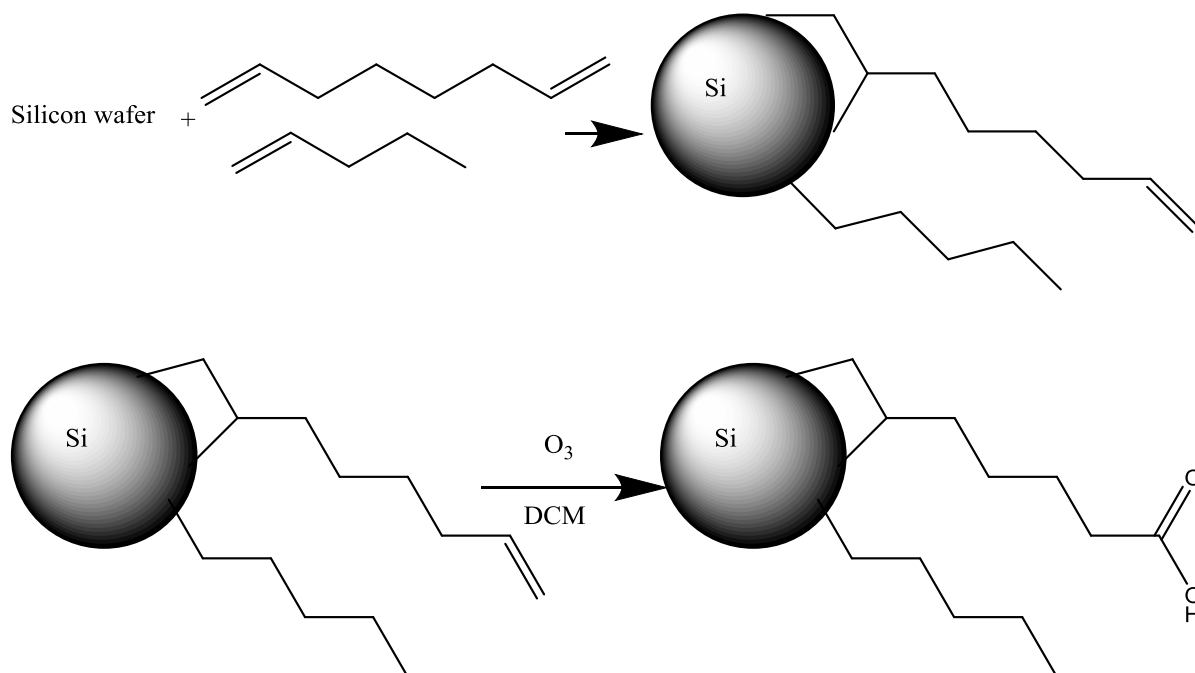
The ability for silicon nanoparticles to be used for biological processes is enhanced by the presence of a carboxylic acid functionality. This allows for the covalent conjugation of biomolecules to the silicon nanoparticles in an efficient manner. One such method that is common in probe immobilization on surfaces is to prepare a surface with a succinimidyl ester surface layer.²⁻⁵ This allows then for the reaction of the biomolecule with an amine functionality to be immobilized on the surface. This can be done with a DNA sequence or with a lysine group on the surface of a protein.²⁻⁴ This is an efficient method that can easily be applied to silicon nanoparticles. However, rather than creating an immobile surface, the nanoparticles with low cytotoxicity⁶ can be circulated throughout the human body and be

targeted to the area of interest, such as a cancer tumor.⁷⁻⁸ Silicon nanoparticles have been previously used for non-targeted fluorescent staining labels, because of their resistance to photobleaching.⁹⁻¹⁰ However, with the ability to covalently link targeting molecules to the silicon nanoparticles, the specificity of the labeling increases and the concentration of the nanoparticles at the intended target is greatly increased.¹¹

In order for this method of using silicon nanoparticles to be successful, the nanoparticles must meet several requirements. They must be safe, water soluble, high fluorescence yield, and be compatible with the molecules that are to be attached.¹⁰ These requirements are met by the design for the synthesis of the silicon nanoparticles.

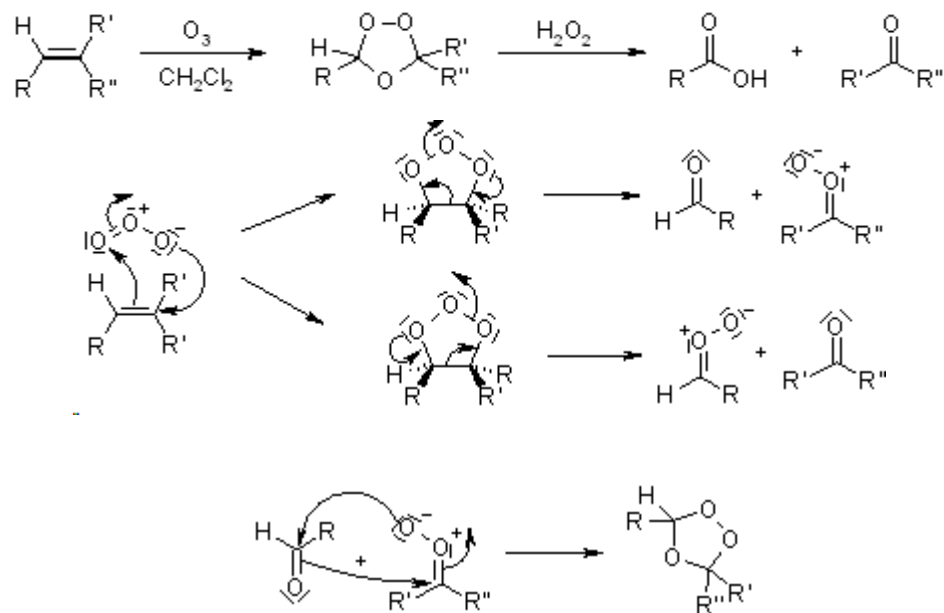
First, the issue of steric hindrance is dealt with by using 1,7-octadiene as the passivating linker molecule. The α -olefin reacts with the fresh silicon surface during ball milling to covalently attach the linker molecule to the silicon nanoparticle. The length of the linker molecule is also chosen to be long enough that there is flexibility to the chain to allow for different conformations to be adopted. The spacer passivating molecule, 1-pentene, is chosen so that it is shorter than the linking molecule. This is done to aid in the ease of the terminal olefin interacting with other molecules.

The silicon nanoparticle must be water soluble. The use of carboxylic functionality is designed to aid in the meeting of this requirement. The terminal olefin is oxidized to a terminal olefin by an ozonolysis reaction.¹² This is illustrated in scheme 3.1 below.



Scheme 3.1 Reaction scheme for the production of carboxylic acid functionalized silicon nanoparticles from silicon wafers and 1,7-octadiene/1-pentene.

One possibility for the conversion of a terminal alkene to a carboxylic acid is the reaction with ozone. The general reaction mechanism is described by Criegee and is shown in scheme 3.2.



Scheme 3.2 General mechanism of ozonolysis reaction.¹²

As shown, the ozone cleaves the alkene double bond in a cyclization addition reaction to form the primary ozonide. However, this then undergoes a conversion to the secondary more stable ozonide. This is then reacted with hydrogen peroxide to give the resultant carboxylic acid product. Byproducts have been shown to be formaldehyde and formic acid.¹³ Park *et al.* had previously demonstrated a similar reaction of an organic monolayer of 5-hexenyldimethylchlorosilane on quartz nanoparticles.¹³

One function for the incorporation of a polar functionality is colloidal stability of the nanoparticle in an aqueous solvent. Even though the majority of the nanoparticle (1,7-octadiene and 1-pentene) surface is nonpolar and contains hydrophobic molecules. The nanoparticles must be water soluble and resist oxidation (by the surface being passivated) by

the environments that they are in which can be different pH ranges and different salt concentration.^{7, 14-15}

The fluorescence quantum yield of the silicon nanoparticles have been shown to have excellent yields making them acceptable candidates for use as labels.^{1, 7, 9, 16-18} Different methods of preparation and functionalization lead to different quantum yields for the silicon nanoparticles but silicon nanoparticles have been proven to be acceptable candidates for use in biological labelling applications especially since they are resistant to photobleaching which is a major problem with conventional organic dyes that have been used as labels.

Recently, the cytotoxicity of silicon nanoparticles was found to be dependent on surface functionality and the size of the nanoparticles. Positive surface charges have been shown to increase toxicity of the particles. However, negatively charged carboxylic acid functionalized nanoparticles were shown to have little or no toxicity in rat lung and human colon cell lines.¹⁹ Also, it was shown that only particles <5.5 nm are effectively cleared by the kidneys. This makes silicon nanoparticles ideal, as only nanoparticles that are below the Bohr radius of about 5.5 nm are luminescent, and so all of the particles that would be used as biolabels, would be able to be cleared from the body. The effects of nanoparticles that are not cleared is also not an issue as silicon nanoparticles are oxidized to silica, which is also safe for the human body.^{17, 20}

The conjugation of carboxylic acid to an amine to form a covalent amide bond is a proven strategy.^{2-3, 16, 21} The covalent attachment of the biomolecule to the silicon nanoparticle helps the particle from losing functionality or stability by the leaching of molecules from the particle. Other methods of synthesizing and functionalizing particles that depend on non-covalent linkage have the added problem of maintaining the particle

throughout the cardiovascular system to the target without losing components due to the different pH and salt concentration environments which the particle must pass.

DNA is a molecule that is essential to life and has become more interesting to a large array of fields of research. The ability to use DNA to target cancer both for imaging purposes and also for therapeutic uses such as photodynamic therapy (PDT) makes it a very attractive targeting molecule.²² PDT is a therapy in which reactive singlet oxygen is synthesized which aids in the destruction of the tumor.²³ While the silicon nanoparticle itself is not by itself useful as a PDT agent, it can act as a scaffold to which both a targeting molecule and a PDT agent can be attached.²³⁻²⁵ DNA also is a great molecule for increasing the water solubility of a nanoparticle, not only do we have target functionality but also the ability to better dissolve in aqueous environments. DNA can be used to target specific complementary strands of DNA located on different proteins and in different organs.

Ethylenediamine conjugation is a simple way to convert the carboxylic acid terminated nanoparticles to amine terminated nanoparticles adding more functionalities to the silicon nanoparticles. Amine terminated nanoparticles have been shown to withstand a wide pH range from 1-13 and temperatures to 120°C.²⁶ Amine terminated silicon nanoparticles have also shown promise in cellular imaging as they also display a low cytotoxicity though still greater than that of the carboxylic acid functionality.¹⁹

Section 3.2 Synthesis

Materials

Silicon wafers were obtained from Silrec Corporation of Lexington Kentucky. The wafers were undoped, with a mirror finish, and of the 111 orientation. 1,7-octadiene (98.5%) and 1-pentene (>98.5%) were obtained from Sigma Aldrich Corporation and were used without an further purification. Deuterated chloroform and methylene chloride-d₂ were obtained from Cambridge Isotope Laboratories, Inc and were used without further purification. Methylene chloride was received from Fisher Scientific and was distilled over calcium chloride. Tetrahydrofuran was received from Fisher Scientific, radical stabilizer butylated hydroxytoluene (BHT) was removed and the solvent was dried, by distillation over sodium metal. Bio-beads SX-1 (200 mesh) were obtained from Bio-Rad Laboratories and were used as the immobile phase for Gel Permeation Chromatography (GPC). Ozone is generated using anT-23 Welsbach Ozonator from the Welsbach Corporation, converting oxygen to ozone via an electrical charge. Hydrogen peroxide (30%) was obtained from Fisher Scientific and used without further purification. Ethylenediamine was obtained from Fisher Scientific and purified by fractional distillation.

Experimental

1,7-Octadiene/1-pentene passivated silicon nanoparticles

A stainless steel milling vial was charged with 1.25 grams of silicon wafers and 25 mL of a 50% molar solution of 1,7-octadiene and 1-pentene (10.6 mL of 1,7-octadiene and 14.4 mL of 1-pentene) was added to the vial in a dry box with an inert atmosphere. Two stainless steel milling balls, each weighing approximately 8.1 grams and 1.2 cm in diameter were also added to the vial. The vial was then sealed to the atmosphere and the sample was milled in a Spex Sample Prep 8000D mixer/mill at 1060 cycles per minute for 12 hours in a cold room with a temperature of 4° C.

After 12 hours of RHEBM, the vial was opened to the atmosphere and the contents were transferred to plastic centrifugation tubes. The mixture was then centrifuged using a Thermo IEC CL2 Centrifuge, at 511 G for 30 minutes. The supernatant was then separated from the insoluble sediments and the solvent was removed using rotary-evaporation. The nanoparticles which were an oily residue of a light brownish color were then re-dissolved using dichloromethane. The crude yield was 45 mg. **¹H NMR(ppm):** 0.7 (s), 1.4 (broad s), 5.0 (m), 5.5 (s), 5.9 (s) **IR:** (KBr, cm⁻¹): 3400 (ν O-H), 3077 (ν =CH₂), 3000-2800 (ν C-H), 2126 (ν Si-H), 1680 (ν C=C), 1457 (δ C-H), 1378 (δ C-H), 1100 (ν Si-O), 727 (ν Si-C)

Synthesis of 1,5-hexadiene /1-pentene (20%) silicon nanoparticles.

A stainless steel vial was charged with 1-pentene (20 mL) and 1,6-hexadiene (4.34 mL) which were degassed by freeze thaw cycles and combined with 1.25 g silicon chips in a dry box. After milling, the milling mixture was centrifuged in plastic centrifuge tubes at 511 G for 30 minutes. The supernatant was then separated from the insoluble sediments. The remaining starting material (1,5-hexadiene and 1-pentene) were removed by rotary

evaporation. The product was a brownish oily liquid. The average yield was 60 mg. **¹H NMR(ppm):** 0.9 (s), 1.4 (broad s), 5.0 (m), 5.4 (s), 5.8 (s) **IR:** (KBr, cm⁻¹): 3081 (ν =CH₂), 3000-2800 (ν C-H), 2108 (ν Si-H), 1680 (ν C=C), 1457 (δ C-H), 1100 (ν Si-O), 805 (ν C-H)

The reaction of vinyl terminated silicon nanoparticles with KMnO₄.

A round bottom flask was (100 mL) was charged with 20 mg of vinyl terminated silicon nanoparticles passivated with 1,7-octadiene/1-pentene (50%) and the nanoparticles were dissolved in 20 mL of tetrahydrofuran. An excess of KMnO₄ (1 g) was added to the flask dissolved in 1 mL of glacial acetic acid. The reaction was allowed to stir for extended periods of time (>24 hours). After the stirring was complete, KMnO₄ was quenched with sodium bisulfite and the THF and acetic acid were removed using dialysis. These reactions were repeated with silicon nanoparticles passivated with 1,5-hexadiene.

Ozonolysis of 50% 1,7-octadiene/1-pentene passivated silicon nanoparticles.

A round bottom flask (50 mL) was charged with 45 mg of 1,7-octadiene/1-pentene (50%) solution of silicon nanoparticles in 15 mL dichloromethane. The solution's temperature was lowered to -78° C using an acetone/dry ice bath. The solution was then purged with ozone until the solution turned blue which was an indication that the reaction was completed as the blue color is unreacted ozone in solution.¹² The solution was then

treated to 30 mL of 30% hydrogen peroxide for the conversion of ozonides to carboxylic acids. The solution was then pumped to dryness using a rotary-evaporator under reduced pressure. The average yield was 20 mg or 44%. **¹H NMR(ppm):** 0.7 (s), 1.4 (broad s), 1.8 (s), 2.4 (broad, s), 9.8 (s) **IR:** 3612-2471 (ν O-H), 3012-2814 (ν C-H), 1712 (ν C=O), 1460 (δ C-H), 1100 (ν Si-O), 739 (ν Si-C)

Reaction with ethylenediamine

The silicon nanoparticles (20 mg) were activated with n-hydroxysuccinimide and reacted with ethylenediamine. The nanoparticles and purified ethylenediamine were allowed to stir under an inert atmosphere for 48 hours at room temperature. The mixture was then washed and the product was collected by extraction with dichloromethane. The yield was 15 mg. **¹H NMR(ppm):** 1.1 (s), 1.5 (broad s), 1.9 (broad, s), 3.5-4.0, 6.6 (s) **IR:** 3474-3050 (ν N-H₂), 2992-2803 (ν C-H), 2120 (ν Si-H), 1651 (C=O), 1448 (δ C-H), 1100 (ν Si-O), 729 (ν Si-C)

Section 3.4: Results and Discussion

1,7-octadiene/1-pentene passivated silicon nanoparticles

1,7-octadiene/1-pentene silicon nanoparticles were imaged using TEM. The resulting images also had EDS performed which showed that silicon was present in the particles

(Figure 3.3) A peak at 1.74 KV that corresponds to silicon is seen in the EDS spectra as seen in Figure 3.1. The majority of the spectra consists of peaks for copper (8, 8.9 KV), carbon (0-0.2 KV), and oxygen (0.3 KV) are from the grid itself which is copper and the formvar membrane which coats the grid which is composed of carbon and oxygen. These results show that the synthesis of silicon nanoparticles has been successful. The nanoparticles were then further investigated with NMR analysis to probe the passivating identity.

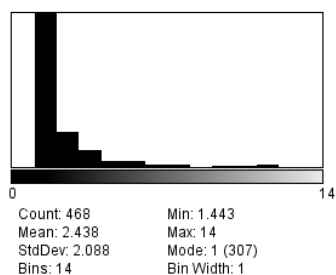
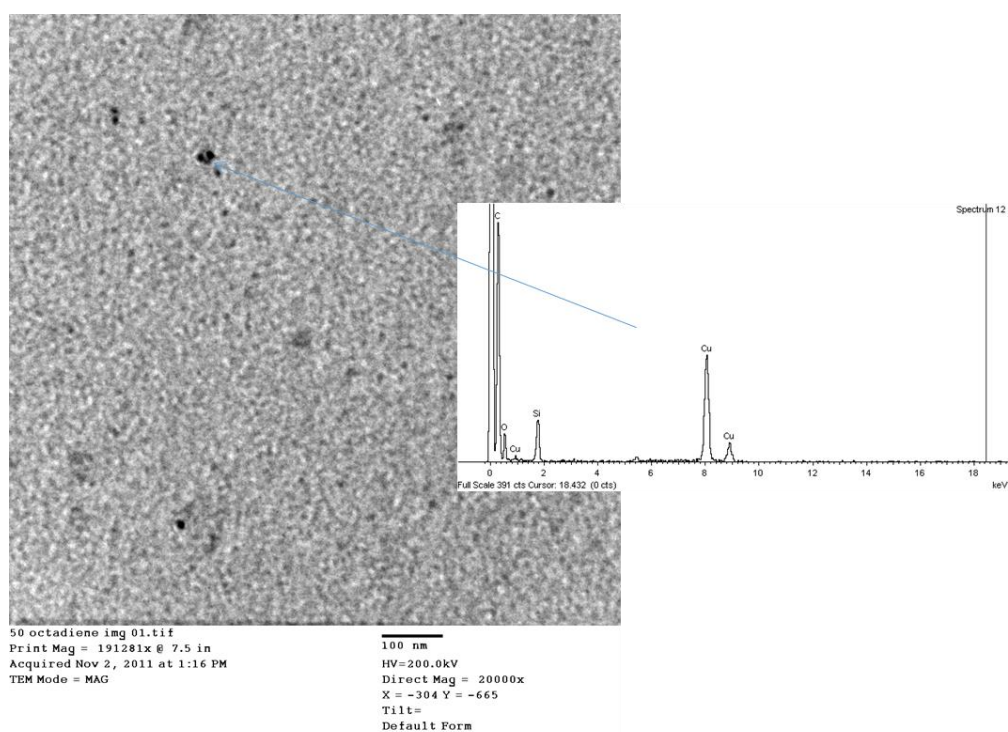


Figure 3.1 TEM and EDS of 50% 1,7-octadiene/1-pentene silicon nanoparticles with histogram

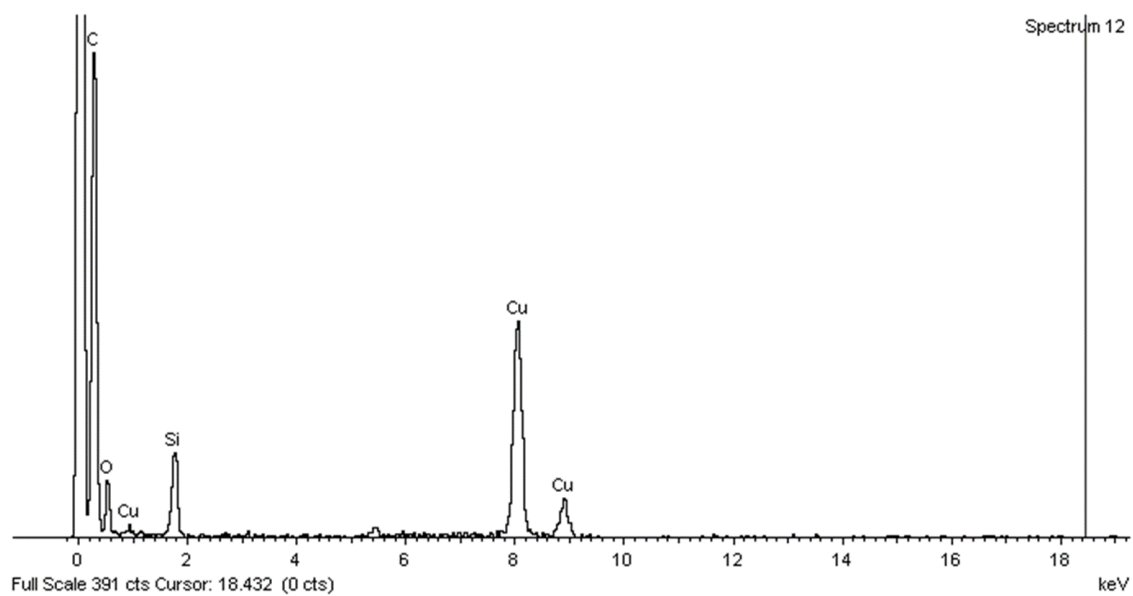


Figure 3.2 EDS of 50% 1,7-octadiene/1-pentene silicon nanoparticles.

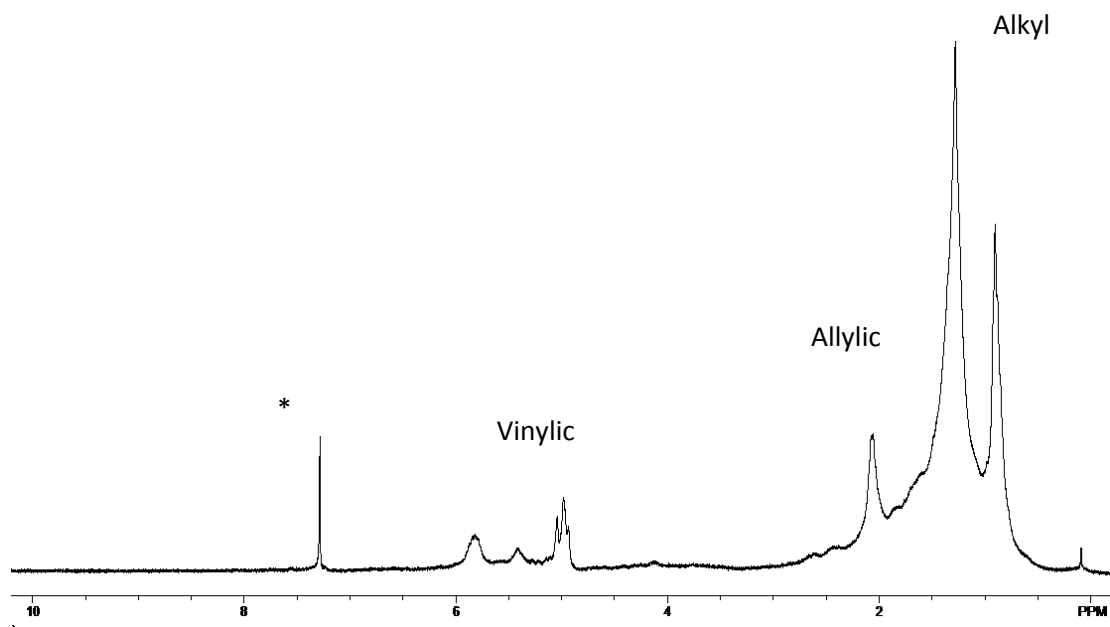


Figure 3.3 NMR spectra of 50% 1,7-octadiene/1-pentene silicon nanoparticles.

The ^1H NMR spectrum of the silicon nanoparticles shows methyl and alkyl regions centered around 0.7 ppm and 1.4 ppm (Figure 3.3). The methyl peak is from the 1-pentene and the alkyl peaks are from the solution of both 1,7,-octadiene and 1-pentene. There are three peaks in the olefinic region at 5 ppm, 5.5 ppm, and 5.9 ppm. The peaks at 5 ppm and 5.9 ppm are the vinylic protons and have been assigned to the terminal olefin of 1,7-octadiene. However, the peak at 5.5 is assigned to an internal double bond. This double bond may arise from an “ene” reaction that occurs during passivation during RHEBM.

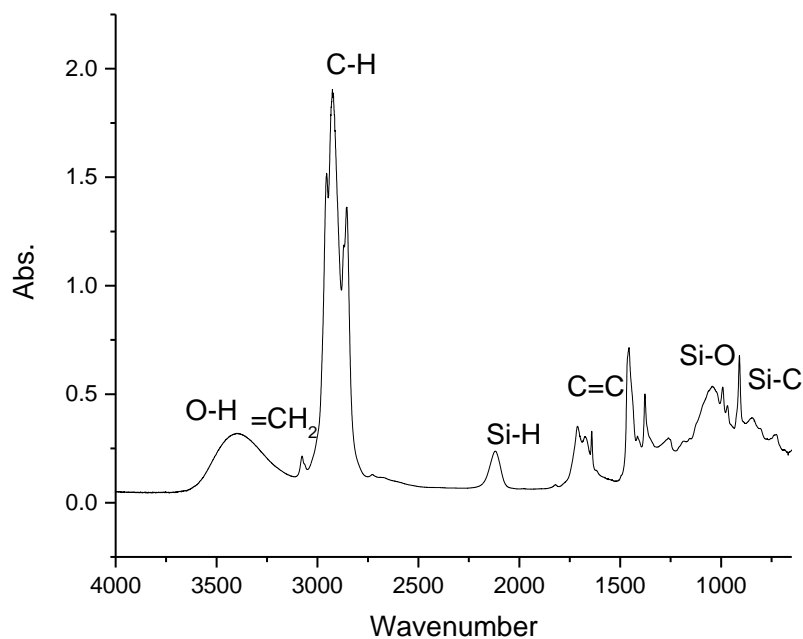


Figure 3.4 infrared Spectra of 50% 1,7-octadiene/1-pentene Silicon Nanoparticles.

The IR spectrum shows a vinyl C-H stretch at 3077 wavenumbers. There is also an O-H stretch present at around 3300 wavenumbers, which is not expected and is probably adventitious water. There is a peak at 911 wavenumbers for silicon- carbon stretching. A Si-H stretch is seen at 2114 wavenumbers along with a C=C stretch at 1640 wavenumbers.

Photoluminescence spectra was taken with dichloromethane as the solvent. Dichloromethane was chosen as it was the solvent used to dissolve the nanoparticles. The solution concentration was adjusted till optical density was 0.3 at 300 nm. The resulting spectra of the 50% 1,7-octadiene/1-pentene silicon nanoparticle solution is shown in Figure 3.5.

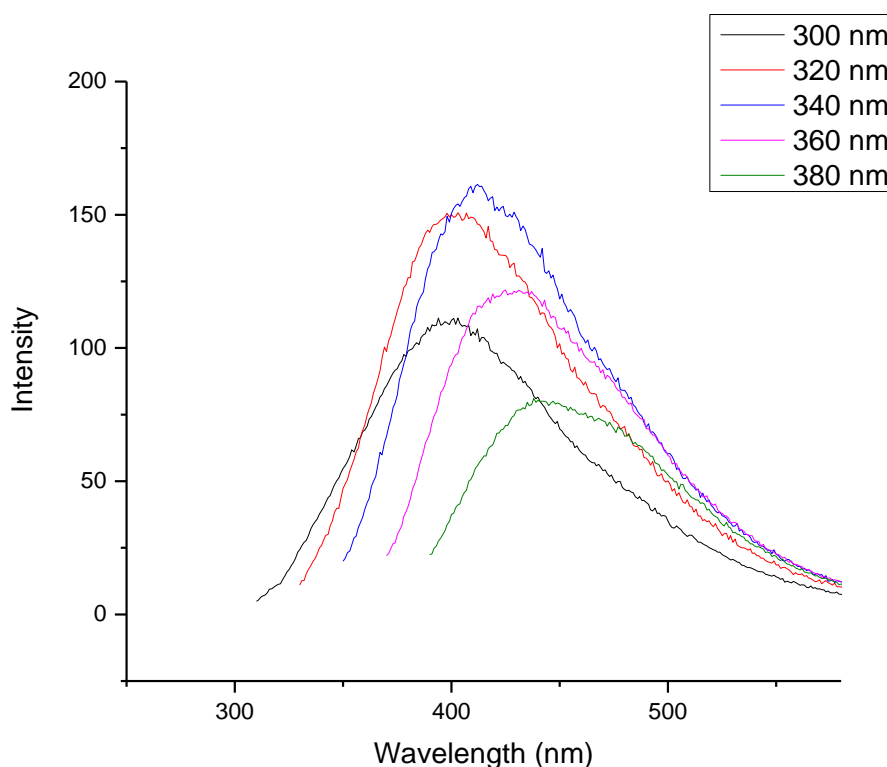


Figure 3.5 Photoluminescence of 1,7-octadiene/1-pentene silicon nanoparticles, Normalized by the UV-vis absorbance.

As seen in Figure 3.5 a shift is evident that of increased emission wavelength from the excitation wavelength. The legend shows the excitation wavelengths and the emission maxima can be seen in the spectra. The excitation at 300 shows a maxima at 400 nm, the excitation at 320 shows an emission maxima at 407 nm, and the excitation at 340 nm shows

an emission maxima at 412 nm. The photoluminescence behavior is characteristic of a polydisperse distribution of silicon nanoparticles. As the excitation wavelength increases, populations of larger nanoparticles are excited.¹ The nanoparticle solutions display a blue luminescence rather than a luminescence that changes with the size of the nanoparticles. This can be explained by the luminescence is arising from core-hole recombination at defect states in the surface, rather than photoluminescence across the bandgap.²¹

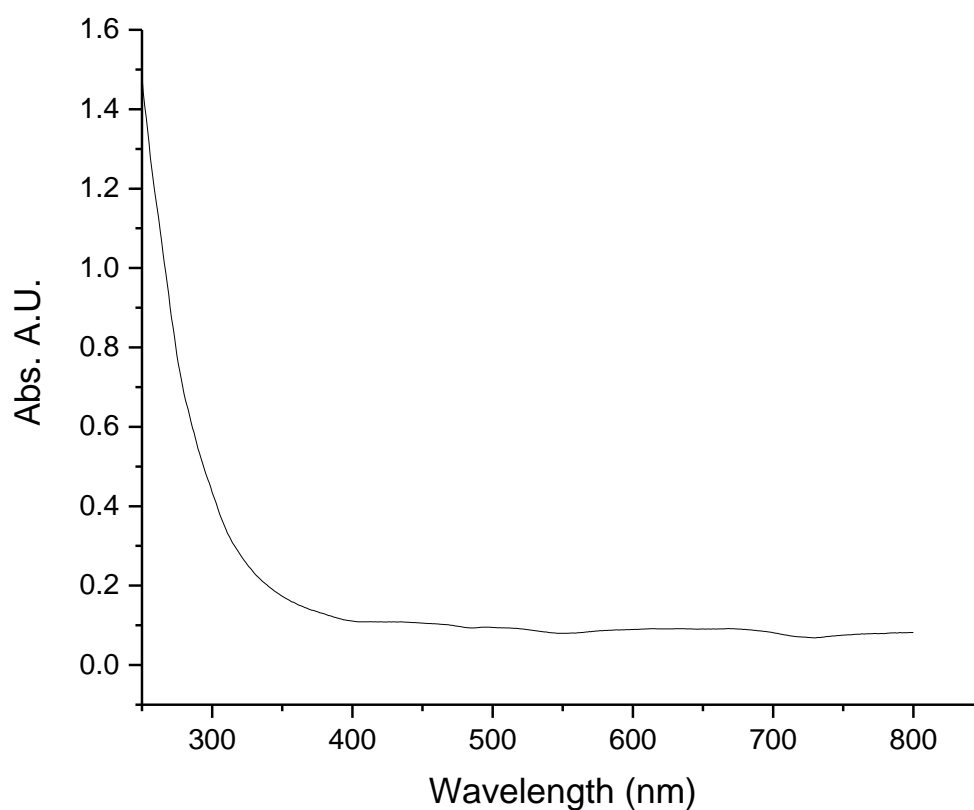


Figure 3.6 Absorption spectrum of 1,7-octadiene/1-pentene silicon nanoparticles.

The absorption spectrum shows a long tail which is consistent with the indirect bandgap of the silicon nanoparticles.^{18, 21, 27} This has been observed in all of the silicon nanoparticle solutions produced by the mechanochemical milling process.

1,6-hexadiene (20%)/ 1-pentene passivated silicon nanoparticles.

The steric properties of the different reactive organic molecules was taken into account with the design of the reactions. 1-Pentene was chosen as the main passivating alkene as it has a shorter chain length than that of the 1,6-hexadiene (6 carbons versus 5 carbons). This may be important for both the oxidation of the olefin to a carboxylic acid and also for the reaction of the carboxylic acid with an amine to form an amide bond.

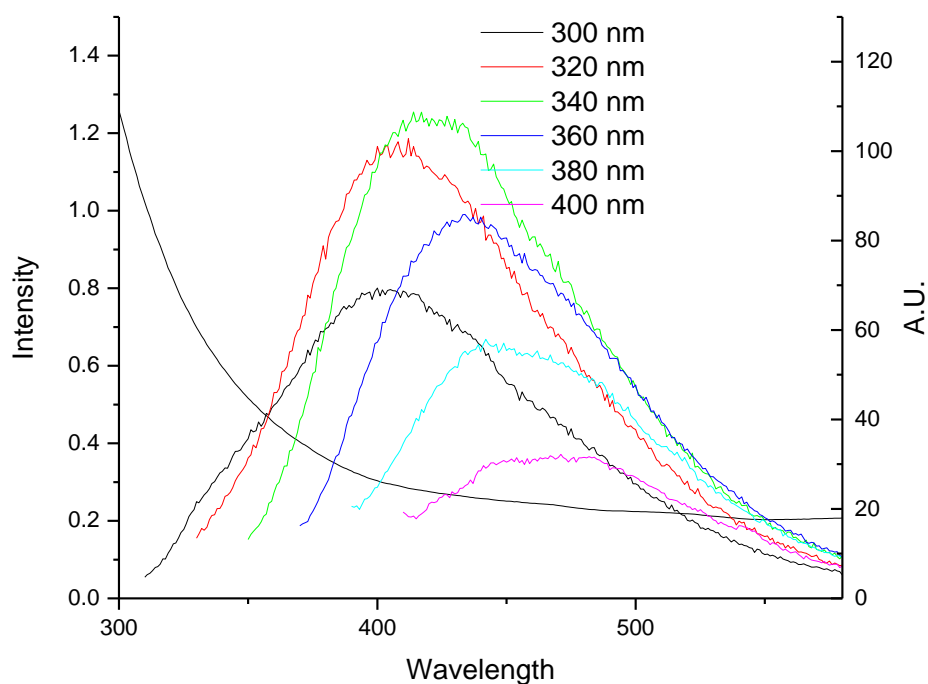


Figure 3.7 Photoluminescence of 1,6-hexadiene(20%)/1-pentene passivated silicon nanoparticles, normalized by UV-vis absorbance.

The photoluminescence of the alkene passivated silicon nanoparticles is also an advantage over the carboxylic acid passivated silicon nanoparticles. As seen in figure 3.7 the maximum of emission reaches 100 arbitrary units as compared to 65, with the valeric acid/pimelic acid passivated silicon nanoparticles, which was the most intense luminescence seen from all of the carboxylic acid passivated systems studied.

As with the carboxylic acid passivated silicon nanoparticles, a shift is seen between the absorbing wavelength and the emission maxima. The first absorbing wavelength at 300 nm has an emission maxima at 405 nm. The second absorbance wavelength of 320 nm has its emission maxima at 411. The third absorbance wavelength at 340 nm having an emission maxima at 417 nm.

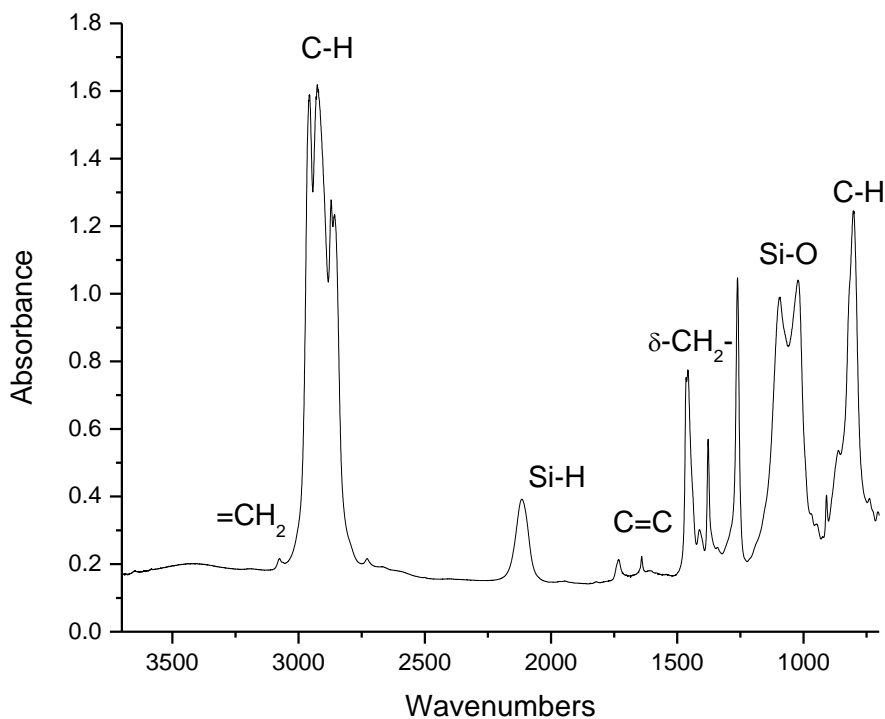


Figure 3.8 Infrared spectrum of 1,6-hexadiene (20%)/1-pentene passivated silicon nanoparticles.

The infrared spectrum of the 1,6-hexadiene(20%)/1-pentene passivated silicon nanoparticles shows an absorption for vinylic C-H stretch at 3076 wavenumbers. There is also weak vinyl stretching vibration at 1640 wavenumbers. A strong alkane stretch is observed at 2900 wavenumbers for the aliphatic hydrogens. The Si-O stretch is seen at around 1100 wavenumbers and is fairly strong. The Si-O is most likely due to oxygen that was on the surface of the starting material wafers. A strong C-H bending vibration is observed at 804 wavenumbers.

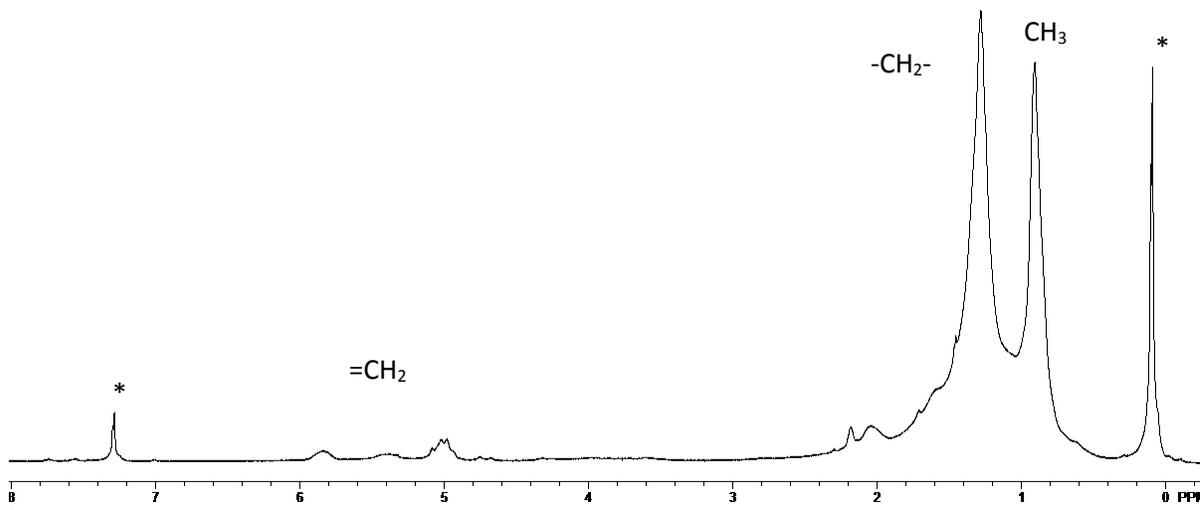


Figure 3.9 ^1H NMR spectrum of 1,6-hexadiene (20%)/1-pentene passivated silicon nanoparticles (in CDCl_3).

The ^1H NMR spectrum shows peaks at 5.0 and 5.8 ppm corresponding to the terminal olefin, while the small peak at 5.5 ppm is indicative of an internal olefin.²⁸ The methyl group of the 1-pentene is seen at 0.9 ppm. The aliphatic region from 1 to 2 ppm is derived from both the 1,6-hexadiene and the 1-pentene.

The ease of removal of the low boiling alkenes and the dialkenes makes them a more suitable correctant compared to the high boiling carboxylic acids. The ability to modify the terminal functionality is also a huge asset. The solubility of the dicarboxylic acids severely limited the synthesis of carboxylic acid passivated silicon nanoparticles with terminal carboxylic functionality, with the greatest percentage of terminal carboxylic acid functionality achieved being only 5% with the valeric acid/pimelic acid system. In contrast, the alkene/ dialkene solution molar composition was able to be adjusted to any mole fraction desired.

3.5 Oxidation of the terminal vinyl groups.

Conversion of the terminal vinyl groups were first attempted by using KMnO_4 as the oxidant. The passivated silicon nanoparticles used were synthesized by milling of silicon chips with a mixture of 1,7-octadiene/ 1-pentene (50%) in a nitrogen gas atmosphere. The nanoparticles were dissolved in THF and 1 gram of KMnO_4 was added to the solution. The mixture of the two phases were stirred for >24 hours. After the reaction, the KMnO_4 was quenched with sodium bisulfite and the nanoparticles were purified using dialysis.

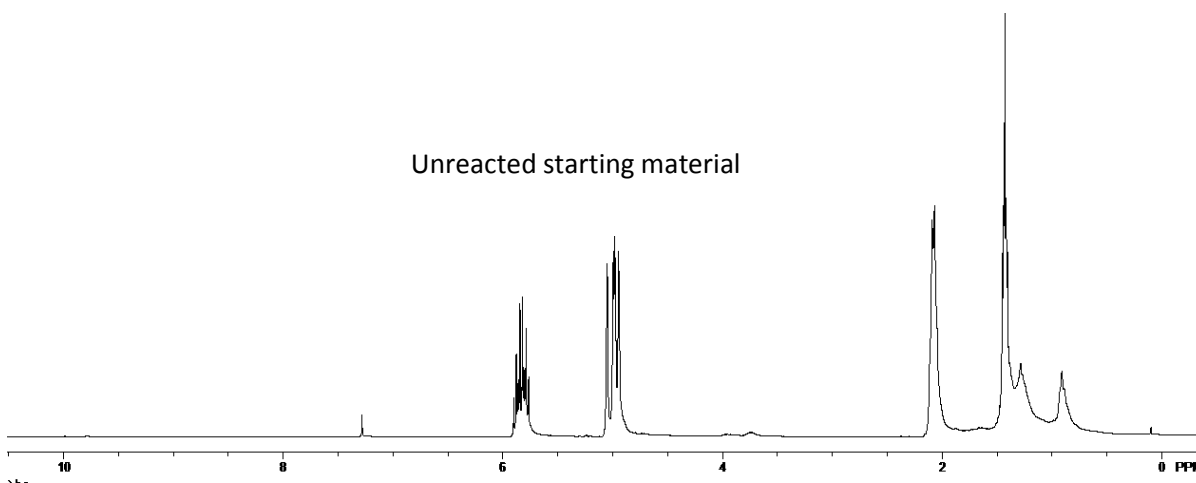


Figure 3.10 ^1H NMR of 1,7-octadiene/1-pentene (50%) Silicon nanoparticles after KMnO_4 oxidation. The unreacted olefin can be seen at 5 ppm and 5.9 ppm.

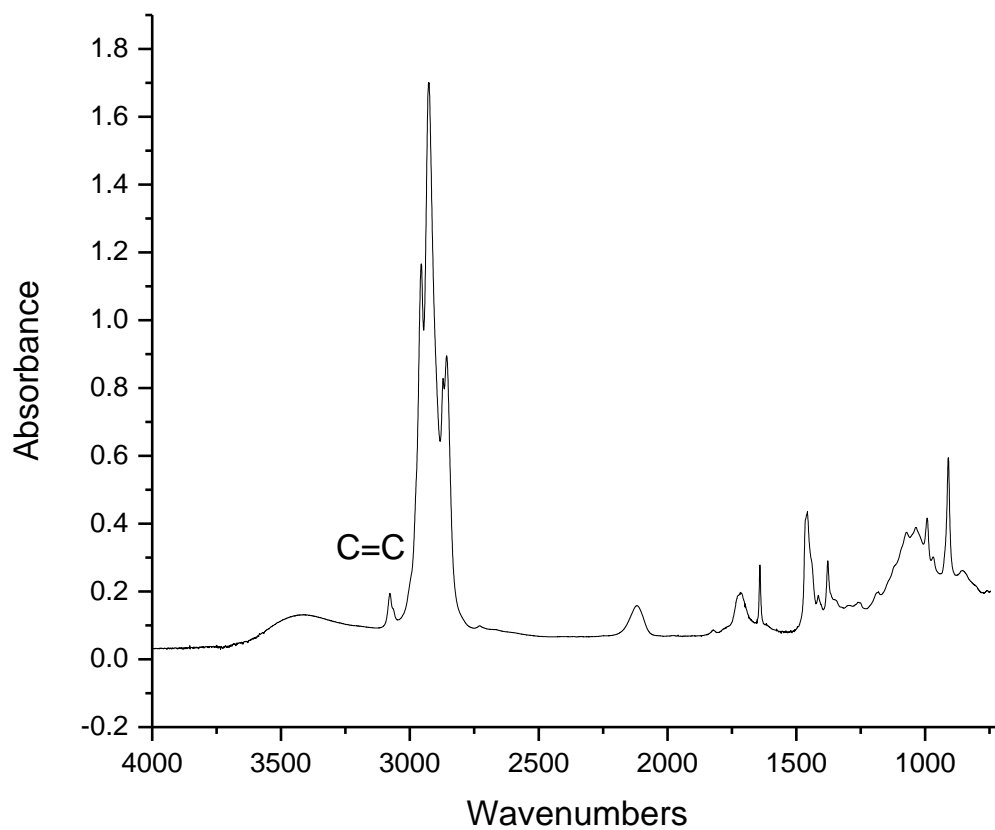


Figure 3.11 IR of 1,7-octadiene/1-pentene (50%) silicon nanoparticles after reaction with KMnO_4 .

The NMR and IR spectra show that mostly starting material remains after reaction with KMnO_4 . Since this reaction is a two phase system, mixing was a factor in the ability of the reagents to mix and react. With more vigorous mixing and longer mixing times, better results were seen, however, more byproducts were produced as seen in Figure 3.12 below.

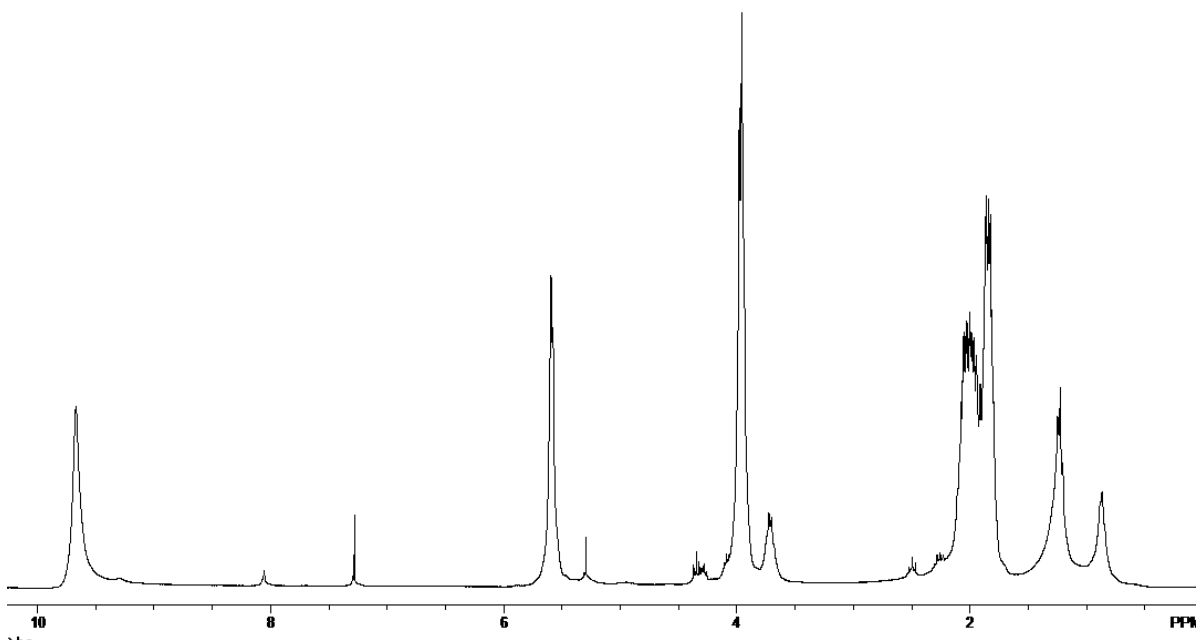


Figure 3.12 ^1H NMR of 1,7-octadiene/1-pentene (50%) silicon nanoparticles after increased reaction time (>72 hours stirring with KMnO_4).

The problems presented by the heterogenous mixing of the reaction and the production of byproducts which were not easily removed by purification presented a challenge for obtaining pure nanoparticle products. This ultimately led to a search for a more efficient route of conversion that would allow for the reaction to scale more easily. The goal of the project is to find a route of production of carboxylic acid terminated nanoparticles in as few as steps as possible, with as few byproducts easy route of purification of the products. This lead to the search for a new method of oxidizing the terminal vinylic group.

Ozonolysis proved to be an efficient route to carboxylic acid functionality. This method resulted in few byproducts, was easy to purify, and spectral analysis suggests that the reaction proceeded to completion. One nice feature of the ozonolysis reaction is the color

indicator that the reaction has completed. This is shown by a blue color of the solution when all of the alkenes have been consumed and unreacted ozone begins to dissolve in the solution.¹² This can be seen Figure 3.13 below.



Figure 3.13 Characteristic blue color of dichloromethane containing dissolved ozone.

The 1,7-octadiene (50%)/ 1-pentene passivated silicon nanoparticles were dissolved in dichloromethane. The solution was cooled in an acetone/dry ice bath to -72°C . Ozone was then bubbled through the solution till the dark blue color indicative of dissolved excess ozone. This normally took place within 20 minutes, with the solution getting progressively darker in blue. The ozonide was then oxidized to carboxylic acid functionality by the

addition of hydrogen peroxide. The products were then pumped to dryness and the nanoparticles dissolved in dichloromethane.

Photoluminescence of carboxylic acid terminated silicon nanoparticles

The resultant product was characterized using a combination of ^1H NMR, IR, UV-Vis, and Photoluminescence. The photoluminescence is shown in Figure 3.14. It shows a decrease in the intensity of emission (corrected by normalization to the absorption) for all exciting wavelengths.

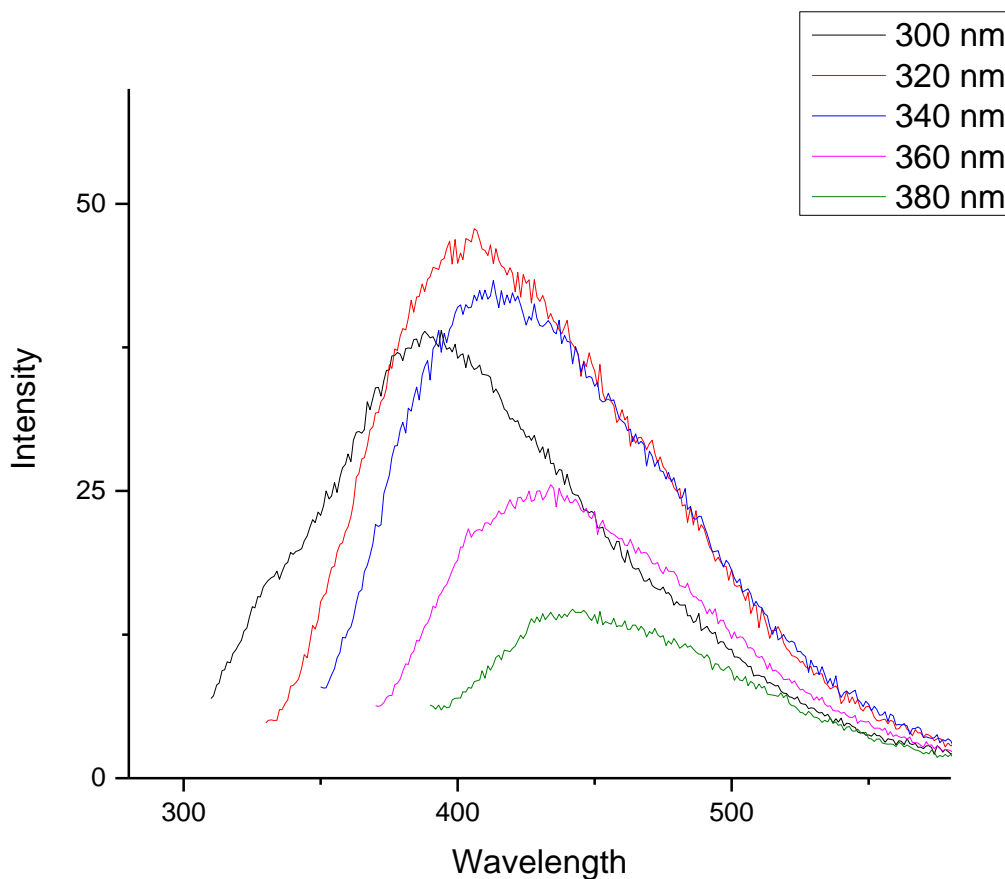


Figure 3.14 Photoluminescence of carboxylic acid terminated silicon nanoparticles.

There is still the characteristic excitation/emission shift that is characteristic of nanoparticle populations. The different size nanoparticles absorb different wavelengths based on their bandgap. However, the normalized emission has been decreased perhaps by oxidation of unprotected surface areas of the silicon nanoparticle by the small molecule ozone. There is also the possibility that this decrease is simply a function of the solvent interactions with the carboxylic acid terminated nanoparticles as the luminescence intensity has been shown to be a function of the pH of the solution.²⁹ The solubility of the nanoparticles may also play a key role. The particles are not water soluble, likely due to the formation of dimers between the carboxylic acid functional groups, and the pH had to be increased in order to obtain absorption and emission spectra of the carboxylic acid terminated nanoparticles. This can be seen below in the two photos of the carboxylic acid nanoparticles solutions at different pH.

As can be seen the water solubility of the carboxylic acid terminated nanoparticles is greatly dependent on the pH of the water solution. This is seen in Figure 3.15 as a non-dispersed colloid on the left and a dispersed solution on the right.

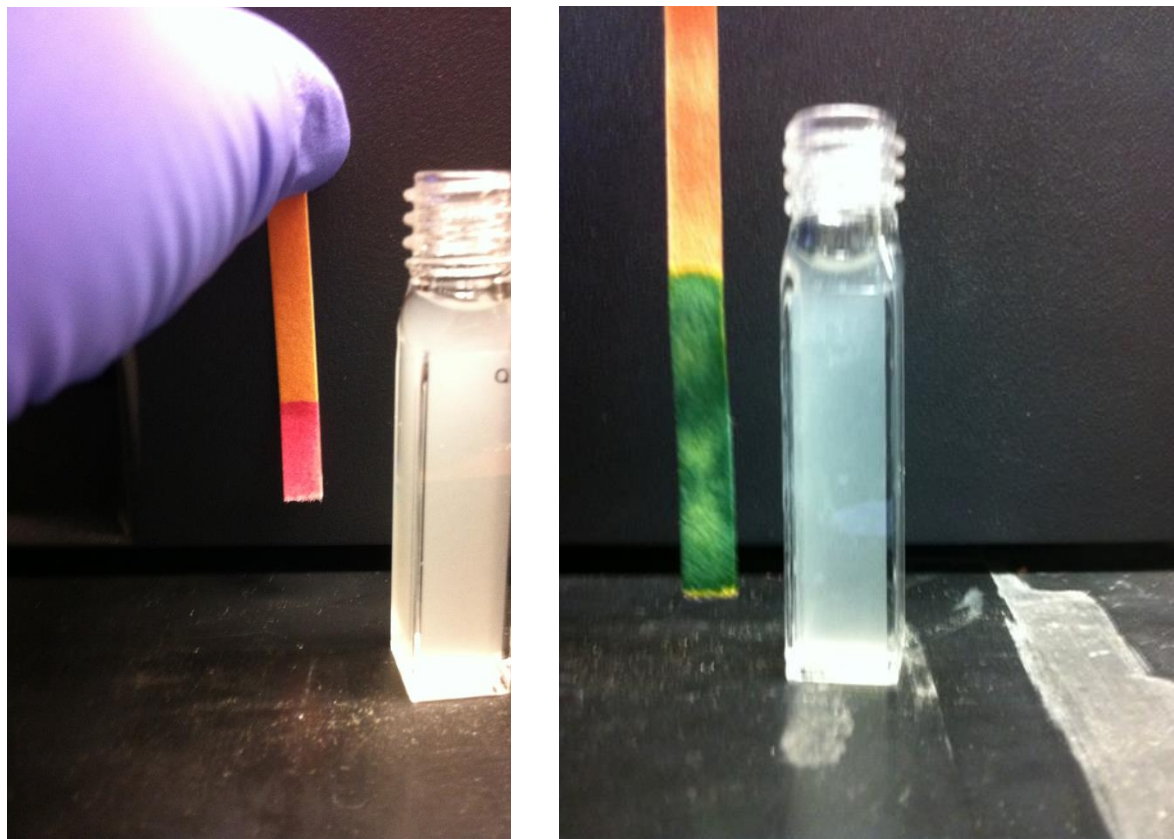


Figure 3.15 Water solubility of carboxylic acid terminate nanoparticles at pH 2 on the left and at pH 8 on the right.

IR analysis shows strong evidence for the formation of carboxylic acid functionality. The spectra is shown in Figure 3.16 below.

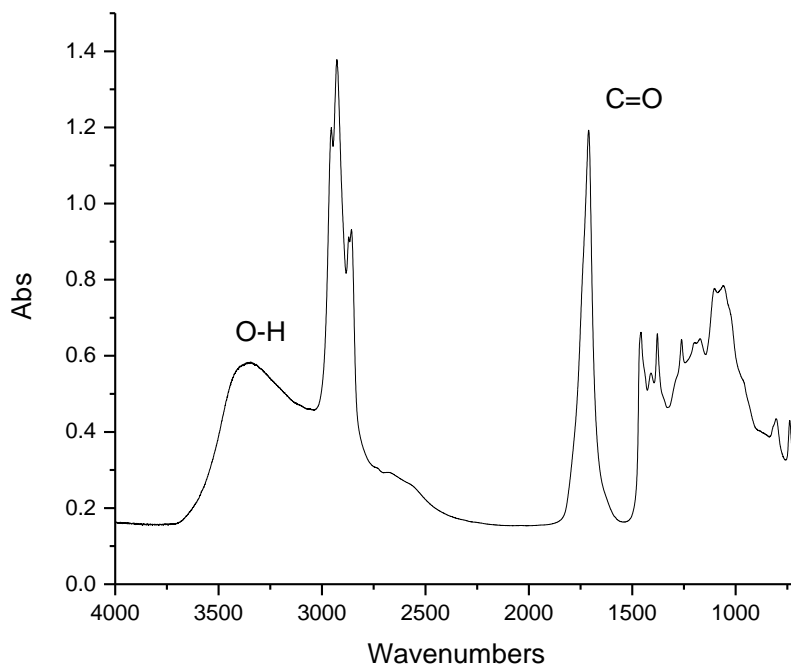


Figure 3.16 Infrared spectra of carboxylic acid terminated silicon nanoparticles.

The characteristic broad absorption from $3600\text{-}2300\text{ cm}^{-1}$ is very indicative of a carboxylic acid functionality. Also, there is now the prominent peak at 1711 cm^{-1} which is now present that is evidence of a carbonyl group. These two features lend strong evidence of a conversion from terminal olefin to a carboxylic acid functionality. However, it is not clear that the conversion of the vinylic group proceeded totally to the carboxylic acid functionality. The reaction goes through an aldehyde intermediate, which is oxidized by the hydrogen peroxide to carboxylic acid. It is possible that some of the aldehyde functionality remains. The carbonyl peak should be expected at 1760 wavenumbers for a free carboxylic acid functionality. The dimer appears at $1706\text{-}1720\text{ cm}^{-1}$, which could also account for the

observed carbonyl stretching vibration. However, the aldehyde C-H stretch should appear in the range of 2695-2830 cm^{-1} , the observed peak in this spectrum is at 2856 cm^{-1} .

The ^1H NMR spectra is shown in Figure 3.17 below.

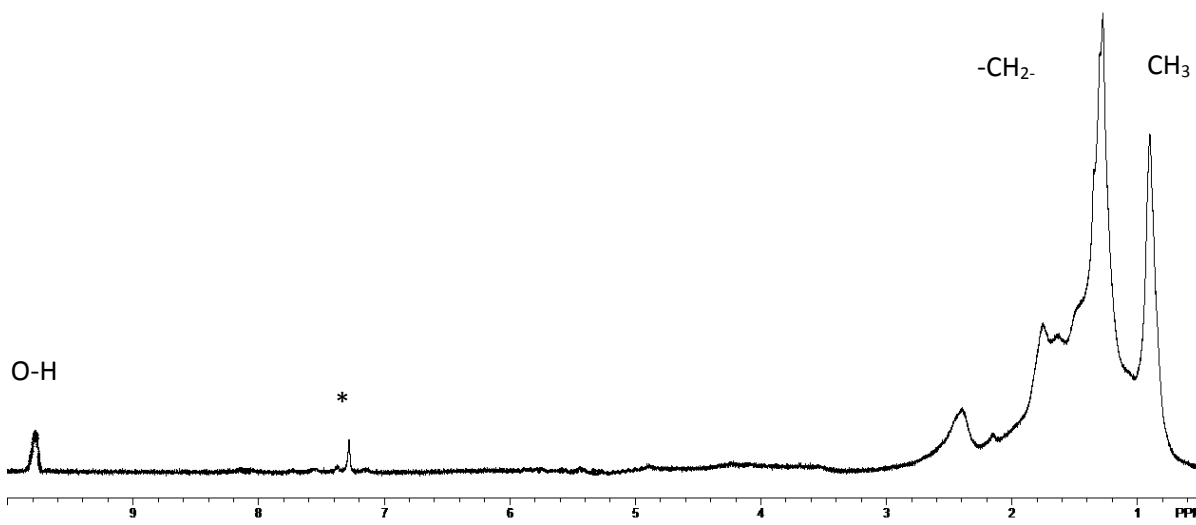


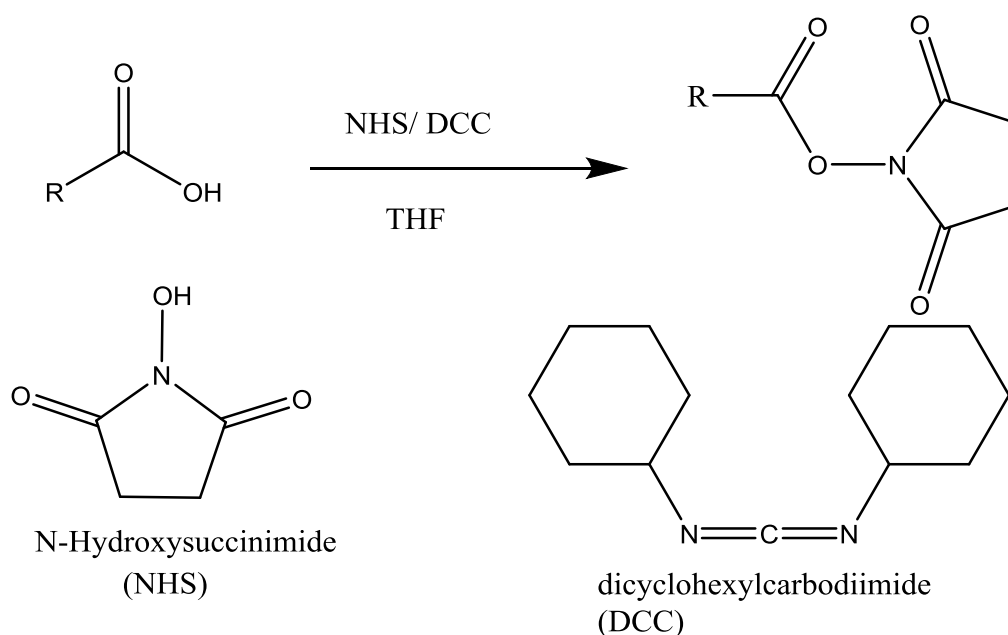
Figure 3.17 ^1H NMR of carboxylic acid terminated silicon nanoparticles in CDCl_3 .

The ^1H NMR shows a carboxylic acid or aldehyde proton at 9.8 ppm. The alkyl and the methyl regions appear as expected. The ^1H NMR confirms that the terminal olefin has been converted from a terminal vinylic functionality. These spectra show that the characterization of whether the reaction has completed the oxidation to a carboxylic acid functionality, or if it was incomplete with a percentage of the product remaining as an aldehyde functionality. The presence of a terminal carboxylic acid functionality was confirmed by the conjugation of ethylenediamine to the free carboxylic acid.

3.6 Conjugation of amine to carboxylic acid terminated silicon nanoparticles.

Method of conjugation

Conjugation between carboxylic acid and amines proceeds slowly without first activating the carboxylic by adding a better leaving group. This was done by the reaction with N-hydroxysuccinimide (NHS) in the presence of dicyclohexylcarbodiimide (DCC). This reaction was carried out in dry THF. A scheme is shown in Scheme 3.2.



Scheme 3.3 Activation of carboxylic acid.

The formation of the amide can be facilitated by a good leaving group in the regeneration of NHS which helps to drive the reaction towards completion. To insure that all of the carboxylic acid moieties on the surface of the silicon nanoparticle were activated, a 10 fold excess by mass was used. The excess DCC and NHS are easy to separate in a washing purification step and have no impedance on the progression of the reaction. The formation of

water in dried THF provides a driving force for the increased yield of conversion for the reaction.

Characterization of amine terminated silicon nanoparticles.

Silicon nanoparticles with a terminal carboxylic acid functionality were prepared by milling silicon chips with 1,7-octadiene (50%)/1-pentene. The silicon nanoparticles which then had a terminal vinylic group which was oxidized using ozone as described in the previous section. The carboxylic acid terminated silicon nanoparticles were then activated by reacting the carboxylic acid functionality with DCC and NHS in THF as described above. The activated nanoparticles were then stirred with ethylenediamine in dried THF for 24 hours. The starting material was attempted to be purified by dialysis.

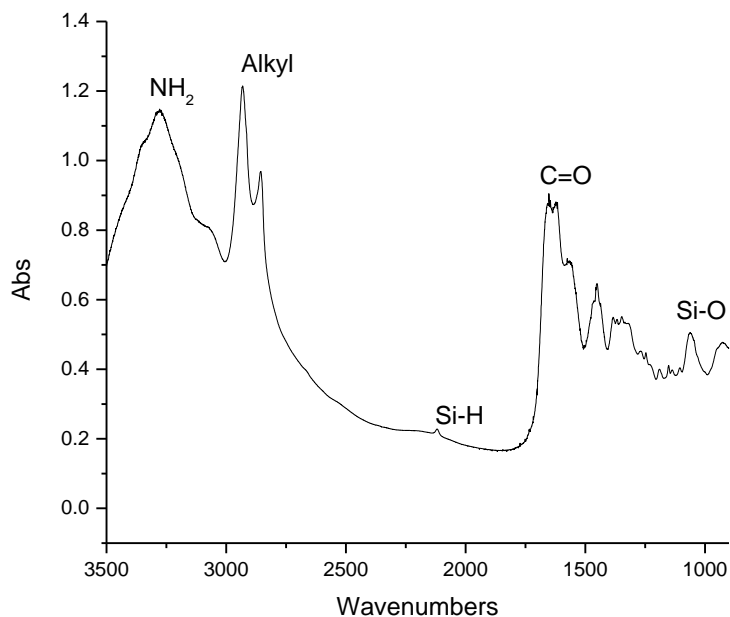


Figure 3.18 Infrared spectra of Amine terminated silicon nanoparticles.

The IR spectra of the amine terminated nanoparticles shows a very broad peak centered around 3300 cm^{-1} which is the hydrogen bonding of the terminal amine functionality. Also, the carbonyl peak which was seen at 1711 cm^{-1} has shifted down to 1650 cm^{-1} . This is indicative of the carbonyl from the carboxylic acid converting to a carbonyl of an amide group.³⁰ These two features lend very good evidence for the conversion of the carboxylic acid functionality to an amine functionality.

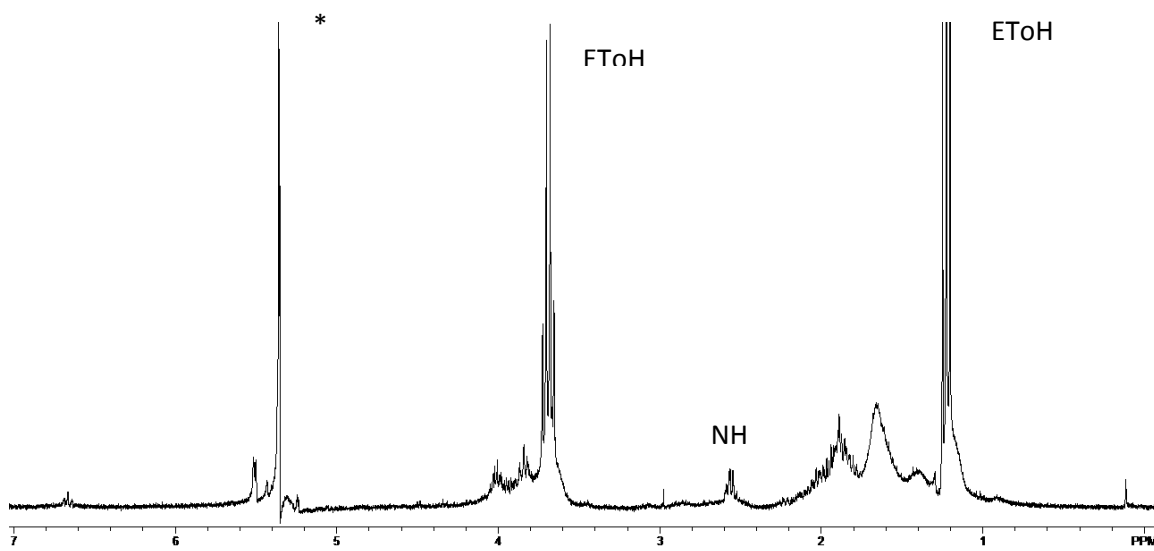


Figure 3.19 ^1H NMR of amine terminated silicon nanoparticles in CD_2Cl_2 .

The ^1H NMR spectra of the amine terminated silicon nanoparticles shows three distinct regions. There is the methyl region at 1.1 ppm that is the methyl functional group of the 1-pentene functional group. There are also two broad peaks at 1.5 ppm and 1.9 ppm that are alkyl regions that represent the alkyl carbon chains of the 1-pentene and the 1,7-octadiene passivating layer. The peaks between 3.5 and 4.0 are assigned to the amine functionality of the terminal amine. Also, a small peak at 6.6 is representative of the amide bond.

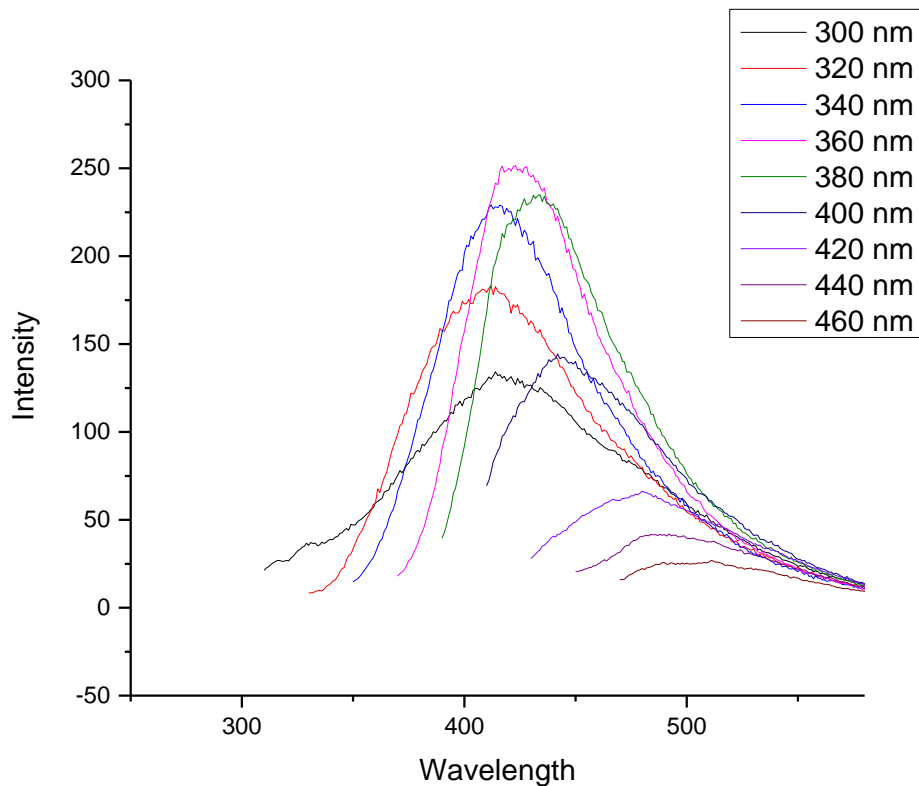


Figure 3.20 Photoluminescence of amine terminated silicon nanoparticles.

The photoluminescence of the amine terminated particles when normalized to the absorbance of the solution, shows an increase in luminescence over both the carboxylic acid nanoparticles and the starting material 50% 1,7-octadiene/1-pentene silicon nanoparticles. It was theorized earlier that the decrease in the luminescence of the carboxylic acid terminated nanoparticles could be due to the ability of ozone, a small molecule, to be able to penetrate the passivating layer and oxidized the silicon surface at defect sites. However, the luminescence of the amine terminated particles surpasses even that of the starting material (1,7-octadiene/1-pentene silicon nanoparticles) in intensity. Whether this is due to solvent effects and there was no oxidation during the ozonolysis step is a question that remains unanswered.

Conjugation with DNA

For further proof of the ability to conjugate biological molecules of interest to the carboxylic acid terminated silicon nanoparticles, a collaborative project was undertaken to attach a short DNA sequence to the nanoparticles. This was done in collaboration with Cooper Battle of Dr. Jayawickramarajah's group. Two conjugations were successfully completed using first a single strand (5'-TCAA CAT CAG TCT GAT AAG CTA-C₅NH₂-3') as the short strand of DNA that was conjugated. The coverage of the terminal carboxylic acid functionality were varied between 50% in the one reaction and 25% in the second. The second conjugation was carried out with hybridized DNA containing a complementary sequence to the original strand of DNA (3'-GTC AGA ATA TTC GAT-5'). After purification of the conjugation reaction product, gel electrophoresis was performed in an polyacrylamide gel.

Silicon nanoparticles that were passivated using 1,7-octadiene (50%)/1-pentene were oxidized to a carboxylic acid functionality using ozone as described previously. The carboxylic acid functional groups were then activated using DCC and NHS. The amine terminated DNA strand was then stirred with the silicon nanoparticles . The reaction was then purified using centrifugation filters with a 30 KD cutoff. The results of these conjugation reactions are shown below.

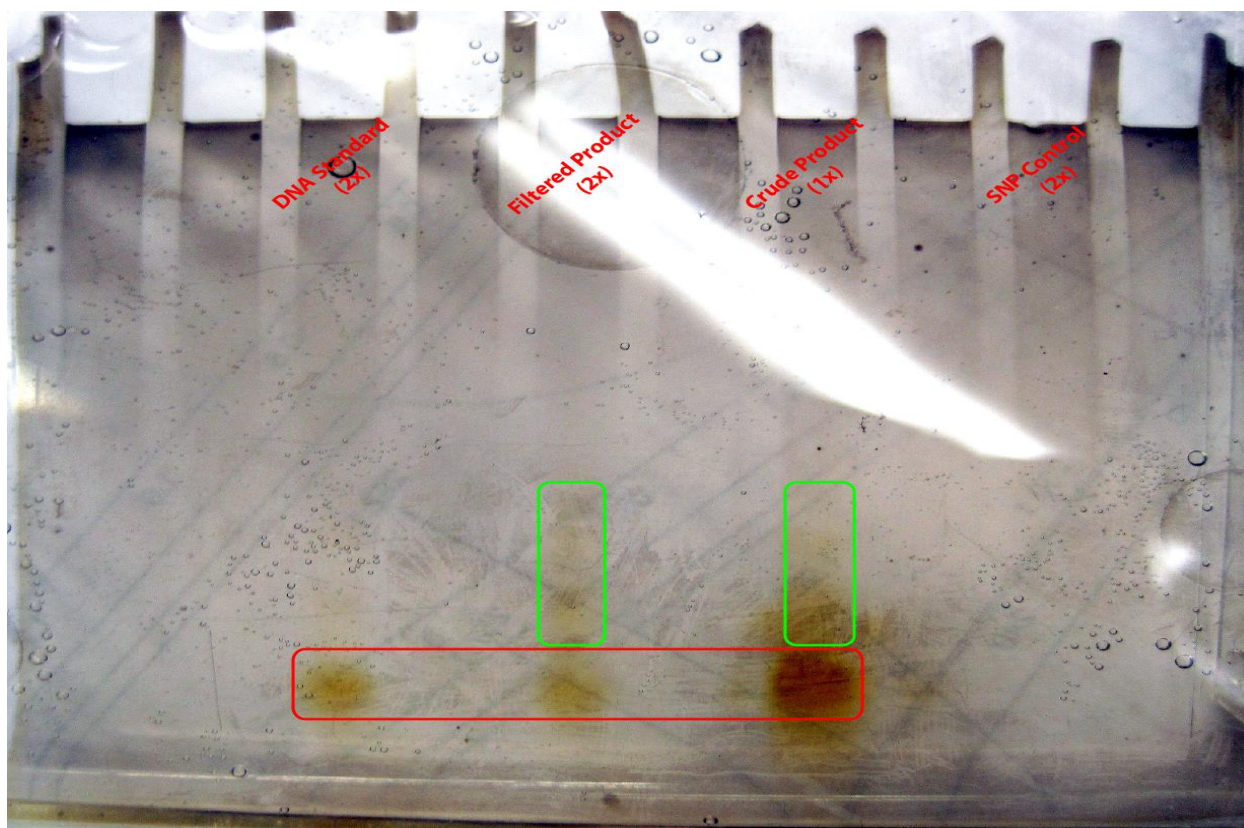


Figure 3.21 polyacrylamide gel of 1,7-octadiene/1-pentene (50%) silicon nanoparticles conjugated with DNA (5'-TCAA CAT CAG TCT GAT AAG CTA-C₅NH₂-3') and stained with silver ion solution.

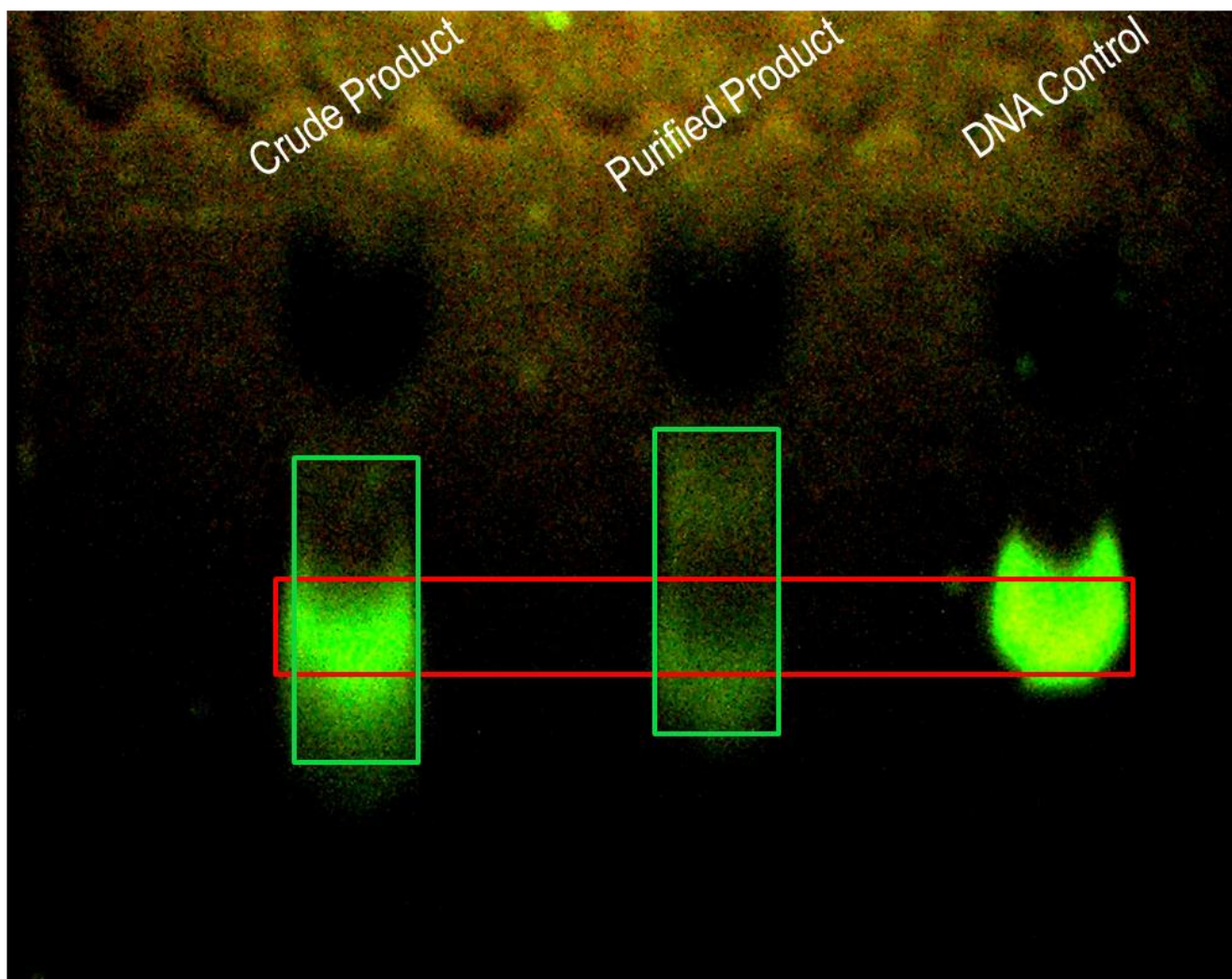


Figure 3.22 polyacrylamide gel of 1,7-octadiene/1-pentene (25%) silicon nanoparticles conjugated with hybridized DNA which was incubated with Sybr-green, an intercalating fluorescent marker.

The gels are a comparison of the position of the free DNA sequence that was run as a control, with the lanes containing silicon nanoparticles that have been conjugated with the DNA, shows that the distance traveled differs from the control. The gel uses two different

properties to separate the materials, size and charge. The DNA sequences have the same charge whether it has been conjugated or is free. However, the conjugated silicon nanoparticles will have a significant larger size allowing for the gel to separate the conjugates from the free DNA based on the size difference. TEM images were also taken of the 1,7-octadiene/1-pentene (25%) silicon nanoparticles conjugated with the DNA sequence.

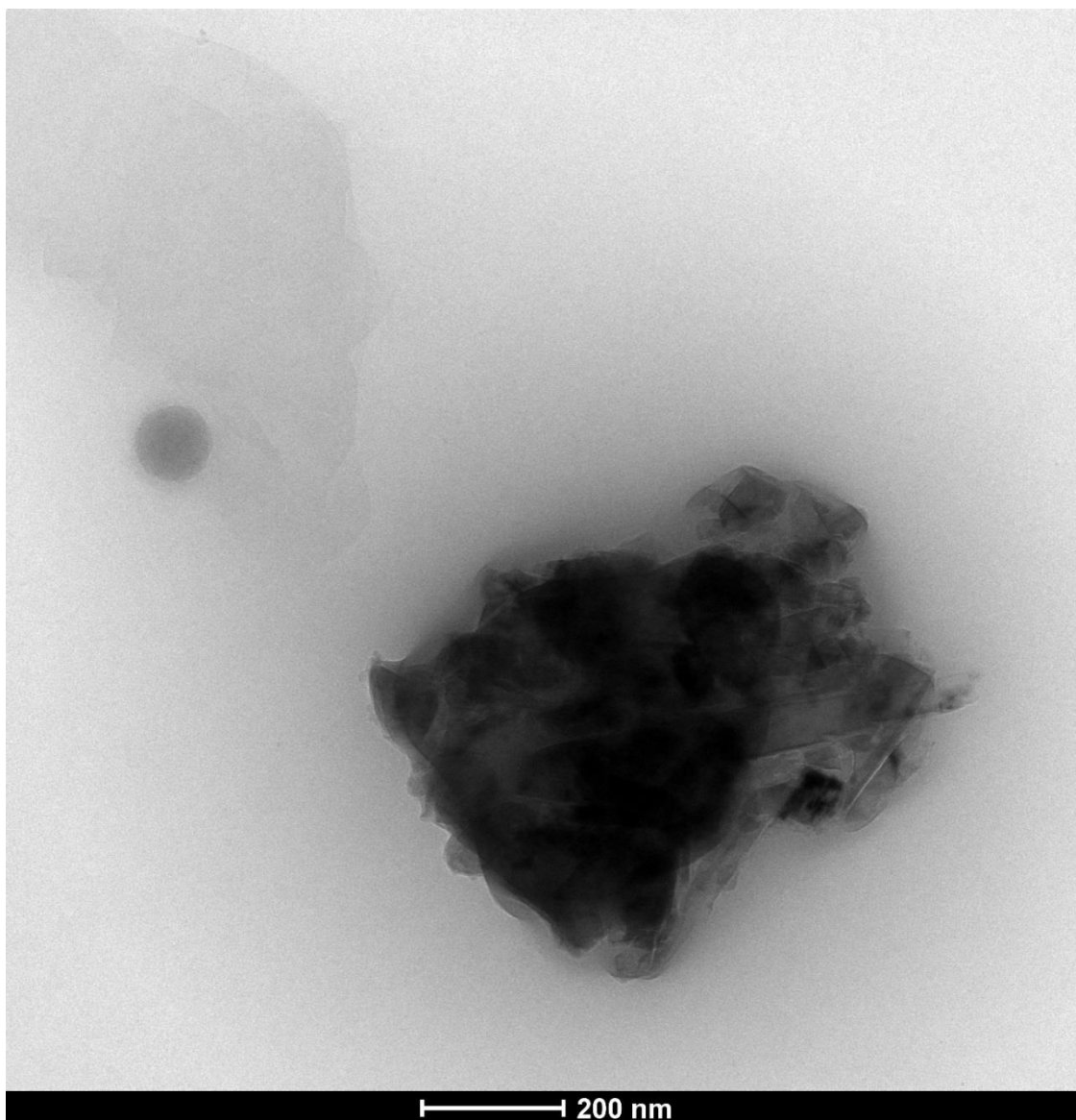


Figure 3.23 TEM of 1,7-octadiene/1-pentene (25%) silicon nanoparticles conjugated to DNA.

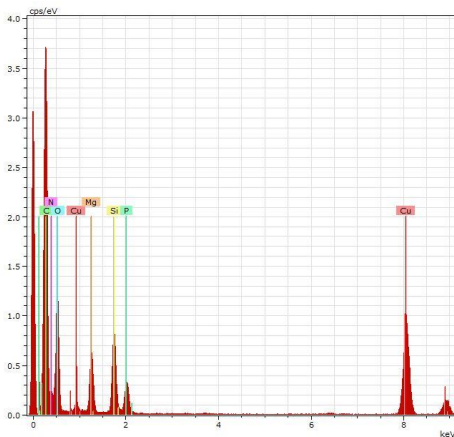


Figure 3.24 EDS of TEM of 1,7-octadiene/1-pentene (25%) silicon nanoparticles conjugated to DNA.

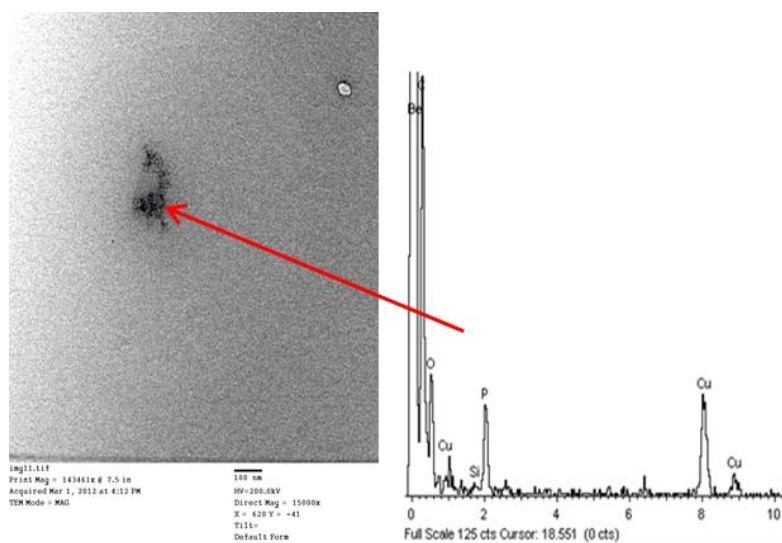


Figure 3.25 TEM and EDS of 1,7-octadiene/1-pentene (50%) silicon nanoparticles conjugated with DNA.

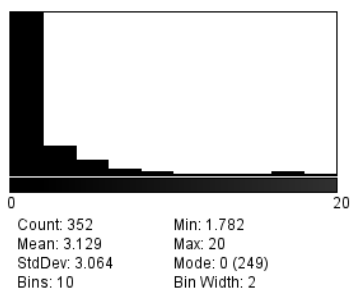


Figure 3.26 Histogram of TEM particles of 1,7-octadiene/1-pentene (50%) passivated silicon nanoparticles conjugated with DNA.

The TEM and EDS show that there are silicon nanoparticles present and that the EDS also shows the elements of silicon for the nanoparticles, magnesium, phosphorous, and nitrogen which are expected from the DNA sequence.

3.7 Conclusion

Based on the spectral analysis of the silicon nanoparticles, it appears that there is strong evidence that the 50% 1,7-octadiene/1-pentene silicon nanoparticles did undergo a conversion of their terminal functionality from olefin to carboxylic acid, and finally to amine. This was supported by the IR of the functionalities and also by the ^1H NMR of the nanoparticles as they progressed through their functionalities. This has led to a method of synthesizing both carboxylic acid and amine terminated nanoparticles. However, other methods have been shown to be easier routes as both functionalities can be gained by RHEBM with the appropriate, though expensive, reactants. This is an economically feasible route as all of the reactants were fairly cheap and common reactants found in the laboratory. However, the many steps coupled with the fact that not all reactions and conversions went to completion means that this route needs to begin with a larger amount of starting material which does not lend itself to being an efficient method of synthesis even though it may be a cheaper route.

The ability to conjugate amines to a carboxylic acid functionalized silicon nanoparticle opens up many interesting avenues of research. It is possible to conjugate almost any biomolecules that have a free amine without steric hindrance preventing the conjugation. The water solubility of the carboxylic acid functionalized nanoparticle is not ideal however. Most reactions were carried out in organic solvents which show a markedly improved solubility for the nanoparticle. It may be necessary to add a water soluble spacer group to take the place of 1-pentene to increase the water solubility of the carboxylic acid functionalized nanoparticles. Similar reactions as to those described here were performed but with a 25% molar solution of 1,7-octadiene/1-pentene silicon nanoparticle solution. There

was no recognizable difference by inspection to the difference in solubility between these two molar concentrations. This seems to suggest that the carboxylic acid functionality does not impart much water soluble character to the nanoparticles, probably due to the formation of dimers. Perhaps a water soluble spacer group will increase the water solubility as the water solubility property is very important with respect to the nanoparticles ability to be a good platform for biomolecules which will be more likely to be water soluble.³¹

The amine functionalized silicon nanoparticles were more water soluble than the carboxylic acid functionalized silicon nanoparticles. However, they still show only partial water solubility and will aggregate with time when left exposed to water. After aggregation, it is very difficult to re-disperse the nanoparticles in even organic solvents such as dichloromethane, which showed excellent solubility prior to aggregation.

The increased luminescence of the amine terminated silicon nanoparticles is important to note. The luminescence is an important physical property which is of great use in many biological roles. These particles coupled with a biomolecule that is targeted to a tumor would prove very useful in detection of remaining cancerous cells during a surgical procedure to remove cancerous tissue.

References

1. Heintz, A. S.; Fink, M. J.; Mitchell, B. S., Mechanochemical Synthesis of Blue Luminescent Alkyl/Alkenyl-Passivated Silicon Nanoparticles. *Advanced Materials* **2007**, *19* (22), 3984-3988.
2. Sam, S.; Touahir, L.; Salvador Andresa, J.; Allongue, P.; Chazalviel, J. N.; Gouget-Laemmel, A. C.; Henry de Villeneuve, C.; Moraillon, A.; Ozanam, F.; Gabouze, N.; Djebbar, S., Semiquantitative Study of the EDC/NHS Activation of Acid Terminal Groups at Modified Porous Silicon Surfaces. *Langmuir* **2010**, *26* (2), 809-814.
3. Yang, M.; Teeuwen, R. L. M.; Giesbers, M.; Baggerman, J.; Arafat, A.; de Wolf, F. A.; van Hest, J. C. M.; Zuilhof, H., One-Step Photochemical Attachment of NHS-Terminated Monolayers onto Silicon Surfaces and Subsequent Functionalization. *Langmuir* **2008**, *24* (15), 7931-7938.
4. Guo, D.-J.; Xiao, S.-J.; Xia, B.; Wei, S.; Pei, J.; Pan, Y.; You, X.-Z.; Gu, Z.-Z.; Lu, Z., Reaction of Porous Silicon with Both End-Functionalized Organic Compounds Bearing α -Bromo and ω -Carboxy Groups for Immobilization of Biomolecules. *The Journal of Physical Chemistry B* **2005**, *109* (43), 20620-20628.
5. Voicu, R.; Boukherroub, R.; Bartzoka, V.; Ward, T.; Wojtyk, J. T. C.; Wayner, D. D. M., Formation, Characterization, and Chemistry of Undecanoic Acid-Terminated Silicon Surfaces: Patterning and Immobilization of DNA. *Langmuir* **2004**, *20* (26), 11713-11720.
6. Barroso, M. M., Quantum Dots in Cell Biology. *Journal of Histochemistry and Cytochemistry* **2011**, *59* (3), 237-251.
7. Erogbogbo, F.; Yong, K.-T.; Roy, I.; Xu, G.; Prasad, P. N.; Swihart, M. T., Biocompatible Luminescent Silicon Quantum Dots for Imaging of Cancer Cells. *ACS Nano* **2008**, *2* (5), 873-878.
8. Tabasi, O.; Falamaki, C.; Khalaj, Z., Functionalized mesoporous silicon for targeted-drug-delivery. *Colloids and Surfaces B: Biointerfaces* **2012**, *98* (0), 18-25.
9. Li, Z. F.; Ruckenstein, E., Water-Soluble Poly(acrylic acid) Grafted Luminescent Silicon Nanoparticles and Their Use as Fluorescent Biological Staining Labels. *Nano Letters* **2004**, *4* (8), 1463-1467.
10. Choi, J.; Wang, N. S.; Reipa, V., Conjugation of the Photoluminescent Silicon Nanoparticles to Streptavidin. *Bioconjugate Chemistry* **2008**, *19* (3), 680-685.
11. Erogbogbo, F.; Yong, K.-T.; Roy, I.; Hu, R.; Law, W.-C.; Zhao, W.; Ding, H.; Wu, F.; Kumar, R.; Swihart, M. T.; Prasad, P. N., In Vivo Targeted Cancer Imaging, Sentinel Lymph Node Mapping and Multi-Channel Imaging with Biocompatible Silicon Nanocrystals. *ACS Nano* **2011**, *5* (1), 413-423.

12. Criegee, R., Mechanism of Ozonolysis. *Angewandte Chemie International Edition in English* **1975**, *14* (11), 745-752.
13. Park, J.; Gomez, A. L.; Walser, M. L.; Lin, A.; Nizkorodov, S. A., Ozonolysis and photolysis of alkene-terminated self-assembled monolayers on quartz nanoparticles: implications for photochemical aging of organic aerosol particles. *Physical Chemistry Chemical Physics* **2006**, *8* (21), 2506-2512.
14. Tilley, R. D.; Yamamoto, K., The Microemulsion Synthesis of Hydrophobic and Hydrophilic Silicon Nanocrystals. *Advanced Materials* **2006**, *18* (15), 2053-2056.
15. Tu, C.; Ma, X.; House, A.; Kauzlarich, S. M.; Louie, A. Y., PET Imaging and Biodistribution of Silicon Quantum Dots in Mice. *ACS Medicinal Chemistry Letters* **2011**, *2* (4), 285-288.
16. Wang, L.; Reipa, V.; Blasic, J., Silicon Nanoparticles as a Luminescent Label to DNA. *Bioconjugate Chemistry* **2004**, *15* (2), 409-412.
17. Park, J.-H.; Gu, L.; von Maltzahn, G.; Ruoslahti, E.; Bhatia, S. N.; Sailor, M. J., Biodegradable luminescent porous silicon nanoparticles for in vivo applications. *Nat Mater* **2009**, *8* (4), 331-336.
18. Kuang, L.; Mitchell, B. S.; Fink, M. J., Silicon nanoparticles synthesised through reactive high-energy ball milling: enhancement of optical properties from the removal of iron impurities. *Journal of Experimental Nanoscience* **2014**, 1-9.
19. Bhattacharjee, S.; Rietjens, I. M. C. M.; Singh, M. P.; Atkins, T. M.; Purkait, T. K.; Xu, Z.; Regli, S.; Shukaliak, A.; Clark, R. J.; Mitchell, B. S.; Alink, G. M.; Marcelis, A. T. M.; Fink, M. J.; Veinot, J. G. C.; Kauzlarich, S. M.; Zuilhof, H., Cytotoxicity of surface-functionalized silicon and germanium nanoparticles: the dominant role of surface charges. *Nanoscale* **2013**, *5* (11), 4870-4883.
20. Dasog, M.; Yang, Z.; Regli, S.; Atkins, T. M.; Faramus, A.; Singh, M. P.; Muthuswamy, E.; Kauzlarich, S. M.; Tilley, R. D.; Veinot, J. G. C., Chemical Insight into the Origin of Red and Blue Photoluminescence Arising from Freestanding Silicon Nanocrystals. *ACS Nano* **2013**, *7* (3), 2676-2685.
21. Manhat, B. A.; Brown, A. L.; Black, L. A.; Ross, J. B. A.; Fichter, K.; Vu, T.; Richman, E.; Goforth, A. M., One-Step Melt Synthesis of Water-Soluble, Photoluminescent, Surface-Oxidized Silicon Nanoparticles for Cellular Imaging Applications. *Chemistry of Materials* **2011**, *23* (9), 2407-2418.
22. Brevet, D.; Gary-Bobo, M.; Raehm, L.; Richeter, S.; Hocine, O.; Amro, K.; Loock, B.; Couleaud, P.; Frochot, C.; Morere, A., Mannose-targeted mesoporous silica nanoparticles for photodynamic therapy. *Chemical Communications* **2009**, (12), 1475-1477.

23. Couleaud, P.; Morosini, V.; Frochot, C.; Richeter, S.; Raehm, L.; Durand, J.-O., Silica-based nanoparticles for photodynamic therapy applications. *Nanoscale* **2010**, *2* (7), 1083-1095.
24. Bechet, D.; Couleaud, P.; Frochot, C.; Viriot, M.-L.; Guillemin, F.; Barberi-Heyob, M., Nanoparticles as vehicles for delivery of photodynamic therapy agents. *Trends in biotechnology* **2008**, *26* (11), 612-621.
25. Cheng, S.-H.; Lee, C.-H.; Chen, M.-C.; Souris, J. S.; Tseng, F.-G.; Yang, C.-S.; Mou, C.-Y.; Chen, C.-T.; Lo, L.-W., Tri-functionalization of mesoporous silica nanoparticles for comprehensive cancer theranostics—the trio of imaging, targeting and therapy. *Journal of Materials Chemistry* **2010**, *20* (29), 6149-6157.
26. Rosso-Vasic, M.; Spruijt, E.; Popovic, Z.; Overgaag, K.; van Lagen, B.; Grandidier, B.; Vanmaekelbergh, D.; Dominguez-Gutierrez, D.; De Cola, L.; Zuilhof, H., Amine-terminated silicon nanoparticles: synthesis, optical properties and their use in bioimaging. *Journal of Materials Chemistry* **2009**, *19* (33), 5926-5933.
27. Sato, S.; Swihart, M. T., Propionic-Acid-Terminated Silicon Nanoparticles: Synthesis and Optical Characterization. *Chemistry of Materials* **2006**, *18* (17), 4083-4088.
28. Kuang, L. Mechanochemical Synthesis, Characterization, and functionalization of Vinyl-Terminated Silicon Nanoparticles. Tulane, 2014.
29. Zhang, H.; Zhou, Z.; Yang, B.; Gao, M., The Influence of Carboxyl Groups on the Photoluminescence of Mercaptocarboxylic Acid-Stabilized CdTe Nanoparticles. *The Journal of Physical Chemistry B* **2003**, *107* (1), 8-13.
30. Robert M. Silverstein, F. X. W., David J. Kiemle, *Spectrometric Identification of Organic Compounds*. 7 ed.; John Wiley & Sons: Hoboken, 2005.
31. L. Wang, V. R., and J. Blasic, Silicon Nanoparticles as a Luminescent Label to DNA. *Bioconjugate Chem.* **2004**, *15*, 409-412.

Chapter 4. X-ray investigation and characterization of silicon nanoparticles.

Section 4.1: Introduction

X-ray absorption near edge spectroscopy (XANES) is an experiment which is dependent on a synchrotron light source compatible with the energy levels needed for the observed atom. One of the limiting factors of using XANES for silicon is the need for a soft x-ray source. Silicon requires a relatively low energy source, below 10 KeV, compared to a large majority of synchrotron sources that are currently available for use. The increase in the power of light sources is shown graphically in Figure 4.1.

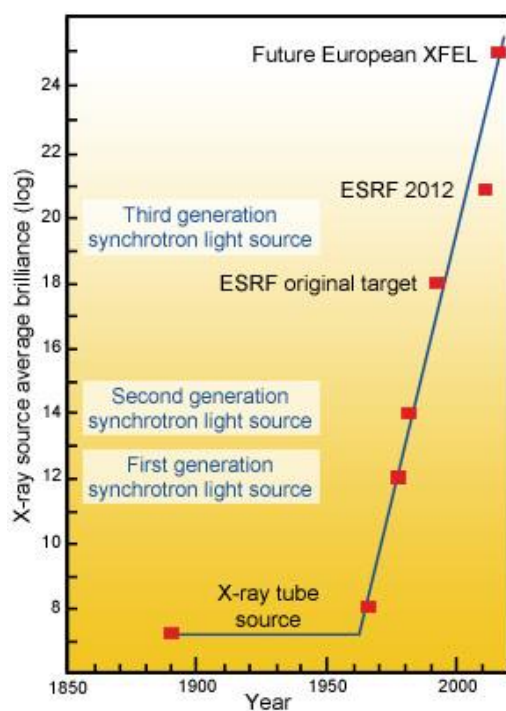


Figure 4.1. Energy levels of synchrotrons.¹

Synchrotron light was developed at General Electric laboratories in 1947.² When electrons are accelerated in a circular orbit at speeds approaching the speed of light they emit x-rays at a tangent to their orbit. The Center for Advanced Microstructures and Devices (CAMD) has a synchrotron light source that is compatible for silicon experiments. The synchrotron operates with a 1.5 GeV storage ring. It is located in Baton Rouge and is affiliated with Louisiana State University. It was the accessibility of this light source which allowed for this project to go forward.

XANES is a technique that provides detailed information on the electronic properties of a material such as silicon nanoparticles. A synchrotron is used to provide x-rays which are tuned to the threshold energy of the material which causes an exciton to be formed by the excitation of a core electron to an unoccupied or continuum state. The secondary processes are then observed such as Auger electrons, x-ray fluorescence, or visible fluorescence.³

XANES provides elemental specific information on the oxidation state and the coordinating environment of components of a material.⁴ There are three ways in which this experiment is generally conducted. The experiment can be done in transmission mode, electron yield, or in fluorescence mode.

The transmission method of XANES detection depends on the sample being able to be transparent to the x-ray. The method of measuring the transmission method is a series of ionization chambers that are on either side of the sample.⁵

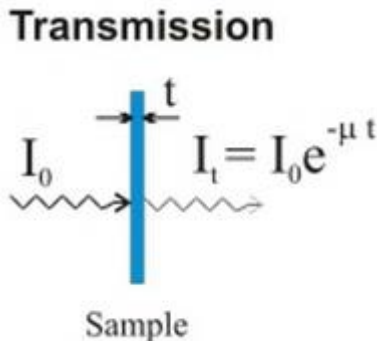


Figure 4.2 Transmission experiment setup of sample in ionization chamber.⁶

This method is a direct measurement of the x-ray absorption by the sample. This method also is able to probe the entire depth of the sample and is not sensitive to the surface as with the total electron yield method (TEY).⁶ The absorbance is measured as the intensity which is equal to the original intensity of the ion chamber before the sample multiplied by an exponential function of the negative of the absorbance coefficient (μ), multiplied by the thickness of the sample, as seen in figure 4.2.

The electron yield method is not a direct measure of the absorbance of the x-rays as with the transmission method. The total electron yield (TEY) method measures the Auger electrons that are caused by the core electron being excited to an excited state. These creates holes in the valence band that are then filled by Auger decay. The primary Auger electrons interact with the environment around the primary absorber creating secondary scattering electrons which dominate the TEY method. This method is more sensitive to the surface of the sample and does not penetrate the sample more than a few nanometers.

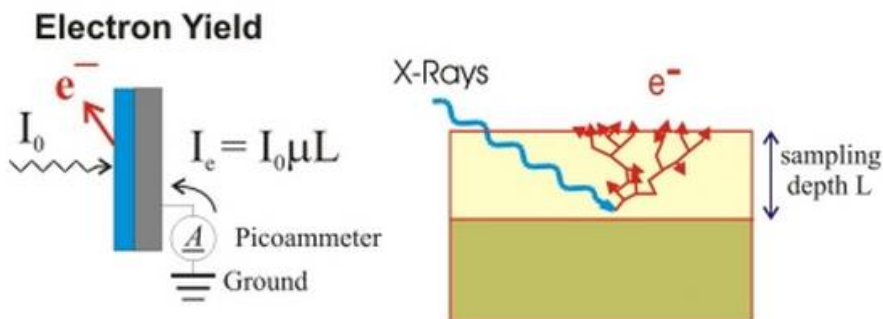


Figure 4.3 Total electron yield method.⁶

In this method the absorbance is calculated as seen in Figure 4.3, as the intensity of absorbance is equal to the original intensity multiplied by the absorption coefficient (μ) and the sample depth.

A third method of detection is the measurement of the fluorescence of the sample. This method is very similar to the method of taking the photoluminescence of the sample. The sample is excited and the radiative recombination of the core and hole is measured by the photons emitted which is measured by a silicon drift detector.

Once the experimental data is collected, the analysis can be done in a few ways. Fingerprinting is a method in which standards of high purity that have also had their XANES spectra taken are compared to the experimental unknown spectra.⁷⁻⁸ This method however, is mostly constrained to identifying known compounds in the sample. However, this technique is closely related to linear combination analysis.⁹ In this method a series of known compounds is compared to the unknown. This is most useful when comparing a sequential range of oxidation states to an unknown sample. This method is used with great results with transition metal elements. XANES has the specificity and ability to detect low concentrations of material which makes this method very useful.

A third method for analyzing XANES samples is to model the XANES spectra of compounds that may comprise your sample. The theoretical XANES spectra can be produced by such software packages as FEFF. FEFF is a software package that can calculate the x-ray absorbance of materials based on Green's Theory.¹⁰⁻¹¹ The theoretical spectra can be compared to the experimental spectra much as one would with the fingerprinting method.¹² Also, a series of compounds could be modeled to create a theoretical linear combination to fit the experimental spectra.¹³

XANES has been used extensively with silicon compounds. XANES has been used to study gases such as methylflurosilane, minerals (Figure 4.5), polymers,^{4, 14-15} and nanoparticles.¹⁶⁻¹⁸ The results of such studies, which were performed at CAMD, were a starting point for the interpretation of the silicon nanoparticle XANES results. Some of the same features can be seen and have already been identified. One such feature is the broad peak that is present in many spectra of both the nanoparticles and of the minerals and methylflurosilane, which was attributed to the ionization potential of the core electron from the K edge.¹⁹

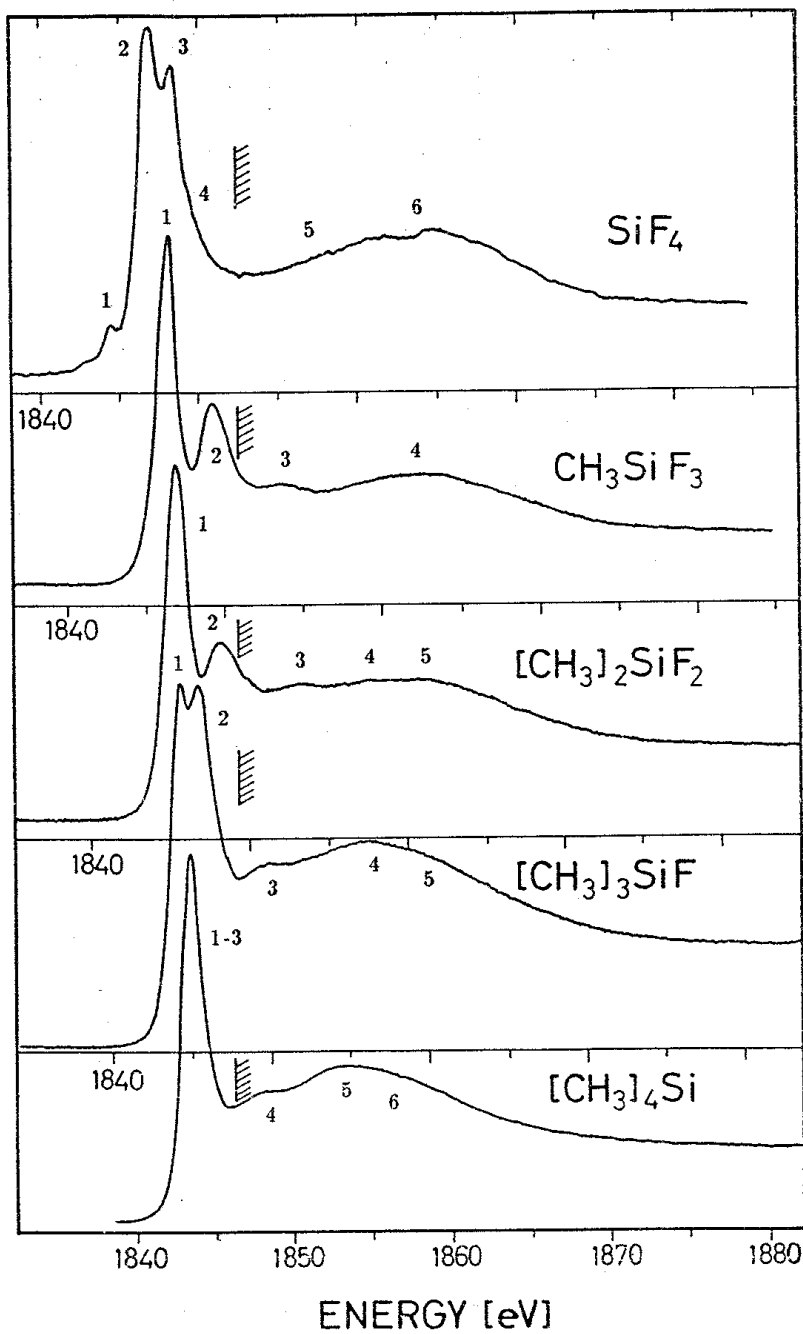


Figure 4.4 Silicon K-edge XANES of methylfluorosilane.¹⁹ Antenna denotes ionization potential.

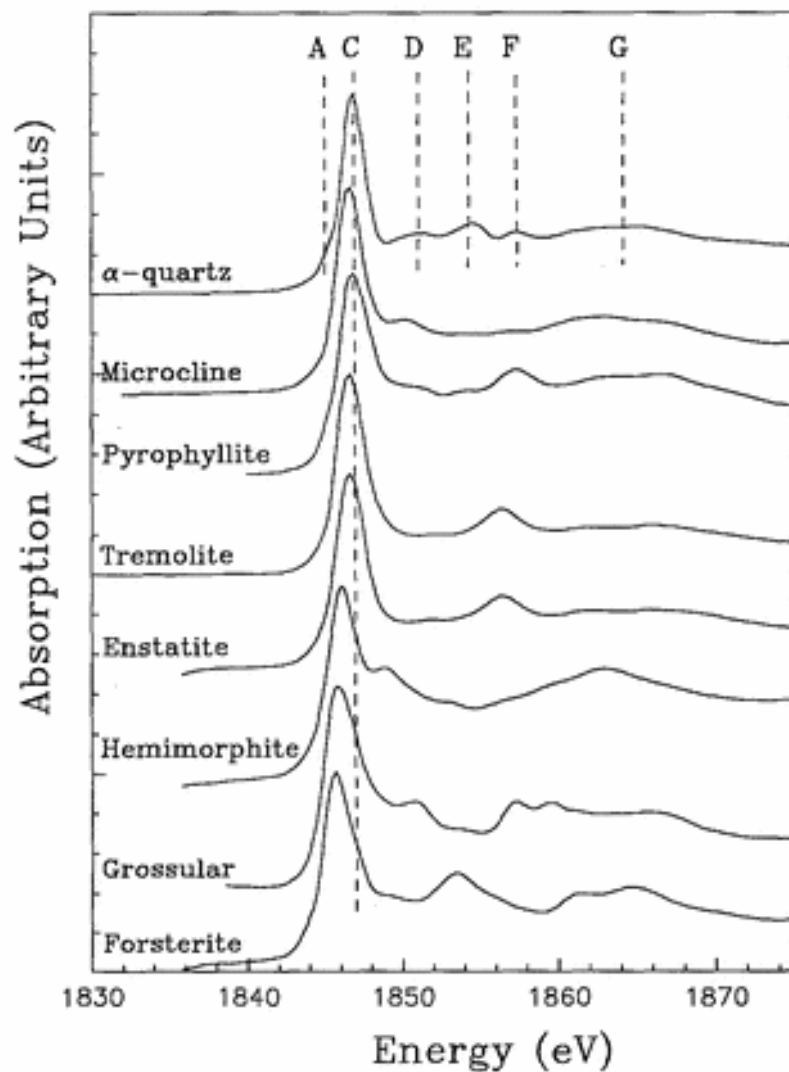


Figure 4.5 Silicon K-edge XANES of silicon minerals.²⁰

The Veinot group has also studied the XANES of monodisperse size samples of silicon nanoparticles and the results obtained are compared to the results of silicon nanoparticles synthesized by reactive high energy ball milling and show good agreement.

Section 4.2: Experimental

All XANES experiments were performed at the Center for Advanced Microstructures and Devices (CAMD) on the campus of the Louisiana State University (LSU). The samples that were used for the XANES experiments were nanoparticle samples that were prepared using the reactive high energy ball milling technique that is described in chapters 2 and 3. The other samples are standards that were purchased.

Samples were prepared in two ways. First, the silicon nanoparticle samples were dissolved in dichloromethane and then deposited on a Kimwipe which was taped to the sample holder. This simple preparation was found to be the most efficient method, as the Kimwipe was thin enough to allow the beam pass through the sample and was devoid of any residual silicon species used in the manufacturing process. Secondly, the powdered standard samples were ground using a mortar and pestle and were then sealed inside a mylar pouch. The mylar pouch was constructed of a piece of mylar that had the sample sprinkled onto it, folded over and then taped with scotch tape. The ground particles of the samples clung to the mylar, and were situated on the sample holder so that the beam passed through a portion of the mylar pouch that was populated with the powdered sample.

The XANES experiments were performed on the double crystal monochromator (DCM) beam line. The set up for the DCM beam line is shown in Figure 4.6.

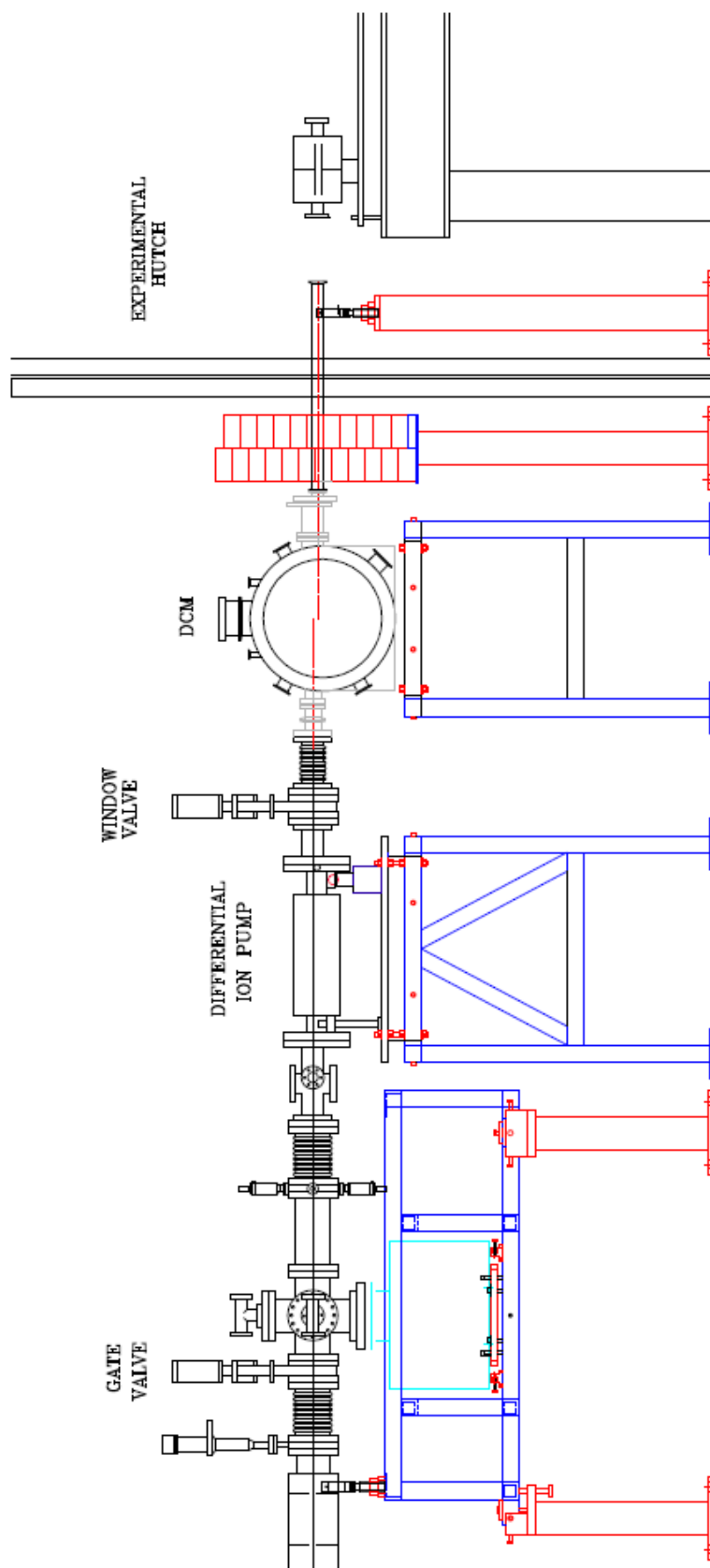


Figure 4.6. Schematic drawing of double crystal monochromator.²¹

The DCM beam line is situated on a bending magnet 5 and accepts 2 mrad of radiation. The beam line has been in operation since 1994 and uses a Lemmonier-Bonn type of double crystal monochromator.²¹ The crystal used for silicon K-edge experiments were YB₆₆ (400) which are useful between 1170 – 4090 eV. The k-edge of silicon is 1842 eV, well within the range of these crystals. A bremsstrahlung shutter has been added downstream from the monochromator, so that the samples can be changed in the experimental hut, while the monochromator is still exposed to light. This is of great help as the crystals are constantly exposed to light and the thermal equilibrium of the crystals is maintained while the samples are being changed. This allows for data from the samples to immediately be taken, without a required time period for the crystal to once again reach thermal equilibrium.

The DCM beam line can detect data by three means; there is a 13- element germanium diode array fluorescence detector, a Lytle fluorescence and electron yield detectors, and ionization chambers. This allows for data to be collected by transmission, fluorescence, and electron yield modes. The experiments discussed in this chapter will all be data that was collected using the ionization chambers to collect transmission data.

The experimental set up consisted of preparing the sample by making the mylar pouch or by evaporating the nanoparticle samples on a strip of Kimwipe. The samples were then affixed to the sample holder which was positioned perpendicular to the radiation beam. The ionization chamber was then pumped down till it was a steady 0.2 atm. The fill gas used was nitrogen which is the suggested gas for samples below 3 KeV.²² The hutch was then secured and the bremsstrahlung shutter was opened allowing radiation into the ionization chamber.

Two silicon nanoparticle systems were investigated, nanoparticles passivated by 1-octyne and 1-octene. The particles were prepared by reactive high energy ball milling using the same methods previously described in Chapters 2 and 3 and reported by Heintz.³³ The systems were all fractionated using a gel permeation chromatography column. This separated the molecular impurities from the nanoparticles while also separating the nanoparticles by size. The earlier fractions contain nanoparticles that are larger and the later fractions contain nanoparticles that are smaller. These fractions were then individually investigated using XANES.

Section 4.2.1: Results and discussion

XANES Spectroscopy

The experiment is calibrated by using two standards. The first is silicon dioxide which is known to have a strong peak at 1848 eV. This can be seen in Figure 4.7 below.

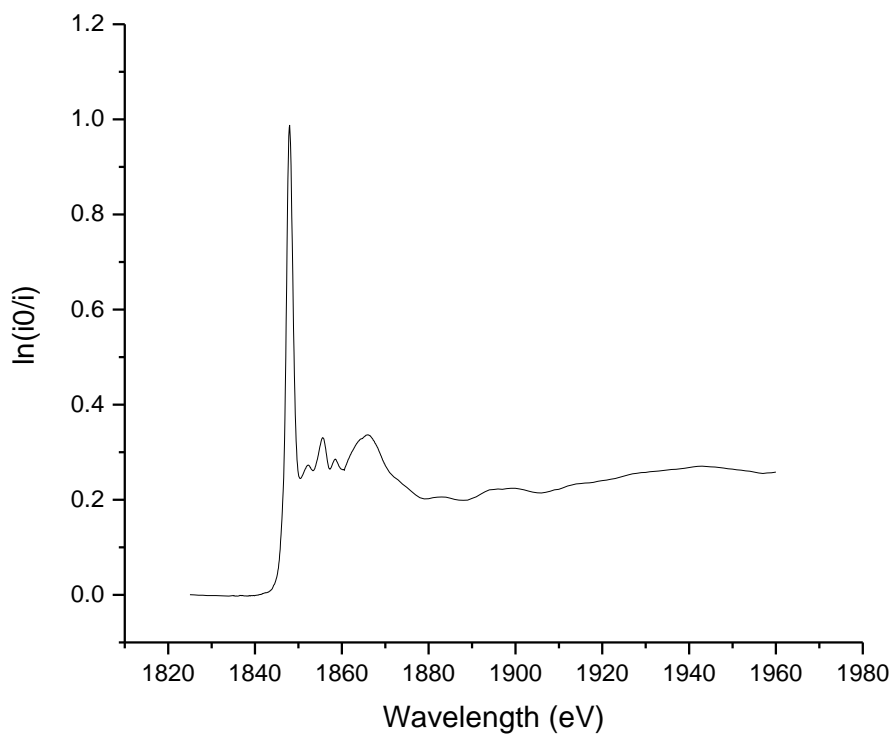


Figure 4.7. XANES spectra of silicon dioxide standard.

The other standard that was used for calibration was powdered silicon that was ground using a mortar and pestle right before the experiment so that the surface of the silicon would not be overly oxidized. This can be seen in Figure 4.8.

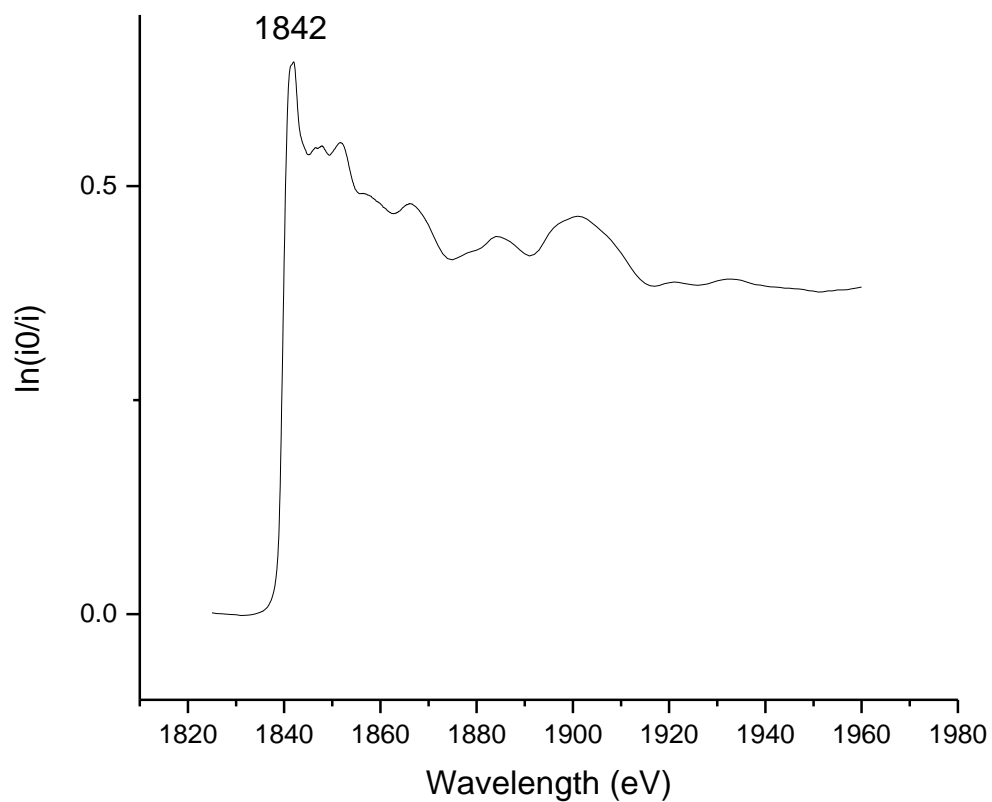


Figure 4.8. Silicon powder standard.

Calibration was done daily with silicon dioxide to insure that the data recorded was correctly calibrated. The two silicon nanoparticle systems were then recorded. Below in Figure 4.9, the XANES spectra for 1-octyne passivated silicon nanoparticles can be seen. These nanoparticles were prepared by Dr. Tapas Purkait in 2010.

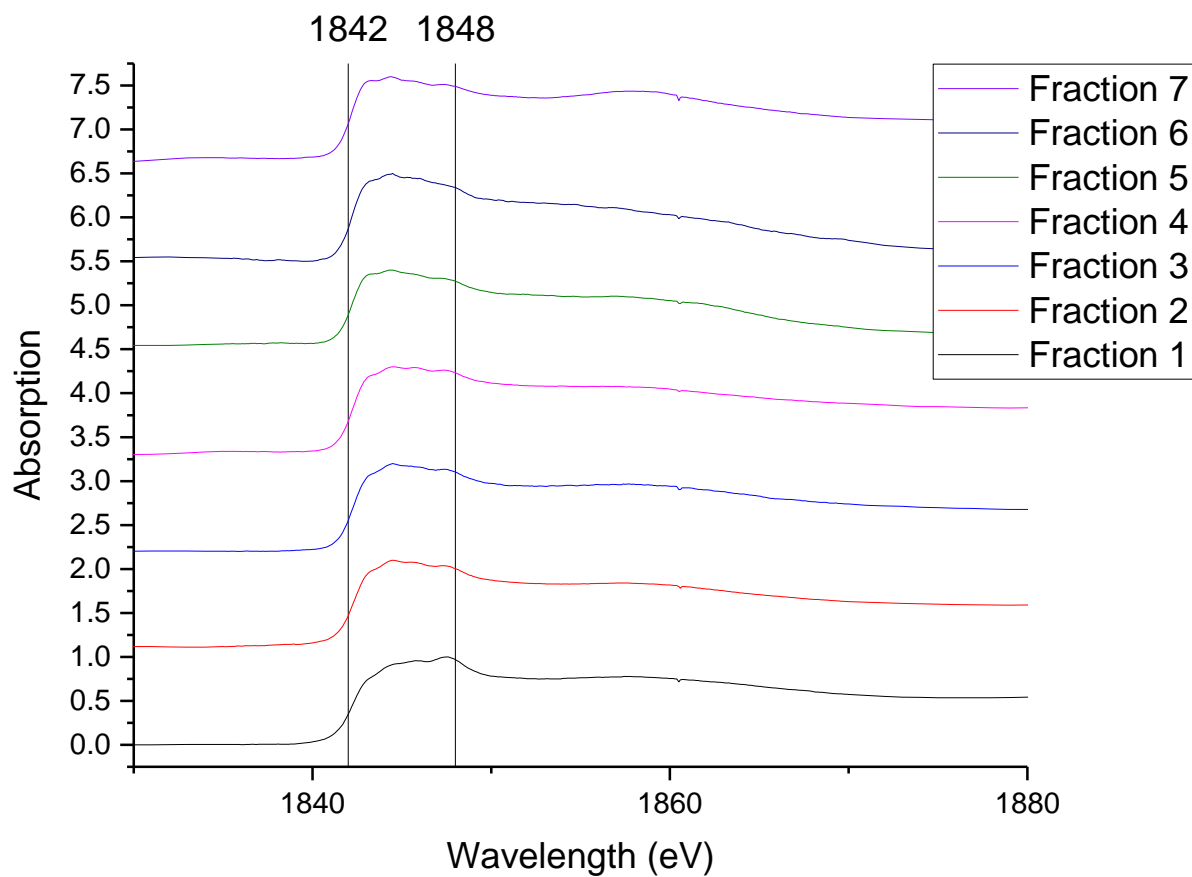


Figure 4.9 XANES results of 1-octyne passivated silicon nanoparticle fractions.

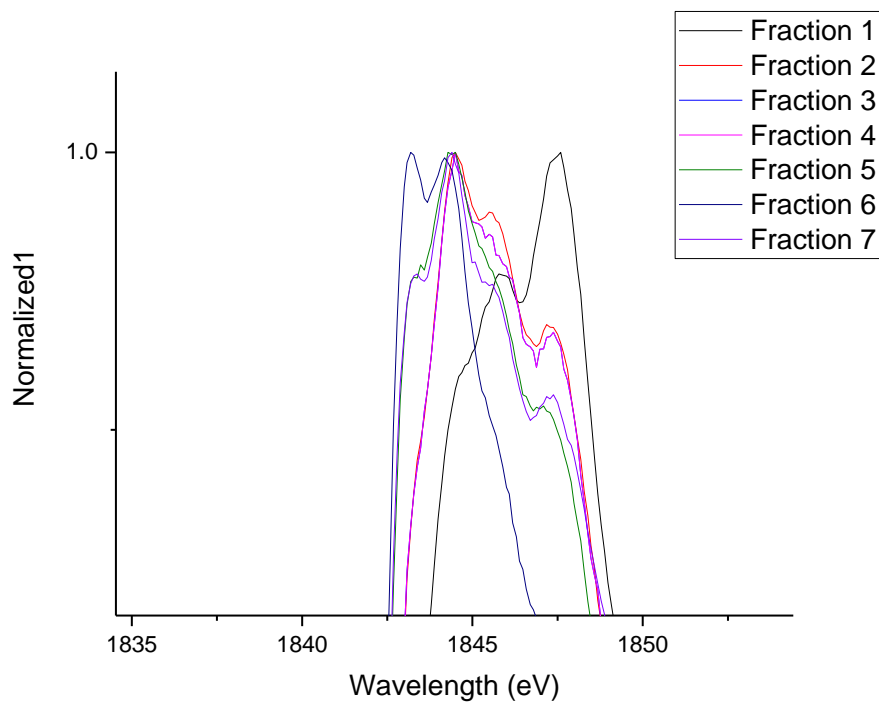


Figure 4.9B. Close up view of all normalized peaks of 1-octyne passivated silicon nanoparticles over laid, showing trend for later fractions to have moved to lower wavenumbers.

As seen in the XANES spectra of silicon nanoparticles passivated by 1-octyne, there is a trend of the major peak observed first being observed at 1848 eV and then trends towards 1842 eV with later fractions. This is explained by the first fractions having more oxygen present on the surface of the silicon nanoparticles. There is a secondary feature that is seen that lies between the bordering peaks at 1842 eV and 1848 eV. This is a fine peak splitting feature that is the focus of this project. The assignment of this peak splitting will be discussed later in the modeling section.

The XANES spectra of 1-octene passivated silicon nanoparticles is seen in Figure 4.10. These nanoparticles were prepared by Dr. Zejing Xu.

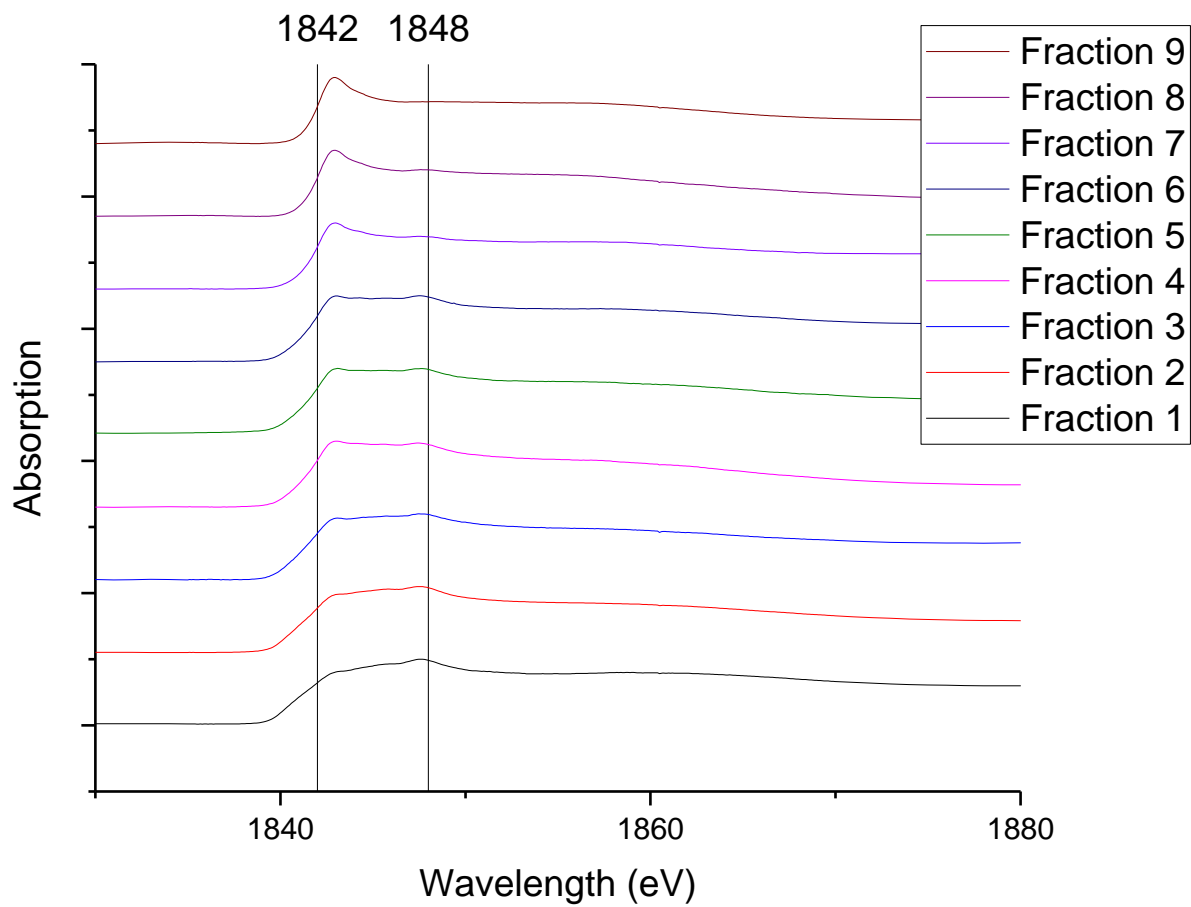


Figure 4.10 XANES results of 1-octene passivated silicon nanoparticles.

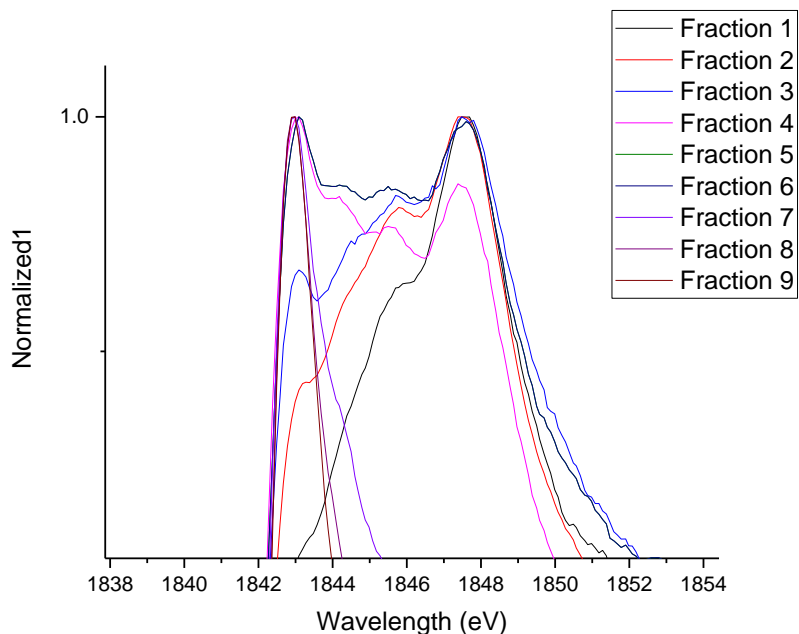


Figure 4.10B. Close up view of all normalized peaks of 1-octene passivated silicon nanoparticles overlaid, showing trend for later fractions to have moved to lower wavenumbers.

The same trend can be seen in the 1-octene passivated silicon nanoparticles as was seen in the 1-octyne passivated silicon nanoparticles. The early fractions show the major peak occurring at 1848 eV, which is where silicon dioxide is observed. This indicates that there is oxygen on the surface of the nanoparticles which is not unexpected. This is a common trend with the silicon nanoparticles prepared by reactive high energy ball milling and is observed in the infrared spectra of the particles as seen in the IR spectra of 1-octene passivated silicon nanoparticles in Figure 4.11.

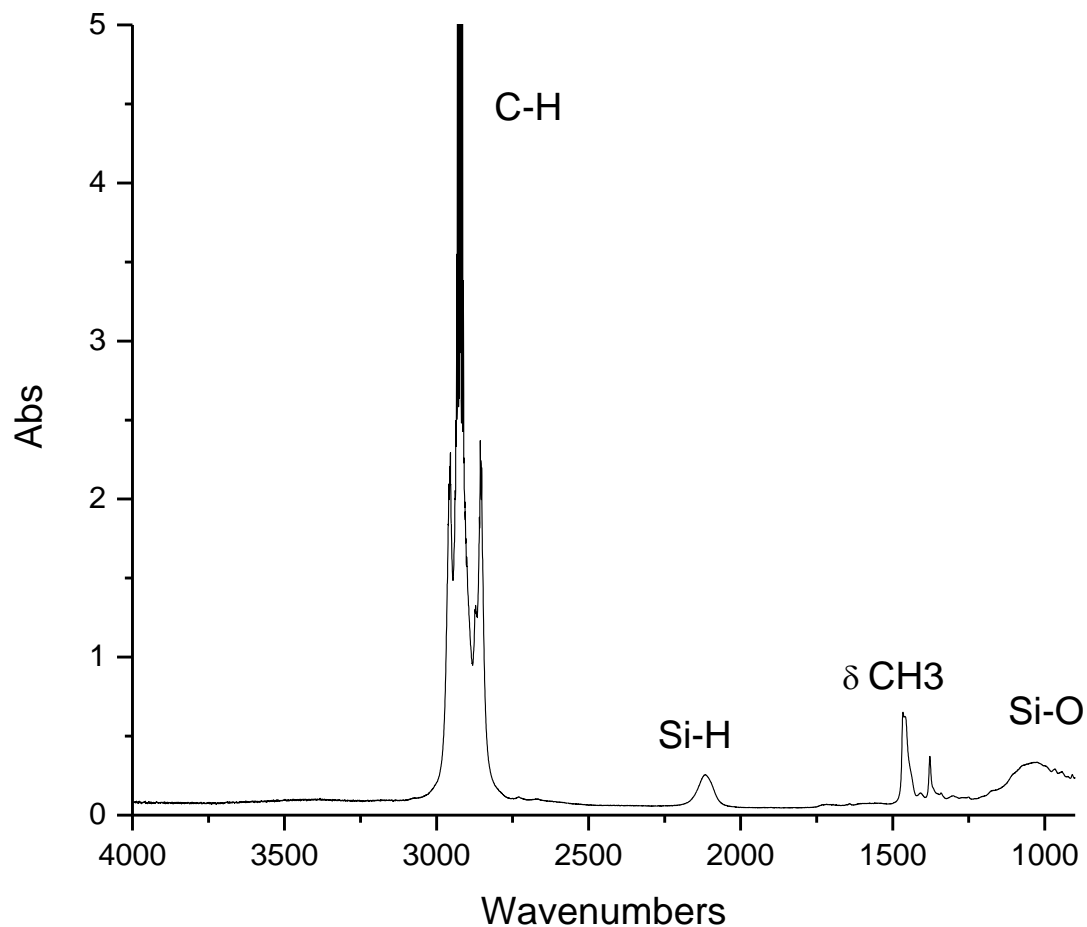


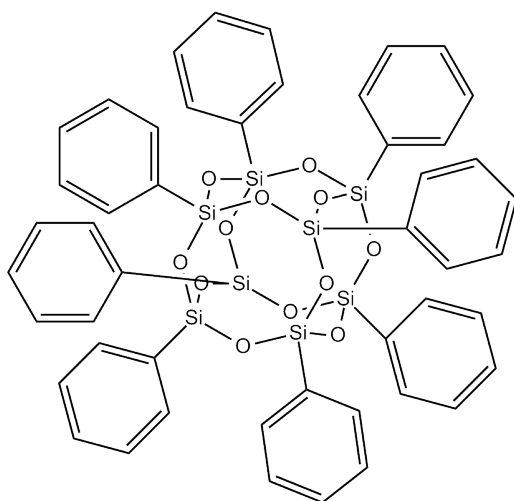
Figure 4.11 Infrared spectra of 1-octene nanoparticles.

The later fractions trend towards 1842 eV, the same trend that was observed with the 1-octyne passivated silicon nanoparticles. Once again, an intermediate peak is also observed.

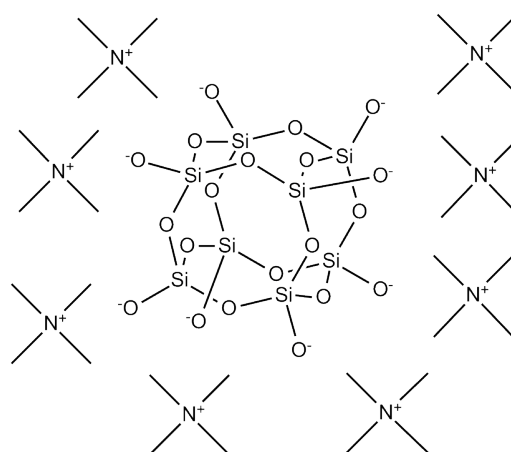
The nature of the intermediate peak was investigated by obtaining the XANES of a series of highly pure commercially available silicon standards. The interest in these molecules was to try and identify similar peaks with highly pure molecules, so that the

unknown peak could be assigned. This method is the fingerprinting method that was described in the introduction to this chapter. The molecules and their corresponding XANES spectra are shown.

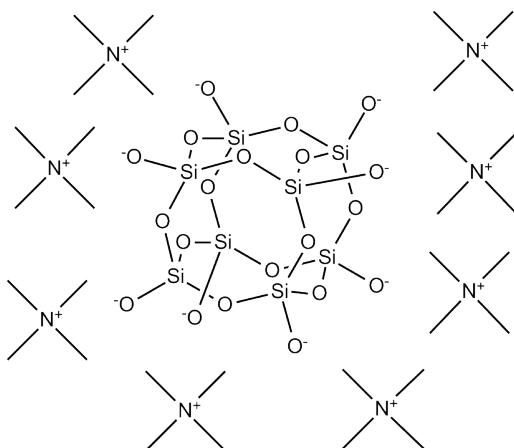
Silicon standards:



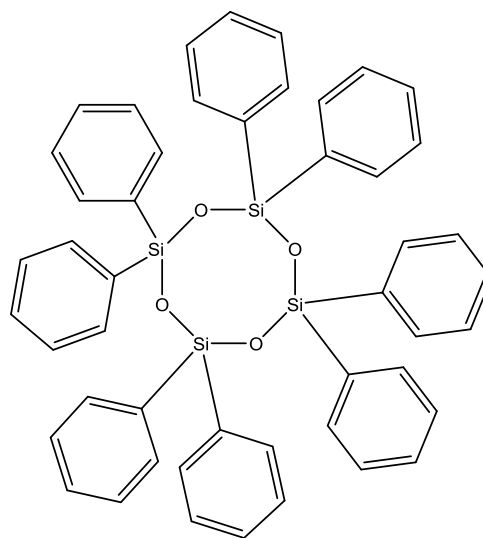
Octaphenyl-T8-silsesquioxane



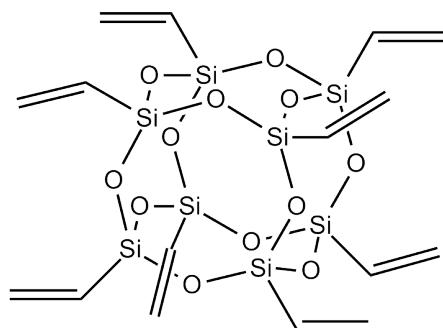
Octakis(tetramethylammonium)-T8-silsesquioxane hydrate



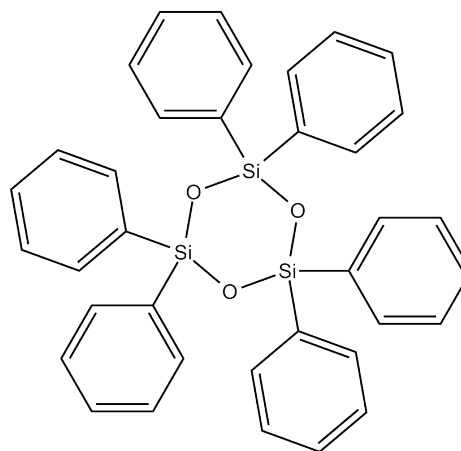
Octakis(dimethylsiloxy)-T8-
silsesquioxane



Octaphenylcyclotetrasiloxane



Octavinyl-T8-silsesquioxane



Hexaphenylcyclotrisiloxane

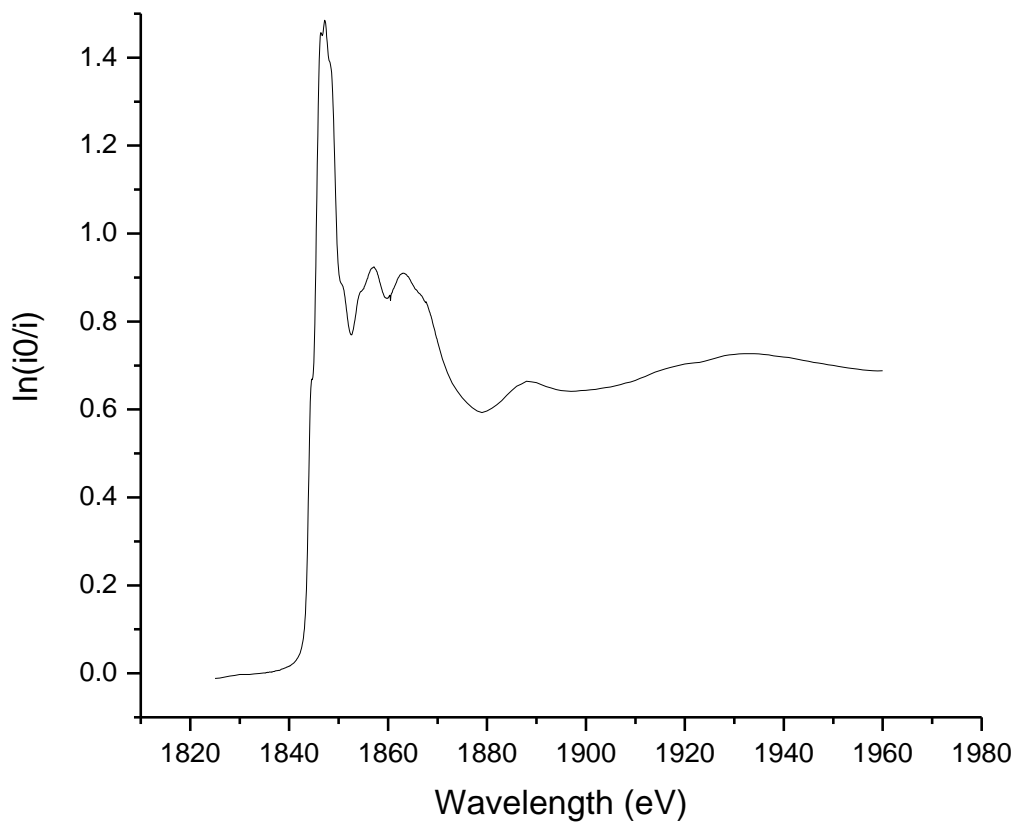


Figure 4.12 XANES spectra of octaphenyl –T8- silsesquioxane.

The XANES spectra of octaphenyl –T8- silsesquioxane, $(\text{PhSiO}_{3/2})_8$ shows a strong major peak at 1848 eV. This is expected as there multiple Si-O bonds in the molecule.

However, there are slight shoulders that appear at 1844 and 1845 eV. These shoulders appear to correspond to Si-C bonds.

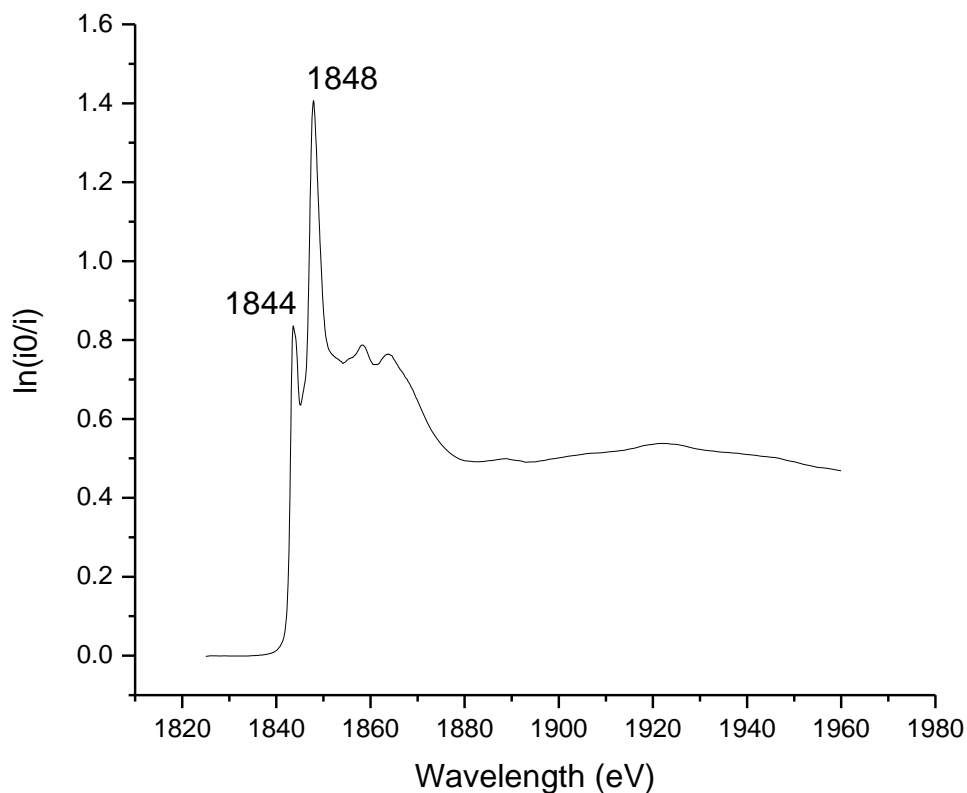


Figure 4.13 XANES spectrum of octakis(dimethylsiloxyl)-T8-silsesquioxane.

The XANES spectrum of octakis(dimethylsiloxyl)-T8-silsesquioxane, $((\text{CH}_3)_2\text{SiHSiO}_{3/2})_8$ shows a very defined strong peak at 1844, as compared to the slight shoulder seen in octaphenyl-T8-silsesquioxane. Here however, there are bonds to both methyl groups and also hydrogen that could be assigned to this peak. There is no separate peak observed for Si-C and Si-H. Once again, as expected, the major peak is the peak at 1848 eV for the Si-O bonds.

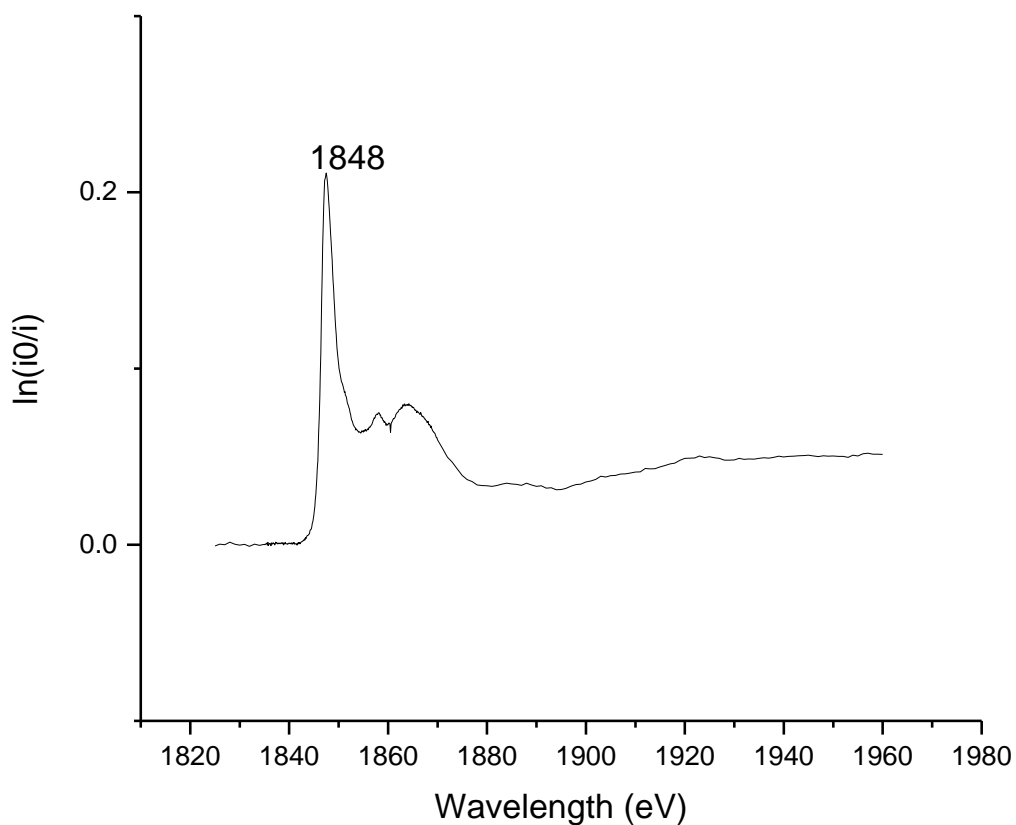


Figure 4.14 XANES spectra of octakis(tetramethylammonium)-T8-silsesquioxane hydrate

Octakis(tetramethylammonium)-T8-silsesquioxane hydrate, $((\text{CH}_3)_4\text{NSiO}_{3/2})_8$ was chosen as there are no bonds except for Si-O bonds. However, there are counter ions of tetramethylammonium. However, as seen in the spectra, there is no peak or shoulder present for any scattering interaction with the counter ion.

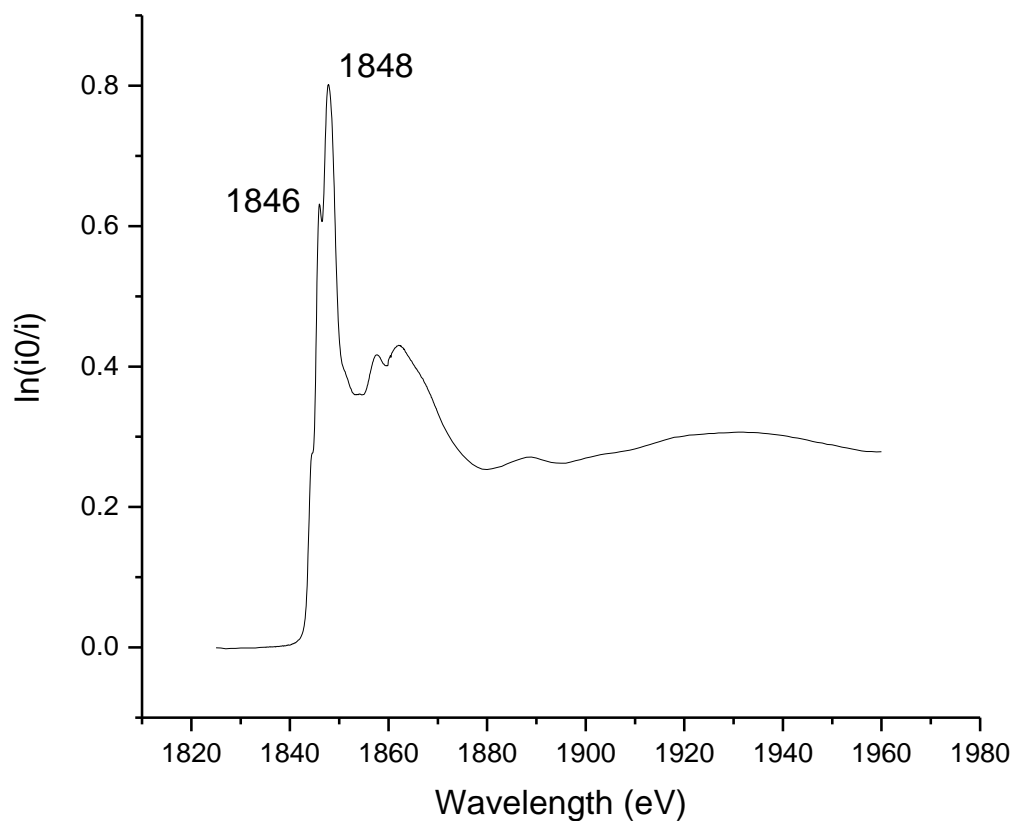


Figure 4.15 XANES spectra of octavinyl-T8-silsesquioxane

Octavinyl-T8-silsesquioxane, $(C_2H_3SiO_{3/2})_8$ was chosen as a standard because of the vinyl group attached to the silicon atoms. The location of the peak that was associated with this feature should be comparable to both the 1-octyne and the 1-octene passivated silicon nanoparticles which both have possible bonding modes with an sp^2 hybridized carbon. As seen there is a distinct peak, however, not a strong peak, at 1846 eV. Once again the major peak is the Si-O peak at 1848 eV.

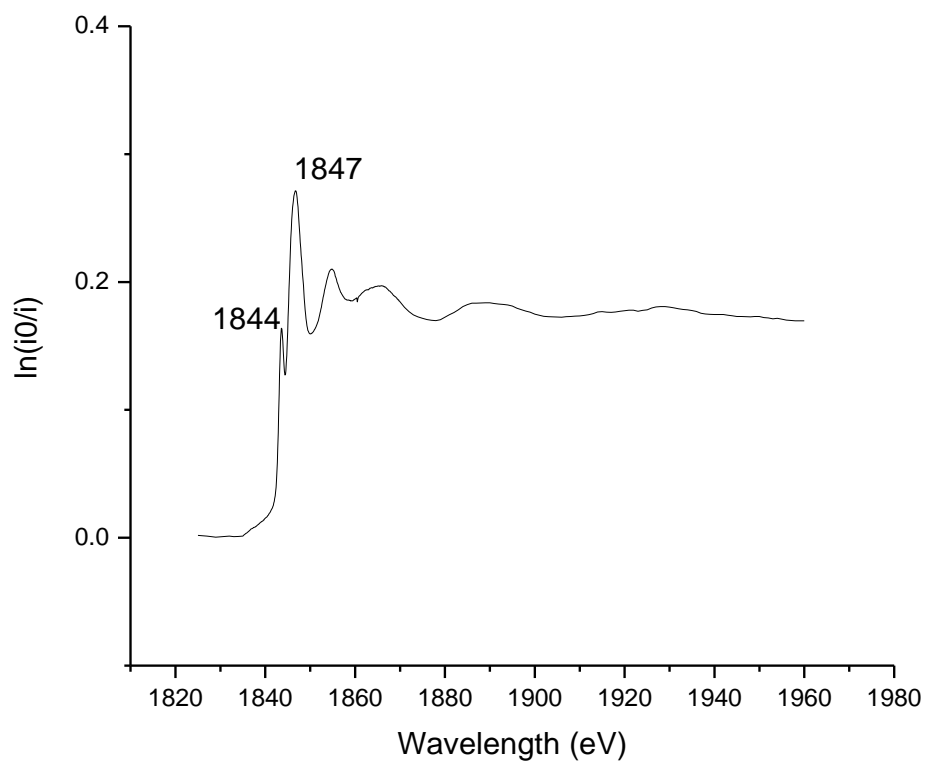


Figure 4.16 XANES spectra of octaphenylcyclotetrasiloxane.

The spectra of octaphenylcyclotetrasiloxane, $(\text{Ph}_2\text{SiO})_4$ shows a major peak at 1848 eV that corresponds to the multiple Si-O bonds. Also, there is a minor peak at 1844 eV that corresponds to the Si-C bond with the phenyl groups.

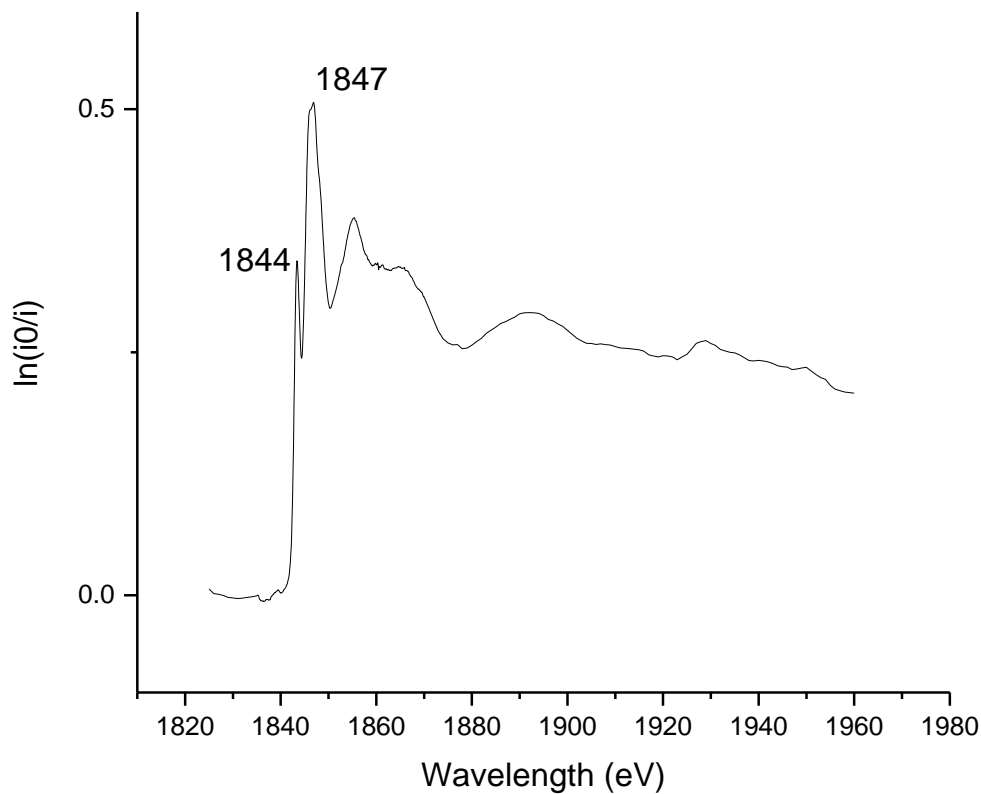


Figure 4.17 XANES spectra of hexaphenylcyclotrisiloxane.

The XANES spectra of hexaphenylcyclotrisiloxane shows the same trend. The Si-O peak is seen at 1848 eV as is seen in all the other silicon standards with an Si-O bond. There is also a minor peak seen at 1844 eV that corresponds to the Si-C bond of the phenyl group.

With the information gained from the highly pure standards, the assignment of bonds was attempted as with the fingerprint method of assignment. The Si-O bond is represented by a strong peak at 1848 eV. However, the assignment of the intermediate

peak could not be accomplished by the finger printing method. Whether there was a Si-H or an Si-C bond, the peak was between 1844 and 1846 eV. The peak did not correspond to a change in the hybridization of the carbon that was attached to the silicon. The phenyl groups of hexaphenylcyclotrisiloxane and octaphenylcyclotetrasiloxane showed a peak at 1844 eV which is the same as the methyl groups bonded to silicon in octakis(dimethylsiloxy)-T8-silsesquioxane.

The XANES of our nanoparticles can be compared to an earlier XANES study conducted by the Veinot group. These results are of silicon nanoparticles prepared from the etching of silicon rich powders prepared by thermal annealing of hydrogen silsesquioxane as described in chapter 1. As seen in Figure 4.18 the silicon nanoparticles are shown plotted with a silicon standard, a silicon dioxide standard, a control, and the styrene and 1-hexene passivated silicon nanoparticles. The control refers to silicon nanoparticles that are freshly etched and have a surface of hydrogen.

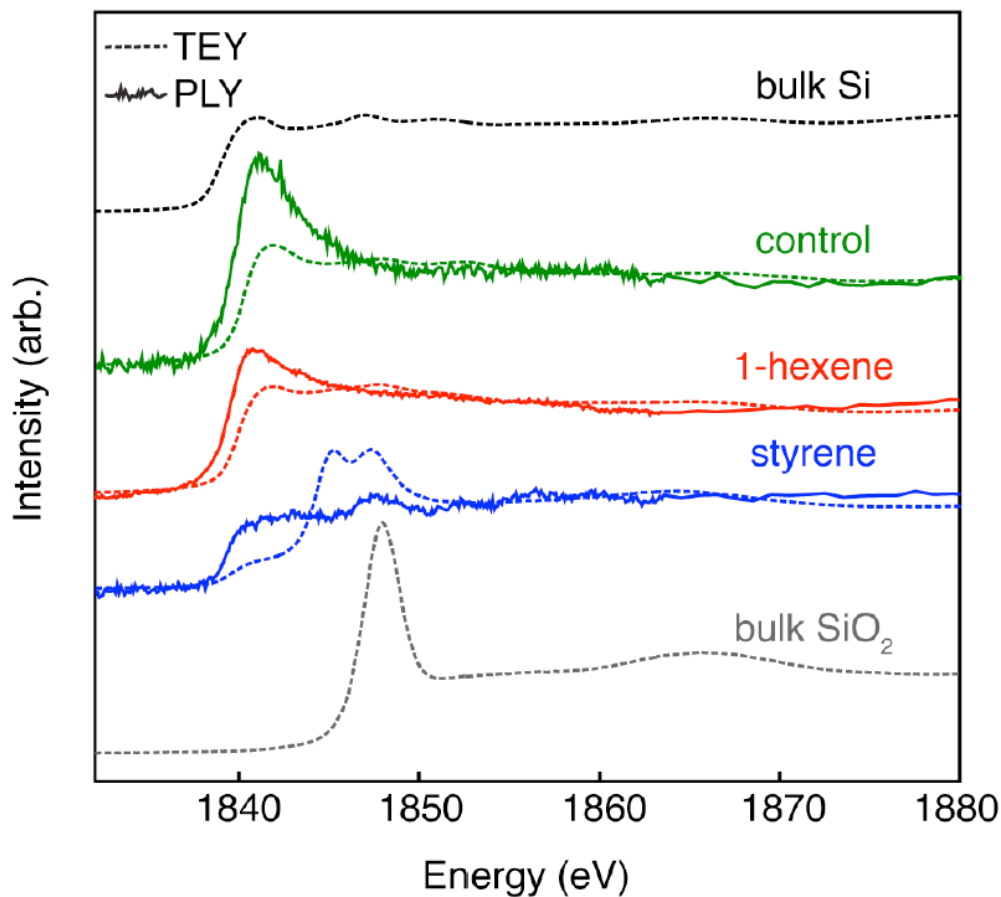


Figure 4.18 XANES K-edge spectra of silicon nanoparticles prepared as described in chapter 1 from silicon rich silicon oxides.^{17, 23}

As seen in Figure 4.18 the total electron yield (TEY) and the photoluminescence yield (PLY) offer two different sets of information. The TEY is more of a surface technique while the PLY shows information that is mainly from the core of the silicon nanoparticle. While the TEY of the styrene nanoparticles shows that the nanoparticles are mostly oxidized, the PLY shows mostly the silicon core contribution with a small peak for the oxidized surface.

The XANES spectra of the control, 1-hexene, and styrene passivated samples all show a major peak at 1842 eV corresponding to the K-edge of the silicon. There is also a smaller peak in each spectra around 1844-1846 eV that corresponds to the passivating layers of hydrogen, hexane, or styrene. These results are in good agreement with our results.

The investigation of the silicon XANES of different passivated silicon films containing nitrogen shows similar peak features (Figure 4.19).

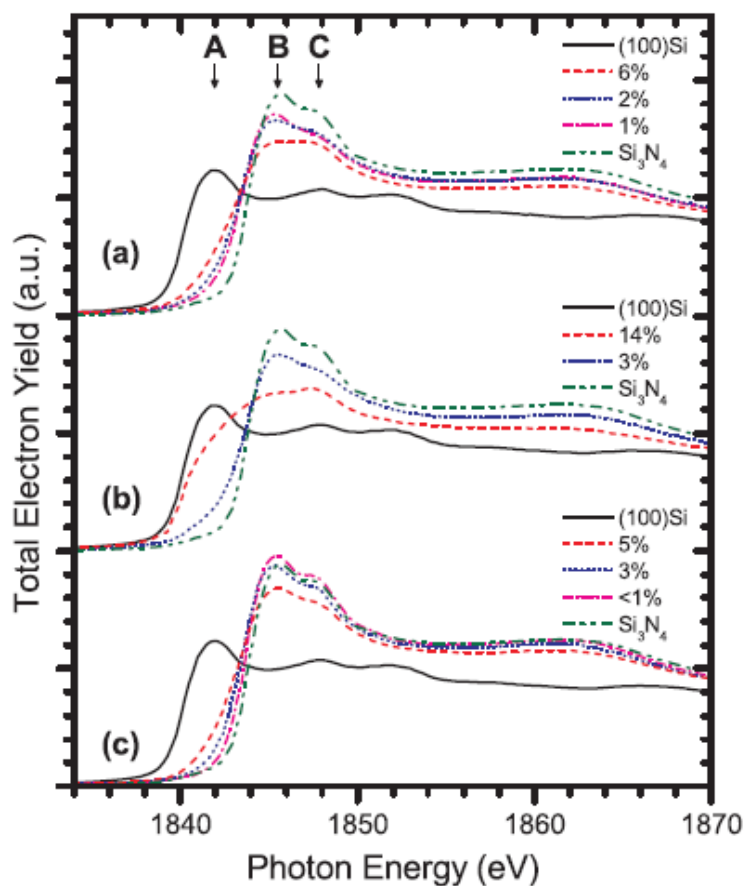


Figure 4.19 TEY-XANES spectra for silicon rich silicon nitride films (a) plasma enhanced chemical vapor deposition (PECVD), (b) electron cyclotron resonance PECVD, and (c) inductively coupled plasma chemical vapor deposition films at the Si K-edge. A,

B, and C indicate the peak positions for Si-Si, Si-N, and Si-O resonances, respectively. The percentages in the legend refer to the excess silicon content of the silicon rich silicon nitride films.²⁴

There is an onset of silicon absorbance (1842 eV) and also a peak at 1844-1846 eV for the nitrogen that is bonded to silicon. The percentage of nitrogen is varied in the silicon films, producing different line shapes, however, the same trends of a peak between 1844-1846 eV for a molecular species bonded to the silicon is present. This doesn't change with the hybridization of the carbon atom directly attached to the silicon, nor does it change with the element that is attached to the silicon. Since assignment of the intermediate peak was not successful using the finger printing method by comparing with pure standard compounds, another method of interpreting the XANES spectra was needed. This was attempted by using modeling of the silicon nanoparticle clusters using FEFF9.

Section 4.3: Modeling

Modeling the silicon nanoparticles was the next step in trying to assign the intermediate peak between 1844 and 1846 eV. FEFF9 is an *ab initio* multiple scattering software package available from the University of Washington Physics department. The program allows for the multiple scattering calculation of XANES.¹¹ This allows for the silicon nanoparticles to be modeled with the basis of the model being the optimized structure coordinates of the silicon nanoparticles. This was accomplished using the SPARTAN software package. Silicon nanoparticles modeled and the structure was optimized using Merck molecular force field (MMFF) calculations.

The models were first constructed to determine the effect of the passivating organic molecule. A 29 atom silicon nanoparticle with T_d symmetry was attached with a range of alkyl chains (1-8 carbons in length). The model was optimized using MMFF and the coordinates of the model were inputted into the FEFF9 modeling program. The program requires that an absorbing atom be identified. With the nanoparticle having T_d symmetry, there were three levels of silicon atoms in the model. The silicon at the core, which was surrounded by 4 silicon atoms (second “level”) and then 24 silicon atoms that were surface atoms (third “level”). This can be seen in Figure 4.

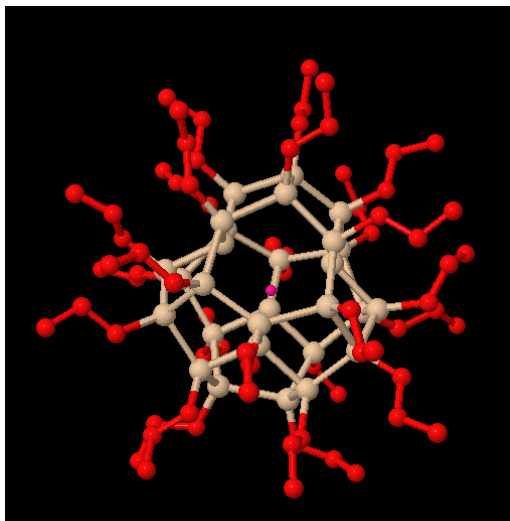


Figure 4.20 Model of 29 at silicon nanoparticle with propyl chains passivating surface.

The symmetry of the nanoparticle allows for only one atom at each level to be designated as the absorbing atom. Then the three “levels” are weighted by their frequency and a composite model XANES structure can be derived. The results of this modeling with the differing chain lengths can be seen in Figure 4.19.

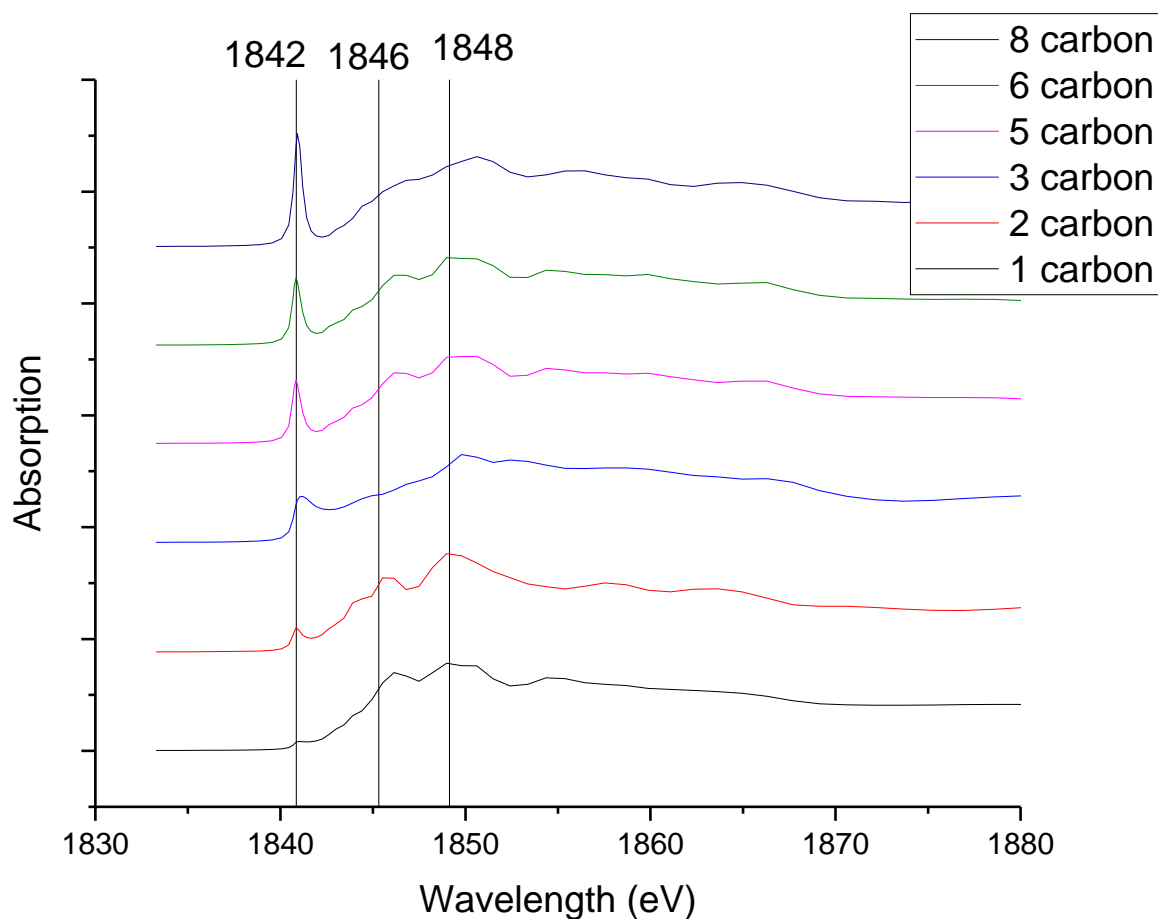


Figure 4.21 FEFF calculations of chain length on 29 atom silicon nanoparticle (0.8 nm).

The results of the FEFF calculations on chain length shows no trend as was seen with the 1-octyne and 1-octene passivated silicon nanoparticles. There is a trend however, that the longer the chain length the stronger the Si-Si peak at 1842 eV is. There is no trend however, that smaller nanoparticles (including the chain length) have a major peak at 1842 eV, while the larger particles have a major peak at 1848 eV. This can be explained as there are no Si-O bonds in these silicon clusters. There is a constant peak at 1850 eV. This peak lies outside of the range that was observed experimentally that was

bordered by 1842 and 1848 eV. There was an experimental constant peak that showed no change that appears at about 1860 eV. However, the intermediate peak that is of interest is seen at 1846 eV. The peak is very well defined in some FEFF spectra while only seen as a shoulder in other spectra such as the propyl passivated silicon nanoparticle.

A second aspect of the silicon clusters that was investigated by modeling was the effect of the silicon cluster size on the XANES spectra. This was accomplished by constructing silicon clusters with larger diameters corresponding to different “layers” of silicon atoms surrounding the silicon core. A 119 atom cluster was constructed and then its geometry was optimized using MMMFF calculations using the SPARTAN program as was done for the silicon 29 clusters. The diameter of the 119 silicon atom cluster was 1.5 nm. A third cluster was also constructed using 232 silicon atoms. This cluster has a diameter of 2 nm. This cluster was optimized using MMFF calculations and the optimized geometry structural coordinates inputted into the FEFF program as were with the other two silicon cluster sizes. A larger cluster was constructed, however, the FEFF program was not able to handle the larger cluster and crashed, limiting the size of the clusters that could be studied.

The results from the modeling of the different cluster sizes is shown below in Figure 4.22

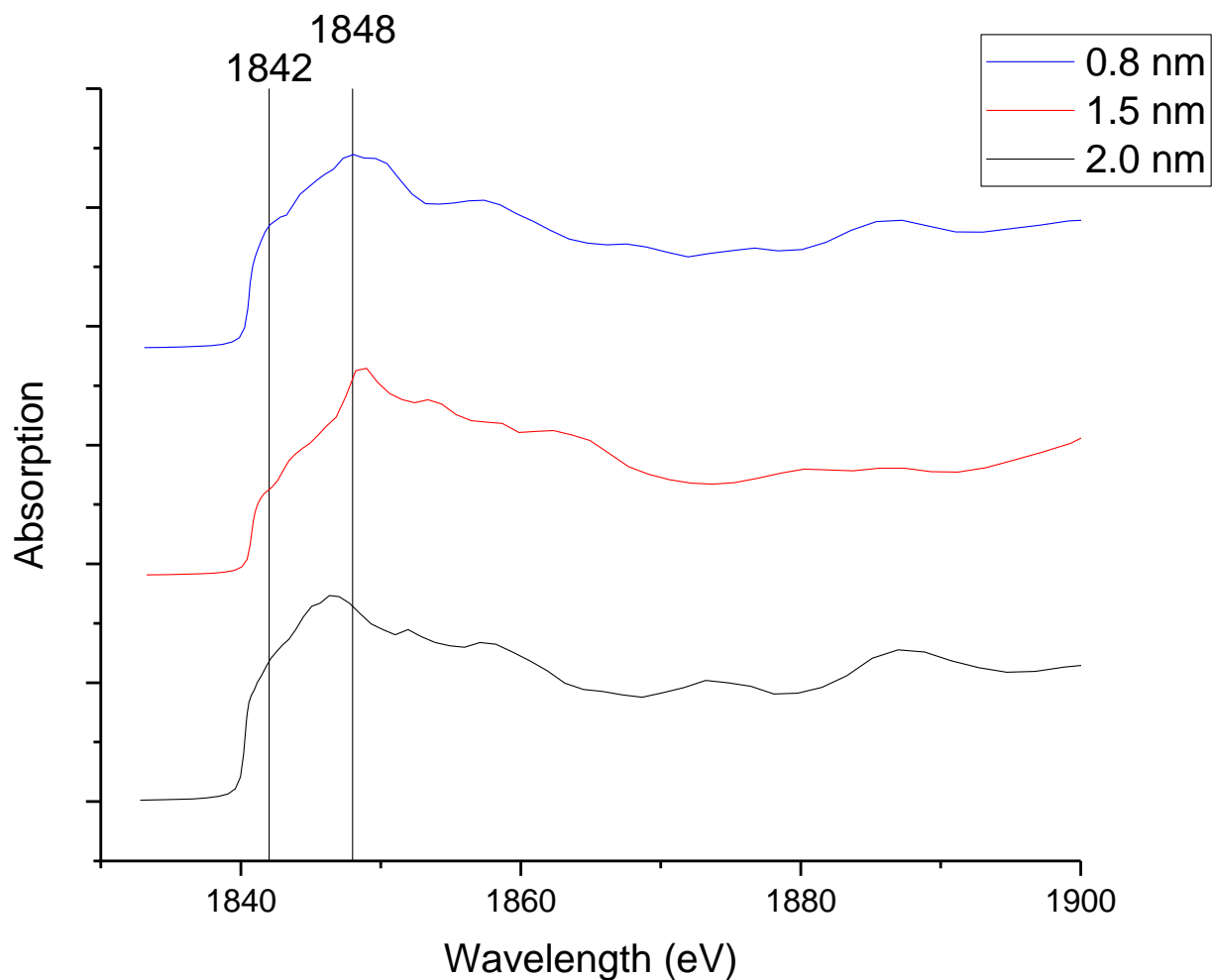


Figure 4.22 FEFF calculations of propyl passivated silicon nanoparticle size.

The results of the cluster size modeling shows a trend that smaller nanoparticles have a major peak around 1848 eV. This peak becomes more defined with the larger cluster of 1.5 nm and then shifts to 1842 eV for the cluster with a diameter of 2 nm. This suggests that a size effect could be present in the experimental silicon nanoparticle XANES spectra. This has been observed in systems with gold nanoparticles²⁵⁻²⁸ and with copper nanoparticles²⁹.

An *in situ* experiment that monitors the growth of gold nanoparticles using a microfluidic reactor monitors the change in the Au L₃ edge of the gold nanoparticles. The microfluidic reactor is shown in Figure 4.23.

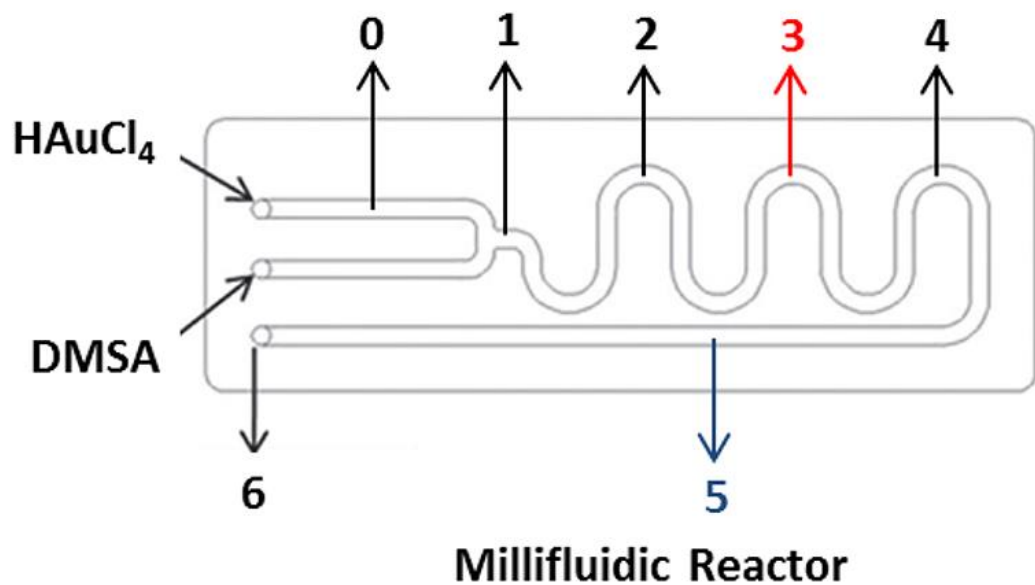


Figure 4.23 Microfluidic chip reaction that allows for the *in situ* monitoring of the growth of gold nanoparticles using L₃ edge XANES.²⁵

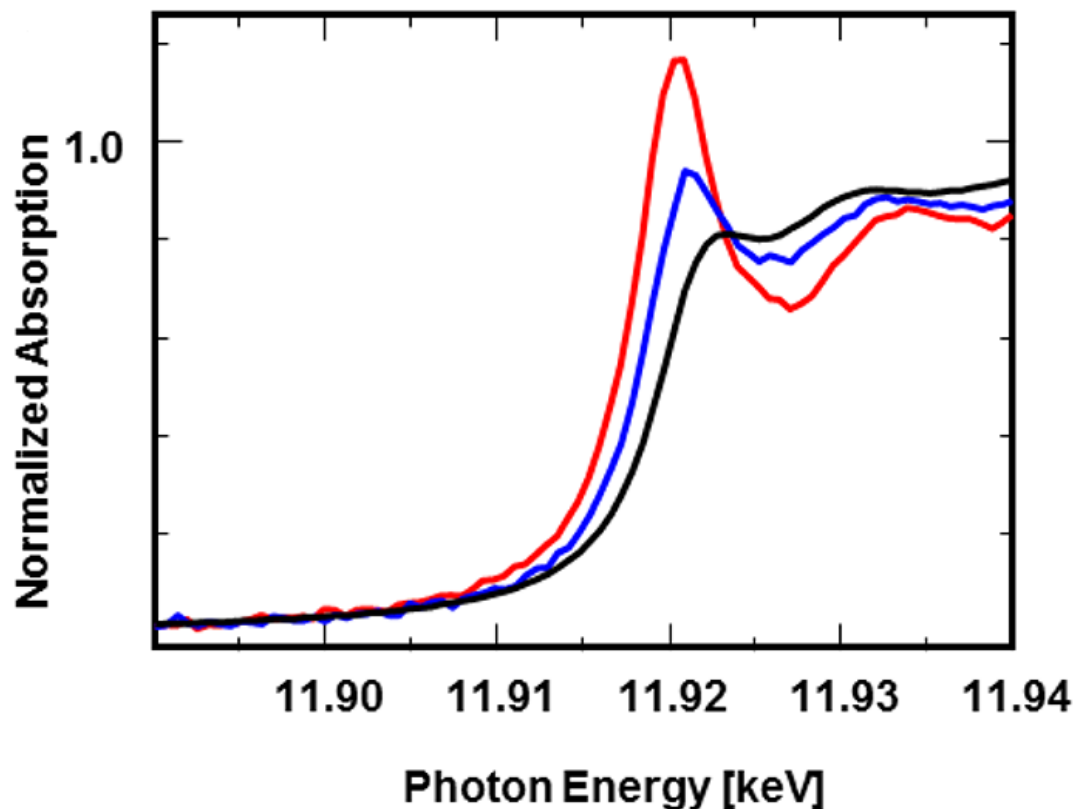


Figure 4.24 XANES spectra of Au L_3 -edge of gold nanoparticles monitored using XANES as they grow. Red denotes zone 3 blue is zone 5, and black is zone 6 as denoted in Figure 4.21.²⁵

Figure 4.24 shows the evolution of the Au L_3 edge of gold nanoparticles as they are grown. The trend here is the opposite of the trend that we observe for silicon nanoparticles in modeling studies. However, these data are not directly comparable as they are of both a different element and also a different edge. However, they do show that the size of the particle can affect the XANES spectra of the nanoparticle.

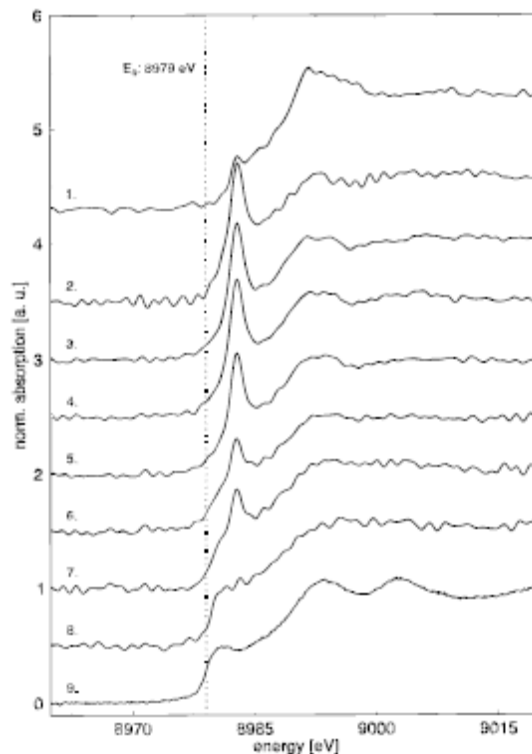


Figure 4.25 XANES spectra of time resolved formation of colloidal copper nanoparticles.²⁹ 1: $[\text{N}(\text{octyl})_4]_2 [\text{CuCl}_2\text{Br}_2]$, 2-7: Cu^+ intermediate growth (~ 2 minutes between spectra), 8: colloidal copper, 9: Copper foil standard

Figure 4.25 shows the evolution of molecular copper to colloidal nanoparticles as monitored by copper K-edge XANES. This also shows that the growth of the nanoparticles has an effect on the XANES spectra and that the size of the nanoparticles has an effect, as seen by the modeling done on the silicon nanoparticles.

This size effect is caused by the strain affecting the particle as the size constrains the bond lengths and angles caused by the differing size of the nanoparticle. As the particle increases in size, these strains decrease as the particle has the crystal structure that is more characteristic of elemental silicon in its natural state. Conversely, smaller particles show greater strains, exhibiting XANES results that could be mistaken for Si-O.

Section 4.4: XPS

X-ray photoelectron spectroscopy (XPS) is a surface sensitive technique that reveals the elemental composition of a sample. The 1-octyne and 1-octene passivated silicon nanoparticles were used for silicon and carbon XPS to try and quantify the surface of the nanoparticles.

The samples were made by dissolving the silicon nanoparticles in dichloromethane and then depositing them on a sample holder which was covered with copper tape. The dichloromethane was allowed to evaporate, leaving a thin film of the silicon nanoparticles. Powder standards were simply spread on the copper tape without any further processing. The samples were then loaded into the VG Scientific MKII system using Mg K α excitation source ($h\nu = 1253$ eV). The pressure in the chamber during analysis was $<5 \times 10^{-8}$ mbar.

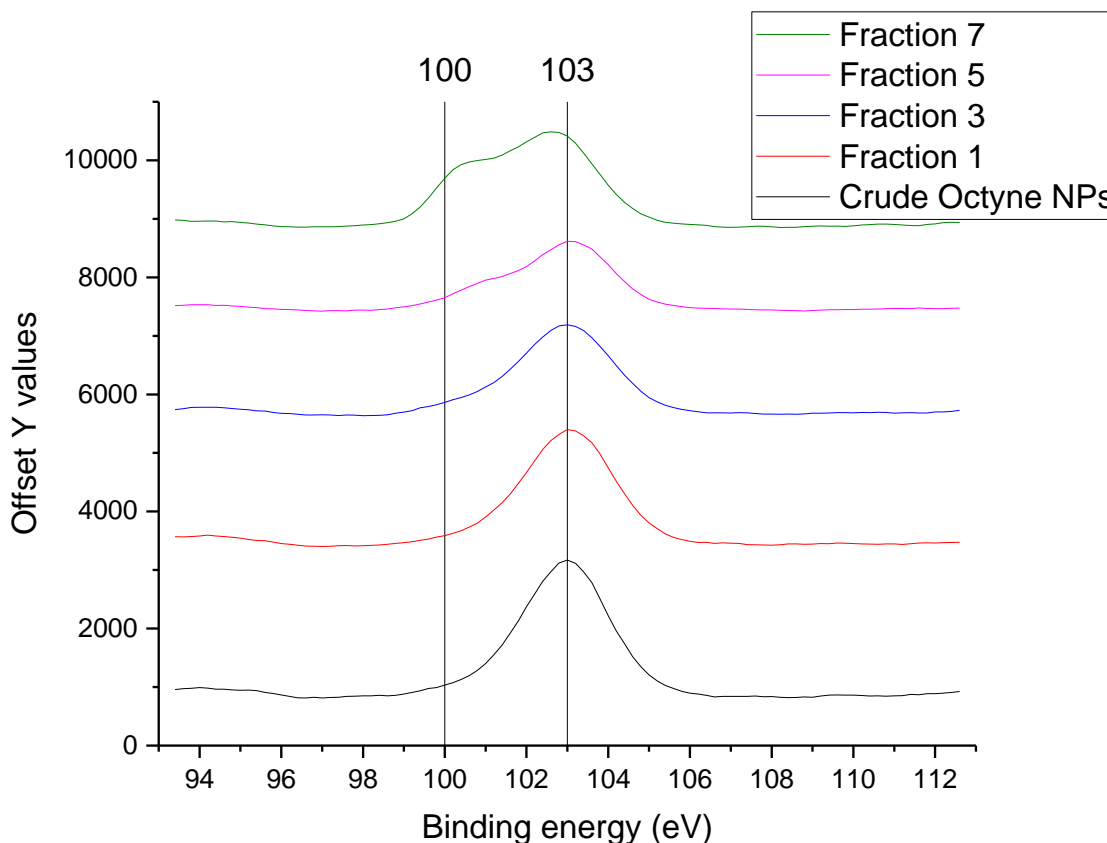


Figure 4.26 Silicon XPS of 1-octyne passivated silicon nanoparticles.

The silicon XPS spectra shows a large peak in every spectra at 103 eV which is where Si-O bond is expected. The Si-C bond is expected at 99-100 eV which is observed in the spectra of fraction 7.³⁰ The earlier fractions are dominated by Si-O. However, this may not mean that only Si-O is present. The angle of the incident x-rays on the source has been shown to effect the resultant spectra, with a 90° angle showing the best results.³¹⁻³² The instrument used on these experiments was fixed angle of 37.5° and so it is possible with better instrumentation that the earlier fractions also might be resolved to show Si-C bonding.

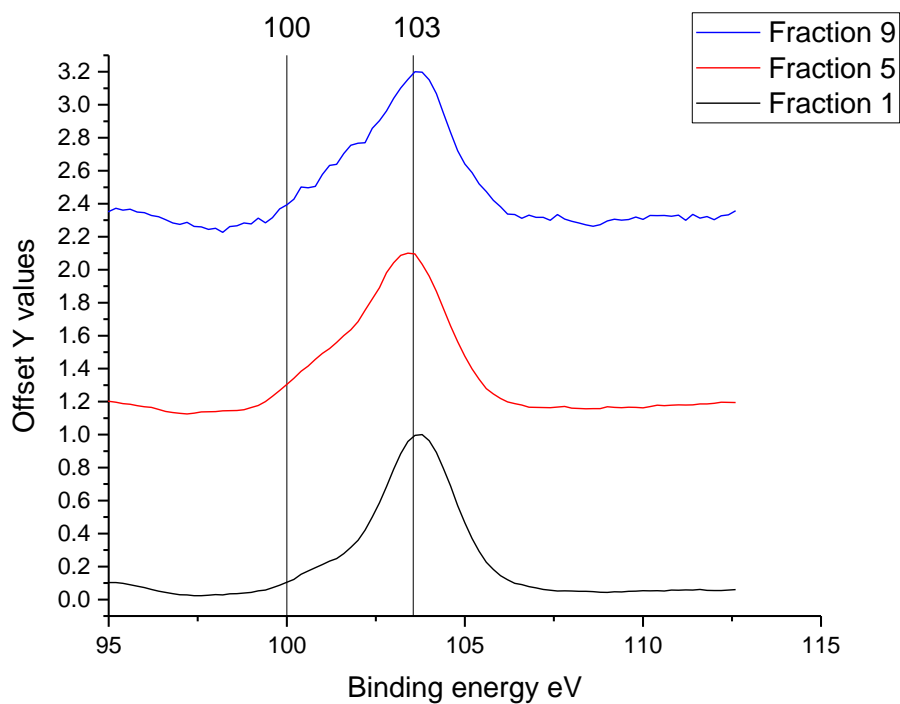


Figure 4.27 Silicon XPS of 1-octene passivated silicon nanoparticles.

The silicon XPS of 1-octene passivated silicon nanoparticles shows the Si-O bond at 103 eV as the major peak. Unlike the 1-octyne passivated silicon nanoparticles, Si-C was not observed for these samples. The limitations of the instrument might be a factor in this. The signal to noise ratio for the ninth fraction decreased, which might be extrapolated to show that there was less oxygen on the surface of the later fraction, as was seen with the 1-octyne passivated silicon nanoparticles.

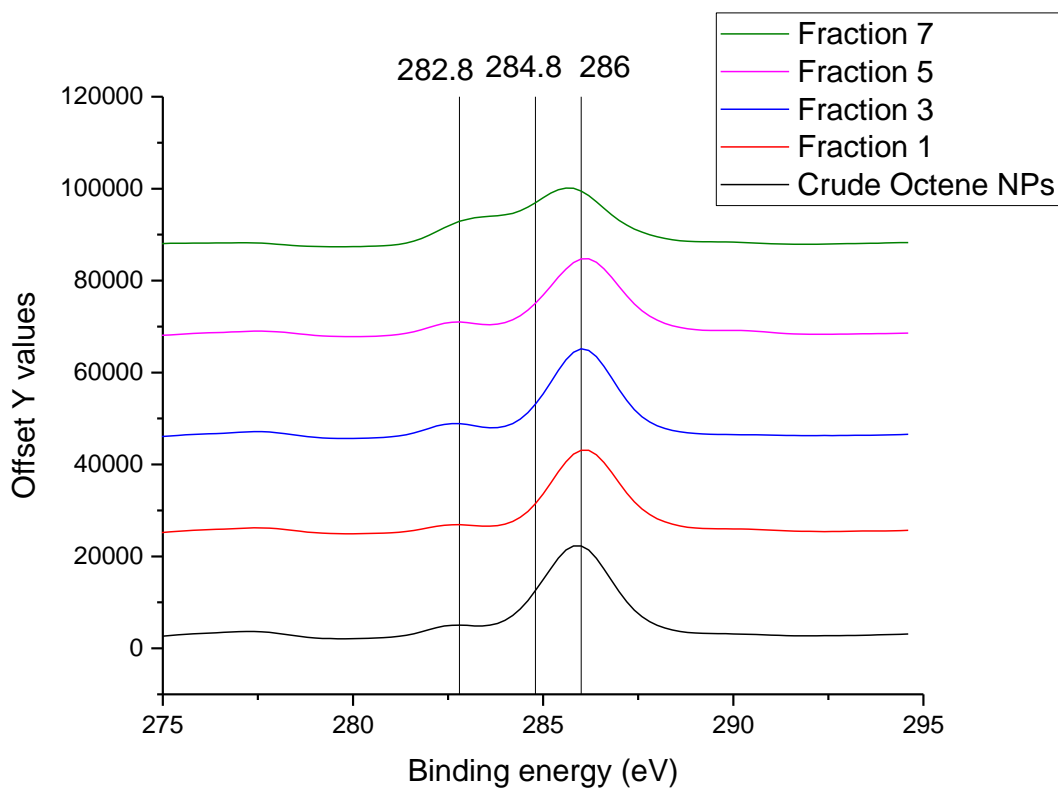


Figure 4.28 Carbon XPS of 1-octyne passivated silicon nanoparticles.

The carbon XPS spectra shows a large peak for the C-O bond at 286 eV. Also seen is a peak at 282.8 eV which corresponds to the C-Si bond.³⁰ The C-C bond is expected a 284.8 eV. The peak intensity of the C-O bond versus the C-Si bond decrease as the retention time and the fractions increase with smaller particle size. That is to say smaller nanoparticles have less oxygen present on the surface of the silicon nanoparticles.

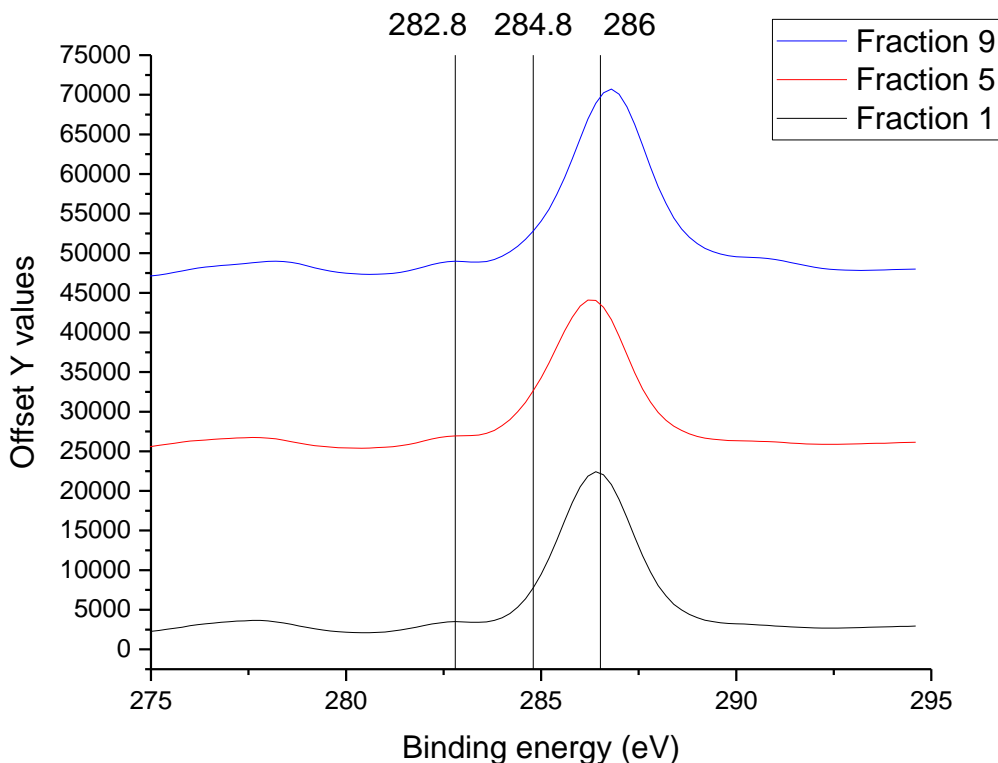


Figure 4.29 Carbon XPS of 1-octene passivated silicon nanoparticles.

The carbon XPS of 1-octene passivated silicon nanoparticles shows the C-O bond at 286 eV as seen with the 1-octyne passivated silicon nanoparticles. Also there is the C-Si bond seen at 282.8 eV. The silicon XPS spectra does not show good results for Si-C, however this carbon XPS spectra does show that there are silicon nanoparticles with covalent bonds to the alkyl passivating agent 1-octene.

The presence of the C-O bond is not indicative of bonding with the silicon nanoparticles. The C-O bond is present in all of the samples and is seen even when a blank is run with no sample. The C-O bond is seen when control experiments of the copper tape and the copper tape are washed with dichloromethane to remove the adhesive from the copper tape, which is shown in Figure 4.30.

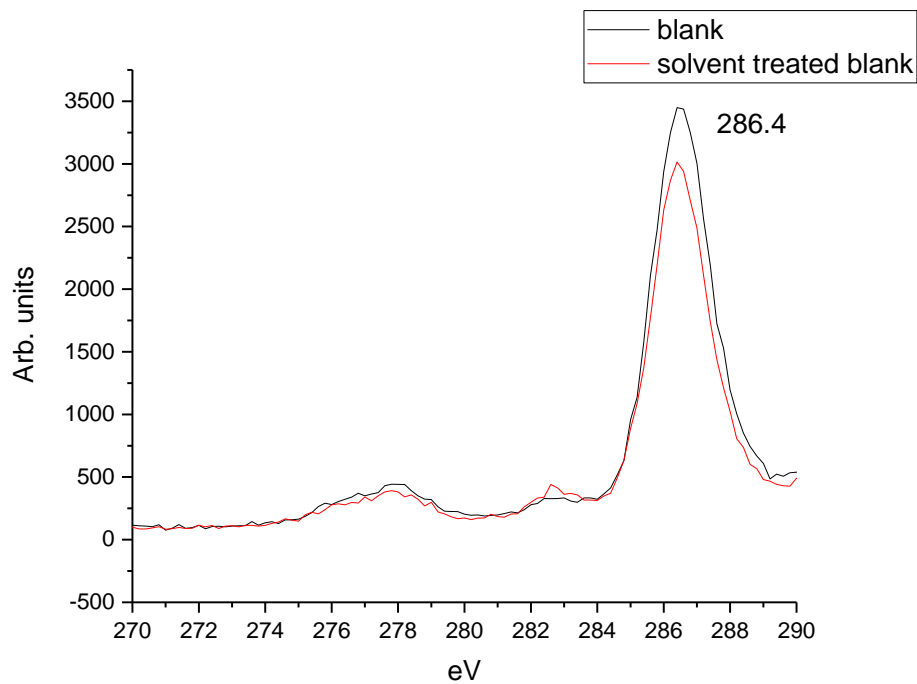


Figure 4.30. XPS control experiments with the copper tape only on the sample holder (blank) and the copper tape after it has been washed with dichloromethane to try and remove any adhesive.

This impurity from the copper tape makes any C-O bonding unable to be assigned to the sample. Different preparation methods, sample holders, and access to a multi angle XPS would be very useful in elucidating the results of the silicon nanoparticles using XPS.

Section 4.5: Conclusion

Silicon nanoparticles that were passivated with 1-octyne and 1-octene were investigated using XANES, modeling and theoretical XANES, and XPS. The results show that the nanoparticles are covalently bound with Si-C strong linkages as expected. Also, the results are in good agreement with other silicon nanoparticles synthesized by the Veinot group.

The peaks in the fine edge structure of the XANES experiments between 1844-1846 eV are indicative of a covalent bond. The XANES spectra of octakis(tetramethylammonium)-T8-silsesquioxane hydrate which has only covalent bonds between silicon and oxygen, shows no peaks in the range of 1844-1846 eV. Literature results of both silicon bound with carbon and with nitrogen moieties shows the same peak features from 1844-1846 eV for covalently bound molecules. These results provide good evidence that the nanoparticles synthesized by reactive high energy ball milling are passivated with covalent strong Si-C bonds.

The shifts of the major peak from 1848 eV for early fractions to 1842 eV for later fractions shows the decrease in the oxygen content on the silicon surface. This is expected as IR spectra of silicon nanoparticle fractions show Si-O features, especially in the earlier fractions. The XPS data shows that Si-O is present in all fractions, however, the ratio decreases in the later fractions which is in agreement with the XANES and IR data.

The modeling of the silicon nanoclusters and their theoretical XANES spectra using the FEFF9 software package confirm the results of the XANES experiments.

Modeling is useful as the time at the beamline is limited and the use of modeling can show the expected results and is a great tool in designing future experiments. The effect of the chain length of the passivating organic molecules was investigated and shows no effect on the peak fine splitting between 1844-1846 eV. The modeling of the effect of the silicon cluster size shows that the smaller clusters have a major peak that is slightly shifted to higher energies. This is seen in Figure 4.22. This might also account for some of the shoulders seen in the XANES spectra at 1848 eV which can also be interpreted as Si-O, but the size effect may be a conflating variable in that assignment. The XPS as stated before shows Si-O in all fractions, however, the contribution of a size effect is something that is interesting and requires further experimentation.

There are several factors that affect the XANES spectra, there is the chemical environment that the absorbing silicon atom is in. The neighbors are of great importance as the scattering off of these atom forms the basis for the XANES experiment. As can be seen with the chain length modeling experiment, the FEFF9 software shows greater resolution with more neighbors to calculate this scattering from. However, the silicon nanoparticles are not a crystal with orderly and repetitive unit cells. This differing chemical environment can best be replicated by modeling of a similar environment as was done with the chain length and size study.

These two studies showed us that there was not trend observed for the differing chain length, rather than greater resolution of the absorbance at 1842 for silicon with longer chain lengths. However, the size study showed a trend that smaller nanoparticles, with more strain, but less oxygen, will exhibit the major peak closer to 1848 eV. Larger

particles show the major peak in between 1842 and 1848 eV. These results are in opposition to the results concerning oxygen bound to the silicon.

Oxygen bound to silicon results in a prominent peak at 1848 eV. As the early fractions have shown, this is the major peak which corresponds to the data from IR and from XPS confirming that the early fractions have more oxygen present. However, the early fractions are also the larger fractions. This would tend to broaden the peaks and also give rise to shoulders or small peaks in the range of 1844-1848 eV. As the later fractions show less oxygen present, this is in agreement with the IR and XPS data. However, the size study using FEFF9 shows that smaller particles show a peak closer to 1848 eV. This would also broaden and give rise to small shoulders and peaks in the range from 1844-1848 eV.

Literature searches have also shown that XANES spectra of silicon bound to carbon and nitrogen also display peaks in this range from 1844-1846 eV. This is shown in films, plastics, and minerals where there is no side effect. There are therefore three variables affecting the XANES spectra: 1) oxygen bound to the surface, 2) size effect, and 3) the ligand bound to the silicon surface.

In order to properly investigate the size effect which has been documented in gold and copper nanoparticles, silicon nanoparticles that have a high monodispersity of size are required. The top down method of reactive high energy ball milling provides a polydisperse size population that requires further size separation than the techniques used in this study.

The results of the x-ray characterization show that there is silicon covalently linked to the carbon chains of the passivating layer. The results of XANES and XPS agree with the data from IR, that the earlier larger fractions have more oxygen bound to the surface of the silicon nanoparticle. The later fractions have smaller particles with less oxygen present, once again confirming the IR data. The XANES data shows that there is a complex process that results from the presence of oxygen, the size of the nanoparticle, and also from passivating alkyl chains covalently bound to the surface.

References

1. The European Synchrotron. <http://www.esrf.eu/about/synchrotron-science/synchrotron-light>.
2. Elder, F. R.; Gurewitsch, A. M.; Langmuir, R. V.; Pollock, H. C., Radiation from Electrons in a Synchrotron. *Physical Review* **1947**, *71* (11), 829-830.
3. Calvin, S., *EXAFS for Everyone*. CRC Press: Boca raton, 2013.
4. Chaboy, J.; Barranco, A.; Yanguas-Gil, A.; Yubero, F.; González-Elipe, A. R., Si K-edge XANES study of amorphous polymeric materials. *Physical Review B* **2007**, *75* (7), 075205.
5. Bunker, G., *Introduction to XAFS. A Practical Guide to X-Ray Absorption Fine Structure Spectroscopy*. Cambridge University Press: New York, 2010; p 260.
6. Stohr, J., *Nexafs Spectroscopy*. 1996.
7. Owens, A., XANES fingerprinting: a technique for investigating CCD surface structures and measuring dead layer thicknesses. *Nuclear Instruments and Methods in Physics Research Section A: Accelerators, Spectrometers, Detectors and Associated Equipment* **2004**, *526* (3), 391-398.
8. Singh, A.; Baur, K.; Brennan, S.; Homma, T.; Kubo, N.; Pianetta, P. In *X-ray absorption spectroscopy on copper trace impurities on silicon wafers*, MRS Proceedings, Cambridge Univ Press: 2002; p B1. 4.
9. Harp, G.; Han, Z.; Tonner, B., X-ray absorption near edge structures of intermediate oxidation states of silicon in silicon oxides during thermal desorption. *Journal of Vacuum Science & Technology A* **1990**, *8* (3), 2566-2569.
10. Rehr, J. J.; Albers, R. C., Theoretical approaches to x-ray absorption fine structure. *Reviews of Modern Physics* **2000**, *72* (3), 621-654.
11. Rehr, J. J.; Kas, J. J.; Vila, F. D.; Prange, M. P.; Jorissen, K., Parameter-free calculations of X-ray spectra with FEFF9. *Physical Chemistry Chemical Physics* **2010**, *12* (21), 5503-5513.
12. Murata, H.; Taniguchi, T.; Hishita, S.; Yamamoto, T.; Oba, F.; Tanaka, I., Local environment of silicon in cubic boron nitride. *Journal of Applied Physics* **2013**, *114* (23), 233502.
13. Bugaev, L. A.; Bokhoven, J. A. v.; Khrapko, V. V.; Avakyan, L. A.; Latokha, J. V., Effect of Aluminum on the Local Structure of Silicon in Zeolites as Studied by Si K Edge

X-ray Absorption Near-Edge Fine Structure: Spectra Simulation with a Non-Muffin Tin Atomic Background. *The Journal of Physical Chemistry B* **2009**, *113* (14), 4614-4618.

14. Ade, H.; Zhang, X.; Cameron, S.; Costello, C.; Kirz, J.; Williams, S., Chemical contrast in X-ray microscopy and spatially resolved XANES spectroscopy of organic specimens. *Science* **1992**, *258* (5084), 972-975.

15. Franke, R.; Bender, S.; Jüngeremann, H.; Kroschel, M.; Jansen, M., The determination of structural units in amorphous Si–B–N–C ceramics by means of Si, B, N and CK–XANES spectroscopy. *Journal of electron spectroscopy and related phenomena* **1999**, *101*, 641-645.

16. Kelly, J. A.; Henderson, E. J.; Hessel, C. M.; Cavell, R. G.; Veinot, J. G. C., Soft X-ray spectroscopy of oxide-embedded and functionalized silicon nanocrystals. *Nuclear Instruments and Methods in Physics Research Section B: Beam Interactions with Materials and Atoms* **2010**, *268* (3-4), 246-250.

17. Kelly, J. A.; Henderson, E. J.; Clark, R. J.; Hessel, C. M.; Cavell, R. G.; Veinot, J. G. C., X-ray Absorption Spectroscopy of Functionalized Silicon Nanocrystals. *The Journal of Physical Chemistry C* **2010**, *114* (51), 22519-22525.

18. van Buuren, T.; Dinh, L. N.; Chase, L. L.; Siekhaus, W. J.; Terminello, L. J., Changes in the Electronic Properties of Si Nanocrystals as a Function of Particle Size. *Physical Review Letters* **1998**, *80* (17), 3803-3806.

19. Chauvistré, R. Absorptionsspektroskopie an Atomen und kleinen Molekülen im weichen

Röntgengebiet. University of Bonn, 1987.

20. Li, D.; Bancroft, G. M.; Fleet, M. E.; Feng, X. H., Silicon K-edge XANES spectra of silicate minerals. *Phys Chem Minerals* **1995**, *22* (2), 115-122.

21. LSU CAMD Double Crystal Monochromator (DCM). **2008**.

22. Mueller, A. Guide to XAFS Measurements at SSRL. <http://www-ssrl.slac.stanford.edu/mes/xafs/index.html#Gas>.

23. Kelly, J. A. Surface Modification of Group 14 Nanocrystals. University of Alberta, 2012.

24. Wilson, P. R. J.; Roschuk, T.; Dunn, K.; Normand, E. N.; Chelomentsev, E.; Zalloum, O. H. Y.; Wojcik, J.; Mascher, P., Effect of thermal treatment on the growth, structure and luminescence of nitride-passivated silicon nanoclusters. *Nanoscale Research Letters* **2011**, *6* (1), 168-168.

25. Sai Krishna, K.; Navin, C. V.; Biswas, S.; Singh, V.; Ham, K.; Bovenkamp, G. L.; Theegala, C. S.; Miller, J. T.; Spivey, J. J.; Kumar, C. S., Millifluidics for time-resolved

mapping of the growth of gold nanostructures. *Journal of the American Chemical Society* **2013**, *135* (14), 5450-5456.

26. Zhang, P.; Sham, T. K., X-Ray Studies of the Structure and Electronic Behavior of Alkanethiolate-Capped Gold Nanoparticles: The Interplay of Size and Surface Effects. *Physical Review Letters* **2003**, *90* (24), 245502.

27. van Bokhoven, J. A.; Miller, J. T., Electronic and Geometric Structures of Small Gold Metal Particles: Particles Size Effects and the Relationship to Catalytic Activity. *AIP Conference Proceedings* **2007**, *882* (1), 582-584.

28. Polte, J.; Ahner, T. T.; Delissen, F.; Sokolov, S.; Emmerling, F.; Thünemann, A. F.; Kraehnert, R., Mechanism of Gold Nanoparticle Formation in the Classical Citrate Synthesis Method Derived from Coupled In Situ XANES and SAXS Evaluation. *Journal of the American Chemical Society* **2010**, *132* (4), 1296-1301.

29. Rothe, J.; Hormes, J.; Bönnemann, H.; Brijoux, W.; Siepen, K., In Situ X-ray Absorption Spectroscopy Investigation during the Formation of Colloidal Copper. *Journal of the American Chemical Society* **1998**, *120* (24), 6019-6023.

30. Chen, L.; Yang, C.; Bhusari, D.; Chen, K.; Lin, M.; Lin, J.; Chuang, T., Formation of crystalline silicon carbon nitride films by microwave plasma-enhanced chemical vapor deposition. *Diamond and related materials* **1996**, *5* (3), 514-518.

31. Singh, P.; Shivaprasad, S. M.; Lal, M.; Husain, M., Angle-dependent XPS analysis of silicon nitride film deposited on screen-printed crystalline silicon solar cell. *Solar Energy Materials and Solar Cells* **2009**, *93* (1), 19-24.

32. Wasserman, S. R.; Tao, Y. T.; Whitesides, G. M., Structure and reactivity of alkylsiloxane monolayers formed by reaction of alkyltrichlorosilanes on silicon substrates. *Langmuir* **1989**, *5* (4), 1074-1087.

33. Heintz, A. S.; Fink, M. J.; Mitchell, B. S., Silicon nanoparticles with chemically tailored surfaces. *Applied Organometallic Chemistry* **2010**, *24* (3), 236-240.

Chapter 5. Attempts to elucidate the nature of Si-H bond on alkenyl passivated silicon nanoparticles.

Section 5.1. Synthesis of 1-octene passivated silicon nanoparticles.

Silicon nanoparticles synthesized by RHEBM with alkenyl and alkynyl organic ligands display an Si-H stretching vibration in the IR spectra. It is thought that this arises from the abstraction of protons from the milling solvent. However, no study has yet been completed to definitively prove that this is the origin of the Si-H bond on the surface of the silicon nanoparticles.

Section 5.2: Experimental

Synthesis of 1-octene passivated silicon nanoparticles synthesis

A stainless steel milling vial with a gas side arm (Figure 5.1) was charged with 1.25 grams of silicon wafers and 30 mL of 1-octene. Two stainless steel milling balls, each weighing approximately 8.1 grams and 1.2 cm in diameter were added to the vial. The vial was then sparged with nitrogen for 20 minutes to degas the milling solution. The vial was sealed to the atmosphere and then milled for 12 hours using a SPEX SamplePrep 8000D mixer/mill at 1060 cycles per minute in a 4° C cold room.

The stainless steel milling vial was adapted from an 8007 stainless steel grinding vial obtained from SPEX SamplePrep. The Vial was adapted by drilling a hole in the side of the vial 1 cm from the bottom of the vial with the use of a diamond tipped drill. The vial was then welded to a 90° elbow that was fitted with a SwageLok gas tight tube fitting

that was cut so that the arm protruded 1.5 cm from the side of the milling vial. A SwageLok gas tight quarter turn valve was fitted to the SwageLok tube fitting. The apparatus was determined to be gas tight by the lack of any bubbles observed when the vial was charged with a pressured gas and then submerged in water for a period of time. The vial is shown in Figure 5.1 and Figure 5.1B.



Figure 5.1. Stainless steel milling vial with adapted gas sidearm.

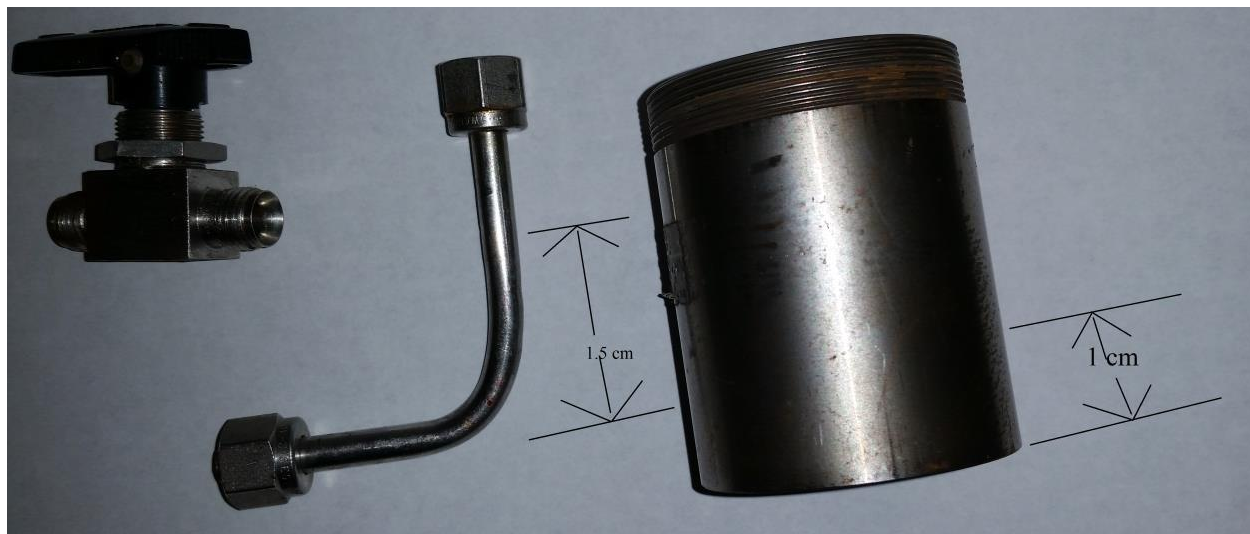


Figure 5.1B. Dimensions for the adaptation of stainless steel milling vial.

After 12 hours of RHEBM, the vial was opened to the atmosphere and the contents were transferred to plastic centrifugation tubes. The mixture was then centrifuged using a Thermo IEC CL2 Centrifuge, at 511 G for 30 minutes. The supernatant was then separated from the insoluble sediments and the solvent was removed using rotary-evaporation. The nanoparticles which were an oily residue of a light brownish color were then re-dissolved using dichloromethane. The crude yield was 45 mg. $^1\text{H NMR}$ (ppm): 0.9(s), 1.5(broad s), 2.1 (s) $\text{IR}(\text{KBr cm}^{-1})$: 3000-2800 (ν C-H), 2126 (ν Si-H), 1464 (δ C-H), 1100 (ν Si-O)

Section 5.3: Results and Discussion.

The synthesis of the silicon nanoparticles passivated by 1-octene closely follows the synthesis of the other alkene passivated silicon nanoparticles as laid out in chapter 3. The ^1H NMR spectra shows a methyl peak at 0.9 ppm and a broad alkane region that is centered at 1.5 ppm. There is also a small peak at 2.1 ppm that is where the protons of CH_2 next to a $\text{C}=\text{C}$ bond appear. There are no vinylic protons in the region between 5 and 6 ppm however. There is a possibility of a structure, where an internal double bond could be formed. However, since this NMR was taken in CD_2Cl_2 , that region (5.5 pm) is obscured.¹

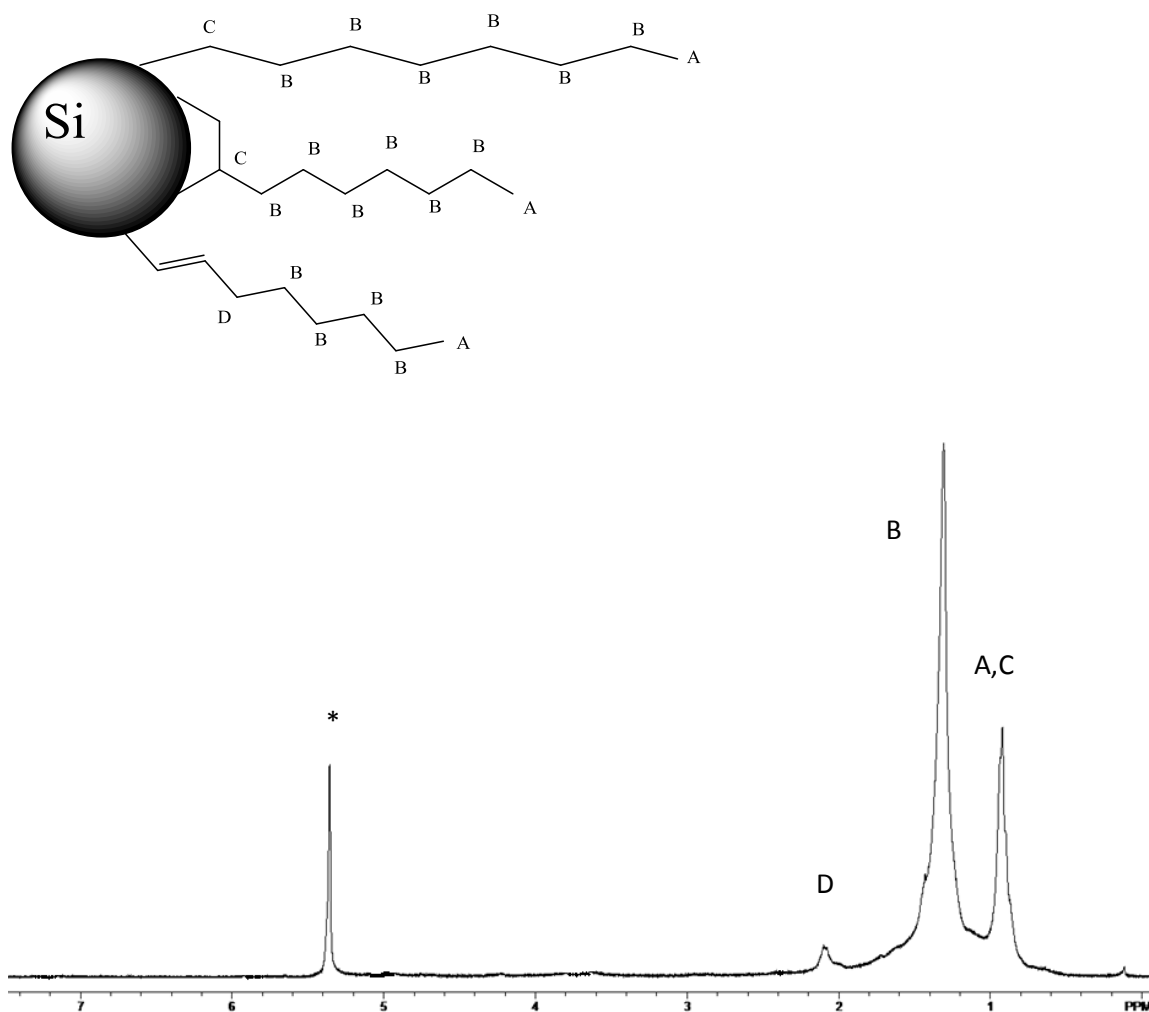


Figure 5.2. ^1H NMR of 1-octene passivated silicon nanoparticles, in CD_2Cl_2 .

The FTIR spectra of the 1-octene passivated silicon nanoparticles is shown in Figure 5.3. There is the expected alkane C-H stretch at 2800 to 3000 cm^{-1} . Also observed is the Si-H stretch that is seen at 2126 cm^{-1} . The C-H bending symmetric and antisymmetric modes can be seen at 1279 and 1466 cm^{-1} .

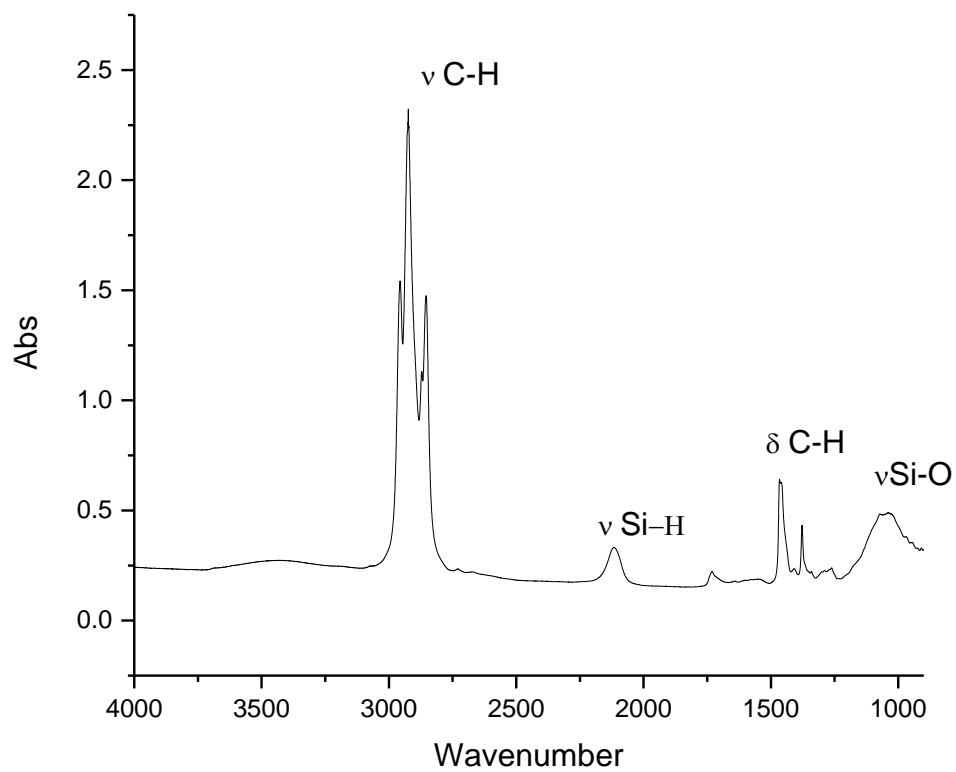


Figure 5.3. FTIR spectra of 1-octene passivated silicon nanoparticles.

The luminescence spectra can be seen in Figure 5.4 and has been normalized to the absorption using the UV data. This data also shows a red shift that corresponds to the excitation of populations of larger sized nanoparticles with longer wavelength excitation.

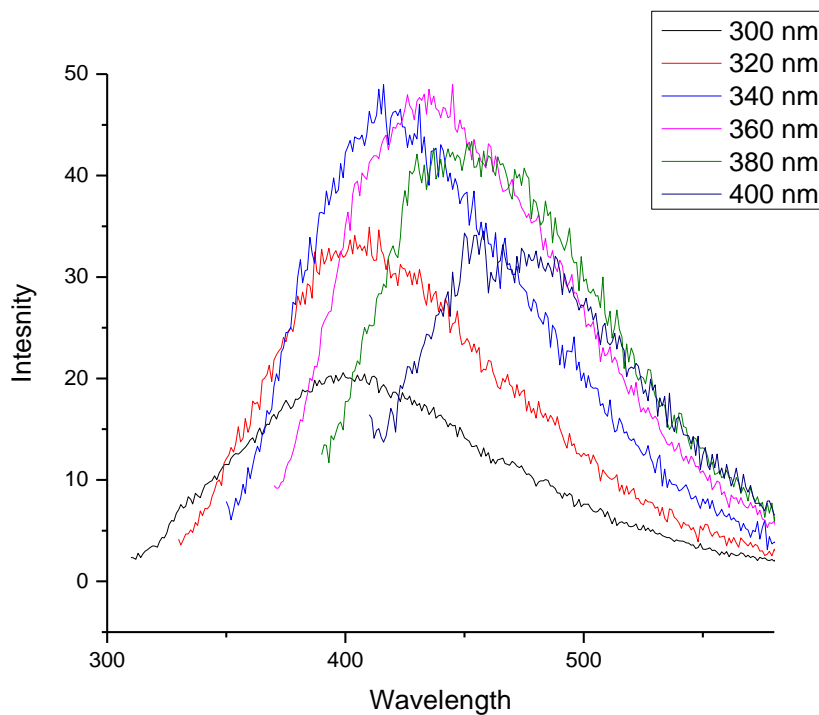


Figure 5.4. Photoluminescence of the 1-octene passivated silicon nanoparticles.

Section 5.4.1: Reaction of D₂O with silicon nanoparticles

In order to investigate the possible reaction of dangling silicon bonds by atmospheric water which would lead to an increase in silanol species on the surface of the silicon nanoparticles, an experiment using D₂O was proposed. The purpose is to determine if the silicon surface is susceptible to reactions with atmospheric water. To determine this, D₂O was substituted as water in order to show isotopic shifts in the IR spectra of the silicon nanoparticles.

Silicon nanoparticles were prepared as described in the previous section. However, as soon as the milling was completed D_2O was introduced to the milling vial. This was done by attaching a nitrogen gas feed through the gas side arm to exclude any atmospheric gasses from entering the vial. The vial was then capped for another 24 hours as the D_2O was allowed to react with the milling mixture. The vial was then opened and the contents were centrifuged as was done in the previous section. The starting materials were separated by vacuum pump leaving the silicon nanoparticles as a semisolid mass of about 45 mg.

The photoluminescence showed no change as is shown in Figure 5.5.

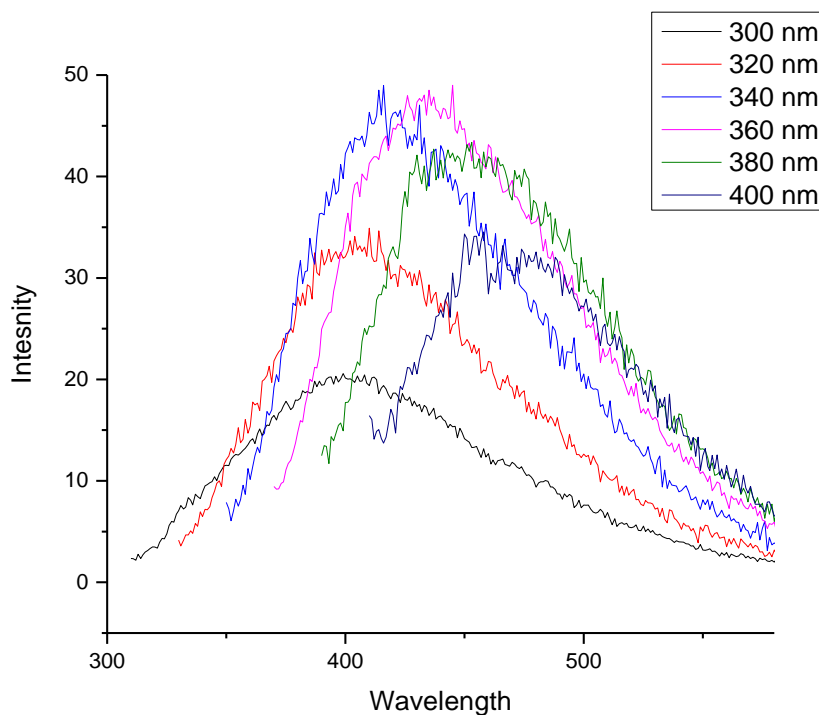


Figure 5.5. Photoluminescence of 1-octene passivated silicon nanoparticles after 24 hours exposure to D_2O .

The FTIR spectra also showed no changes as can be seen in the comparison of IR spectra of the 1-octene passivated silicon nanoparticles and the 1-octene nanoparticles that had been exposed to D₂O for 24 hours. This is shown in Figure 5.6.

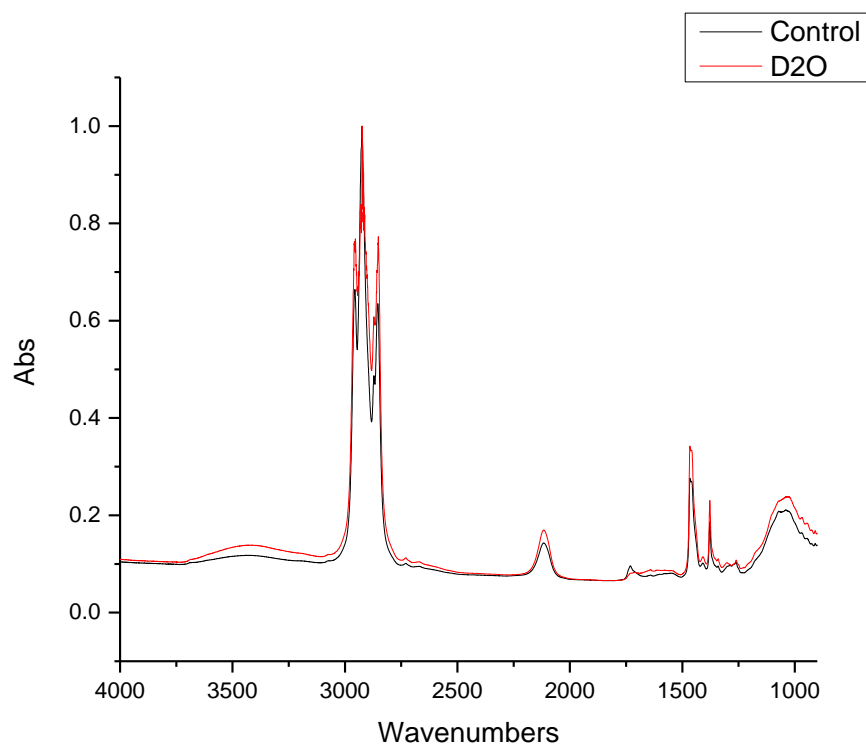


Figure 5.6. 1-octene passivated silicon nanoparticles denoted as control and 1-octene passivated silicon nanoparticles that had been exposed to D₂O for 24 hours, denoted as D₂).

To rule out that the negative result could be caused by the polarity differences of the 1-octene and the D₂O and thus cause the nanoparticles to remain in the organic phase and not in contact with the D₂O a mixing of the two phases was required. Milling with 5 mL of D₂O in the milling vial also produced no results, which lends evidence to the

possibility that the two phases are not mixing. So the next step was to repeat the experiment using sonication to insure mixing of the phases.

Section 5.4.2: Reaction of silicon dangling bonds using D₂O and sonication

Sonication was employed to mix the two phases. The 1-octene passivated silicon nanoparticles were synthesized and exposed to D₂O as stated in the previous section. However, the vial was sonicated for 12 hours to mix the two phases. This was done to surpass any energy input normally experienced by shaking or moving of the milling liquid prior to the separation of the D₂O and 1-octene starting material from the nanoparticles. That is to say, that these two phases were agitated more than the nanoparticle samples normally were by normal handling and if atmospheric water was reacting with the nanoparticles, this experiment should react to an even greater degree due to the large input of energy into the vial using sonication.

The photoluminescence spectra are shown below in Figure 5.7.

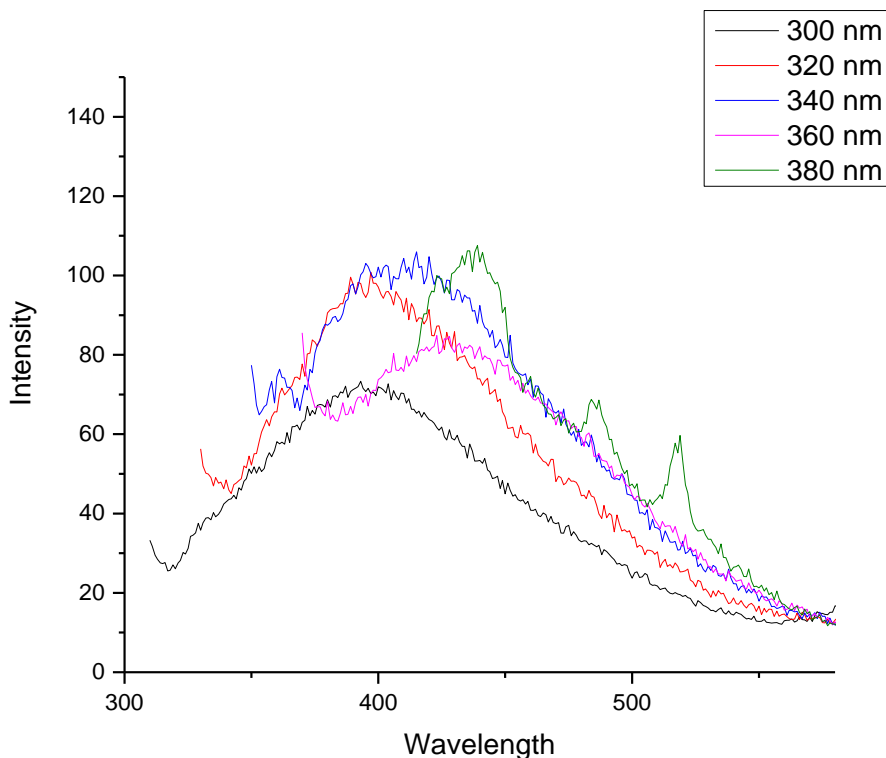


Figure 5.7. 1-octene passivated silicon nanoparticles after 12 hours sonication with D₂O, normalized by the absorption.

The photoluminescence shows an increase of about 100% over the original nanoparticles and also the nanoparticles that had been exposed to D₂O for 24 hours as shown in the last section. This increase is initially surprising as an increase in the oxidation of the surface is thought to decrease the luminescence of the nanoparticles.² However, it is also possible that some of the remaining starting material, 1-octene, could have also reacted with the silicon nanoparticles further passivating the surface.

The IR of the nanoparticles after 12 hours of sonication with D₂O showed the Si-H stretch to still be a prominent feature and no additional features that would indicate the presence of D₂O bonding with the silicon nanoparticle surface. This is shown in Figure 5.8.

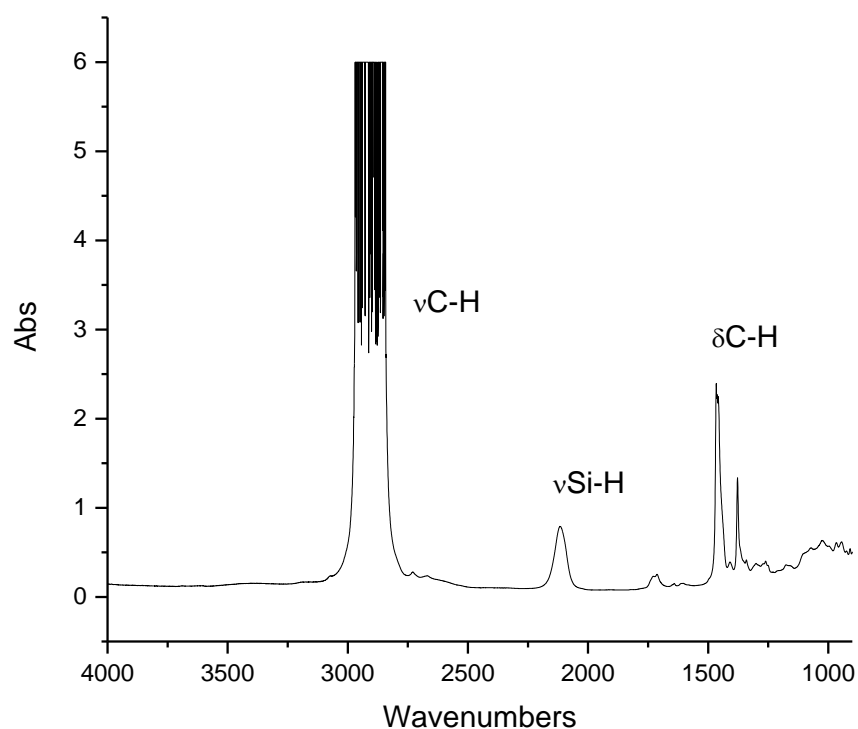


Figure 5.8. IR spectra of 1-octene passivated silicon nanoparticles after sonication for 12 hours with D₂O.

There is a small feature at 1729 cm⁻¹ that does resemble an Si-D bond, however, it is also seen in the control IR of just 1-octene passivated silicon nanoparticles. It is also slightly too high a wavenumber to be Si-D though as Si-D appears at about 1550 cm⁻¹. This can be seen in Figure 5.9 as shown below.

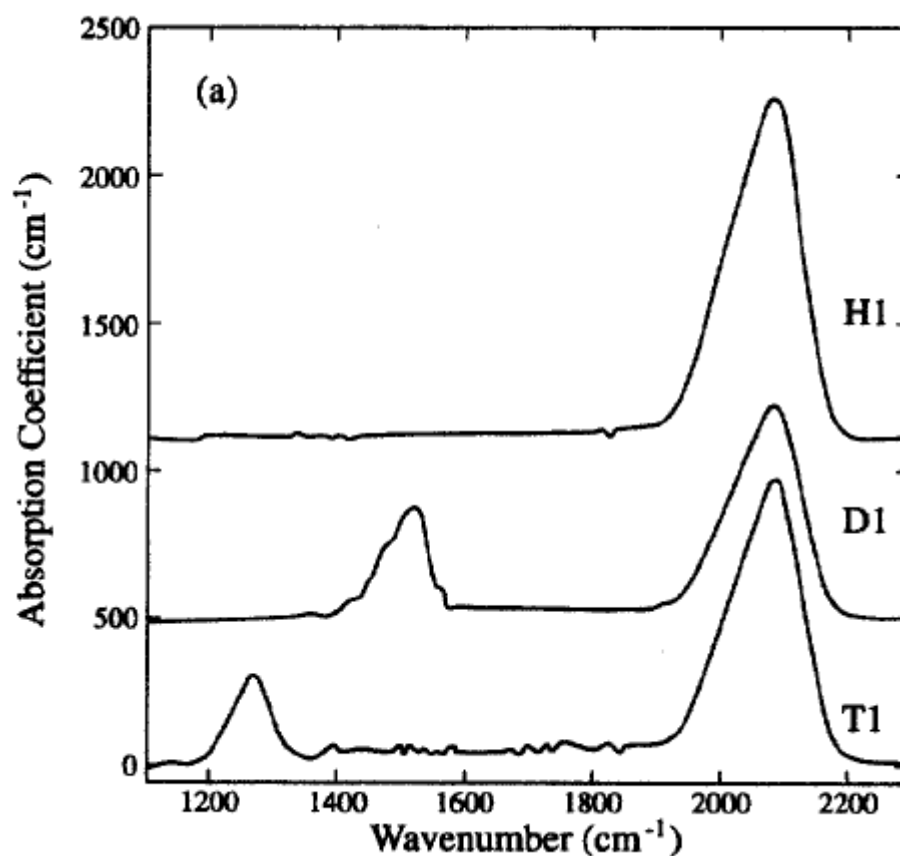


Figure 5.9. The IR spectra of hydrogen, deuterium, and tritium bound to silicon.³

The absence of any new features in the IR spectra suggests that atmospheric water is not having a large impact on the silicon nanoparticles. By exposing the silicon nanoparticle mixture to both D₂O for an extended period of time (24 hours) and also exposing it to a large energy input in the form of sonication and reaction between the silicon nanoparticles and the D₂O should have been apparent in the IR spectra. The sonication did increase the luminescence of the silicon nanoparticles solutions that had been normalized by the absorbance using UV-vis. This allows for the comparison of the two samples which shows an increase of about 100%. This could be caused by the

sonication breaking apart larger silicon particles which reacted with the 1-octene that was still in the milling vial. This type of reaction was investigated by Mitchell et al and has been shown to work, albeit with a sonic horn with higher energy input.⁴

Section 5.5: Hydrosilation of passivated silicon nanoparticles.

Increased passivation of the silicon nanoparticle surface should lead to a better protected surface against small molecules such as oxygen and ozone. To test this theory a series of reactions were carried out to attempt to further passivate the silicon surface by conversion of Si-H bonds to a stronger Si-C bond through the use of hydrosilation. Si-C bonds are stronger and the increase in organic chains covalently bound to the surface will also increase the steric protection of any remaining dangling bonds and Si-H sites.

The Si-H bond has been shown to undergo hydrosilation reactions throughout the literature on flat silicon⁵ and with silicon nanoparticles^{2, 6-7}. The route chosen that would be the best for the silicon nanoparticles was UV light assisted hydrosilation. A photoreactor with 254 nm emitting bulbs was used in a 4°C cold room. The solutions were all degassed to lessen the possibility of oxidation of the silicon nanoparticles. The hydrosilation was done by bubbling ethylene through a solution of the nanoparticles under 254 nm light and also the use of halogen solvents to assist in the hydrosilation.

Section 5.5.1: Hydrosilation of 1-octene passivated silicon nanoparticles.**Purging of ethylene through 1-octene passivated silicon nanoparticles under 254 nm light.**

Silicon nanoparticles passivated by 1-octene were prepared as stated in the first section. These nanoparticles were dissolved in dichloromethane in a quartz tube and degassed using nitrogen gas. The tube was fitted with a septum allowing gas to be pumped in and the pressure to be released through a needle, maintaining a positive pressure. The solution was then monitored by photoluminescence after thirty minutes and an hour. The reaction was stopped after 12 hours to allow for IR to be taken to determine the loss of the Si-H stretch. The photoluminescence after 30 minutes of purging ethylene through the solution under 254 nm light can be seen in Figure 10. This can be compared to Figure 5.4 of the photoluminescence of 1-octene passivated silicon nanoparticles, which shows a roughly 300% increase in luminescence.

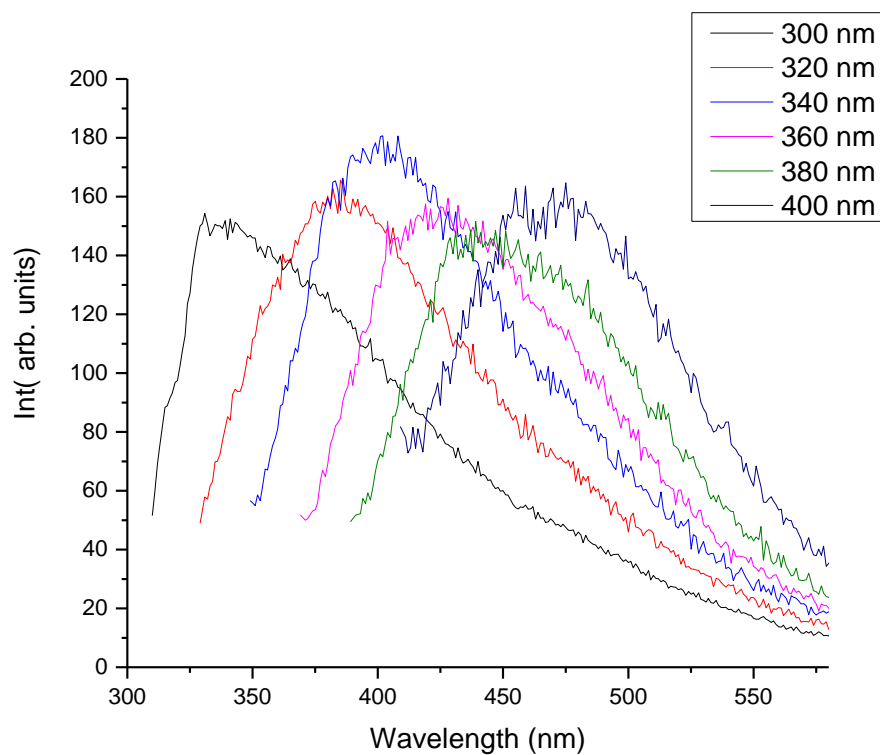


Figure 5.10. 1-octene passivated silicon nanoparticles, purged with ethylene under 254 nm light for 30 minutes. (Normalized by absorbance of UV-Vis)

The photoluminescence of the solution was also recorded after 1 hour. This can be seen in Figure 5.11.

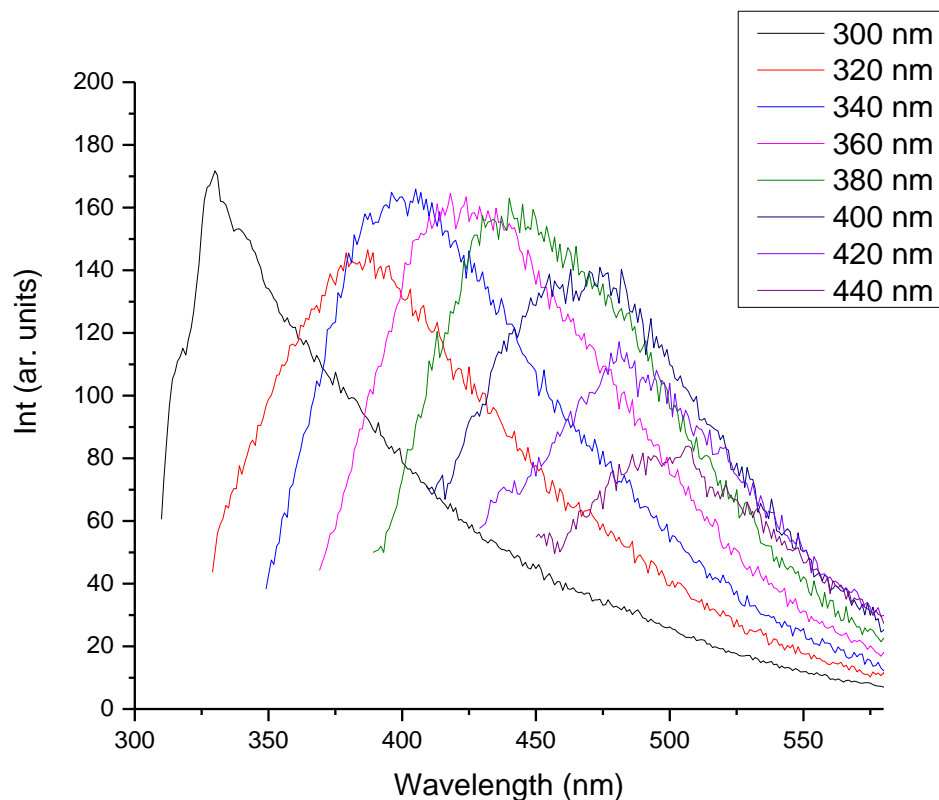


Figure 5.11. 1-octene passivated silicon nanoparticles, purged with ethylene under 254 nm light for 1 hour. (Normalized by absorbance of UV-Vis)

As can be seen by the comparison between 30 minutes and 1 hour, there is not any appreciable increase in intensity of the normalized luminescence. This would suggest that the reaction proceeds quickly under the 254 nm light. The IR was then taken after 12 hours to assess the reactions impact on the Si-H stretch. This is shown in Figure 5.12.

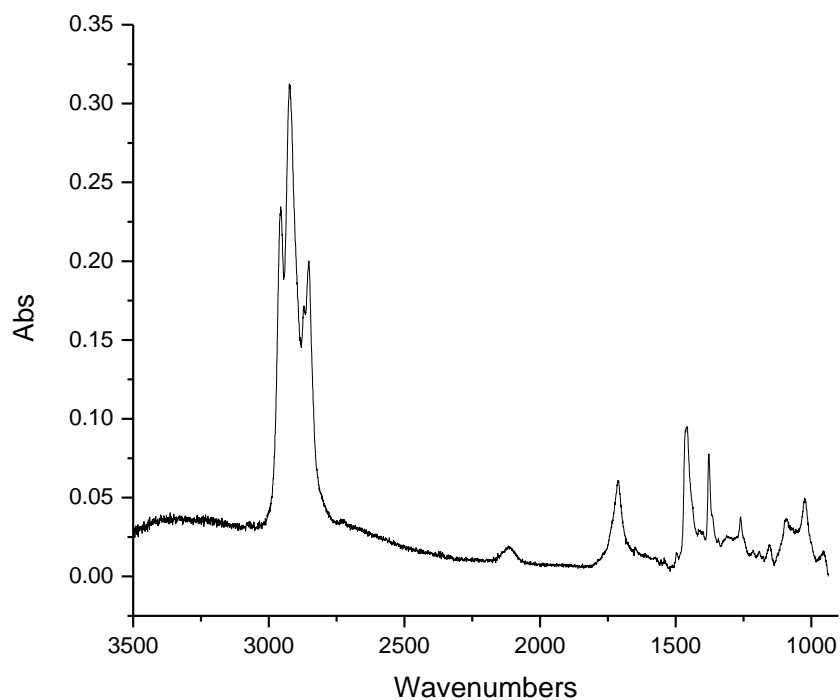
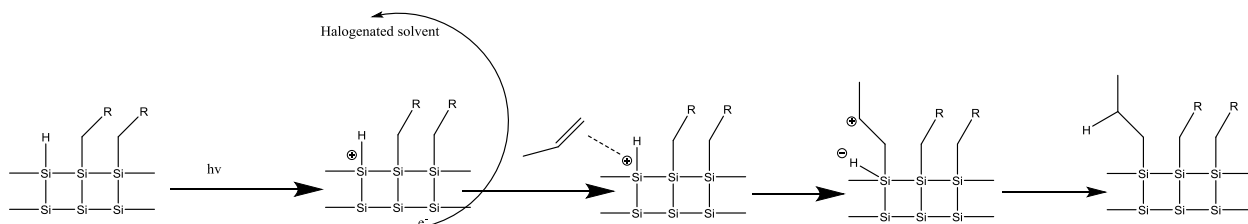


Figure 5.12. IR of 1-octene passivated silicon nanoparticles, purged with ethylene under 254 nm light for 12 hours.

As seen from the IR of the silicon nanoparticles after 12 hours of purging with ethylene under 254 nm light, there is still a significant Si-H stretch observed at 2126 cm^{-1} . This reaction did increase the luminescence of the nanoparticles as seen by comparing the normalized luminescence of the 1-octene passivated silicon particles (Figure 5.4) and the nanoparticles after purging with ethylene under 254 nm light.

Section 5.5.2: Hydrosilation of 1-octene passivated silicon nanoparticles with halogenated solvents.

Buriak et al have shown that exciton mediated hydrosilation can improve the hydrosilation results.⁸⁻⁹ By using a solvent with a high reduction potential the exciton is quenched with the acceptance of the electron by the oxidant, making the positively charged silicon surface a much more attractive target for the π electrons of the alkene.⁹ This is shown in reaction Scheme 5.1. The level of reduction potential vs porous silicon is shown in Figure 5.13. Testing the theories set forth by Buriak on porous silicon on silicon nanoparticles led to the use of carbon tetrachloride to promote hydrosilation reactions on 1-octene passivated silicon nanoparticles.



Scheme 5.1. Exciton mediated hydrosilation mechanism on silicon nanoparticle

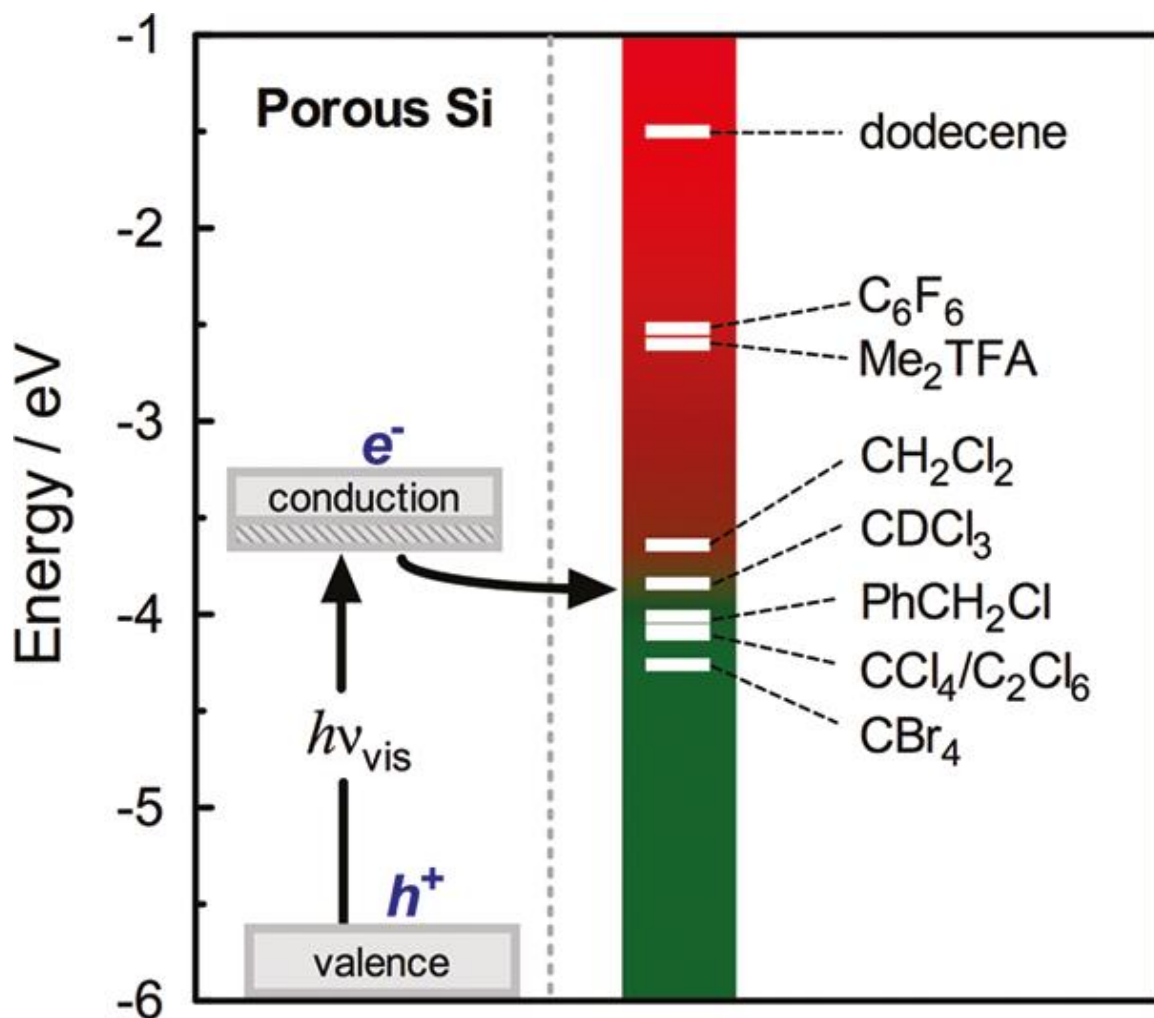


Figure 5.13. Reduction potentials of halogenated solvents compared to porous silicon.⁹

Hydrosilation with chloroform.

1-Octene passivated silicon nanoparticles were prepared as stated in the first section. The nanoparticles were dissolved in dichloromethane with an addition of 5 mL of $CHCl_3$. The solution was degassed by sparging with nitrogen in a quartz tube sealed with a rubber septum with a needle as a relief valve. The quartz tube was then placed in a

photoreactor and ethylene gas was bubbled through the solution, maintaining a positive pressure. The reaction was allowed to run for 12 hours.

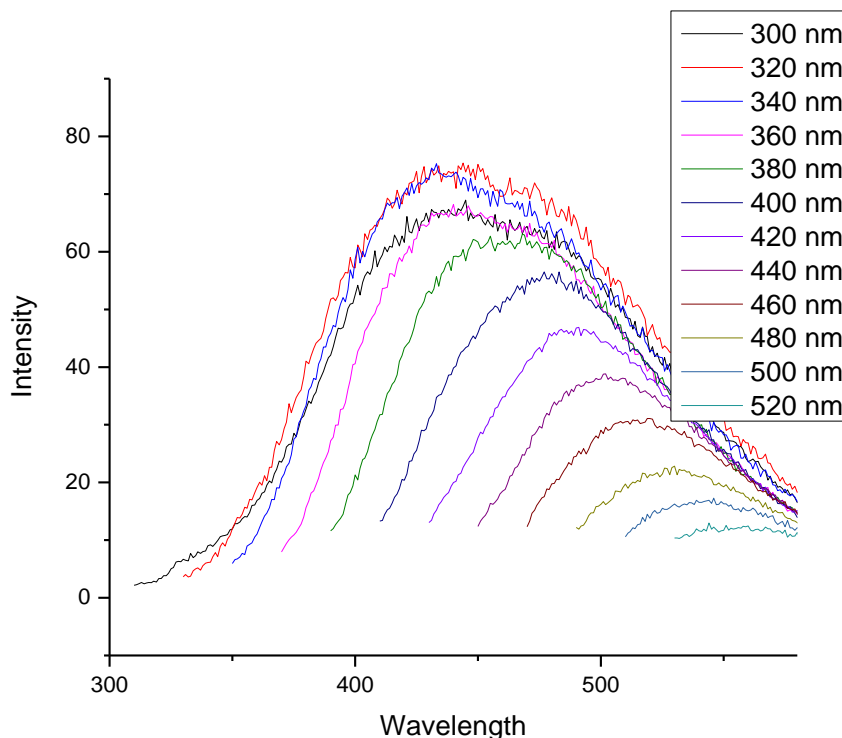


Figure 5.14. 1-Octene passivated silicon nanoparticles purged with ethylene in CHCl_3 for 12 hours under 254 nm light.

As seen from Figure 5.14, the hydrosilation using CHCl_3 did not result in a large increase in the luminescence. Comparison of this normalized intensity to that in Figure 5.4 shows only an increase of 33%. The IR of the silicon nanoparticles is shown in Figure 5.15 below. The Si-H stretch is no longer apparent, however, there is a new stretch in the region in which ketones appear. This may be a results of impurity in the chloroform or side reactions that may have occurred during the reaction. However, these undesirable

results led to abandoning chloroform in favor of carbon tetrachloride which has a more desirable reduction potential.

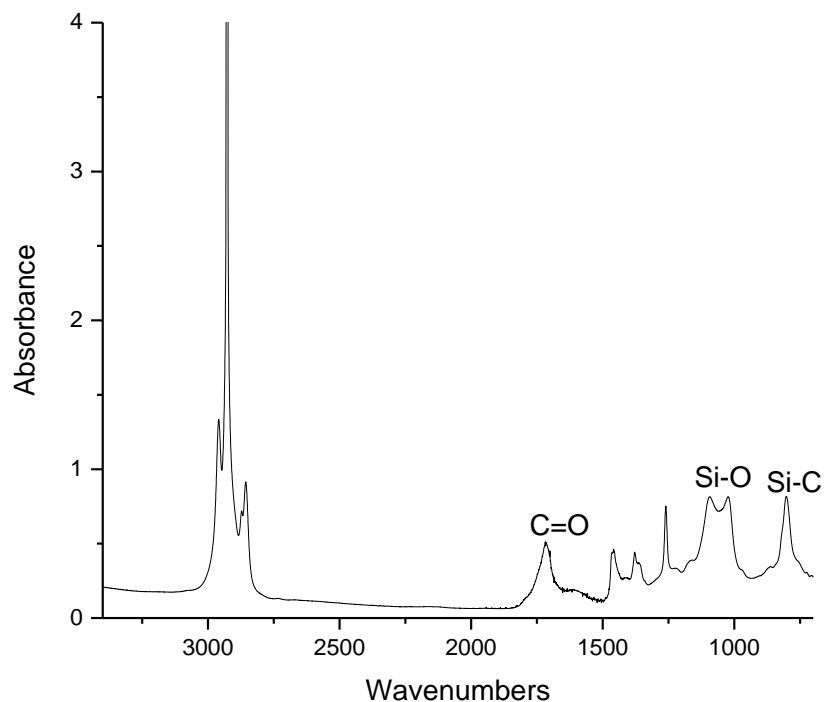


Figure 5.15. IR of 1-octene passivated silicon nanoparticles purged with ethylene for 12 hours under 254 nm light with chloroform.

Hydrosilation with carbon tetrachloride.

1-octene passivated silicon nanoparticles were prepared as stated in the first section. The nanoparticles were dissolved in dichloromethane with an addition of 5 mL of CCl_4 . The solution was degassed by sparging with nitrogen in a quartz tube sealed with a rubber septum with a needle as a relief valve. The quartz tube was then placed in a

photoreactor and ethylene gas was bubbled through the solution, maintaining a positive pressure. The reaction was allowed to run for 12 hours.

The photoluminescence results of the first three fractions are shown below in

Figure 5.16-5.18.

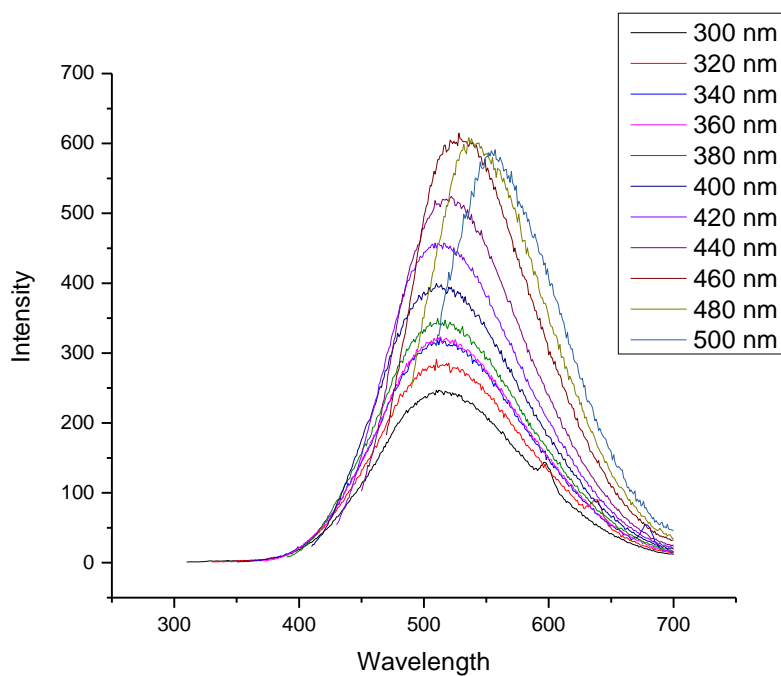


Figure 5.16. 1-Octene passivated silicon nanoparticles purged with ethylene in CCl_4 for 12 hours under 254 nm light, fraction 1.

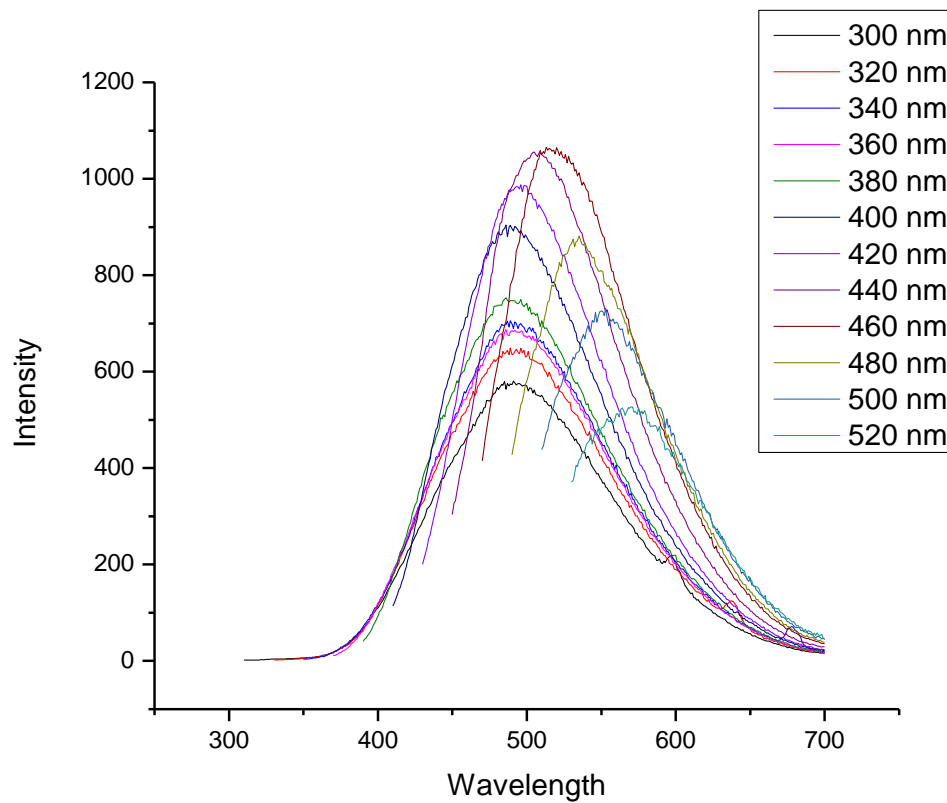


Figure 5.17. 1-Octene passivated silicon nanoparticles purged with ethylene in CCl_4 for 12 hours under 254 nm light, fraction 2.

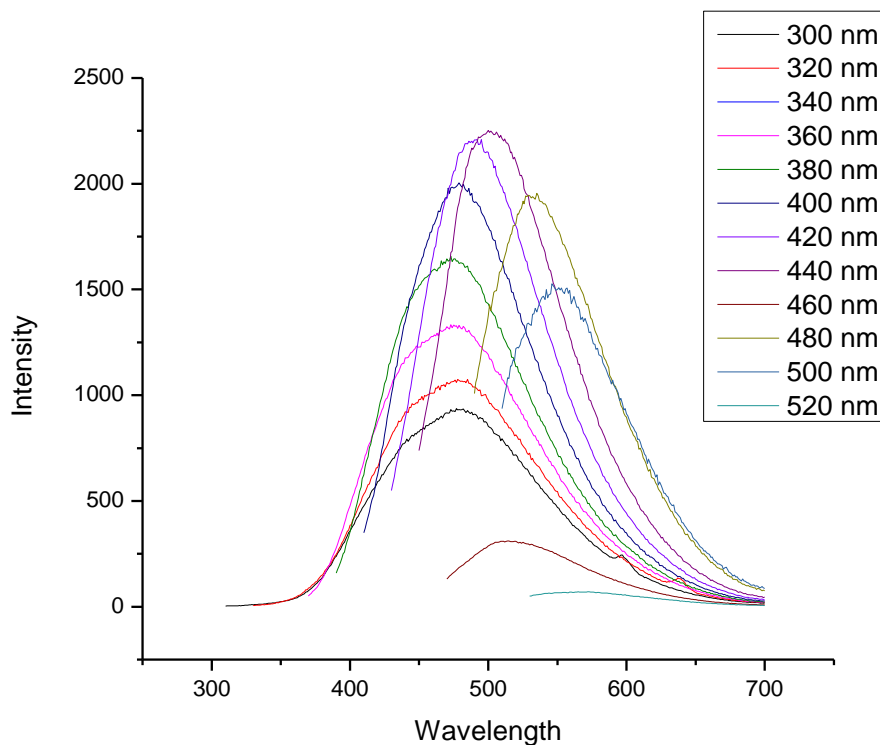


Figure 5.18. 1-Octene passivated silicon nanoparticles purged with ethylene in CCl_4 for 12 hours under 254 nm light, fraction 3.

As seen from the three normalized fractions, the luminescence of the silicon nanoparticles has increased by more than an order of magnitude from the silicon nanoparticles in Figure 5.4. This is a great result as the greater the quantum yield, the better the nanoparticles are for applications such as biological labeling as discussed in Chapter 3. This is the most luminescent solution of silicon nanoparticles that have been observed throughout all of the projects in this thesis.

The reason for this increased luminescence is attributed to increased passivation of the silicon nanoparticle surface. This however, has not been investigated in great detail

and the exact reason is not known. The increased passivation however does further protect the surface from oxidation and provide steric hindrance to small molecules which may interact with the silicon surface. The silicon surface may also be undergoing a reorganization during the photo assisted hydrosilation reaction. Silacation sites may increasingly occur after the ejection of the electron to the halogenated solvent, which would allow for dangling bonds to recombine, removing defect states and traps. Silacation sites behave similar to cations, which the mobility of is well known, allowing for the silacation sites to move and reorganize the surface of the silicon nanoparticle. Reductions in traps and defects states have been proven to influence the photophysics and quantum yield of silicon nanoparticles.¹⁰ The IR also shows that the reaction has proceeded close to completion based on the disappearance of the Si-H stretch. This is shown in Figure 5.19.

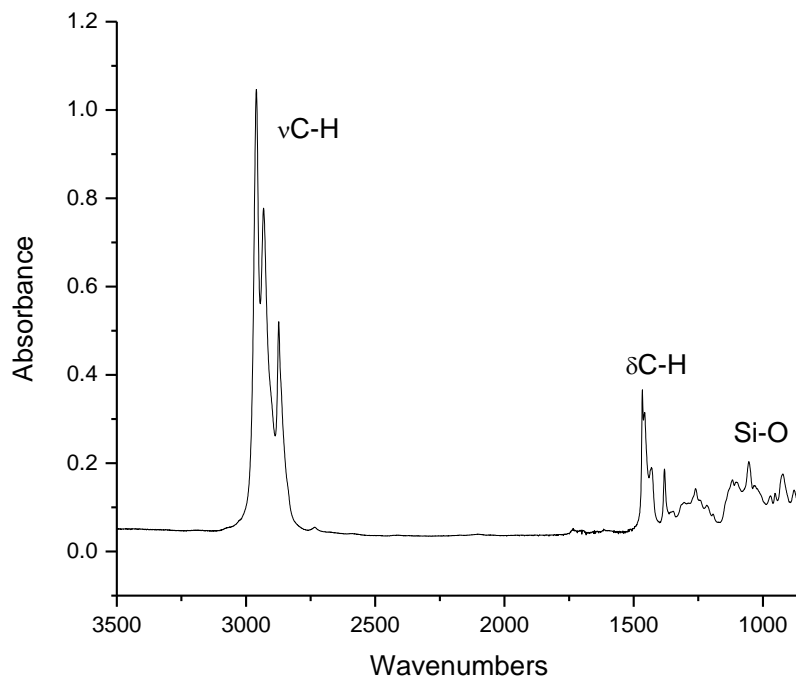


Figure 5.19. IR of 1-octene passivated silicon nanoparticles purged with ethylene in CCl_4 under 254 nm light for 12 hours.

The lack of a Si-H stretch in the IR is good evidence that the hydrosilation reaction had worked and gone to completion as far as could be evaluated by IR. There is also no broad O-H stretch in the region around 3400 cm^{-1} which could have pointed to oxidation and thus hydrolysis of the Si-H rather than hydrosilation. There is a small peak around 1100 cm^{-1} which is in the region in which Si-O-Si is reported, but this occurs normally during the process of the ball milling and has not shown any increase with the hydrosilation reaction.

Section 5.6: Future work.

The next step in investigating the origin of the Si-H is the need for isotopic labeling studies. A crude attempt at this was done with milling in the presence of methanol-D₄. However, the results were not clear as to where the deuterium originated. Ethanol-D was also used to mill with, however, no change was seen. This however could be from the hydrogen was abstracted from the third position, or another aliphatic C-H, or that the ethanol did not mix well with the 1-octene. The correct experiment would be to procure 1-octene that was labeled with deuterium in the third position. This would give definitive proof whether or not the proton is abstracted from the third carbon position.

Section 5.7: Conclusion:

There is more work that needs to be performed on these series of experiments. The hydrolysis experiments showed the ability of the nanoparticles to withstand oxidation with atmospheric water. The carbon tetrachloride experiments are of great interest as they have shown the ability to greatly increase the luminescence of the silicon nanoparticles, while also further passivating the surface, without an increase in oxidation of the surface; as was seen with the chloroform experiments. These experiments have also shown that only a few simple steps can lead to a very large increase in the luminescence of the nanoparticles.

These experiments also show that the surface is fairly well protected due to the steric hindrance of the passivating organic layer. The only successful reactions with the silicon surface were all with small molecules only. This validates the reasoning behind choosing longer chain length organic ligands to passivate the surface, as they do protect the surface from interactions with larger molecules and polar molecules such as KMnO_4 .

The increase in luminescence greatly increases the value of the nanoparticles for biological application where the luminescence is of supreme importance such as tagging of cancerous cells to aid in the efficient removal of cancerous cells without having to remove as much healthy cells as is the practice now in order to insure that as much of the cancer is removed as possible. As discussed in Chapter 3, the silicon nanoparticles are nontoxic and a good candidate for a wide array of biologically relevant procedures.

References

1. Kuang, L. Mechanochemical Synthesis, Characterization, and functionalization of Vinyl-Terminated Silicon Nanoparticles. Tulane, 2014.
2. Hua, F.; Erogbogbo, F.; Swihart, M. T.; Ruckenstein, E., Organically Capped Silicon Nanoparticles with Blue Photoluminescence Prepared by Hydrosilylation Followed by Oxidation. *Langmuir* **2006**, 22 (9), 4363-4370.
3. Sidhu, L. S.; Kosteski, T.; Zukotynski, S.; Kherani, N. P., Infrared vibration spectra of hydrogenated, deuterated, and tritiated amorphous silicon. *Journal of Applied Physics* **1999**, 85 (5), 2574-2578.
4. Wang, H.; Xu, Z.; Fink, M. J.; Shchukin, D.; Mitchell, B. S., Functionalized silicon nanoparticles from reactive cavitation erosion of silicon wafers. *Chemical Communications* **2015**, 51 (8), 1465-1468.
5. Buriak, J. M., Organometallic Chemistry on Silicon and Germanium Surfaces. *Chemical Reviews* **2002**, 102 (5), 1271-1308.
6. Hua, F.; Swihart, M. T.; Ruckenstein, E., Efficient Surface Grafting of Luminescent Silicon Quantum Dots by Photoinitiated Hydrosilylation. *Langmuir* **2005**, 21 (13), 6054-6062.
7. Li, Z. F.; Ruckenstein, E., Water-Soluble Poly(acrylic acid) Grafted Luminescent Silicon Nanoparticles and Their Use as Fluorescent Biological Staining Labels. *Nano Letters* **2004**, 4 (8), 1463-1467.
8. Stewart, M. P.; Buriak, J. M., Exciton-Mediated Hydrosilylation on Photoluminescent Nanocrystalline Silicon. *Journal of the American Chemical Society* **2001**, 123 (32), 7821-7830.
9. Huck, L. A.; Buriak, J. M., UV-Initiated Hydrosilylation on Hydrogen-Terminated Silicon (111): Rate Coefficient Increase of Two Orders of Magnitude in the Presence of Aromatic Electron Acceptors. *Langmuir* **2012**, 28 (47), 16285-16293.
10. Nirmal, M.; Brus, L., Luminescence photophysics in semiconductor nanocrystals. *Accounts of Chemical Research* **1999**, 32 (5), 407-414.

Chapter 6: Summary and Prospectus

This project originated from the idea of synthesizing a silicon nanoparticle with carboxylic acid functional groups which could be used for biological applications by conjugating biomolecules. This was first attempted in a direct fashion by the reactive high energy ball milling (RHEBM) of carboxylic acids with silicon wafers to form carboxylic acid passivated silicon nanoparticles. A mixture of mono and dicarboxylic acids were milled using RHEBM to add the functionality of the carboxylic acid group, distal to the silicon surface. The disappointing results lead to the need for another route of synthesizing functionalized silicon nanoparticles. This route was chosen to be the oxidation of terminal vinyl functional groups. The luminescence of the silicon nanoparticles was recorded for each process, to determine which synthesis route resulted in the best luminescence yield. These particles were then characterized using TEM, EDS, XPS, XANES, photoluminescence, Uv-vis absorption, NMR, and infrared spectroscopy.

The project was a continuation of a project that was started by Andrew Heintz. He originally tried many different functional groups to see which provided the best yield of passivated silicon nanoparticles. He used 1-octanoic acid to test the passivating ability of carboxylic acids to form silicon nanoparticles. This was the starting point of this project, to try and reproduce his results and then to expand upon those results, with the ultimate goal to produce passivated silicon nanoparticles with a free carboxylic acid functional group for further reactions with the silicon nanoparticles.

The initial experiments showed positive results. Silicon nanoparticles were synthesized that were passivated by 1-octanoic acid, 1-hexanoic acid, and 1-pentanoic acid. The next step was to mix dicarboxylic acids with the mono carboxylic acids to result in a particle that was passivated by carboxylic acid and also had a free carboxylic acid functional group. This plan met resistance due to the fact that the diacids were not significantly soluble in the monocarboxylic acids. The best results were from the 1-pentanoic acid and the 1,7- heptanedioic acid but even with this mixture of acids, only 5% of the diacid would dissolve in the monoacid. This limited the amount of carboxylic acid functional groups that could be added to the silicon nanoparticle for further reactions. The use of an inert solvent to increase the solubility of the diacids was met with failure due to the practical limitation of the milling vial and milling process (volume limits and increase in material hampering fracture of the silicon wafer).

A new direction was sought for the synthesis of passivated nanoparticles that had carboxylic acid functionality or that could be converted to carboxylic acid functionality. The route that was chosen was the use of alkenes which had been extensively studied in the Fink and Mitchell groups. The chemistry behind the passivation of the silicon nanoparticles by alkenes was known and as such the focus could be on the oxidation of the terminal vinyl group.

Oxidation of the terminal vinyl groups was first attempted by using KMnO_4 . This did not have successful results for a reaction time of 24 hours. This however, shows that the passivation layer bound to the silicon surface does protect the surface from oxidation as little difference was seen in the photoluminescence or IR of the nanoparticles. Increased reaction time did lead to oxidation of the terminal vinyl groups, however, it

also created many byproducts as this was not a specific oxidation of only the terminal vinyl group. Literature searches of an oxidation that would target only the terminal vinyl group resulted in using ozone to selectively oxidize the vinyl groups.

Ozone has been used for conversion of alkenes and alkynes to several different products based on the chemical workup of the reaction. As discussed in Chapter 3, the oxidizing environment produced by the addition of H_2O_2 resulted in the formation of carboxylic acid functional groups. Use of ozone proved successful on silicon nanoparticles that had been passivated with 1-pentene/1,7-octadiene. IR spectra showed a strong carbonyl stretch at 1711 cm^{-1} and a broad O-H stretch indicative of hydrogen bonding that was centered around 3300 cm^{-1} . The ^1H NMR data showed a peak at about 9.8 ppm which could be an aldehyde (one of the steps that the mechanism proceeds through) or a low field shifted carboxylic acid proton. The oxidizing environment produced by the H_2O_2 should oxidize all aldehydes, but it is possible that the reaction did not proceed to completion. The IR data showed evidence of a carboxylic acid, so it is possible that the greater sensitivity of the NMR experiment revealed a small byproduct of unreacted aldehyde.

Ethylenediamine was used to test the ability to conjugate amines to the carboxylic acid functional group, which converted the terminus of the silicon nanoparticles functionality to an amine group. This was done by an activation step using *n*-hydroxysuccinimide which was then followed by simply stirring of the ethylenediamine with the activated silicon nanoparticle. The characterization revealed that the carbonyl peak shifted to 1650 cm^{-1} which is indicative of an amide bond.

A short strand of DNA was conjugated to the carboxylic acid functionalized silicon nanoparticles to further test the ability to conjugated biomolecules. A second experiment using hybridized strand of DNA was also performed. Both experiments showed positive results of a successful conjugation. Polyacrylamide gel electrophoresis showed that the size of the nanoparticle conjugated to the DNA caused the complex to proceed at a slower rate through the gel than the free DNA strands.

After successfully showing that silicon nanoparticles had been passivated, functionalized, and conjugated to a biomolecule the focus shifted to better characterizing the silicon nanoparticles. Especially the surface of the silicon nanoparticle was of interest. The use of x-ray absorption near edge spectroscopy (XANES) was used to try and determine the modes of bonding and also the composition of the silicon nanoparticle surface. XANES spectra were taken using the synchrotron at the Center for Advanced Microstructures and Devices (CAMD) at Louisiana State University (LSU).

The XANES experiments on 1-octyne and 1-octene passivated silicon nanoparticles showed that the nanoparticles exhibited two major peaks. The peak at 1842 eV corresponded to elemental silicon and a peak at 1848 eV that matched the silicon dioxide calibration standard. The nanoparticle solutions were fractionated using gel permeation chromatography (GPC) to have size separated fractions. These fractions showed a trend of the larger earlier fractions having a major peak at 1848 eV which matched the silicon dioxide peak and was in agreement with IR data that showed the earlier fractions had more oxygen present on the surface of the silicon nanoparticle. The later fractions showed the major peak being closer to 1842, matching the elemental silicon peak. There was also minor intermediate peaks observed between 1842-1848 eV.

A series of XANES spectra of silicon standards were obtained to see if the intermediate peaks could be matched to these standards (a method known as fingerprinting). The fingerprinting method did not reveal the exact cause of these intermediate peaks. The silicon standards did show similar peaks, but did not show a relationship between the peak position and different binding modes or functional groups.

The next step was to model the silicon nanoparticles and produce theoretical XANES spectra. This was done using the software package FEFF9. This is an *ab initio* multiple scattering program based on Green's theories on calculations in real space. A study was undertaken of the affect that chain length has on the XANES spectra and also of the effect of the size of the nanoparticle. The results showed that while the increased chain length increased the resolution of the theoretical XANES spectra, especially at 1842 eV, no trend could be seen that would explain the intermediate peaks between 1842-1848 eV. The size study (0.8 nm, 1.5 nm, and 2.0 nm) of the silicon nanoparticle showed a size effect. The smaller nanoparticles showed a major peak at 1848 eV while the larger (2.0 nm) nanoparticles showed a major peak in the intermediate range.

While a factor which results in a peak that is seen in the intermediate range was found, there is still more study that needs to be done. There are three factors that affect the XANES spectra: 1) oxygen, 2) size, and 3) covalent bonding of molecules to the silicon surface. A series of monodisperse samples of silicon nanoparticles of known sizes needs to be obtained to experimentally determine the effect of the size of the nanoparticles. This would leave only two remaining variables which should provide more data from which a better conclusion could be drawn about the nature of the surface of the silicon nanoparticle.

One of the main themes that are part of all of these different projects is the photoluminescence yield. Comparison of the photoluminescence yield is important as the luminescence is one of the main attractions of using silicon nanoparticles for bioimaging purposes as it has shown to be a better biolabel than many molecular dyes. The first project with the passivation by carboxylic acids showed the lowest photoluminescence yield. The passivation of the silicon nanoparticles by alkenes increased the photoluminescence yield by at least doubling it in most experiments.

A feature that is seen in the IR spectra is an Si-H stretch. It was hypothesized that by increasing the passivation of the surface that the luminescence yield might increase. This was tested by photoassisted hydrosilation using ethylene gas. Initial reactions showed an increase in the yield of the luminescence but the Si-H stretch still remained. This increase could possibly be caused by the promotion of silications on the surface by the formation of excitons. These silications may be able rearrange the silicon nanoparticle surface, eliminating dangling bonds which will eliminate trap states and defects that could reduce luminescence yield. The use of halogenated solvent greatly increased the luminescence yield by an order of magnitude. This is thought to have happened by the halogenated solvent trapping the ejected electron and therefore increasing the amount of silications on the silicon nanoparticle surface.

These projects which are all interconnected with the main goal being the synthesis of highly luminescent silicon nanoparticles with terminal carboxylic acid functional groups that can be conjugated to biomolecules. This has been done by the passivation of silicon nanoparticles with alkenes with terminal vinyl groups which were oxidized to carboxylic acid functional groups. These nanoparticles were then conjugated to DNA

strands to prove that the conjugation to biomolecules was feasible. The silicon nanoparticles were then characterized by XANES and XPS to try and confirm the surface of the silicon nanoparticles, finding a trend involving oxygen that validates the IR data of the silicon nanoparticles. Finally a post processing method of increasing the photoluminescence yield was developed using photoassisted exciton mediated hydrosilation to greatly increase the photoluminescence yield.

Biography

Ted Shaner was born in Phoenixville, Pennsylvania on September 25, 1984. He attended Louisa County High School in Virginia, where he lettered in football and wrestling. He was also awarded the co-MVP for the 2001 football season. In 2003 he was awarded the Most Improved wrestler award, for winning the Jefferson District Wrestling title for heavyweight division and placing 5th in the region in his first year of wrestling. Ted Shaner received a Bachelor of Science degree from Randolph Macon College in Ashland, Virginia in the spring of 2007. He was awarded the American Institute of Chemists Student award in 2007. After college, he entered the Graduate School of Science and Engineering of Tulane University to pursue a Doctor of Philosophy degree in chemistry.